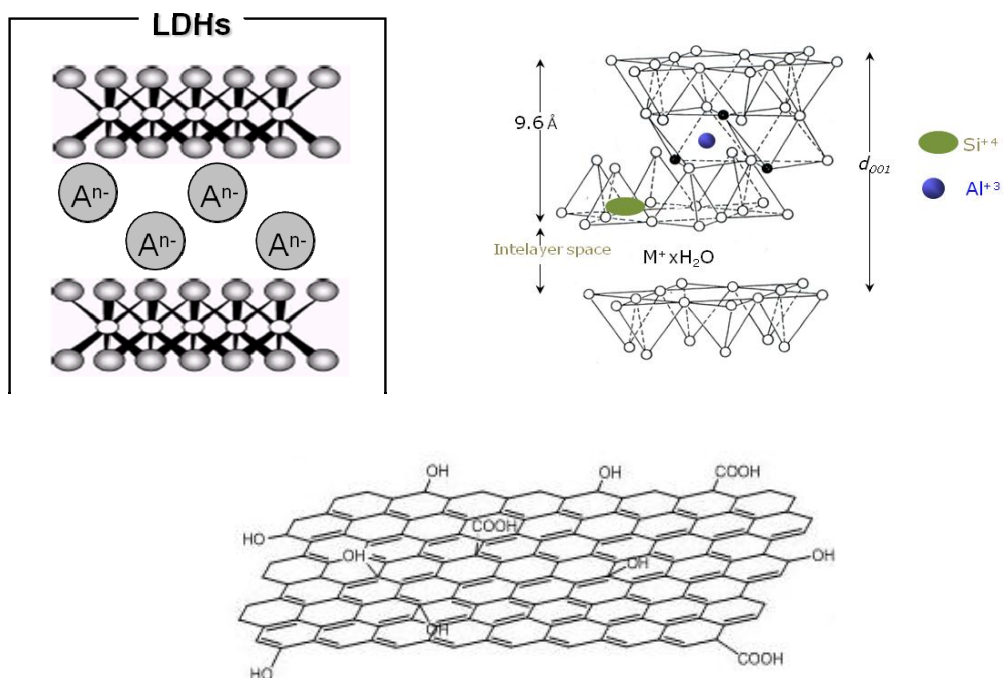


Hybrid nanostructured fillers for polymer electrolytes in the PEM Fuel Cells

Kristina Angjeli

University of Calabria
Doctorate school Bernardino Telesio
Department of Chemistry
2012





Dipartimento di Chimica – Facoltà di Scienze Matematiche Fisiche e Naturali

Bernardino Telesio – Scuola di Dottorato di Scienza e Tecnica

Curriculum: Mesofasi e Materiali Molecolari

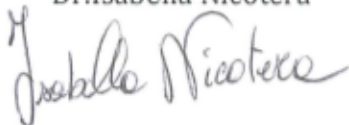
Settore disciplinare: CHIM02

XXV ciclo

Hybrid nanostructured fillers for polymer electrolytes in the PEM Fuel Cells

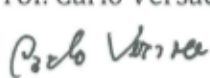
Supervisore

Dr. Isabella Nicotera



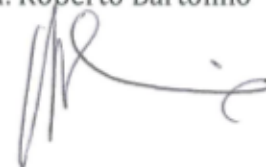
Coordinatore

Prof. Carlo Versace



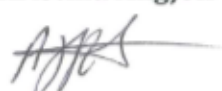
Direttore

Prof. Roberto Bartolino



Candidata

Kristina Angjeli



PREFAZIONE

Le celle a combustibile a idrogeno e metanolo diretto (DHFC/DMFC) che utilizzano come elettrolita una membrana di tipo PEM costituiscono dei sistemi per la generazione di potenza non inquinanti adatti per applicazioni su veicolo elettrico/ibrido o per applicazioni portatili, in virtù della loro elevata efficienza di conversione energetica (~50%) ed emissioni zero.

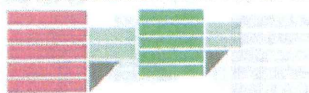
Tuttavia, i principali ostacoli alla commercializzazione su vasta scala delle PEMFC sono l'alto costo, la bassa conduttività protonica alle basse umidità e le scarse proprietà meccaniche a temperature superiori ai 130°C. Per superare queste difficoltà, sono allo studio membrane nanocomposite innovative basate su polimeri perfluorosulfonati-acidi (PFSA) come il Nafion.

In questo lavoro di dottorato membrane ibride nanocomposite sono state preparate a partire da tre classi di filler stratificati e nano strutturati: (i) argille smectite (sintetici e naturali), (ii) ossido di grafene (GO), e (iii) idrossidi doppi strati (LDHs).

Questi materiali opportunamente sintetizzati e funzionalizzati sono stati caratterizzati da una combinazione di diffrazione di raggi X, spettroscopia FTIR, analisi termica (DTA / TGA), Raman, microscopia elettronica a scansione (SEM) e analisi dinamica meccanica.

Uno degli obiettivi principali in questo lavoro è stato quello di coniugare un'intensa attività di ricerca di base, al fine di comprendere i meccanismi molecolari alla base della conduzione ionica in sistemi così complessi, con la progettazione, la sintesi e la caratterizzazione di nuovi nano compositi con opportuni requisiti. A tal fine, uno studio approfondito delle proprietà di trasporto dell'acqua confinata nelle membrane elettrolitiche è stato effettuato mediante metodi NMR per comprendere la dinamica molecolare e i meccanismi alla base della conduzione ionica all'interno delle membrane composite e come questi sono influenzati dalla struttura polimerica e dai filler dispersi.

UNIVERSITÀ DELLA CALABRIA



Dipartimento di Chimica

School "BERNARDINO TELESIO"



Department of Chemistry
Department of Physics

Bernardino Telesio – Doctorate School of Science and Technique

Curriculum: Mesophases and Molecular Materials – CHIM02

XXV cycle

Hybrid nanostructured fillers for polymer electrolytes in the PEM Fuel Cells

Submitted in partial fulfillment of requirements for the Degree of Doctor of Philosophy in Science and
Technique.

Supervisor

Dr. Isabella Njeotera

Coordinator

Prof. Carlo Versace

Chairman

Prof. Roberto Bartolino

Candidate

Kristina Angjeli

This thesis is dedicated to my family

Hybrid nanostructured fillers for polymer electrolytes in the PEM Fuel Cells

Kristina Angjeli

© Kristina Angjeli 2012

PhD Dissertation

Laboratory: PC_SM “Mario Terenzi”

Department of Chemistry

University of Calabria

Ponte P. Bucci, 14D

87036-Rende (CS)

Italy

ABSTRACT

The present thesis is focused on the development of novel nanocomposite membranes, prepared by the incorporation of two-dimensional inorganic layered structures such as (i) smectite clays (synthetic and natural), (ii) graphene oxide (GO), and (iii) layered double hydroxides (LDHs) with different compositions into the polymer matrix of Nafion, for use as electrolytes in Proton Exchange Membrane fuel cells. The characteristics of the membranes were studied mainly, in terms of transport properties by NMR spectroscopy, in order to study the water dynamics inside the electrolyte membranes. For this purpose the Pulse-Field-Gradient Spin-Echo NMR (PFGSE-NMR) method was employed to obtain a direct measurement of water self-diffusion coefficients on the water-swelled membranes in a wide temperature range (25-140 °C). This technique together with the ^1H -NMR spectral analysis and NMR spin-lattice relaxation times (T_1) conducted under variable temperature.

Furthermore, both pristine materials (fillers and Nafion) as well as the resulted nanocomposite membranes were characterized by a combination of X-ray diffraction, FTIR spectroscopy, thermal analysis (DTA/TGA), Raman spectroscopies and scanning electronic microscopy (SEM).

LIST OF PAPERS

1. I. Nicotera, A. Enotiadis, K. Angjeli, L. Coppola and D. Gournis
“Evaluation of smectite clays as nanofillers for the synthesis of nanocomposite polymer electrolytes for fuel cell applications”
International Journal of Hydrogen Energy (2012) 37, 6236-6245.
2. I. Nicotera, A. Enotiadis, K. Angjeli, L. Coppola, G. Ranieri, D. Gournis
“Effective improvement of water-retention in nanocomposite membranes using novel organomodified clays as fillers for high temperature PEMFCs”
Journal of Physical Chemistry B (2011) 115, 29, 9087-9097.
3. A. Enotiadis, K. Angjeli, N. Baldino, I. Nicotera, D. Gournis
“Graphene-based Nafion nanocomposite membranes. Enhanced Proton Transport and Water Retention by Novel Organo-Functionalized Graphene Oxide Nanosheets”
Small (2012), 8, 3338-3349. (DOI: 10.1002/smll.201200609)
4. Isabella Nicotera, Kristina Angjeli, Luigi Coppola, Antonino S.Aricò and Vincenzo Baglio. “NMR and Electrochemical investigation of the Transport Properties of Methanol and Water in Nafion and Clay-Nanocomposites Membranes for DMFCs”
Membranes (2012), 2, 325-345.

SUBMITTED PAPER

- 1 K. Angjeli, I. Nicotera, M. Baikousi, A. Enotiadis, D. Gournis, A. Saccà, E. Passalacqua, A. Carbone
“Investigation of Layered Double Hydroxide (LDH) Nafion-Based composite membranes for high temperatures PEMFCs”
Submitted to Solid State Ionics.

CONFERENCES PRESENTATIONS

- International Conference on Solid State Ionics July 3-8 2011, Warszawa, Poland. Oral presentations “Novel nanocomposite membranes based on organo-modified graphite oxide for lowhumidity pem fuel cells”, K. Angjeli, A. Enotiadis, I. Nicotera , C. Oliviero, L. Coppola, G.A. Ranieri ,D. Gournis.

-
- Symposium on Porous Materials, 30th June – 1st July 2011, Crete, Greece. Oral presentation “Improvement of water retention on polymer electrolyte membranes using layered structures” A. Enotiadis, K. Angjeli, I. Nicotera and D. Gournis 5th PanHellenic.

 - 9th Conference on Solid State Chemistry 10 September- 15 September 2010 Prague, Czech Republic. Poster presentation “Laponite-clay functionalized for nafion nanocomposite membranes in the pem fuel cells applications: water mobility”, K. Angjeli, A. Enotiadis, I. Nicotera , C. Oliviero, L.Coppola, G. A. Ranieri ,D. Gournis.

 - XXII International Symposium on Polymer Electrolytes 29 August - 3 September 2010, Padova, Italy. Poster presentation “Evaluation of smectite clays as nanofillers for the synthesis of nanocomposite polymer electrolytes for fuel cell applications” I. Nicotera, A. Enotiadis, K. Angjeli, C. Oliviero, L. Coppola, G. A. Ranieri ,D. Gournis.

 - 3rd International CARISMA Conference, 3-5 September 2012 Copenhagen, Denmark. Poster presentation “Inorganic-organic membranes from the short side chain perfluorosulfonic acid ionomer for direct methanol fuel cell.” K. Angjeli, I. Nicotera, D. Jones and J. Rozière.

 - XXVI International Conference on Solid State Protonic Conductors- SSPC 16- Grenoble (France), 10-14 Sept. 2012. “Investigation of Layered Double Hydroxide (LDH) Nafion-Based composite membranes for high temperatures PEMFCs”. A. Carbone, K. Angjeli, D. Gournis, I. Nicotera, A. Saccà, E. Passalacqua.

CONTENT INDEX

INTRODUCTION	1
1. GENERAL ASPECTS AND APPLICATIONS	4
1.1 HYDROGEN ECONOMY AND FUEL CELLS	4
1.2 HISTORY OF FUEL CELL TECHNOLOGY	5
1.2.1 Types of Fuel Cells	8
1.3 PROTON EXCHANGE MEMBRANE MATERIALS FOR PEMFCS	15
1.3.1 Nafion polymer	18
1.4 PROTON CONDUCTION MECHANISMS IN PEM	26
1.5 HIGH TEMPERATURE PEM FUEL CELLS (HT-PEMFCS)	30
1.5.1 Composite Membranes	32
References	35
2. MATERIALS	38
2.1 CLAYS	38
2.2 GRAPHENE – GRAPHITE OXIDE	42
2.3 LAYERED DOUBLE HYDROXIDE (LDH)	47
References	51
3. EXPERIMENTAL TECHNIQUES	53
3.1 NUCLEAR MAGNETIC RESONANCE (NMR)	53
3.1.1 Temperature dependence of T1 and T2	58
3.1.2 NMR PGSE Techniques	60
3.2 SCANNING ELECTRON MICROSCOPY	64
3.3 DYNAMIC MECHANICAL ANALYSIS	66
References	68
4. RESULTS AND DISCUSSION	69
4.1 CLAYS-BASED NANOCOMPOSITES FOR PEMFCS (PAPER I)	70
4.1.1 Structural properties of clays-nanocomposites membranes	70

4.1.2. Water transport properties in clays-based PEM	72
4.2 CLAY-NANOCOMPOSITES FOR DIRECT METHANOL FUEL CELLS (DMFCS) (PAPER II)	76
4.3 ORGANO-MODIFIED CLAYS FOR HT-PEMFCS (PAPER III)	83
4.3.1 Preparation of organo-modified clay nanofillers	83
4.3.2 Properties of SWy-organoclays nanocomposites	85
4.3.3 Properties of Laponite-organoclays nanocomposites	91
4.4 ORGANO-FUNCTIONALIZED GRAPHENE OXIDE (GO) – BASED NANOCOMPOSITES MEMBRANES (PAPER IV)	92
4.4.1 Synthesis of organo-modified GO nanofillers	93
4.4.2 Preparation of organo-GO nanocomposites	94
4.4.3 Properties of the organo-GO nanocomposites	96
4.5 LDH-BASED NANOCOMPOSITES FOR PEMFCS (PAPER V)	99
4.5.1 LDH-based nanocomposites by using Nafion 1000 EW as ionomer	99
4.5.2 LDH -- based nanocomposites by using Nafion 1100 EW	101
4.6 AQUIVIONTM-ZRP COMPOSITE MEMBRANES	104
4.6.1 Zirconium Phosphate	105
4.6.2 Preparation of Composite Membrane	106
4.6.3 Structural and Morphological Characterization	108
4.6.4 Physicochemical Characterization and Proton Conductivity	112
References	115
COLCLUSIONS	118
ACKNOWLEDGEMENTS	121

Introduction

The issue of renewable energy is becoming significant due to increasing power demand, instability of the rising oil prices and environmental problems. Among the various renewable energy sources, fuel cell is gaining more popularity due to their higher efficiency, cleanliness and cost-effective supply of power demanded by the consumers.

In the recent scenario, proton exchange membrane fuel cells (PEMFCs) are one of the most promising clean energy technologies. The potential advantages of PEMFCs are related to their possible use in electric and hybrid vehicles or portable apparatuses through (a) the high energy conversion efficiency (~ 50%), (b) the reduced environmental impact for the low CO₂ emissions (zero in the case where the primary fuel is hydrogen) and (c) the flexibility respect to the fuel, in fact, besides hydrogen (DHFC), they can be fed with methanol (DMFC).

The key constituent of a PEMFC is a dense proton-exchange membrane, which is responsible for proton migration from the anode to the cathode. Typically is based on perfluorosulfonic acid (PFSA) polymer membranes, such as Nafion (by Du Pont), which currently represents the most widely used polymer for its unique combination of chemical inertia, mechanical, thermal stability and high proton conductivity; therefore, it constitutes a term of comparison for all new electrolyte materials. Polymer electrolyte fuel cells based upon PFSA membranes have typically been operated in a temperature range between approximately 50 and 90 °C. This temperature range is a compromise between competing factors.

In recent years, increasing interest has been devoted to the development of *high temperature proton conducting polymer electrolyte fuel cell systems*. In fact, most of the *key issues and shortcomings* of PEMFC technology, such as water management, CO poisoning, cooling and heat recovery, can be solved or avoided by developing alternative membranes with suitable ionic conductivity and stability up to 120-130 °C. Polymer membranes able to operate above 120 °C could benefit from both enhanced carbon monoxide (CO) tolerance and improved heat removal. But, the most significant

barrier to running a polymer electrolyte fuel cell at elevated temperatures is maintaining the proton conductivity of the membrane.

For this reason substantial efforts are devoted by the academia and industry to the development of novel fuel cell membrane materials, driven by the need for membranes with improved functionality (e.g., ionic conductivity, robustness) and more cost-efficient polymers.

A number of alternative strategies have been proposed to satisfy these requirements and to maintain membrane conductivity in a dehydrating environment (i.e. elevated temperature and reduced relative humidity). One of these is to integrate hygroscopic materials in the polymer matrix, obtaining nanocomposites membranes. Nanocomposites, that are the object of my doctoral project, generally consist of an ionomer (usually containing acid or superacid $-SO_3H$ groups) in which inorganic or inorgano-organic solid particles are dispersed. The properties of these composite membranes not only depend on the nature of the ionomer and the solid used but also on the amount, homogeneous dispersion, size, and orientation of the solid particles dispersed in the polymeric matrix. Additionally, the introduction of inorganic materials into the polymeric matrix can be considered as a good approach to improve the proton transport, the retention to the swelling and the resistance to the methanol cross-over in DMFC (direct methanol fuel cells) working conditions (membrane in equilibrium with liquid water-methanol mixture).

The work presented in this thesis is the result of a Ph.D. project carried out during a period of about three years from 2009 – 2012, in the Physical Chemistry Soft Matter Laboratory “Mario Terenzi” (PC_SM Mario Terenzi) at the Department of Chemistry in the University of Calabria. The thesis was written as part of the requirements for obtaining the doctor of philosophy degree. Aim of the present thesis is the development of proton conducting nanocomposite membranes based on Nafion polymer, for use as electrolytes in Proton Exchange Membrane fuel cells. The research study focused on the incorporation of two-dimensional inorganic layered structures such as (i) **smectite clays** (synthetic and natural), (ii) **graphene oxide (GO)**, prepared by oxidizing powdered graphite, and (iii) **layered double hydroxides (LDHs)** with different compositions (various combinations of interlayer anions and molar ratios of divalent to trivalent cations), into the polymer matrix of Nafion for the creation of novel hybrid nanocomposites membranes for operation above 100 ° C. Nafion hybrid membranes,

were synthesized by solution intercalation, while the effect of the solvent, temperature and filler loading were examined in order to determine the optimum conditions for the preparation of highly homogeneous composites.

Water-transport properties inside the membranes were investigated by NMR spectroscopy, including pulsed-field-gradient spin-echo (PFGSE), spectral analysis and spin-lattice relaxation time (T₁) conducted under variable temperature. In addition, both pristine materials (fillers and Nafion) as well as the resulted nanocomposite membranes were characterized by a combination of X-ray diffraction, FTIR spectroscopy, thermal analysis (DTA/TGA), Raman spectroscopies, scanning electronic microscopy (SEM) and dynamic mechanical analysis.

The results obtained all these three years have been published in four scientific papers in different international journals. All of the papers are reported in appendices to the end of the thesis. The results obtained using as nanofillers the LDH materials have been divided in two papers, the first is recently submitted in the Solid State Ionics and is also reported in appendix, while the second is in preparation.

During my Ph.D. stage for a period of five months, in the Institute Charles Gerhardt ICGM – AIME, CNRS - University of Montpellier II, in France, under the supervision of Dr. Deborah Jones, the research study focused mainly on the preparation of composite membranes using an alternative polymer to Nafion. In the work presented in this thesis, the short side chain perfluorosulfonic acid ionomeric matrix (Aquivion™), has been used as template for α -type ZrP inorganic particle growth. The membranes were characterized by measurements of water uptake and dimensional change, determination of proton conductivity as a function of relative humidity, observation of structure by SEM and TEM, ³¹P NMR spectroscopy, and X-ray diffraction. The differences of the characteristics of the Aquivion™ -ZrP nanocomposite membrane compared to the pure Aquivion™ membrane were investigated. The results obtained of this work were presented in a poster at the 3rd International Carisma Conference 2012, in Copenhagen, Denmark.

1. General aspects and applications

1.1 Hydrogen economy and fuel cells

Energy is one of the most important topics in the 21st century. With the rapid depletion of fossil fuels and increasingly worsened environmental pollution caused by vast fossil-fuel consumption, there is high demand to make efficient use of energy and to seek renewable and clean energy sources that can substitute fossil fuels to enable the sustainable development of our economy and society. Energy storage can be dated back to ancient times and it is quite simple and natural. With the rapid development of modern industries and the durative increase of global population, the rate of electrical energy consumption has dramatically increased and its consumption manner is diversified. Energy storage becomes even more complex and important, desirable and high-performance energy storage techniques are needed to enable efficient, versatile, and environmentally friendly uses of energy including electricity⁶. Moreover worldwide reduction of CO₂ emission to reduce the risk of climate change (greenhouse effect) requires a major restructuring of the energy system. The use of hydrogen as an energy carrier is a long-term option to reduce CO₂ emissions. The optimal endpoint for conversion to the hydrogen economy is the substitution of clean hydrogen for the present fossil fuels. The clean way to produce hydrogen from water is to use sunlight in combination with photovoltaic cells and water electrolysis. **Hydrogen** is hailed as a non-polluting synthetic fuel that could replace oil, especially for transport applications. Hydrogen is the lightest (density 0.08988 g/L) and the most abundant chemical element on Earth. It constitutes about 75% of all normal matter in the universe and nearly 90% of all atoms. The chemical energy per mass of hydrogen (142 MJ kg⁻¹) is at least three times larger than that of other chemical fuels (for example, the equivalent value for liquid hydrocarbons is 47 MJ kg⁻¹). Thus Hydrogen has the best ratio of valence electrons to protons (and neutrons) of all the periodic table, and the energy gain per electron is very high⁷. At standard temperature and pressure, Hydrogen is colorless,

odorless, tasteless, non metallic, high combustible diatomic gas with the molecular formula H_2 . Hydrogen plays a particularly important role in acid-base chemistry with many reactions exchanging protons between soluble molecules. The charge density of the hydrogen cation H^+ thus remarkably high and it strongly interacts with other surrounding electron rich elements or molecule moieties. Hydrogen is not in and of itself an energy source, because it is not naturally occurring as a fuel. The main source of hydrogen is water, which is essentially an unlimited resource. Hydrogen is also found in many organic compounds, notably the “hydrocarbons” that make up many of our fuels such as gasoline, natural gas, methanol and propane⁸. It cannot be destroyed unlike hydrocarbons, and it simply changes state from water to hydrogen and back to water—during consumption. Furthermore Hydrogen is carbon-free, non-toxic, and its thermal or electrochemical combustion with oxygen yields nothing but energy and water^{7, 9}. The safety of hydrogen relies on its high volatility and non-toxicity. Nonetheless the chief problem is that hydrogen is a gas at room temperature, so it takes up an impractically large amount of space. The gas must therefore be compressed in some way to make it compact enough for mobile applications. A solid-state storage system that can potentially store more hydrogen per unit volume is being developed. Additionally researchers must overcome several obstacles if hydrogen is to become a major energy resource. Hydrogen is currently more expensive than traditional energy sources; the production efficiency (the amount of energy or feedstock used to produce hydrogen) must improve and an infrastructure to efficiently transport and distribute hydrogen must be developed. However hydrogen production, storage and utilization technologies are continually improving. It is only a matter of time before hydrogen will start replacing fossil fuels on a large scale. Once this is known, the transition to our new economy will progress rapidly. Today, many scientists and engineers, some companies, governmental and non-governmental agencies and even finance institutions are convinced that hydrogen’s physical and chemical advantages will make it an important synthetic fuel in the future. After the successful use of hydrogen for space technology, national hydrogen associations were created and joint ventures started. The future for our planet is bright because hydrogen provides the solution to environmental pollution and dwindling fossil fuels⁷⁻⁹. An engine that burns pure hydrogen produces almost no pollution. As an energy carrier, the inherent energy of the stored hydrogen

can be released and converted into electrical energy when needed. This can be done in another type of electrochemical device, which is often referred to as a **fuel cell**.

Whereas the 19th century was the century of the steam engine and the 20th century was the century of the internal combustion engine, it is likely that the 21st century will be the century of the fuel cell. Fuel cells are presently under development for a variety of power generation applications in response to the critical need for a cleaner energy technology. A fuel cell is an energy conversion device that generates electricity and heat by electrochemically combining a gaseous fuel (hydrogen) and an oxidant gas (oxygen from the air) through electrodes and across an ion conducting electrolyte. During this process, water is formed at the exhaust. The fuel cell does not run down or require any recharging, unlike a battery it will produce energy as long as fuel is supplied. The principle characteristic of a fuel cell is its ability to convert chemical energy directly to electrical energy giving much higher conversion efficiencies than any conventional thermo–mechanical system thus extracting more electricity from the same amount of fuel, to operate without combustion so they are virtually pollution free and have quieter operation since there are no moving parts¹⁰. Table 1.1 shows a comparison of different generation systems such as wind turbine, photovoltaic, micro-turbines. It is observed that the efficiency of fuel cells is always higher as compared with conventional system and other distributed generation systems. Fuel cell converts up to 40–60% of available fuel to electricity (90% with heat recovery). While comparing the fuel cell with other distributed generation technologies, it offer more advantages like high energy conversion efficiency, zero emission, modularity, scalability, quick installation and gives good opportunities for cogeneration operations^{10, 11}.

Table 1.1 : Comparison of different generation systems (data reported in 2009)

	<i>Reciprocating engine: Diesel</i>	<i>Turbine generator</i>	<i>Photo voltaic</i>	<i>Wind turbine</i>	<i>Fuel cells</i>
Capacity Range	500 kW to 5 MW	500 kW to 25 MW	1kW to 1MW	10kW to 1MW	200kW to 2MW
Efficiency	35%	29-42%	6-19%	25%	40-60%
Capital Cost (\$/kW)	200-350	450-870	6600	1000	1500-3000

1.2 History of Fuel Cell Technology

Fuel cell is an electrochemical apparatus that convert the chemical energy in electrical energy without fuel combustion. Therefore, in a fuel cell system, the chemical energy related to electrochemical reaction of the fuel (hydrogen) with oxidant (oxygen), directly change into the water, electricity and heat¹². The basic principle of the fuel cell was discovered in the year 1838 by Swiss scientist Christian Friedrich Schönbein. In 1839 Sir William Grove developed the first fuel cell based on reversing the electrolysis of water by an accident¹⁰. Andùjar and Segura¹³ recently held a detailed review of the history of fuel cells, which describe the main stations as shown in Figure 1.2.1.

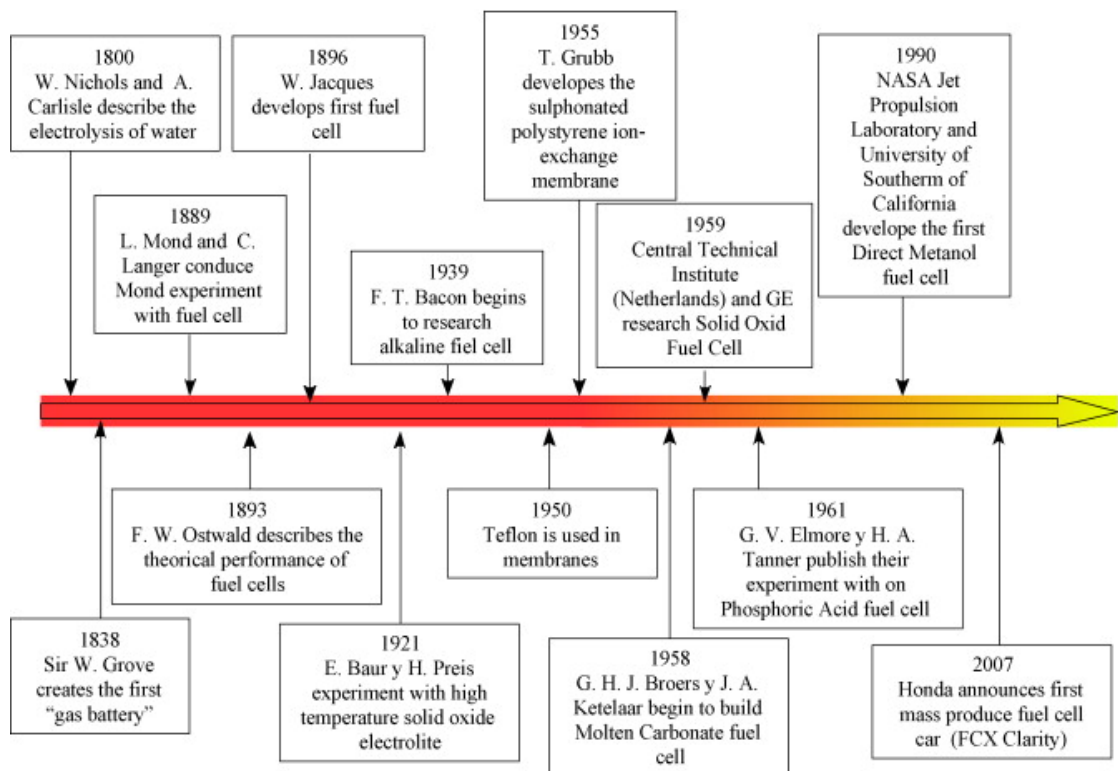


Figure 1.2.1: Historical review of fuel cells¹³

In 1950 Francis Bacon at the Cambridge University demonstrated the first 5 kW alkaline fuel cell. After the successful development of alkaline fuel cells, NASA needed a compact system to generate electricity for space shuttle applications. In 1970s, international fuel cells developed a 12 kW alkaline fuel cell for NASA's space shuttle orbiter to supply reliable power without the use of any backup powers like batteries. Beginning in the mid-1960s, the research work was focused on further development of various fuel cells for applications like stationary powers and transportations. Further the government agencies in the USA, Canada and Japan have significantly increased their funding for fuel cell in R&D¹⁴. But in many countries it was taken into account after 50 years, because of its major drawback of higher installation cost. After the development of power conversion devices much more researches are going on fuel cells to reduce its higher installation cost¹¹. Moreover, in 2007, the vehicle manufacturer Honda presented the model FCX Clarity at Los Angeles automobile saloon. This model is available for the consumer since the summer of 2008. This is the first fuel cell vehicle platform-exclusive in the world manufactured in series¹³.

1.2.1 Types of Fuel Cells

Several different types of fuel cells have been developed throughout the years, so they come in many varieties, however, all work in the same general manner. The main difference consists in the type of electrolyte. Each fuel cell type has its own unique chemistry, such as different operating temperatures, catalysts, and electrolytes. Figure 1.2.2 illustrates schematically the operating characteristics for the alkaline fuel cell (AFC), proton exchange membrane (PEM) fuel cell, direct methanol fuel cell (DMFC), molten carbonate fuel cell (MCFC), phosphoric acid fuel cell (PAFC), and solid oxide fuel cell (SOFC). These different types of fuel cells are briefly described bellow with special emphasis on the proton exchange membrane (PEM) fuel cells, the type of fuel cell studied in this thesis. In table 1.2 are summarized the anode and cathode reactions of each fuel cell types.

Table 1.2: The cathode and anode reactions of the different fuel cell types

Fuel Cell type	Cathode reaction	Anode reaction
alkaline (AFC)	$O_2 + 4e^- + 2H_2O \rightleftharpoons 4OH^-$	$2H_2 + 4OH^- \rightleftharpoons 4H_2O + 4e^-$
solid oxide (SOFC)	$O_2 + 4e^- \rightleftharpoons 2O^{2-}$	$2H_2 + 2O^{2-} \rightleftharpoons 2H_2O + 4e^-$
molten carbonate (MCFC)	$O_2 + 2CO_2 + 4e^- \rightleftharpoons 2CO_3^{2-}$	$2H_2 + 2CO_3^{2-} \rightleftharpoons 2H_2O + 2CO_2 + 4e^-$
phosphoric acid (PAFC)	$\frac{1}{2}O_2 + 2e^- + 2H^+ \rightleftharpoons H_2O$	$H_2 \rightleftharpoons 2H^+ + 2e^-$
direct methanol (DMFC)	$\frac{3}{2}O_2 + 6H^+ + 6e^- \rightleftharpoons 3H_2O$	$CH_3OH + H_2O \rightleftharpoons CO_2 + 6H^+ + 6e^-$
proton exchange membrane (PEM)	$\frac{1}{2}O_2 + 2e^- + 2H^+ \rightleftharpoons H_2O$	$H_2 \rightleftharpoons 2H^+ + 2e^-$

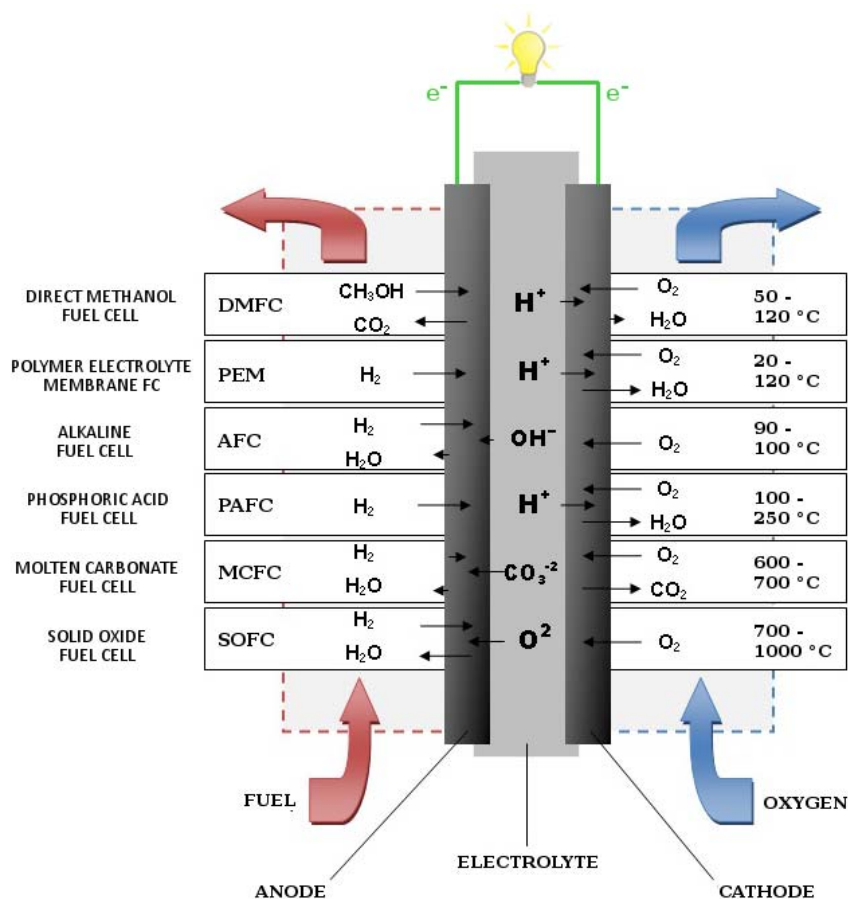


Figure 1.2.2: Schematic representation of different fuel cell types. alkaline fuel cell (AFC), proton exchange membrane (PEM) fuel cell, direct methanol fuel cell (DMFC), molten carbonate fuel cell (MCFC), phosphoric acid fuel cell (PAFC), and solid oxide fuel cell (SOFC).

The **alkaline fuel cell (AFC)** is one of the earlier fuel cell system employed for NASA's space missions. Formerly it is also called as Bacon fuel cell after its British inventor. It operates at low temperature around 100 °C and it has the capability to reach 60–70% of efficiency. It uses an aqueous solution of the potassium hydroxide (KOH) as an electrolyte. It transports negative charged ions from anode to cathode and releases water as its by product. This fuel cell gives quick start, one of its advantages. It is also possible to use electrodes made of non-noble and relatively cheap materials such as nickel or nickel based compounds. The major disadvantage is the high sensitivity to the CO₂ because it takes more time to react and consumes the alkaline in the electrolyte thereby reducing the concentration of hydroxide ion during chemical reactions¹⁵. It needs a separate system to remove the CO₂ from the air. The use of a corrosive electrolyte is also a disadvantage because it has shorter life span¹¹.

The **solid oxide fuel cell (SOFC)** utilizes a solid ceramic electrolyte material based on for example sintered yttria or scandia stabilized zirconia. The SOFC produce electricity at a high operating temperature of about 800-1000 °C. For the electrodes, metals such as nickel or cobalt are used. The electrolyte is solid avoiding the problems of liquid handling. Additionally they allow spontaneous internal reforming fuel. Because the oxide ions travel through the electrolyte, fuel cell can be used to oxidize any combustible gas¹³. There is no need of noble metal catalysts due to the high catalytic activity of alternative metallic or ceramic materials as a result of the high temperature. The slow start up, high cost and intolerant to sulfur content of the fuel cell are some of its drawbacks. This type of fuel cells is used in stationary applications or such as auxiliary power systems (APU).

Molten carbonate fuel cells (MCFC) use an electrolyte composed of a mixture of lithium carbonate and potassium. By this electrolyte circulating carbonate ions (CO₃²⁻) from the cathode to the anode (the reverse of most fuel cells). Fuel cells are working at high temperatures (around 650 °C) and pressures between 1 and 10 atm. The high operating temperature at about 650 °C allows for non-noble metal electrode materials, spontaneous internal reforming fuel, high-speed reactions as well as high efficiencies This cell is intolerant to sulfur and slow start up is one of its drawbacks. It is mainly used for medium and large power applications¹⁵.

The **phosphoric acid fuel cell (PAFC)** operates at about 175–200 °C. Such fuel cells use an electrolyte that conducts hydrogen ions (H⁺) from the anode to the cathode.

The electrolyte is formed, as its name indicates, of a liquid phosphoric acid within a matrix of silicon carbide. There are some fuel cells that use an electrolyte of sulphuric acid. These fuel cell is very tolerant to impurities in the reformed hydrocarbon fuels and may use air directly from the atmosphere. The cogeneration is also possible due to its high operating temperature and the potential is also available for hot water supply as well as electricity depending on the heat and electricity load profile. However the PAFC cost increases due to use of platinum as a catalyst, while they have a maximum tolerance of 2% CO and they utilize liquid electrolyte, which is corrosive to average temperatures, which involves handling and safety problems. PAFC have been developed to the first stage of commercialization. The 100, 200 and 500 kW size plants are available for stationary and heat applications. A 1.3MW system is already tested in Milan¹⁶.

The **direct methanol fuel cell (DMFC)** technology is relatively new when compared to rest of the fuel cells. Such fuel cells are replacing traditional batteries in some applications. It is expected to gain space in the market because they have a higher lifetime compared to the lithium ion battery and can be recharged by simply changing the cartridge of fuel. Like PEM fuel cell, the DMFC uses polymer electrolyte. But DMFC uses liquid methanol or alcohol as fuel instead of reformed hydrogen fuel. During chemical reactions, the anode draws hydrogen by dissolving liquid methanol (CH_3OH) in water in order to eliminate the need of external reformer. At the cathode, the recombination of the positive ions and negative ions takes place, which are supplied from anode through external circuit and it is combined with oxidized air to produces water as a byproduct. The two main barriers to economic DMFCs are methanol crossover and slow anode kinetics. Methanol crossover is the diffusion of methanol through the membrane from the anode side to the cathode. This reduces DMFC efficiency, primarily because (1) the crossed-over methanol is essentially wasted, and (2) the cathode's catalyst can be poisoned by the carbon atoms in the methanol. This generally limits methanol concentrations at the anode compartment to around 2–5 wt%, and may require recirculation of water produced in the cathode compartment back to the anode compartment in order to keep the methanol dilute. Such constraints generally limit the overall DMFC efficiency to around 15–20% and the power density to around 30 mW/cm². Methanol crossover losses can be 30% or higher of the methanol fuel for some DMFC membranes and design configurations^{17, 18}. Yet even now, one potential

area of application can be recognized distinctively: for relatively low-power energy sources in electronic equipment such as notebooks, cameras and video cameras, DVV players, and some medical devices. So far, another potential field of application of DMFC as power sources for electric vehicles is too remote. Work is needed to achieve the futures of longer lifetime and greater efficiency¹⁹.

The **proton exchange membrane fuel cell (PEMFC)**, also called the solid polymer fuel cell (SPFC), was first developed by General Electric in the United States in the 1960s for use by NASA on their first manned space vehicles. Today, the PEM fuel cell technology has been recognized as an efficient and environmentally benign concept for electrical power generation, especially for portable and automotive applications. The PEMFC typically operates at temperatures between 60 and 100 °C, in specific configurations around 180 °C. This technology has drawn the most attention because of its simplicity, viability and quick start-up. The most important part and in the other words the central core of the fuel cell is the membrane electrode assembly (MEA) which is consist of two part namely electrocatalyst and membrane, that has some unique capabilities, this part will be further discussed in chapter 1.3. It is impermeable to gases but it conducts protons (hence Proton Exchange Membrane name). The membrane, which acts as the electrolyte is responsible for proton migration from the anode to the cathode, is squeezed between the two porous, electrically conductive electrodes. These electrodes are typically made out of carbon cloth or carbon fiber paper. At the interface between the porous electrode and the polymer membrane there is a layer with catalyst particles, typically platinum supported on carbon. Schematic representations of cell configuration and MEA are shown in Figure 1.2.3. Hydrogen gas (H_2) is oxidized at the anode on catalyst particles that disassociate to $2H^+$ (protons) and $2e^-$. The protons (associated with water molecules) are transferred through the polymer electrolyte (membrane) to the cathode, where they react with oxygen to produce water and heat. PEM fuel cells can be operated at high power densities which means that the total active area of the MEAs can be minimized, allowing for a compact design of the fuel cell stack. Other advantages of the PEM fuel cell are its higher power density and quick start up for automotive vehicles. The low operating temperature makes the technology competitive in transportation and commercial applications like laptop computers, bicycle, and mobile phones. The major

drawbacks of the PEM fuel cell are its lower operating efficiency (40–45%) and use of high cost platinum catalyst. It is also intolerant to carbon monoxide.

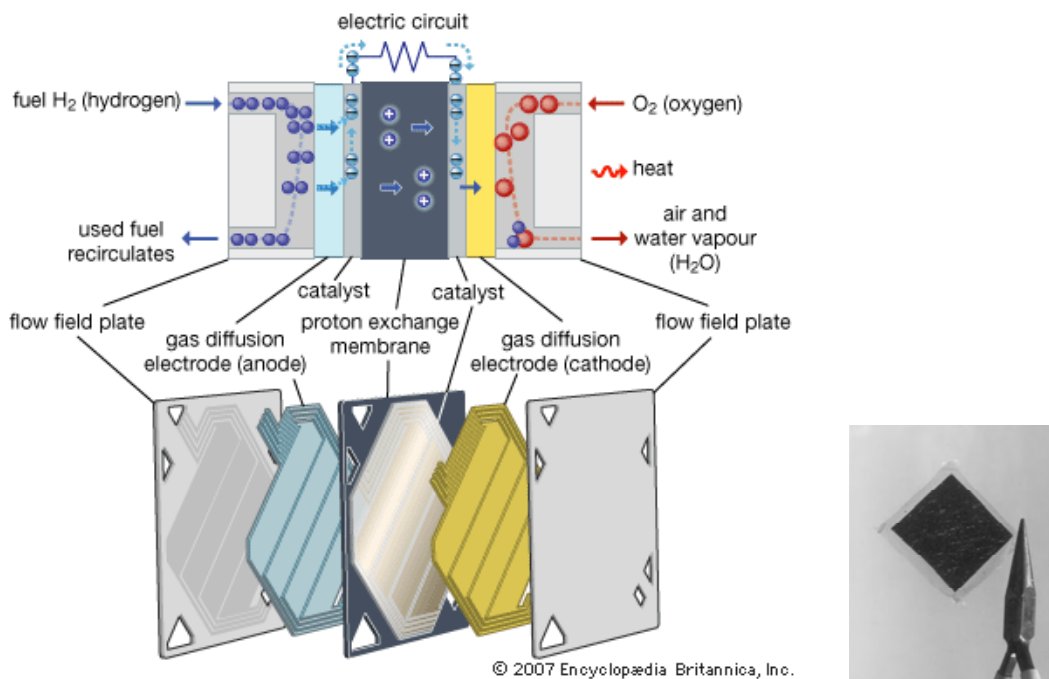
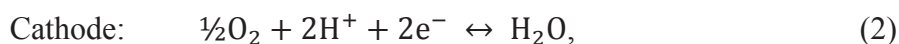
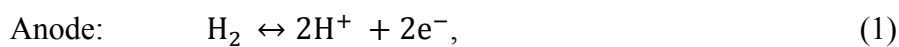


Figure 1.2.3: schematic representation of PEM fuel cell (left) and an example of a membrane electrode assembly (MEA). The membrane is a little larger than the electrodes that are attached. These electrodes have the gas diffusion layer attached, which gives it a ‘grainy’ texture. The membrane is typically 0.05 to 0.1mm thick, the electrodes are about 0.03mm thick, and the gas diffusion layer is between 0.2 and 0.5-mm thick.²⁰

The reactions taking place in PEMFC are



The Gibbs free energy change (ΔG°) of reaction (3) is related to the cell voltage by

$$\Delta G^\circ = -nFV_0, \quad (4)$$

where n is the number of electrons involved in the overall reaction, F the Faraday constant, and V_0 the cell voltage at thermodynamic equilibrium in absence of the

current flow, i.e. under open-circuit condition. V_0 is the difference of the equilibrium electrode potentials at the cathode and the anode of the cell, and is calculated from

$$V_0 = -\Delta G/nF = 1.23V. \quad (5)$$

Ideally, PEMs should have high ionic conductivity, good chemical, thermal and physical stability, and be relatively inexpensive. In essence, the efficiency of the PEMFC is dependent upon the transport properties or the ionic mobility of the PEM being used. The expectation is that the greater the ionic mobility, the greater the efficiency of the PEMFC. For this reason, one main focus of researchers has been on the development of PEMs with high ionic conductivities⁴. In 1970s, DuPont developed a perfluorosulfonic acid called “Nafion” that not only showed a two-fold increase in the specific conductivity of the membrane but also extended the lifetime by four orders of magnitude (10⁴-10⁵ h). This soon became a standard for PEMFC and remains so till today. In the next section is extensively analyzed the structure of this membrane.

1.3 Proton Exchange Membrane Materials for PEMFCs

As is mentioned in the chapter 1.2, membrane is the core component of the PEM fuel cell. To achieve high efficiency the membrane must possess the following desirable properties:

- high proton conductivity
- zero electronic conductivity
- low react permeability
- mechanical strength and flexibility
- durability
- compatibility
- availability

Proton conductivity above $10^{-2} \text{ S cm}^{-1}$ is required in order to support high currents with minimal resistive losses. However, the membrane has to be electronically insulating, in order to avoid short circuit of the cell, and a good barrier for the reactants. Reactant cross-over results in poor fuel utilization and voltage losses in fuel cells. High cross-over rate might also be connected with safety issues due to the formation of explosive gas mixtures. Additionally the mechanical strength and the flexibility of the membrane are important parameters in the membrane processing and production of MEAs. Thermal cycling of the electrochemical cell will induce stresses in contact points between different cell components, which ultimately might lead to physical membrane failure. The membrane has to be tolerant to the harsh oxidative conditions in the operating cell. For example the polymer matrix has to withstand aggressive radicals, high potentials, extreme pH and eventually high temperatures. Moreover compatibility of the membrane with the cell hardware as well as the electrode materials is required in order to allow for good reaction kinetics. Finally reaching widespread commercial utilization of the PEM technology the cost of the membrane material has to be minimized^{21, 22}. In general, the materials used in synthesis of the polymer electrolyte membranes can be classified into three vast groups: perfluorinated ionomers (or partially perfluorinated), nonfluorinated hydrocarbons (including aliphatic or aromatic structures), and acid-base complexes²³.

The *perfluorinated sulfonic acid (PFSA)* membranes have been the subject of intense research. The key polymers used currently in portable fuel cell applications have perfluorinated structures with attached sulfonic acid groups. The perfluorinated polymer used most extensively and produced by DuPont goes by the trade name of Nafion®, known as a long-side-chain (LSC) ionomer. In recent years, alternative polymers with a structure similar to Nafion® but with a shorter pendant side-chain (SSC) carrying the sulphonic group, developed by Dow, 3 M, Gore, Asahi glass, Solvay-Solexis, etc²⁴⁻²⁶ (see Figure 1.3.1) have been investigated for fuel cell operation. Membranes of PFSA, such as Nafion®, are generally prepared by melt extrusion or by casting from a solvent solution or from a dispersion of PFSA in a mixture of water and light alcohols. The casting technique and the thermal history of the membrane are directly related to the degree of crystallinity of the polymer and hence the physiochemical properties of the membrane²⁷. However due to the relatively high cost of PFSA membranes, alternative PEM materials based on sulfonated non-fluorinated or partially fluorinated aliphatic or aromatic polymers or multiblock copolymers are under active development^{28, 29}.

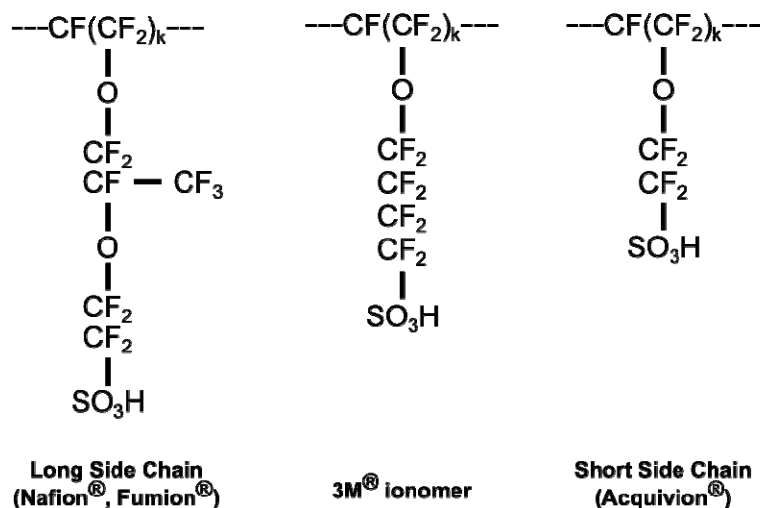


Figure 1.3.1: Chemical structures of LSC and SSC perfluorinated ionomers.

Non-fluorinated hydrocarbon polymers can be aliphatic or aromatic polymers having benzene ring structures in the polymeric backbone of membrane or in the bulky pendant groups from this membrane polymeric backbone. Hydrocarbon membranes

provide some definite advantages over perfluorinated membranes. They are less expensive, commercially available and their structure permits the introduction of polar sites as pendant groups²³. In order to enhance stability at elevated temperatures, aromatic hydrocarbons can be (a) incorporated directly into the backbone of a hydrocarbon polymer or (b) polymers modified with bulky groups in the backbone to render them. Polyaromatic membranes are high temperature rigid polymers with $T_g > 200^\circ\text{C}$ owing to the presence of inflexible and bulky aromatic groups³⁰. The aromatic rings offer the possibility of electrophilic as well as nucleophilic substitution. Polyethersulfones (PESF), polyether ketones (PEK) with varying number of ether and ketone functionalities (such as PEEK, PEKK, PEKEKK, etc.), poly(arylene ethers), polyesters and polyimides (PI), polybenzimidazoles (PBI) are some of the relevant examples of main chain polyaromatics³¹. The addition of a protogenic group (generally a sulfonic acid group) to a polymer can be achieved either by direct sulfonation of the polymer with sulfuric acid or chlorosulfonic acid via sulfonation by chemically grafting a group containing a sulfonic acid function on to a polymer by graft polymer synthesis from monomers bearing sulfonic acid groups. The level of sulfonation is a key parameter, since it is accompanied at too high levels by an unacceptable degree of swelling and unsatisfactory mechanical properties. The conductivity of the membrane is however directly related to the extent of sulfonation (in addition to the degree of relative humidity, temperature, etc.)³². Chemical structures of sulfonated-PEEK and sulfonated-PBI is illustrate in Figure 1.3.2.



Figure 1.3.2: Chemical structures of sulfonated-PEEK and sulfonated-PBI.

Acid-base complexes into an alkaline polymer generally promote proton conduction. The poly(2,2-(*m*-phenylene)-5,5-benzimidazole)/phosphoric acid (PBI/ H_3PO_4) complex is both intriguing and promising at the same time. It has shown a great deal of potential for medium temperature fuel cell applications and hence many

attempts were made to understand and optimize this particular system. Since it is an acid–base complex, the conductivity of doped PBI does not depend on humidity in contrast to Nafion®. Unfortunately, these membranes are less performing at low temperature and do not allow for a rapid start-up as required for automotive applications. Moreover, the power densities that can be achieved with these membranes appear lower than those obtained with perfluorosulfonic acid (PFSA) membranes.

1.3.1 Nafion polymer

In this thesis the Nafion polymer, a perfluorinated sulfonic acid (PFSA) membrane, was studied as a polymer electrolyte for the PEM fuel cells. This ionomer is developed and produced by the E. I. DuPont Company, it is generated by copolymerization of a perfluorinated vinyl ether comonomer with tetrafluoroethylene (TFE), resulting in the chemical structure shown in Figure 1.3.3. Teflon backbone of this structure gives the hydrophobic nature for membrane and hydrophilic sulfonic acid groups (HSO_3^-) have been grafted chemically into backbone. These ionic groups have caused the absorption of the large amount of water by polymer and therefore, lead to hydration of the membrane. Thus, the factors affecting the performance of the suitable proton exchange membrane are the level of hydration and thickness of the membrane which is playing an important role in deciding their suitability for application in fuel cell³³.

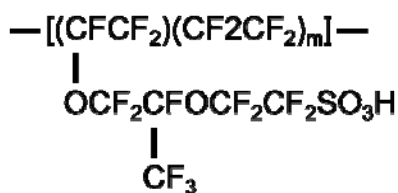


Figure 1.3.3: Chemical structure of Nafion.³⁴

Characteristic feature of Nafion products is the equivalent weight (EW), i.e. the number of grams of dry Nafion per mole of sulfonic acid groups when the material is in the acid form. This is an average EW in the sense that the comonomer sequence distribution (that is usually unknown to the investigator and largely unreported) gives a distribution in m in this formula. EW can be ascertained by acid-base titration, by analysis of

atomic sulfur, and by FT-IR spectroscopy. The relationship between EW and m is: $EW = 100m + 446$ so that, for example in a membrane of 1100 EW, the side chains are separated by around 14 CF_2 units. Furthermore the equivalent weight (EW) and material thickness are used to describe most commercially available membranes, for example in Nafion 117 films, the designation “117” refers to a film having 1100g EW and a nominal thickness of 0.007 in., although 115 and 112 films have also been available. Early-reported studies involved 1200 EW samples as well as special experimental varieties, some being rather thin. In general, a higher EW value corresponds to a lower ionic conductivity and to higher morphological stability. Finally the equivalent weight is related to the property more often seen in the field of conventional ion exchange resins, namely the ion exchange capacity (IEC), by the equation $IEC = 1000/EW$ ³⁴. Curtin et al. performed size exclusion chromatography determinations of the molecular weight distribution in Nafion aqueous dispersions after they were heated to high temperatures (230, 250, and 270 °C)³⁵. Experiments revealed that the radius of gyration had a linear dependence on the molar mass of the aggregates, which suggests that the particles are in the form of rods or ribbons, or at least some elongated structure³⁴. The greatest interest in Nafion in recent years derives from its consideration as a proton conducting membrane in fuel cells. It is clear that the tuning of these materials for optimum performance requires a detailed knowledge of chemical microstructure and nanoscale morphology. It was estimated (DuPont library), based on a coarse literature search, that there were approximately 33.000 papers, patents, and so forth dealing with Nafion, and the number is growing. However, while the quality and quantity of data from state-of-the-art instrumentation, facilities, and methods has increased, a universally accepted morphological model for the solid-state structure of Nafion has yet to be defined. Nafion stems has a random chemical structure that is capable of organizing in the complex formation of ionic and crystalline domains with a significant distribution in dimensions over a wide range of length scales. Since the vast majority of the applications of Nafion involve the hydrated or solvent swollen state and current processing methods for membrane formation often involve solvent casting, considerable attention has been devoted to the influence of swelling solvents (specifically water) on the characteristic morphological features of perfluorosulfonate ionomers. By the late 1970s, experimental evidence for ionic aggregation in Nafion from small-angle scattering data was emerging, and this new information subsequently

lead to extensions of the prevailing models for the structure of ionomers to the interpretation of ionic domain morphology in the perfluorosulfonate ionomer systems³⁴.

Gierke et al. suggested the cluster-network model^{36, 37}, which interprets the properties of Nafion membranes, especially ion and water transport. It is presumed, based on small-angle X-ray scattering (SAXS) studies and several assumptions, that there are ~ 40 Å -in-diameter clusters of sulfonate-ended perfluoroalkyl ether groups that are organized as inverted micelles and arranged on a lattice. These micelles are connected by proposed pores or channels that are ~ 10 Å in size, as is described in Figure 1.3.4. These $-\text{SO}_3^-$ coated channels were invoked to account for intercluster ion hopping of positive charge species but rejection of negative ions (such as OH^-).

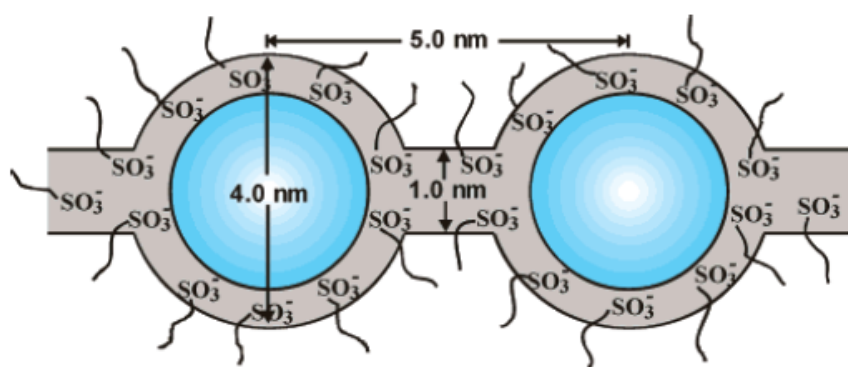


Figure 1.3.4: Cluster-Network model for the morphology of hydrated Nafion.³⁶

Among the earliest concepts, Yeager and Steck proposed a three phase model³⁸ that was significantly different from that of Gierke et al. based on their studies of the diffusion of various ions. As compared with the model of Gierke et al., the clusters do not have a strict geometrical definition (spherical inverted micelles connected by cylindrical pores) and their geometrical distribution has a lower degree of order. Most importantly, there are transitional interphases between hydrophobic and hydrophilic regions (Figure 1.3.5), a concept that is becoming increasingly accepted.

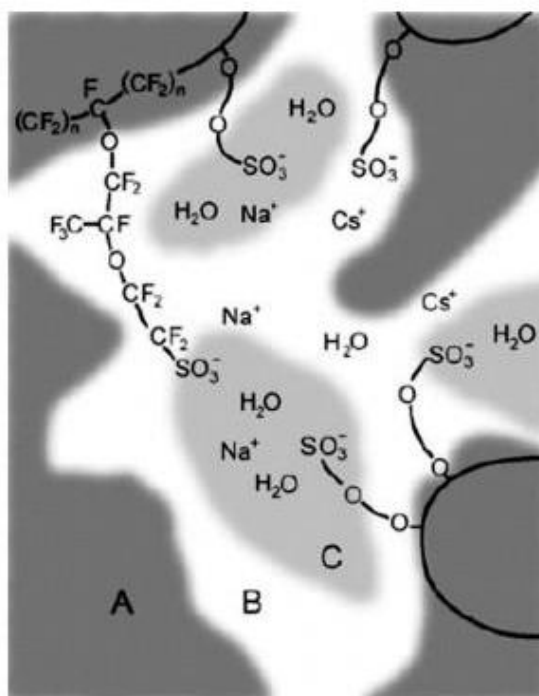
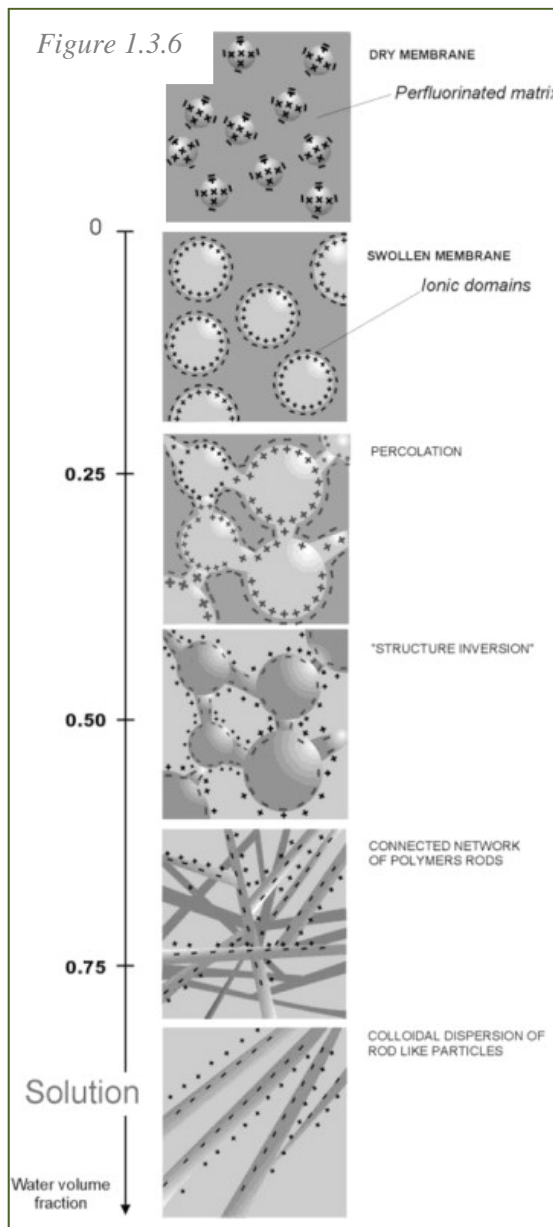


Figure 1.3.5: The three phase model³⁸, region A, B and C are the fluorocarbon polymer, the interfacial and the ionic cluster region, regions respectively.

Gebel³⁹ proposed a conceptual description for the swelling and dissolution process shown schematically in Figure 1.3.6. In dehydrated Nafion, the dry cluster diameter of ~ 1.5 nm is significantly smaller than the inter-cluster distance of ~ 2.7 nm, which explains the extremely low ionic conductivity observed at anhydrous state. With the absorption of water, a modification of the cluster structure occurs, which results in the formation of spherical water pools with the ionic groups at the polymer water interface in order to minimize the interfacial energy. The water pool diameter of ~ 2.0 nm is still lower than the interaggregate distance of ~ 3.0 nm, which is evidenced by the low ionic conductivity at low water content. When the water volume fraction, is larger than 0.2, the large increase of the ionic conductivity happens, indicating a percolation of the ionic aggregates. The origin of percolation can be probably interpreted as a combination of the effect of the interfacial energy and of the limitation of the swelling due to the polymer chain elastic energy. As the water content increases to between $\phi \sim 0.3$ and 0.5, the structure of spherical ionic domains connected with cylinders of water dispersed in the polymer matrix formed. The ionic domain diameter increases from 4 nm to 5 nm, and the increase in ionic conductivity with the water content

increasing reveals that both the connectivity and the diameter increase. At ϕ values larger than 0.5, an inversion of the structure occurs and the membranes correspond to a connected network of rod-like polymer aggregates. Finally, as the membrane “dissolves” into solution, the rod-like structures separate to yield a colloidal dispersion of isolated rods. The structure of highly swollen membranes is then very close to that of the Nafion solution. This model offered a plausible mechanism for the evolution in structure from the widely accepted concept of isolated clusters for membranes containing relatively low water contents to rodlike structures in solution.

The lamellar model proposed by Litt⁴⁰ provides a convenient and simple explanation for the swelling behavior of Nafion. Moreover, it is a variation of the lamellar model proposed by Haubold et al⁴¹, in which synchrotron SAXS studies were performed on acid form Nafion 117 samples. The experiments were conducted on dry samples in air and samples equilibrated with water, methanol, and a range of water/methanol mixtures using an in situ flow cell. The scattering cross section data was fitted to a layered model whose basic structure element (i.e., the scattering particle) is a “sandwich”. The outer portion of this sandwich (the “shell”) consists of the side chains, including the sulfonic acid groups, and the inner liquid portion (the “core”) consists of the water/methanol molecules. To provide channels that serve as conduction pathways for protons through the membrane, these structural elements were



proposed to be juxtaposed in a linear fashion so that the liquid core regions are contiguous as is presented in Figure 1.3.7 below.

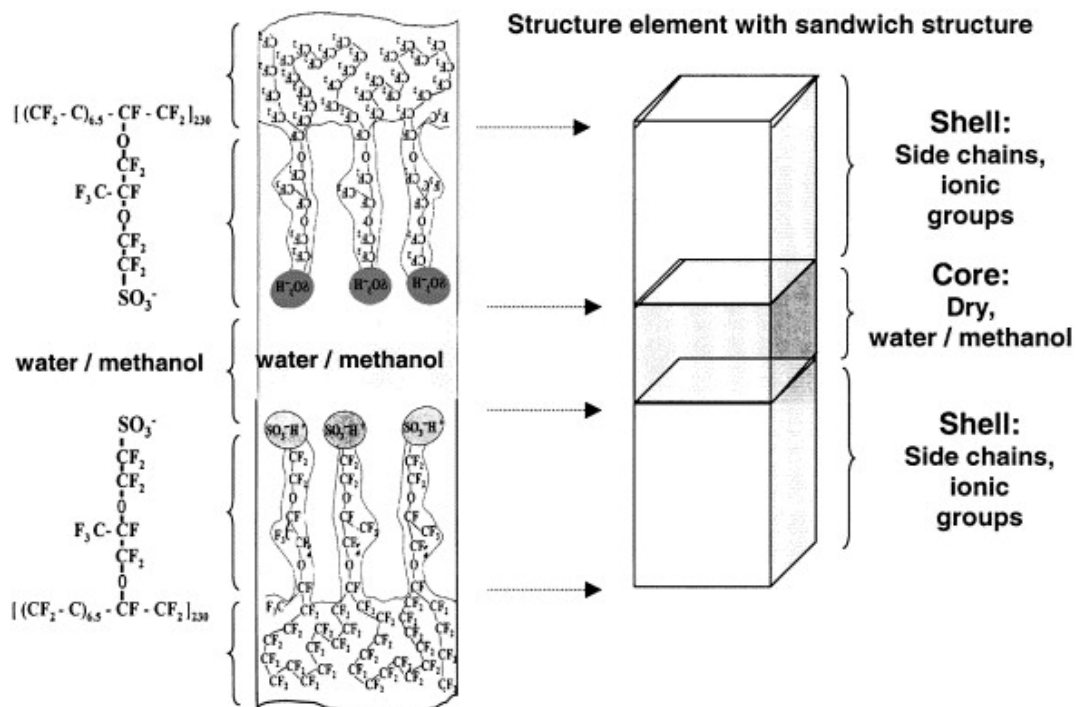


Figure 1.3.7: Sandwich-like structural element proposed for the morphological organization of Nafion.⁴¹

While in 1992 Rubatat⁴² and co-workers, presented a schematic representation (Figure 1.3.8) of an entangled network of elongated rodlike aggregates in Nafion. Long range heterogeneities arising from bundles of locally ordered aggregates are proposed to give rise to the low angle increase in scattered intensity.



Figure 1.3.9: Schematic representation of rodlike structure.⁴²

Finally according to Kreuer²⁸ model perfluorosulfonic polymers naturally combine, in one macromolecule, the extremely high hydrophobicity of the perfluorinated backbone with the extremely high hydrophilicity of the sulfonic acid functional groups. Especially in the presence of water, this gives rise to some hydrophobic/hydrophilic nano-separation. The sulfonic acid functional groups aggregate to form a hydrophilic domain. When this is hydrated, protonic charge carriers form within inner space charge layers by dissociation of the acidic functional groups, and proton conductance assisted by water dynamics occurs. While the well connected hydrophilic domain is responsible for the transport of protons and water, the hydrophobic domain provides the polymer with the morphological stability and prevents the polymer from dissolving in water. The situation in sulfonated polyetherketones was found to be distinctly different with respect to both transport properties and morphological stability. As a result of the smaller hydrophilic/hydrophobic difference (the backbone is less hydrophobic and the sulfonic acid functional group is less acidic and therefore, also less polar) and the smaller flexibility of the polymer backbone, the separation into a hydrophilic and a hydrophobic domain is less pronounced. As schematically illustrated in Figure 1.3.10, the water filled channels in sulfonated PEEKK are narrower compared to those in Nafion. They are less separated and more branched with more dead-end “pockets”. These features correspond to the larger hydrophilic/ hydrophobic interface and, therefore, also to a larger average separation of neighbouring sulfonic acid functional groups. The stronger confinement of the water in the narrow channels of the aromatic polymers leads to a significantly lower dielectric constant of the water of hydration.

The nature of the crystalline component in Nafion has received much less attention than that of the ionic domains, and thus, the relevance of this morphological feature to the technologically important properties of the membranes is still unclear. Since the initial studies of Nafion morphology, the crystalline component has been recognized as an important structural feature and often considered as a necessary component that provides mechanical integrity and a barrier to solvent swelling. With respect to current models, however, the crystallites may be considered to exist within elongated polymeric aggregates or as critical structures that impose the organization of the ionic domains. In the rodlike models, the crystallites may play a minor role to that of entanglements in affecting the mechanical behavior of the swollen membranes. On

the other hand, the lamellar model suggests that the crystallites are the principal factor in limiting ionic domain swelling³⁴.

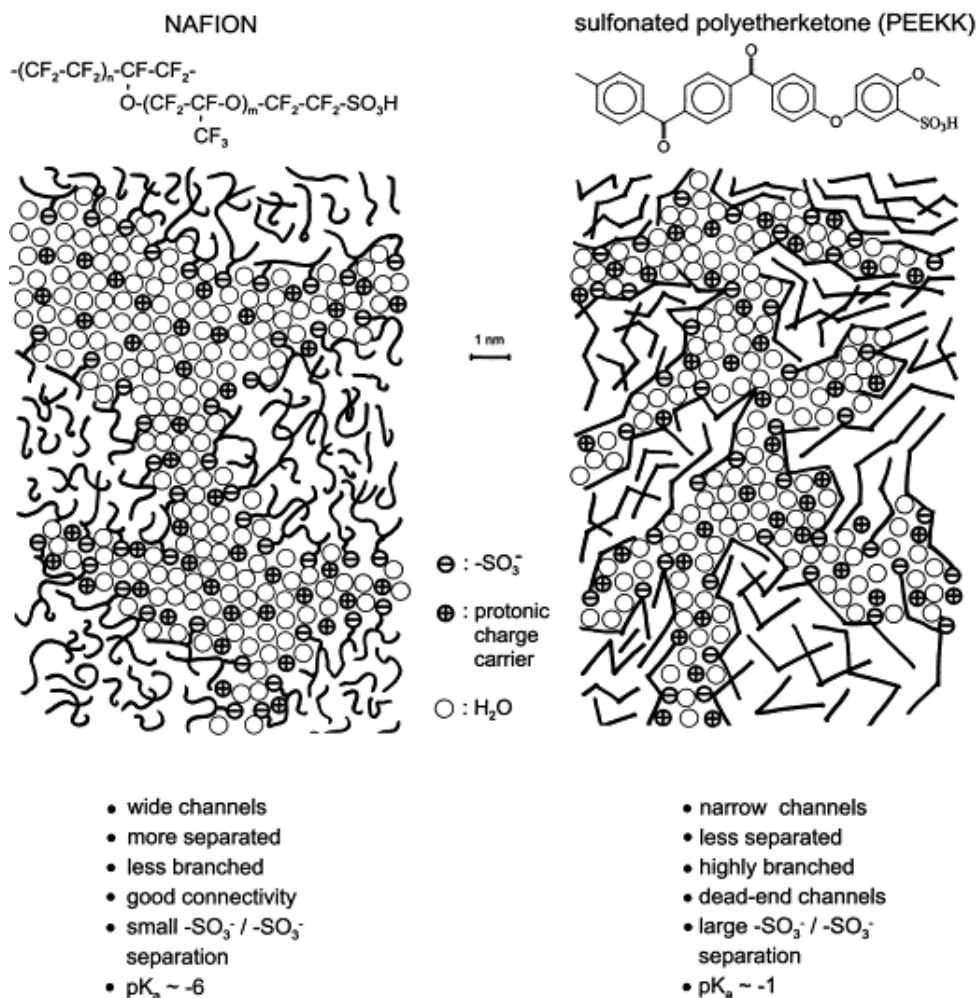


Figure 1.3.10: Schematic representation of the microstructures of Nafion and a sulfonated polyetherketone.²⁸

1.4 Proton Conduction Mechanisms in PEM

In metals, proton transfer generally occurs between the interstitial octahedral or tetrahedral sites, resulting in long-range proton transport, i.e. diffusion. However, in non-metallic environments, the proton mobility requires not only proton transfer reactions within the hydrogen bonds but also structural reorganization, as illustrated schematically in Figure 1.4.1.

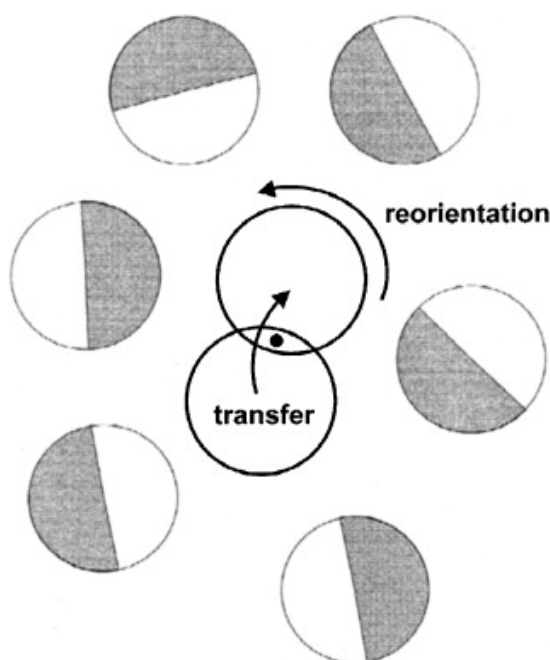


Figure 1.4.1: Schematic diagram of the two reaction steps in long range proton transport.⁴³

Proton transport mechanism through a PEM is basically conduction through water. The dominant intermolecular interaction in water is hydrogen bonding. The introduction of an extra proton leads to proton defects, resulting in a contraction of hydrogen bond in the vicinity of such defects. The binding power of a water molecule depends on the number of hydrogen bonds involve in it. This also leads to relaxation effects in the neighboring hydrogen bonds as a response to the formation and cleavage of hydrogen bonds. When a hydrogen bond is formed, the surrounding bonds are weakened but the cleavage of hydrogen bonds strengthens the neighboring bonds⁴³⁻⁴⁵. Therefore, defects caused by the incorporation of excess protons weaken the

intermolecular interaction by means of breakage and reformation of bonds in combination with large variations in bond length^{43, 46-48}.

Excess protons can be a part of a dimer (H_5O_2^+ , ‘Zundel’ ion) or a part of a hydrated hydronium ion (H_9O_4^+ , ‘Eigen’ ion). The central bond of H_5O_2^+ (≈ 250 pm) is noticeably contracted compared to the average hydrogen bond length in bulk water (≈ 280 pm) but elongated compared to an isolated dimer (≈ 240 pm). Figure 1.4.2 shows the formation of an ‘Eigen’ ion from a Zundel’ ion and the change in protonic charge from one ion to another. In a proton exchange membrane, the hydrated environment, often acidic, acts as a solvent for the diffusion of hydronium and dimer ions formed⁴⁹.

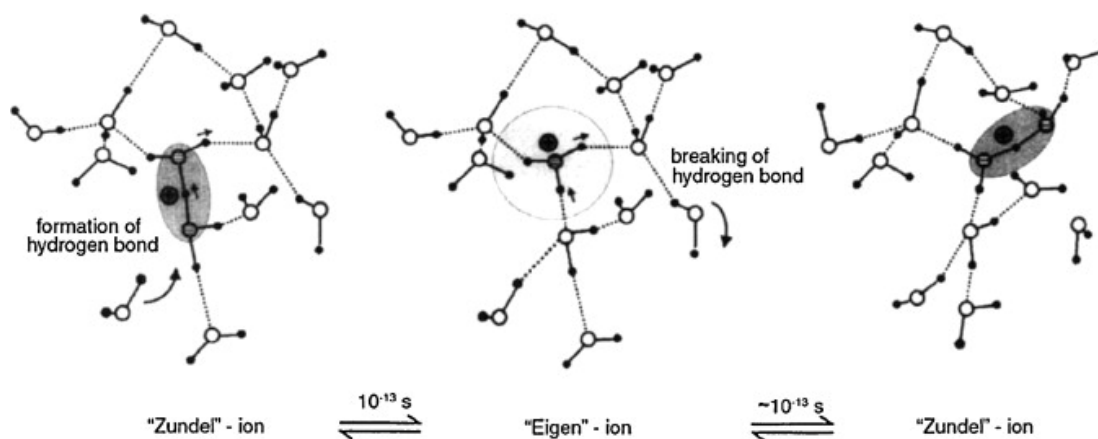


Figure 1.4.2: Transport mechanism of Protonic defects in water.⁴⁶

Proton conduction is fundamental for proton exchange membrane fuel cells and is usually the first characteristic considered when evaluating membranes for potential fuel cell use. High conductivity is essential for the required performance especially at high current density. At a molecular level, the proton transport in hydrated polymeric matrices is in general described on the basis of either of the two principal mechanisms: “proton hopping” or “Grotthus mechanism” and “diffusion mechanism” which water is as vehicle or “vehicular mechanism”⁵⁰⁻⁵². In proton hopping mechanism protons hop from one hydrolyzed ionic site ($\text{SO}_3^- \text{H}_3\text{O}^+$) to another across the membrane. The produced proton by oxidation of hydrogen in anode adheres to water molecule than the provisional hydronium ion is formed and one different proton from same hydronium

ion hops on the other water molecule. In this mechanism, ionic clusters were swelled in presence of water and formed the percolation mechanism for proton transferring. The simple scheme of the hopping mechanism has been shown in Figure 1.4.3. The hopping mechanism has little contribution to conductivity of perfluorinated sulfonic acid membranes such as Nafion¹².

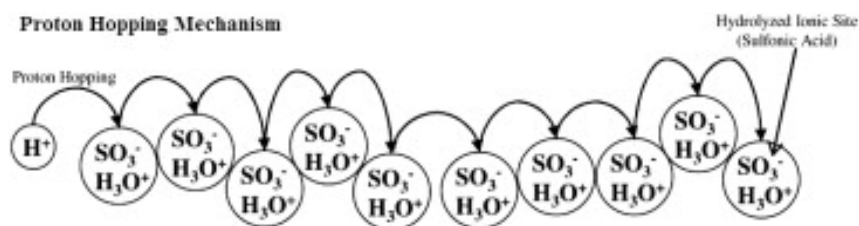


Figure 1.4.3: Scheme of the hopping mechanism.⁵³

The second mechanism is a vehicular mechanism. In this mechanism hydrated proton (H_3O^+) diffuses through the aqueous medium in response to the electrochemical difference. In vehicular mechanism, the water connected protons ($H^+(H_2O)_x$) in the result of the electroosmotic drag carry the one or more molecules of water through the membrane and itself are transferred with them. The major function of the formation of the vehicular mechanism is the existence of the free volumes within polymeric chains in proton exchange membrane which allow the transferring of the hydrated protons through the membrane. The schematic design of the vehicular mechanism in proton conduction in pristine and nanocomposite membranes has been shown in the Figure 1.4.4. Water also has two suggested transport mechanisms: electroosmotic drag and concentration gradient driven diffusion (this probably occurs as self associated clusters: $(H_2O)_y$). The hydrophobic nature of Teflon backbone facilitates the water transfer through the membrane because the surfaces of the hydrophobic holes tend to repel the water molecules⁵³.

The prevalence of one or the other mechanism depends on the hydration level of the membrane. On the other hand, the mechanism of proton transport within nanocomposite and hybrid systems based on the aforementioned membranes is a much more complex process as it involves both the surface and chemical properties of the inorganic and organic phases. Although the exact role of inorganic components in

stabilizing the proton transport properties of nanocomposites based on Nafion and other polymers is still under discussion, it may be presumed that the primary function of the nanoparticles is to stabilize the polymer morphology with increasing temperature. If the inorganic additive happens to be an alternative proton transporter like heteropolyacids, their contribution to the transport processes has also to be analyzed. Proton conductivity improvements would, however, depend upon whether the fraction of bulk water and the bulk proton concentrations are increased as a result of the inorganic additives or not¹².

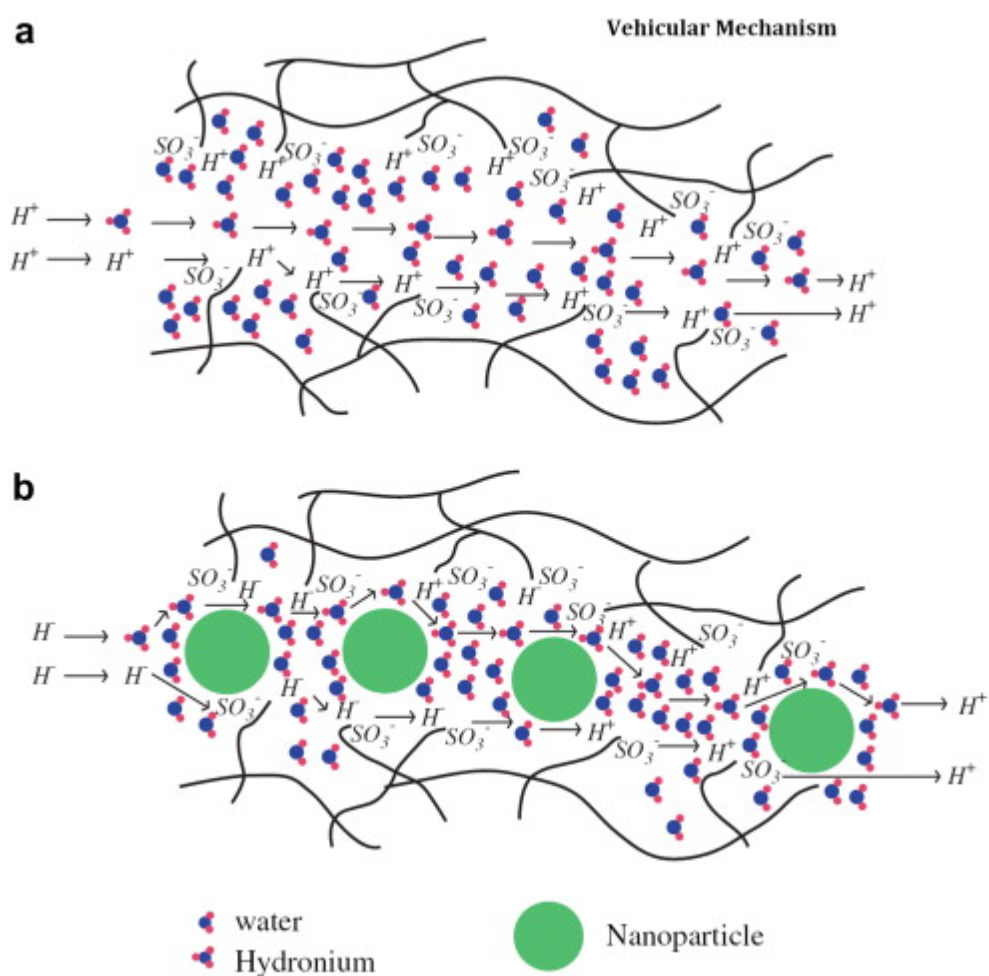


Figure 1.4.4: Schematic design of the Vehicular Mechanism as proton conduction in (a) pristine membranes and (b) polymer/ nano-particle composite membranes.¹²

1.5 High Temperature PEM fuel cells (HT-PEMFCs)

Polymer electrolyte fuel cells based upon PFSA membranes have typically been operated in a temperature range between approximately 50 and 90 °C. This temperature range is a compromise between competing factors. Increasing the operating temperature above room temperature will improve the electrode kinetics of the oxygen reduction reaction. The upper limit of temperature results from the difficulty in maintaining membrane water content at temperatures at or above 100 °C. In addition, temperatures above the polymer glass transition temperature (~110 °C for protonated Nafion) can cause polymer chain rearrangements, which can lead to structural changes in the membrane and lower the membrane stability, performance, and lifetime.

In recent years, increasing interest has been devoted to the development of *high temperature proton conducting polymer electrolyte fuel cell systems*. In fact, most of the *key issues and* shortcomings of the PFSA-based PEMFC technology, such as water management, CO poisoning, cooling and heat recovery, can be solved or avoided by developing alternative membranes with suitable ionic conductivity and stability up to 120-130 °C.

The US Department of Energy (DOE) has a major effort to develop new membranes which can operate under drier conditions and at temperatures up to 120 °C⁵⁴. Polymer membranes able to operate above 120 °C could benefit from both enhanced carbon monoxide (CO) tolerance and improved heat removal²¹. Higher temperature operation includes the following:

- (i) The kinetics for both electrode reactions will be enhanced.
- (ii) Above the boiling point of water, operation of PEMFCs involves only a single phase of water, i.e., the water vapor, and therefore can be simplified.
- (iii) The heat can be recovered as, e.g., steam, which in turn can be used either for direct heating or steam reforming or for pressurized operation. In this way the overall system efficiency will be significantly increased.
- (iv) The operational temperature of a fuel cell around 200 °C is close to temperatures for methanol reforming and for hydrogen desorption of the newly developed high capacity storage materials. This will allow for an

integration of the fuel cell with a methanol reformer or a high-capacity hydrogen storage tank.

- (v) The CO tolerance will be dramatically enhanced

The carbon monoxide concentration CO in the H₂ feed gas affects the performance of a membrane at low temperatures. If the concentration of CO is excessive (~10 ppm), it will strongly adsorb to the platinum (Pt) surface and poison the platinum electro-catalyst⁵⁵⁻⁵⁸ (Figure 1.5.1).

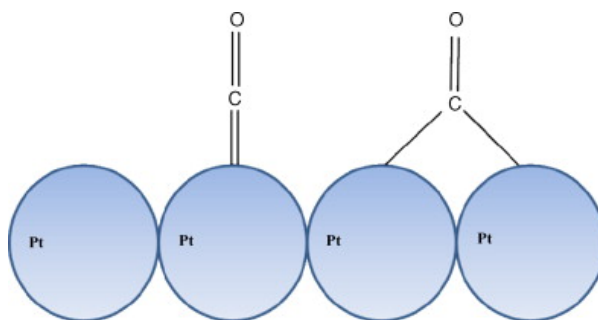


Figure 1.5.1: Adsorption of CO on Pt.⁴⁹

Indeed, the adsorption of CO on Pt is associated with high negative entropy, implying that adsorption is favored at low temperatures, and disfavored at high temperatures⁵⁹. The CO tolerance will be dramatically enhanced, from 10-20 ppm of CO at 80 °C, to 1000 ppm at 130 °C, and up to 30000 ppm at 200 °C²¹.

However, there are also some technical obstacles during high temperature treatment of polymer electrolyte membranes. Polymer membranes are incapable of operating at high temperatures because water from the membrane evaporates out resulting in a loss of proton conductivity⁶⁰. High proton conductivity is essential for achieving a high power density in fuel cells. Dehydration of the membrane at high temperatures may lead to decrease the proton conductivity value and in the process performance of polymeric membranes gets hampered. Water is very essential for the proton conductivity because it promotes the dissociation of protons from the sulfonic acid groups, and provides highly mobile hydrated protons. Hence, hydration is the key factor for maintaining the optimal performance of the membranes. The conductivity of a dry membrane is several orders of magnitude lower than a fully saturated membrane. To keep the membrane hydrated, one or both reactant gas streams must be humidified⁴⁹. However, too much

humidification causes flooding of the electrodes and consequently, the diffusion overpotential increases due to insufficient oxygen and hydrogen supply. In order to reduce these overpotentials, properties such as stable water uptake and high proton conductivity are essential for the electrolyte.

A number of alternative strategies⁶¹⁻⁶⁴ have been proposed to satisfy these requirements and to maintain membrane conductivity in a dehydrating environment (i.e. elevated temperature and reduced relative humidity), such as composite membranes containing finely dispersed fillers in the ionomer matrix. The following section is dealing with these composite membranes, the influence of these particles on membrane properties, such as conductivity and permeability to methanol, is also discussed.

1.5.1 Composite Membranes

As is mentioned in the previous paragraph, the main obstacles to greater commercialization of polymer electrolyte fuel cells are mostly related to the low-proton conductivity at low relative humidity, to the high methanol cross over, and their poor mechanical properties above 100 °C.⁵ Therefore, several approaches have been adopted to modify the polymeric membrane in order to maintain the proton conductivity as well as the performance of the membrane at high temperatures, and can be used in fuel cell applications. An approach is the development of composite membranes, where particles of organic/inorganic fillers homogeneously dispersed in the ionomer matrix. Modified Nafion membranes containing hygroscopic inorganic fillers such as, titania nanotubes⁶⁵ and particles^{66, 67}, SiO₂⁶⁸⁻⁷¹, ZrO₂⁷², Fe₂O₃⁷³, and other compounds characterized by water retention capacity or by proton conduction as hetero-poly-acids (PWA, PMoA, SiWA) or layered zirconium phosphate^{5, 74-77} are valid materials to use as polymer electrolytes in PEMFC. For Nafion ionomer bearing – SO₃H groups, the filling with ZrP, silica, or heteropolyacid nano-particles has a positive effect on fuel cell performance at temperatures higher than 90 – 100 °C, even for relative humidity considerably lower than 100%. This effect can be connected to the notion that these hydrophilic particles replace the loosely bonded water within the hydrophilic Nafion domains⁵. As hydrophilic additives, the presence of these inorganic compounds

decreases the chemical potential of the water inside the membrane and therefore creates an additional pathway for the proton conduction. At the same time, they provide hydrogen-bonding sites for water in the membrane so that the hydration of the membrane will be increased and the transport and evaporation of water will be reduced¹. The water interacting with the surface of the filler is more likely to be retained than loosely bonded water in unmodified Nafion, but still mobile enough to allow fast proton transport. Additionally, the inclusion of inorganic fillers improves the mechanical properties and the membrane water management. The mechanical reinforcement of the membrane, and hence the reduction of the swelling properties play an important role, especially in the temperature range 90 - 110°C, where high humidification conditions can be still obtained at acceptable pressures of the cell. Moreover the properties of these composite membranes not only depend on the ionomer and the solid used but also on the amount, homogeneous dispersion, size, and orientation of the solid particles dispersed in the polymeric matrix. Layered compound can be inserted (i) as powdered particles, (ii) as exfoliated lamellae, (iii) by in situ formation in the ionomer solutions and (iv) by in situ precipitation in membranes of the pure ionomer. Based on the above composite membranes can be prepared according to two main procedures: (i) dispersion of filler particles in an ionomer solution followed by casting, and (ii) growth of the filler particles within a membrane or in an ionomer solution. In the first procedure the solids are first ground until a fine powder is obtained and then dispersed under strong stirring in an organic solution of the polymer. Finally the membrane is obtained by film casting and solvent elimination⁵. Because the composite membrane is obtained by casting an ionomer solution in organic solvents, colloidal dispersions of exfoliated layered materials must be formed in the ionomer solvent or in similar solvents. Depending on the degree of crystallinity of the starting material and on the conditions used in the deintercalation process, it is possible to obtain dispersions of lamellar particles with thickness ranging from ~10 to 100 nm and surface area from ~0.1 to 10 μm^2 .

Furthermore, for each type of the above composite membranes, the properties not only depend on the ionomer and the solid used but also on the particle content, particle size, homogeneous distribution and orientation of the exfoliated particles, and exfoliation degree. If the use of composite membranes is confined to direct methanol fuel cells it is

imperative to overcome the large methanol cross-over of pure ionomer membrane. In Figure 1.5.2 is schematically shown the effect of all the above properties to the performance of the nanocomposite membrane, in this images is shown the increase of the tortuous path encountered by a given diffusing species with increasing degree of exfoliation and/or lamellar particles⁵.

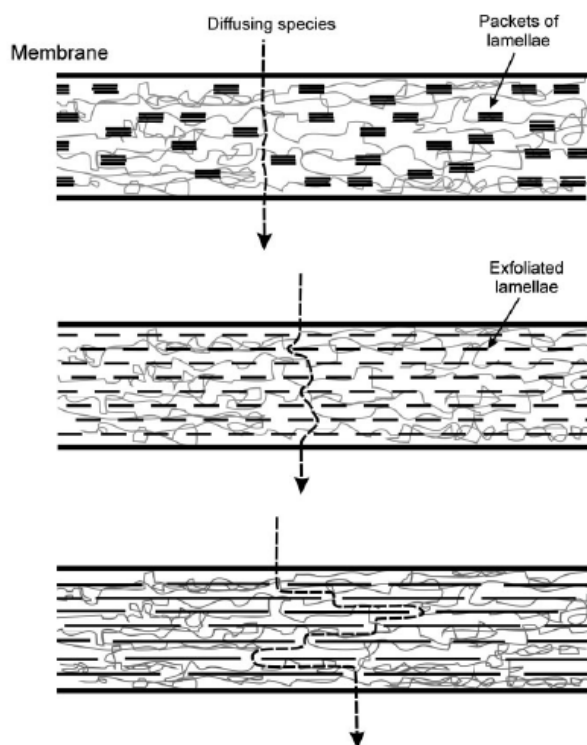


Figure 1.5.2: Schematic view of a hybrid ionomeric membrane containing oriented lamellae of ZrP.⁵

In this present Doctoral thesis, two dimensional (2D) materials, phyllosomorphous materials, such as, Clays, Graphite Oxide and Layered Double Hydroxides (LDHs), were studied as candidates fillers for the polymer electrolyte membranes in PEMFC. Composite membranes, were prepared according the first procedure, dispersing the filler particles in Nafion ionomer solution followed by casting. The study focused on the creation of novel nanocomposite membranes with high proton conductivity and enhanced water retention properties, even at high temperatures.

References

- 1 K. T. Adjemian, S. Srinivasan, J. Benziger, and A. B. Bocarsly, *Journal of Power Sources* **109**, 356 (2002).
- 2 A. S. Arico, P. Creti, P. L. Antonucci, and V. Antonucci, *Electrochem. Solid-State Lett.* **1**, 66 (1998).
- 3 K. T. Adjemian, S. J. Lee, S. Srinivasan, J. Benziger, and A. B. Bocarsly, *J Electrochem Soc* **149**, A256 (2002).
- 4 S. Suarez and S. Greenbaum, *The Chemical Record* **10**, 377 (2010).
- 5 G. Alberti and M. Casciola, *Annual Review of Materials Research* **33**, 129 (2003).
- 6 C. Liu, F. Li, L.-P. Ma, and H.-M. Cheng, *Advanced Materials* **22**, E28 (2010).
- 7 L. Schlapbach and A. Züttel, *Nature* **414**, 353 (2001).
- 8 M. Momirlan and T. N. Veziroglu, *International Journal of Hydrogen Energy* **30**, 795 (2005).
- 9 L. Schlapbach, *Nature* **460**, 809 (2009).
- 10 A. Boudghene Stambouli and E. Traversa, *Renewable and Sustainable Energy Reviews* **6**, 295 (2002).
- 11 A. Kirubakaran, S. Jain, and R. K. Nema, *Renewable and Sustainable Energy Reviews* **13**, 2430 (2009).
- 12 S. J. Peighambaroust, S. Rowshanzamir, and M. Amjadi, *International Journal of Hydrogen Energy* **35**, 9349 (2010).
- 13 J. M. Andújar and F. Segura, *Renewable and Sustainable Energy Reviews* **13**, 2309 (2009).
- 14 C. Brian, *IEEE Proc*, 205 (2002).
- 15 M. Farooque and H. Maru, *IEEE Proc* **89**, 1819 (2001).
- 16 W. G. Coors, *Journal of Power Sources* **118**, 150 (2003).
- 17 G. Apanel and E. Johnson, *Fuel Cells Bulletin* **2004**, 12 (2004).
- 18 V. Neburchilov, J. Martin, H. Wang, and J. Zhang, *Journal of Power Sources* **169**, 221 (2007).
- 19 R. Dillon, S. Srinivasan, A. S. Arico, and V. Antonucci, *Journal of Power Sources* **127**, 112 (2004).
- 20 J. Larminie and A. Dicks, *Fuel Cell Systems Explained* New York (2003).
- 21 Q. Li, R. He, J. O. Jensen, and N. J. Bjerrum, *Chemistry of Materials* **15**, 4896 (2003).
- 22 Q. Li, J. O. Jensen, R. F. Savinell, and N. J. Bjerrum, *Progress in Polymer Science* **34**, 449 (2009).
- 23 B. Smitha, S. Sridhar, and A. A. Khan, *Journal of Membrane Science* **259**, 10 (2005).
- 24 A. Ghielmi, P. Vaccarono, C. Troglia, and V. Arcella, *Journal of Power Sources* **145**, 108 (2005).
- 25 V. Arcella, C. Troglia, and A. Ghielmi, *Industrial & Engineering Chemistry Research* **44**, 7646 (2005).
- 26 A. S. Arico, V. Baglio, A. Di Blasi, V. Antonucci, L. Cirillo, A. Ghielmi, and V. Arcella, *Desalination* **199**, 271 (2006).
- 27 G. Gebel, P. Aldebert, and M. Pineri, *Macromolecules* **20**, 1425 (1987).
- 28 K. D. Kreuer, *Journal of Membrane Science* **185**, 29 (2001).
- 29 M. A. Hickner, H. Ghassemi, Y. S. Kim, B. R. Einsla, and J. E. McGrath, *Chemical Reviews* **104**, 4587 (2004).
- 30 T. Soczka-Guth, J. Baurmeister, G. Frank, and R. Knauf, *International Patent: WO99/29763* (1999).
- 31 V. R. Gowariker, N. V. Vishwanathan, and J. Sridhar, *Polymer science*. New Delhi: New Age International (1999).
- 32 D. J. Jones and J. Rozière, *Journal of Membrane Science* **185**, 41 (2001).
- 33 A. J. Appleby, *Fuel cell handbook*, 1988).
- 34 K. A. Mauritz and R. B. Moore, *Chemical Reviews* **104**, 4535–4585 (2004).

- 35 D. E. Curtin, R. D. Lousenberg, T. J. Henry, P. C. Tangeman, and M. E. Tisack, *Journal of Power Sources* **131**, 41 (2004).
- 36 W. Y. Hsu and T. D. Gierke, *Journal of Membrane Science* **13**, 307 (1983).
- 37 T. D. Gierke, G. E. Munn, and F. C. Wilson, *Journal of polymer science. Part A-2, Polymer physics* **19**, 1687 (1981).
- 38 H. L. Yeager and A. Steck, *Journal of the Electrochemical Society* **128**, 1880 (1981).
- 39 G. Gebel, *Polymer* **41**, 5829 (2000).
- 40 M. H. Litt, *Polymer Preprints* **38**, 80 (1997).
- 41 H. G. Haubold, T. Vad, H. Jungbluth, and P. Hiller, *Electrochimica Acta* **46**, 1559 (2001).
- 42 L. Rubatat, A. L. Rollet, G. Gebel, and O. Diat, *Macromolecules* **35**, 4050 (2002).
- 43 K. D. Kreuer, *Solid State Ionics* **136–137**, 149 (2000).
- 44 K.-D. Kreuer, *Chemistry of Materials* **8**, 610 (1996).
- 45 N. Agmon, *Chemical Physics Letters* **244**, 456 (1995).
- 46 W. H. J. Hogarth, J. C. Diniz da Costa, and G. Q. Lu, *Journal of Power Sources* **142**, 223 (2005).
- 47 M. E. Tuckerman, D. Marx, and M. Parrinello, *Nature* **417**, 925 (2002).
- 48 M. E. Tuckerman, D. Marx, M. L. Klein, and M. Parrinello, *Science* **275**, 817 (1997).
- 49 S. Bose, T. Kuila, T. X. H. Nguyen, N. H. Kim, K.-t. Lau, and J. H. Lee, *Progress in Polymer Science* **36**, 813 (2011).
- 50 A. Z. Weber, J. B. R. Breslau, and I. F. Miller, *Engineering Chemistry Fundamentals* **10**, 554 (1971).
- 51 C. J. T. D. Grotthuss, *Ann Chim (Paris)* **58**, 54 (1806).
- 52 K.-D. Kreuer, S. J. Paddison, E. Spohr, and M. Schuster, *ChemInform* **35**, no (2004).
- 53 N. W. DeLuca and Y. A. Elabd, *Journal of Polymer Science Part B: Polymer Physics* **44**, 2201 (2006).
- 54 J. Marcinkoski, J. P. Kopasz, and T. G. Benjamin, *International Journal of Hydrogen Energy* **33**, 3894 (2008).
- 55 F. Barbir and T. Gómez, *International Journal of Hydrogen Energy* **21**, 891 (1996).
- 56 L. J. Pettersson and R. Westerholm, *International Journal of Hydrogen Energy* **26**, 243 (2001).
- 57 K. Kwon, D. Y. Yoo, and J. O. Park, *Journal of Power Sources* **185**, 202 (2008).
- 58 P. Krishnan, J.-S. Park, and C.-S. Kim, *Journal of Power Sources* **159**, 817 (2006).
- 59 J. J. Baschuk and X. Li, *International Journal of Energy Research* **25**, 695 (2001).
- 60 Y. Sone, P. Ekdunge, and D. Simonsson, *Journal of the Electrochemical Society* **143**, 1254 (1996).
- 61 G. Alberti and M. Casciola, *Annual Review of Materials Research* **33**, 129 (2003).
- 62 B. C. H. Steele and A. Heinzl, *Nature* **414**, 345 (2001).
- 63 M. L. Perry and T. F. Fuller, *J Electrochem Soc* **149**, S59 (2002).
- 64 C. Yang, P. Costamagna, S. Srinivasan, J. Benziger, and A. B. Bocarsly, *Power Sources* **103(1)**, 1 (2001).
- 65 Y. Jun, H. Zarrin, M. Fowler, and Z. Chen, *International Journal of Hydrogen Energy* **36**, 6073 (2011).
- 66 M. Amjadi, S. Rowshanzamir, S. J. Peighambaroust, M. G. Hosseini, and M. H. Eikani, *International Journal of Hydrogen Energy* **35**, 9252 (2010).
- 67 T. Jian-hua, G. Peng-fei, Z. Zhi-yuan, L. Wen-hui, and S. Zhong-qiang, *International Journal of Hydrogen Energy* **33**, 5686 (2008).
- 68 C.-C. Ke, X.-J. Li, Q. Shen, S.-G. Qu, Z.-G. Shao, and B.-L. Yi, *International Journal of Hydrogen Energy* **36**, 3606 (2010).
- 69 I. Nicotera, A. Khalfan, G. Goenaga, T. Zhang, A. Bocarsly, and S. Greenbaum, *Ionics* **14**, 243 (2008).
- 70 V. Baglio, A. S. Aricò, V. Antonucci, I. Nicotera, C. Oliviero, L. Coppola, and P. L. Antonucci, *Journal of Power Sources* **163** 52 (2006).

- ⁷¹ A. S. Arico, V. Baglio, V. Antonucci, I. Nicotera, C. Oliviero, L. Coppola, and P. L. Antonucci, *Journal of Membrane Science* **270**, 221 (2006).
- ⁷² J. Pan, H. Zhang, W. Chen, and M. Pan, *International Journal of Hydrogen Energy* **35**, 2796 (2010).
- ⁷³ L. Sun, S. Wang, W. Jin, H. Hou, L. Jiang, and G. Sun, *International Journal of Hydrogen Energy* **35**, 12461 (2010).
- ⁷⁴ I. Nicotera, T. Zhang, A. Bocarsly, and S. Greenbaum, *Journal of Electrochemical Society* **154**, B466 (2007).
- ⁷⁵ I. Nicotera, L. Coppola, C. O. Rossi, M. Youssry, and G. A. Ranieri, *J Phys Chem B* **113**, 13935 (2009).
- ⁷⁶ G. Alberti, M. Casciola, D. Capitani, A. Donnadio, R. Narducci, M. Pica, and M. Sganappa, *Electrochimica Acta* **52**, 8125 (2007).
- ⁷⁷ D. Jones and J. Rozière, in *Fuel Cells I*, edited by G. Scherer (Springer Berlin Heidelberg, 2008), Vol. 215, p. 219.

2. Materials: Nanostructured Fillers

In this doctoral work, two-dimensional materials, more specifically layered materials, such as Clays, Graphite Oxide and Layered Double Hydroxides (LDHs), were studied as candidates fillers for the creation of novel hybrid nanocomposites membranes for PEMFC applications.

2.1 Clays

Smectite clays^{1, 2} are a class of layered aluminosilicate minerals with a unique combination of swelling, intercalation, and ion exchange properties. The word smectite is derived from the Greek word smectos, σμήγμα, which means soap. They consist of an octahedral alumina layer fused between two tetrahedral silica layers (about 1nm)^{3, 4}. The individual layers are composed of two, three or four sheets. The sheets are formed either by tetrahedrons [SiO₄]⁴⁻, abbreviated as “T”, or by octahedrons, e.g. [AlO₃(OH)₃]⁶⁻, abbreviated as “O”. Smectite clays having two tetrahedral sheets around the central octahedral sheet in each layer (Figure 2.1.1) are known as 2:1 phyllosilicates (T-O-T type). On the other hand, exist also clays with one tetrahedral and one octahedral sheet in each layer, T-O type (1:1 phyllosilicate), as well as the type 2:2 or 2:1:1. The interior of tetrahedrons and octahedrons contains smaller metal cations, their apices being occupied by oxygen from which some are connected with protons (as OH). All these fundamental structural elements are arranged to form a hexagonal network in each sheet. Such clays have a cation exchange capacity, which depends on the substitution of low valent atoms, e.g., Mg²⁺ for Al³⁺ in the octahedral sheet and Al³⁺ for Si⁴⁺ in the tetrahedral sites. As a consequence, the 1nm thick aluminosilicate platelets have a fixed negative charge and neutrality is obtained, for example, by hydrated cations present in the galleries.

The electrically neutral sheets are bonded together by relatively weak dipolar and van der Waals forces.

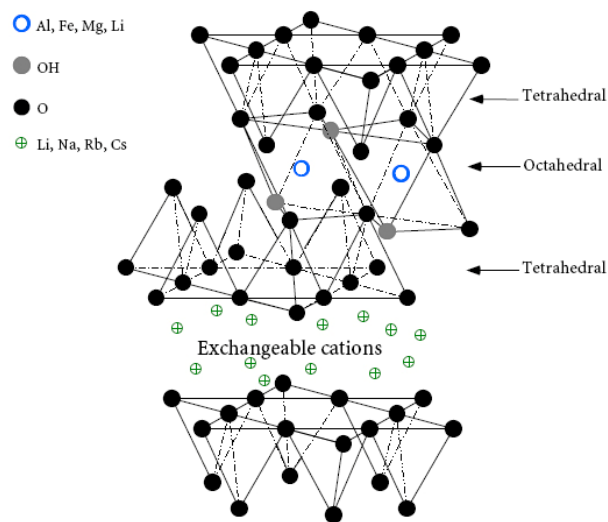


Figure 2.1.1: Clay structure 2:1.⁵

The monovalent ions located between the clay layers allow the absorption of polar solvent, like water (figure 2.12), with good retention capacity so, when incorporated into a polymer membrane, they help to prevent the loss of the hydration water not only at high temperatures but also under low relative humidity environment.

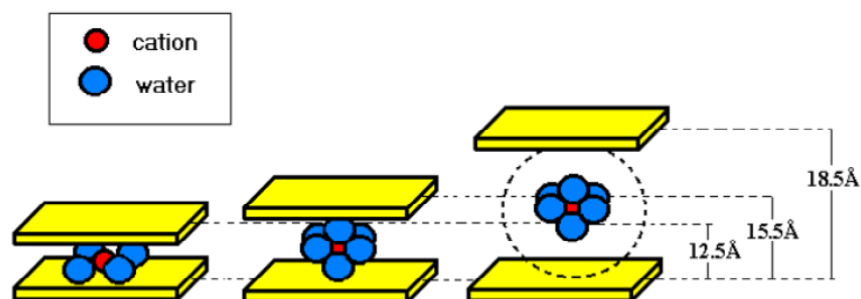


Figure 2.1.2: Schematic representation of the swelling of one clay layer.

The intercalation process in these systems is equivalent to ion exchange, and unlike the intercalation compounds of graphite, it does not involve necessarily charge transfer between the guest and host species⁶. The charge on the layers affects many fundamental properties of the clays, including water holding (an important property for the creation of Nafion nanocomposite membrane), cation fixation, swelling ability, cation exchange capacity and high specific surface area. However the reversibility of the swelling limits the application of clays. Thus, heating the clays at high temperatures

causes removal of intercalated water and leads to precipitation of the sheets, reducing the interlayer space. To prevent the collapse of the interlayer space, bulky cations were developed, which act as pillars and their role is to keep the aluminosilicate sheets apart. During the preparation process of the pillared clays, occurs a cationic exchange reaction of countervailing cations and intrerecalation of the pillar. By calcination of the intercalates, the complexes inserted in the clay interlayer space transform into metal oxide pillars, which support the silicate sheets and keep them apart even at elevated temperatures (up to about 600 °C)⁷. In the figure 2.1.3 is presented the intercalation process of the pillared clays.

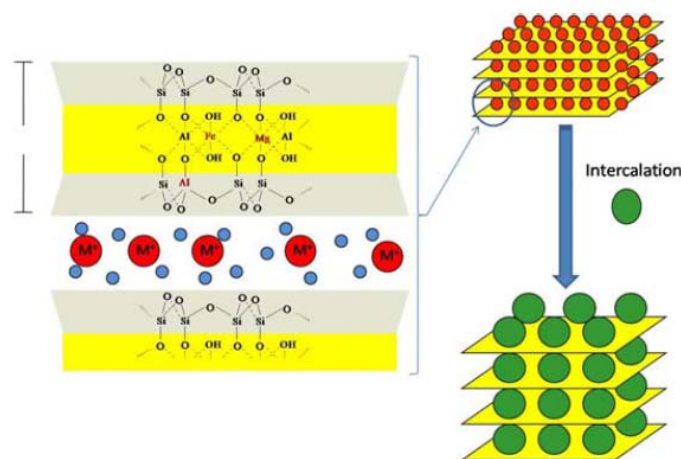
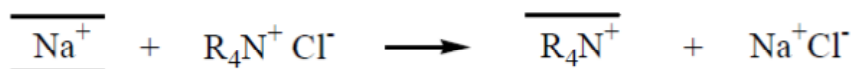


Figure 2.1.3: Schematic illustration of intercalation process.

Easily hydratable cations in the interlayer space of smectites adsorb water. The built cationic hydration coating takes away the three-sheet layers, so that the swelling takes place. Over the last decade a novel class of microporous materials has emerged from the intercalation of swelling clays, i.e. smectites, with oligo- or polymeric cationic complexes of metals⁷. In the principal category of the pillars belong the organic molecules (mainly alkylammoniums $^+\text{NH}_3\text{C}_n\text{H}_{2n+1}$). The intercalation of the alkylammoniums results to organo-clay complexes with organic derivatives. The chemical modification takes part by the cation exchange reaction of the countervailing cations (e.g. Na^+) with positively charged of tetralkylammoniums molecules in aqueous solution:



The positively charged amino group attaches on the negative positions to the clay layer repelling the interlayer water molecules. Depending on the charge density of clay and the cationic surfactant, different arrangements of the organic molecules are possible. In general, the longer the surfactant chain length, and the higher the charge density of the clay, the further apart the clay layers will be forced. This is expected since both of these parameters contribute to increasing the volume occupied by the intergallery surfactant. Depending on the charge density of the clay, the organic surfactants may lie parallel to the clay surface as a monolayer, a lateral bilayer, or an inclined paraffin structure⁸ as illustrated in Fig.2.1.4.

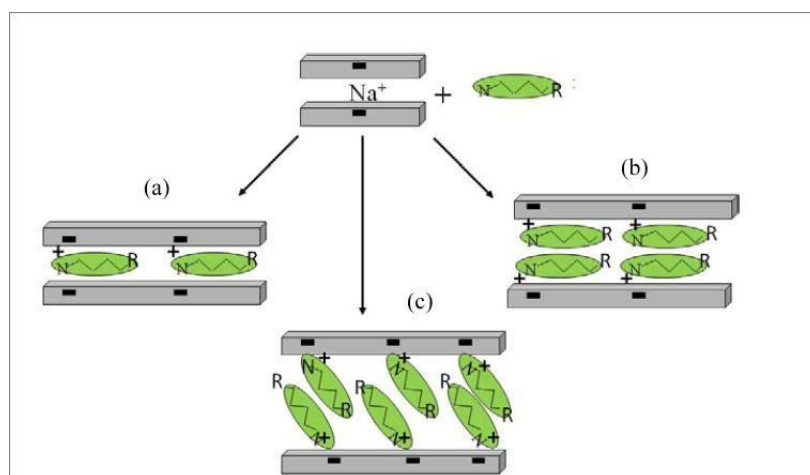


Figure 2.1.4: Orientations of tetralkylammonium ions in the galleries of layered silicates: (a) formation of a monolayer, (b) bilayer, (c) inclined paraffin structure.

Moreover, the properties of the smectite nanoclays can be tailored using simple chemical methods such as intercalation with organic or inorganic guest molecules. Their surface properties, for example, can be easily modified through treatment with an organic surfactant. As a result the presence of the surfactant expands the interlayer gallery rendering the nanoclay compatible with hydrophobic media and polymer matrices. Due to their distinctive structure and properties, these organic–inorganic hybrid materials (so-called “organo-clays”) can be utilized in a wide variety of applications including, construction of modified electrodes, biosensors or biocatalysts,⁹⁻¹¹ adsorbents for environmental remediation (e.g. removal of heavy metal ions for water¹²) but also as nanofillers for polymer reinforcement.¹³⁻¹⁵ Thus a strategy towards the improvement of the water retention of the Nafion membrane is the incorporation in the polymer matrix hybrid nanofillers of modified clays bearing organic functionalities with high affinity for Nafion and increased sites for water trapping.

2.2 Graphene – Graphite Oxide

In the second class of 2D nanofillers, belongs the Graphene extensively studied by Novoselov and Geim on 2004 (Nobel prize in Physics 2010)¹⁶. This material has a number of unique properties, which makes it interesting for both fundamental studies and future applications. Graphene is the name given to a flat monolayer of carbon atoms, tightly packed into a two-dimensional (2D) honeycomb lattice. Carbon is arguably the most fascinating element in the periodic table. It is the base of DNA and all life on the earth. Carbon can exist in several forms, the most common form of carbon is graphite, which consists of several of stacked sheets of carbon with hexagonal structure. Under high pressure diamond is formed, which is metastable form of carbon. A new form of molecular carbon are the so called fullerenes¹⁷. The most common called C₆₀, contains 60 carbon atoms and looks like a football (soccer ball) made up from 20 hexagons and 12 pentagons which allow the surface to form a sphere. The discovery of fullerenes was awarded the Nobel prize in Chemistry in 1996. A related quasi-one-dimensional form of carbon, carbon nanotubes, have been known for several decades¹⁸ and the simple walled nanotubes since 1993¹⁹⁻²¹. These can be formed from graphene sheets which are rolled up to form tubes, and their ends are half spherical in the same way as fullerenes (Figure 2.2.1). Using electron microscopy it has been observed that within graphene monolayers small ripples exist. It is speculated that these imperfections on the surface of graphene are what help to keep it from rolling into nanotubes or other carbonic structures¹⁶. The electronic and mechanical properties of metallic singled walled nanotubes have many similarities with graphene. However graphene like structures were already known of 1960's but there were experimental difficulties in isolating single layers²¹⁻²³, and there were doubts that this was practically possible. Just in 2004, Konstantin Novoselov, Andre Geim and their collaborators¹⁶, showed that such a single sheet of carbon could be isolated and that it was stable. The single layer of carbon is what we call graphene. It is interesting to consider that everyone who has used an ordinary pencil has probably produced graphene-like structures. A pencil contains graphite, and when it moved on a piece of paper, the graphite is cleaved into thin layers and end up on the paper, a small fraction of these thin layers will contain only few layers or even a single layer of graphite, *i.e.* graphene. Thus the difficulty was not to fabricate the graphene structures, but to isolate

successively large individual sheets in order to identify and characterize the graphene and to verify its unique two-dimensional (2D) properties. This is what Geim, Novoselov, and their collaborators succeeded in doing¹⁶.

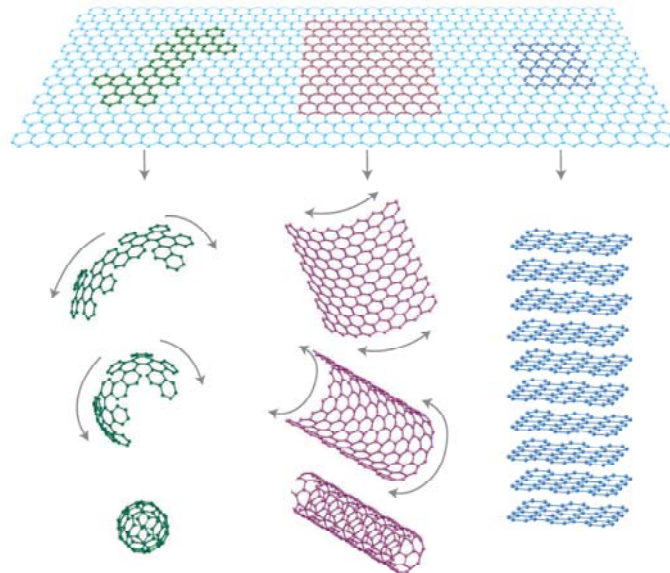


Figure 2.2.1: Representation of all graphitic forms. C60 fullerene molecules, carbon nanotubes, and graphite.²⁴

Graphene is a transparent single layer of carbon atoms arranged in hexagonal “honeycomb” fashion (figure 2.2.2). This structure creates an immensely strong two dimensional material, so strong (breaking strength of 42 N/m) that it is two hundred times the strength of steel. Making graphene the strongest material ever tested. Graphene shows a simultaneously high elasticity, high electrical and thermal conductivity (ten times higher thermal conductivity than copper). In addition the electronic properties of this 2D-material leads to, for instance, an unusual Hall effect²⁵,

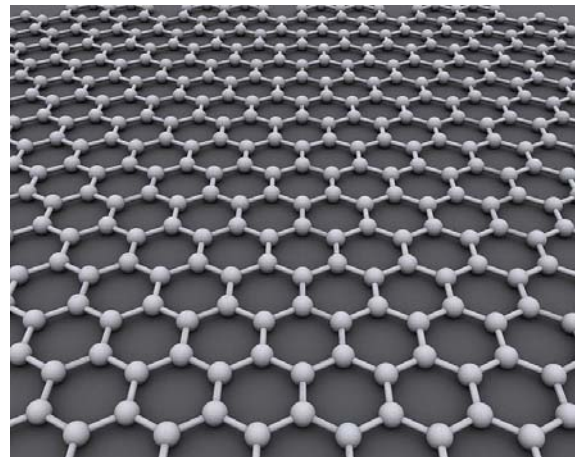


Figure 2.2.2: Schematic representation of Graphene (atomic-scale honeycomb lattice made of carbon atoms).

New types of composite materials based on graphene with great strength and low weight could also become interesting for use in satellites and aircrafts²⁷. Moreover the development of a nano-dispersion of graphene-based materials in a polymer matrix has opened a new and interesting area in materials science in the recent years^{28, 29}. The pristine graphite is inaccessible in the interlayer space and has a tendency to agglomerate in a polymer matrix³⁰ reducing the use of this material. In order to avoid this problem, the functionalization of graphite by chemical oxidation, creating a hydrophilic graphite derivative with covalently attached oxygen-containing groups (hydroxyl, epoxy and carboxyl) to its layers called **graphite or graphene oxide (GO)**³¹, is a particularly attractive solution since it can improve the solubility and processability as well as enhance the interactions with organic and inorganic guest molecules. GO has a history that extends back many decades to some of the earliest studies involving the chemistry of graphite^{32, 33}.

The first, well-known example came in 1859 when British chemist B. C. Brodie was exploring the structure of graphite by investigating the reactivity of flake graphite. One of the reactions he performed involved adding “potash of chlorate” (potassium chlorate; KClO_3) to a slurry of graphite in fuming nitric acid (HNO_3)³⁴. Brodie determined that the final material was composed of carbon, hydrogen, and oxygen, resulting in an increase in the overall mass of the flake graphite. Successive oxidative treatments resulted in a further increase in the oxygen content, reaching a limit after four reactions. The C:H:O composition was determined to be 61.04:1.85:37.11. Brodie found the material to be dispersible in pure or basic water, but not in acidic media, which prompted him to term the material “graphic acid”. Nearly 40 years after L. Staudenmaier improved Brodie’s KClO_3 -fuming HNO_3 preparation by adding the chlorate in multiple aliquots over the course of the reaction (also, with the addition of concentrated sulfuric acid, to increase the acidity of the mixture), rather than in a single addition as Brodie had done. This slight change in the procedure resulted in an overall extent of oxidation similar to Brodie’s multiple oxidation approach (C:O~2:1), but performed more practically in a single reaction vessel³⁵. Hummers and Offeman, 60 years after Staudenmaier, developed an alternate oxidation method by reacting graphite with a mixture of potassium permanganate (KMnO_4) and concentrated sulfuric acid (H_2SO_4), again, achieving similar levels of oxidation³⁶. The Brodie and Staudenmaier approaches both use KClO_3 and nitric acid (most commonly fuming [$>90\%$ purity])

and will be treated together. Nitric acid is a common oxidizing agent (e.g. aqua regia) and is known to react strongly with aromatic carbon surfaces, including carbon nanotubes^{37, 38}. The reaction results in the formation of various oxide-containing species including carboxyls, lactones, and ketones. Oxidations by HNO₃ result in the liberation of gaseous NO₂ and/or N₂O₄. Likewise, potassium chlorate, is a strong oxidizing agent, typically an in situ source of dioxygen, which acts as the reactive species. The Hummers method uses a combination of potassium permanganate and sulfuric acid. Though permanganate is a commonly used oxidant (e.g. dihydroxylations), the active species is, in fact, diamanganese heptoxide³⁹.

The most common source of graphite used for chemical reactions, including its oxidation, is flake graphite, which is naturally occurring mineral that is purified to remove heteroatomic contamination⁴⁰. As such, it contains numerous, localized defects in its π -structure that may serve as seed points for the oxidation process. Furthermore considerable effort has been directed toward understanding the structure of GO, much of it with great success. Many of the earliest structural models of GO proposed regular lattices composed of discrete repeat units. Hofmann and Holst's structure (Figure 2.2.3) consisted of epoxy groups spread across the basal planes of graphite, with a net molecular formula of C₂O⁴¹. Ruess proposed a variation of this model in 1946 which incorporated hydroxyl groups into the basal plane, accounting for the hydrogen content of GO⁴². Ruess's model also altered the basal plane structure to an sp³ hybridized system, rather than the sp² hybridized model of Hofmann and Holst. In 1969, Scholz and Boehm suggested a model that completely removed the epoxide and ether groups, substituting regular quinoidal species in a corrugated backbone.

Finally in the Foster's model, which is the predominant, the epoxy and C-OH functional groups lie above and below each carbon layer, while the -COOH groups are located near the layers' edges^{44, 45}. In conclusion Graphite oxide (GO) is a graphite derivative with covalently attached oxygen-containing groups to its layers. These groups are generated in the course of the GO synthesis by strong oxidation. GO exhibits lamellar structure with randomly distributed unoxidized aromatic regions (sp²-carbon atoms), six-membered aliphatic regions (sp³-carbon atoms) as a result of oxidation, and a high concentration of exposed oxygen-containing functional groups embedded in its carbon layers. Owing to the presence of such hydrophilic polar groups in the solid, GO is quite reminiscent of montmorillonites, which share common

swelling and intercalation properties. As a result, GO is an excellent host matrix for the interlayer accommodation of long chain aliphatic hydrocarbons⁴⁶, transition metal ions³¹, hydrophilic molecules⁴⁷ and polymers. Moreover is also promising for particle engineering processes, especially for the fabrication of thin films with smart properties³¹.

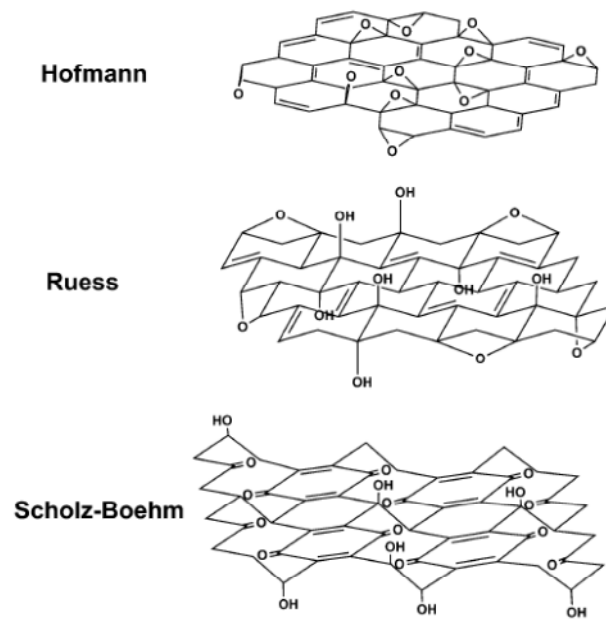


Figure 2.2.3: Structural models of GO⁴³.

2.3 Layered Double Hydroxide (LDH)

Layered double hydroxides (LDHs) belong to a class of nano-sized materials, of anionic clay family, with a unique combination of physicochemical properties that make them valuable nanostructures in diverse fields⁴⁸⁻⁵¹. The first natural material of this family was discovered in Sweden in 1842 (hydrotalcite with the formula $\text{Mg}_6\text{Al}_2(\text{OH})_{16}\text{CO}_3 \cdot 4\text{H}_2\text{O}$), while the first studies for the synthesis, the stability, the solubility and the structure of these materials started in 1930 from Freitknecht⁵². In contrary to the common clays, anionic clays are less known, although exist as naturally occurring minerals, while they are also relatively simple and economical to synthesize. The most interesting properties of LDHs include large surface area, high anion exchange capacity (2–3 meq/g) that is comparable to those of anion exchange resins, and good thermal stability⁵³⁻⁵⁵. The anionic clays structure is similar to brucite $\text{Mg}(\text{OH})_2$ structure shown in Figure 2.3.1, and crystallize in a layer-type lattice. A typical chemical structure of anionic (or hydrotalcite type) clay can be represented as $[\text{M}_{1-x}^{(\text{II})} \text{M}_x^{(\text{III})} (\text{OH})_2]^{x+} [\text{A}^{m-x/m}] \cdot n\text{H}_2\text{O}$, where $\text{M}^{(\text{II})}$ is a divalent metal cation (Mg, Mn, Fe, Co, Ni, Cu, Zn, Ga) and $\text{M}^{(\text{III})}$ is a trivalent metal cation (Al, Cr, Mn, Fe, Co, Ni, and La). A^{m-} represents an interlayer anion, such CO_3^{2-} , OH^- , NO_3^- , SO_4^{2-} or ClO_4^- . The basal spacing (c_0) is the total thickness of the brucite-like sheet and the interlayer region. The octahedral units of M^{2+} or M^{3+} (sixfold coordinated to OH^-) share edges to form infinite sheets (Figure 2.3.2). These sheets are stacked on top of each other and are held together by hydrogen bonding. Such LDHs have an anion exchange capacity, which depends on the isomorphic substitution of Mg^{2+} ions by higher valence cations. As a consequence, the layers have a fixed positive charge and neutrality is obtained, for example, by hydrated anions present in the galleries⁵⁶. The

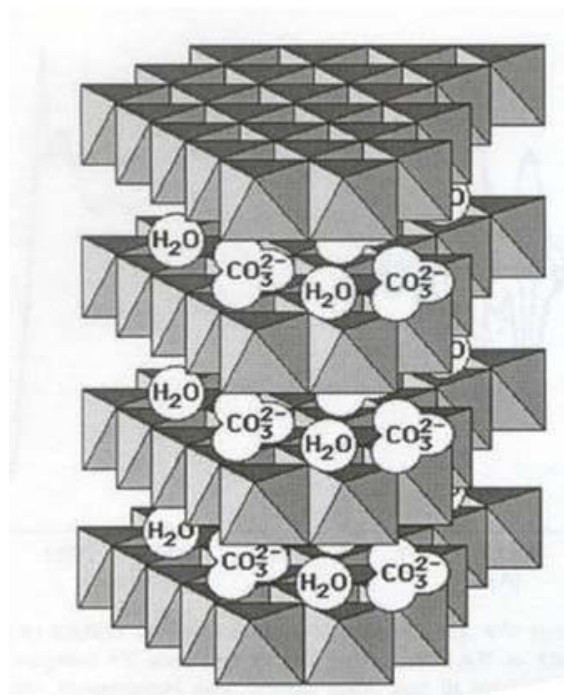


Figure 2.3.1: Schematic representation of the brucite $\text{Mg}(\text{OH})_2$.⁵⁹

positive charge of the layers affects many fundamental properties of the LDHs, including anion exchange capacity, anion fixation, swelling ability, water holding, and high specific surface areas. These materials have the natural ability to absorb organic or inorganic guest anionic species (and even neutral polar molecules) from solutions, and it is this anion “storage” that gives unique properties to LDHs, which can be used in a wide range of applications, such as in the field of catalysis photochemistry, electrochemistry, polymerization, magnetization, biomedical science, and environmental applications^{52, 54, 57, 58}

Moreover there is a great flexibility concerning the anions that can be hosted in the interlayer space of LDHs and counterbalance the positively charged layers. In the literature have reported many types of countervailing anions on LDH such as inorganic ions (Br^- , F^- , Cl^- , I^- , CO_3^{2-} , NO_3^- , OH^- , SO_4^{2-} , ClO_4^- , PO_3^- , PO_4^{3-} , HPO_4^{2-} , H_2PO_4^- , $\text{P}_2\text{O}_7^{2-}$), organic anions (carboxylates, dicarboxylates, alkyl sulfonates, organic dyes), polymeric anions (polyvinyl, polystyrene sulfonate, polyacrylate, polyaniline, polyethylene glycol), complex compounds (CoCl_4^{2-} , NiCl_4^{2-} , IrCl_6^{2-} , $\text{Fe}(\text{CN})_6^{4-}$, $\text{Fe}(\text{CN})_6^{3-}$, $\text{Mo}(\text{CN})_8^{4-}$, $\text{Mo}(\text{CN})_8^{3-}$, $\text{Ru}(\text{CN})_6^{4-}$, $\text{Ru}(\text{CN})_6^{3-}$, $\text{Co}(\text{CN})_6^{3-}$), (POMs) ($\text{Mo}_7\text{O}_{24}^{6-}$, $\text{W}_7\text{O}_{24}^{6-}$, $\text{H}_2\text{W}_{12}\text{O}_{40}^{6-}$, $\text{V}_{10}\text{O}_{28}^{6-}$, biochemical ions (different amino acids, DNA, CMP, AMP, GMP, ATP, ADP)⁶⁰. Unlike the metal to the layers, there is almost no restriction for the nature of the anions in the interlayer space of LDHs.

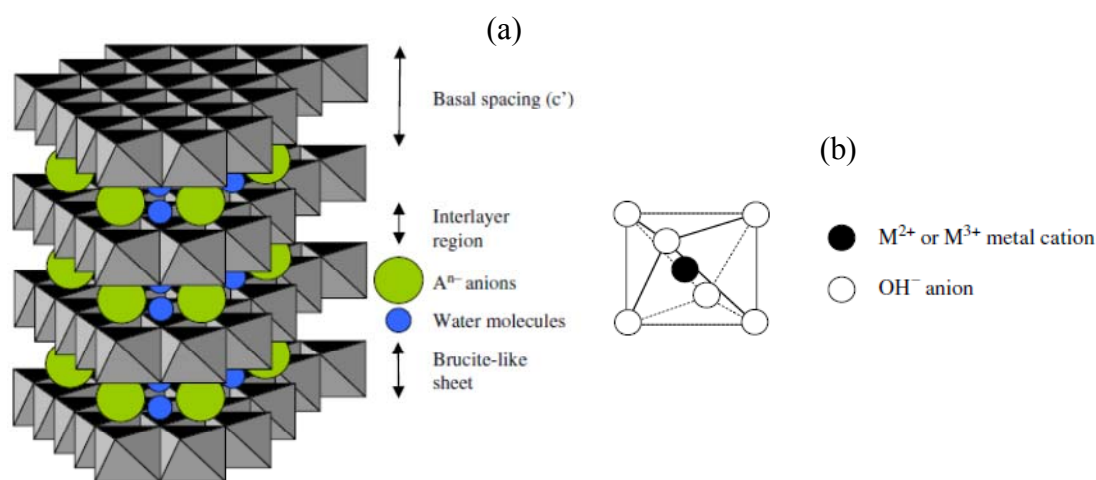


Figure 2.3.2: schematic representations of a) LDH structure and b) octahedral units $M(\text{OH})_6$ of LDH's layers.⁶¹

LDHs can be regarded as a class of materials that are simple to synthesize in the laboratory, although not always as pure phases. In general, there are several approaches to prepare LDHs. The simplest and most commonly used method is coprecipitation. In this method, aqueous solutions of M^{2+} and M^{3+} containing the anion that is to be incorporated into the LDHs are used as precursors, of which Mg and Al are the most frequently used metal precursors. In order to ensure simultaneous precipitation of two or more cations, it is necessary to carry out the synthesis under conditions of supersaturation. There are generally two types of coprecipitation conditions, namely at low supersaturation and at high supersaturation. Coprecipitation at low supersaturation is performed by slow addition of mixed solutions of divalent and trivalent metal salts at the selected ratio into a reactor containing an aqueous solution of the desired interlayer anion. A second solution of an alkali is then added into the reactor simultaneously at such a rate as to maintain the desired pH for coprecipitation of the two metallic salts. In a slight contrast to the former method, coprecipitation at high supersaturation requires the addition of a mixed salt solution to an alkaline solution containing the desired interlayer anion. Coprecipitation at high supersaturation generally gives rise to less crystalline materials compared to those with low supersaturation, due to the formation of a large number of crystallization nuclei. After precipitation at low and high supersaturation, a thermal treatment process is performed to increase the yields and crystallinity of the materials. This is followed by an aging process conducted for a period ranging from a few hours to several days⁵⁴. In order to ensure the purity of the synthesized LDHs, the use of the decarbonated ultrapure water and the application of vigorous stirring in combination with nitrogen purging in the synthesis process are necessary⁶¹. LDHs can be also prepared by the ion exchange method. This method is useful when the coprecipitation method inapplicable, e.g. when the divalent or trivalent metal cations or the anions involved are unstable in the alkaline solution, or when the direct reaction between the metal ions and the guest anions is more favourable. In this method, the guests are exchanged with the anions present in the interlayer regions of the LDHs to produce specific anion-pillared LDHs⁶². Ion exchange method is the most common method for modifying already prepared LDHs. Bish and Bridley in 1977, observed that the treatment of takovite mineral with hydrochloric solutions not change the structure of LDH, but leads to the formation of a new LDH with different interlayer distance between the sheets due to the replacement of carbonate anions (CO_3^{2-}) from

chlorine ions (Cl^-)⁵³. Several factors play important roles in the adsorption process, such as pH, competitive anions, temperature, LDH particle size. Generally when is used LDH which contains carbonate or carboxylate anions, as a precursor, the ion exchange ion takes part at a low pH ($4.5 < \text{pH} < 6$) in order first to accentuate these anions and as result to be more easily removed from the interlayer space of LDH and then to insert the new anions. The most easily exchangeable ions from the interlayer space of LDH's are the nitrate anions (NO_3^-). Depending on the load, the charge density and the ability to hydrogen bonds of anions, they follow the order: $\text{NO}_3^- < \text{Br}^- < \text{Cl}^- < \text{F}^- < \text{OH}^- < \text{CO}_3^{2-} < \text{SO}_4^{2-}$ based on which, some anions are more easily interchangeable than others while the divalent anions are more strongly held in the interlayer than the monolayer anions⁶³.

Another common method to produce LDH is rehydration/reconstruction using the structural “memory effect”. This method involves calcination of LDH to remove the interlayer water, interlayer anions, and the hydroxyl groups, resulting in mixed metal oxides. Besides the aforementioned methods, other reported synthesis methods of LDH include the secondary intercalation method (an intercalation method involving dissolution and the re-coprecipitation method), salt-oxide method, surface synthesis, template synthesis, and others⁶⁴.

References

- 1 R. H. Alonso, L. Estevez, H. Q. Lian, A. Kelarakis, and E. P. Giannelis, *Polymer* **50**, 2402 (2009).
- 2 I. Nicotera, A. Enotiadis, K. Angjeli, L. Coppola, and D. Gournis, *International Journal of Hydrogen Energy* **37**, 6236 (2012).
- 3 Wang J., Merino J., Aranda P., Galvan J.-C., and H.-R. E., *J. Mater. Chem.* **9** 161 (1998).
- 4 B'ebin P., Caravanier M., and G. H., *Journal of Membrane Science* **278** 35 (2006).
- 5 E. Giannelis, R. Krishnamoorti, and E. Manias, edited by S. Granick, et al. (Springer Berlin / Heidelberg, 1999), Vol. 138, p. 107.
- 6 D. Gournis, et al., *Journal of the American Chemical Society* **128**, 6154 (2006).
- 7 D. Petridis, T. Bakas, A. Simopoulous, and N. H. J. Gangas, *Inorganic Chemistry* **28**, 2439 (1989).
- 8 P. C. LeBaron, Z. Wang, and T. J. Pinnavaia, *Applied Clay Science* **15**, 11 (1999).
- 9 J. K. Mbougouen, E. Ngameni, and A. Walcarius, *Anal. Chim. Acta* **578**, 145 (2006).
- 10 A. A. Tziialla, E. Kalogeris, A. Enotiadis, A. A. Taha, D. Gournis, and H. Stamatis, *Materials Science and Engineering B-Advanced Functional Solid-State Materials* **165**, 173 (2009).
- 11 A. A. Tziialla, I. V. Pavlidis, M. P. Felicissimo, P. Rudolf, D. Gournis, and H. Stamatis, *Bioresour. Technol.* **101**, 1587 (2010).
- 12 P. Stathi, K. Litina, D. Gournis, T. S. Giannopoulos, and Y. Deligiannakis, *J. Colloid Interface Sci.* **316**, 298 (2007).
- 13 T. J. Pinnavaia and G. W. Beall, *Polymer-clay nanocomposites* (J. Wiley & Sons, New York, 2001).
- 14 E. P. Giannelis, *Adv. Mater.* **8**, 29 (1996).
- 15 P. C. LeBaron, Z. Wang, and T. J. Pinnavaia, *Appl. Clay Sci.* **15**, 11 (1999).
- 16 K. S. Novoselov, A. K. Geim, S. V. Morozov, D. Jiang, Y. Zhang, S. V. Dubonos, I. V. Grigorieva, and A. A. Firsov, (2004), Vol. 306, p. 666.
- 17 H. W. Kroto, J. R. Heath, S. C. O'Brien, R. F. Curl, and R. E. Smalley, *Nature* **318**, 162 (1985).
- 18 A. Oberlin, M. Endo, and T. Koyama, *Journal of Crystal Growth* **32**, 335 (1976).
- 19 S. Iijima and T. Ichihashi, *Nature* **363** (1993).
- 20 D. S. Bethune, C. H. Klang, M. S. de Vries, G. Gorman, R. Savoy, J. Vazquez, and R. Beyers, *Nature* **363** (1993).
- 21 C. Oshima, A. Itoh, E. Rokuta, T. Tanaka, K. Yamashita, and T. Sakurai, *Solid State Communications* **116**, 37 (2000).
- 22 A. J. Van Bommel, J. E. Crombeen, and A. Van Tooren, *Surface Science* **48**, 463 (1975).
- 23 I. Forbeaux, J. M. Themlin, and J. M. Debever, *Physical Review B* **58**, 16396 (1998).
- 24 A. K. Geim and K. S. Novoselov, *Nature Materials* **6**, 183 (2007).
- 25 K. S. Novoselov, A. K. Geim, S. V. Morozov, D. Jiang, M. I. Katsnelson, I. V. Grigorieva, S. V. Dubonos, and A. A. Firsov, *Nature* **438**, 197 (2005).
- 26 Y. Zhang, Y.-W. Tan, H. L. Stormer, and P. Kim, *Nature* **438**, 201 (2005).
- 27 L. Liao, J. Bai, Y.-C. Lin, Y. Qu, Y. Huang, and X. Duan, *Advanced Materials* **22**, 1941 (2010).
- 28 T. Kuilla, S. Bhadra, D. Yao, N. H. Kim, S. Bose, and J. H. Lee, *Progress in Polymer Science* **35**, 1350 (2010).
- 29 J. R. Potts, D. R. Dreyer, C. W. Bielawski, and R. S. Ruoff, *Polymer* **52**, 5 (2011).
- 30 Y. Geng, S. J. Wang, and J.-K. Kim, *Journal of Colloid and Interface Science* **336**, 592 (2009).
- 31 A. B. Bourlinos, D. Gournis, D. Petridis, T. Szabó, A. Szeri, and I. Dékány, *Langmuir* **19**, 6050 (2003).
- 32 H.-P. Boehm and E. Stumpp, *Carbon* **45**, 1381 (2007).
- 33 C. Schafheutl, *J. Prakt. Chem.* **21**, 129 (1840).

- 34 B. C. Brodie, *Philos. Trans. R. Soc. London* **149**, 249 (1859).
- 35 L. Staudenmaier, *Ber. Dtsch. Chem. Ges.* **31**, 1481 (1898).
- 36 W. S. Hummers and R. E. Offeman, *J. Am. Chem. Soc.* **80**, 1339 (1958).
- 37 P. V. Lakshminarayanan, H. Toghiani, and C. U. Pittman Jr, *Carbon* **42**, 2433 (2004).
- 38 N. Zhang, L.-y. Wang, H. Liu, and Q.-K. Cai, *Surf. Interface Anal.* **40**, 1190 (2008).
- 39 K. R. Koch and P. F. Krause, *J. Chem. Ed.* **59**, 973 (1982).
- 40 M. Wissler, *Journal of Power Sources* **156**, 142 (2006).
- 41 U. Hofmann and R. Holst, *Ber. Dtsch. Chem. Ges. B* **72**, 754 (1939).
- 42 G. Ruess, *Monatsh. Chem.* **76**, 381 (1946).
- 43 T. Szabó, O. Berkesi, P. Forgó, K. Josepovits, Y. Sanakis, D. Petridis, and I. Dékány, *Chemistry of Materials* **18**, 2740 (2006).
- 44 A. Lerf, H. He, M. Forster, and J. Klinowski, *The Journal of Physical Chemistry B* **102**, 4477 (1998).
- 45 N. I. Kovtyukhova, *Chemistry of Materials* **11**, 771 (1999).
- 46 I. Dakany, R. Kreger-Grasser, and A. Weiss, *Colloid and Polymer Science* **276**, 570 (1998).
- 47 P. Liu, K. Gong, and P. Xiao, *Carbon* **37**, 2073 (1999).
- 48 H. F. W. Taylor, *Mineral. Mag.* **39**, 377 (1973).
- 49 B. M. Choudary, M. Lakshmi Kantam, C. R. Venkat Reddy, K. Koteswara Rao, and F. Figueras, *Journal of Molecular Catalysis A: Chemical* **146**, 279 (1999).
- 50 M. J. Climent, A. Corma, S. Iborra, and J. Primo, *Journal of Catalysis* **151**, 60 (1995).
- 51 F. Li and X. Duan, edited by X. Duan and D. Evans (Springer Berlin / Heidelberg, 2006), Vol. 119, p. 193.
- 52 V. Rives, Nova Science Publishers, United states of America (2001).
- 53 D. L. Bish and G. W. Brindley, *American Mineralogist* **62**, 458 (1977).
- 54 F. Cavani, F. Trifiro, and A. Vaccari, *Catalysis Today* **11**, 173 (1991).
- 55 A. Vaccari, *Catalysis Today* **41**, 53 (1998).
- 56 N. Kim, Y. Kim, T. T. Tsotsis, and M. Sahimi, *The Journal of Chemical Physics* **122**, 214713 (2005).
- 57 S. P. Newman and W. Jones, *New Journal of Chemistry* **22**, 105 (1998).
- 58 J. Guo, H. Lou, H. Zhao, D. Chai, and X. Zheng, *Applied Catalysis A: General* **273**, 75 (2004).
- 59 V. Rives, *Materials Chemistry and Physics* **75**, 19 (2002).
- 60 S. M. Auerbach, K. A. Carrado, and P. K. Dutta, *Handbook of layered materials* New York (2004).
- 61 K.-H. Goh, T.-T. Lim, and Z. Dong, *Water Research* **42**, 1343 (2008).
- 62 N. Morel-Desrosiers, J. Pisson, Y. Israeli, C. Taviot-Gueho, J.-P. Besse, and J.-P. Morel, *Journal of Materials Chemistry* **13**, 2582 (2003).
- 63 S. Miyata, in *Clays and Clay Minerals*, 1983), Vol. 31, p. 305.
- 64 J. He, M. Wei, B. Li, Y. Kang, D. Evans, and X. Duan, edited by X. Duan and D. Evans (Springer Berlin / Heidelberg, 2006), Vol. 119, p. 89.

3. EXPERIMENTAL TECHNIQUES

The experimental technique on which focused my experimental work was the Nuclear Magnetic Resonance (NMR), by using different methods and sequence: Pulsed Field Gradient (PFG) NMR, to direct measurements of the diffusion coefficients, inversion recovery and spin echo for relaxation times measurements, and one pulse to acquire NMR spectra.

Scanning Electron Microscopy (SEM) and Dynamic Mechanical Analysis (DMA) are also described in this section.

In collaboration with other laboratories the materials were characterized by X-ray diffraction, FTIR, Raman spectroscopy, thermal analysis, proton conductivity. These techniques are not discussed in this thesis.

3.1 Nuclear Magnetic Resonance (NMR)

Nuclear magnetic resonance (NMR) spectroscopy is a powerful technique that exploits the magnetic properties of certain atomic nuclei to determine physical and chemical properties of atoms or the molecules in which they are contained. It can provide detailed information about the structure, dynamics, reaction state, and chemical environment of molecules. In principle, NMR is applicable to any nucleus possessing spin. The spin is an intrinsic angular momentum of the magnetic nuclei, whose magnitude is $[I(I + 1)]^{1/2} \hbar$. The spin quantum number (I) of some commonly occurring nuclei are given in Table 3.1.

Table 3.1: Some commonly nuclear spin quantum numbers.

I	Nuclei
0	^{12}C , ^{16}O
1/2	^1H , ^{13}C , ^{15}N , ^{19}F , ^{29}Si , ^{31}P
1	^2H , ^{14}N
3/2	^{11}B , ^{23}Na , ^{35}Cl , ^{37}Cl
5/2	^{17}O , ^{27}Al
3	^{10}B

It is worthy to note that ^{12}C and ^{16}O have $I = 0$, i.e. there is no angular momentum, no magnetic moment and consequently no NMR spectra. The angular momentum \mathbf{I} of a spin- I nucleus has just $2I+1$ projections into an arbitrarily chosen axis, name the z axis. That is, the z component of \mathbf{I} , denoted by I_z is quantized:

$$I_z = m \quad (3.1.1)$$

where m , the magnetic quantum number, has $2I+1$ values in integral steps between $+I$ and $-I$, $m = I, I-1, I-2, \dots, -I+1, -I$. In the case of $I=1/2$ (for example ^1H), the angular momentum has two permitted directions, $I_z = \pm 1/2\hbar$, while a nucleus with I (for example ^2H) has three possible state, $I_z = 0, \pm \hbar$. The magnetic moment $\boldsymbol{\mu}$ of a nucleus is directly proportional to \mathbf{I} :

$$\boldsymbol{\mu} = \gamma \mathbf{I} \quad (3.1.2)$$

where γ is the gyromagnetic ratio. γ is equal to $\hbar^{-1}g\mu_N$ where μ_N is the nuclear magneton, and g is the g-factor of the nucleon or nucleus in question.

When nuclei with non-zero spin, and hence non zero magnetic moments, are placed into a static magnetic field, \mathbf{B}_0 , they are subject to various interactions described by the total spin Hamiltonian,

$$\hat{H}_S = \hat{H}_Z + \hat{H}_Q + \hat{H}_{rf} + \hat{H}_D + \hat{H}_{cs} + \hat{H}_J \quad (3.1.3)$$

\hat{H}_Z is the Zeeman interaction and it is the interaction between magnetic moment $\boldsymbol{\mu}$ and magnetic field \mathbf{B}_0 :

$$\hat{H}_Z = -\boldsymbol{\mu} \cdot \mathbf{B}_0 = -\gamma \mathbf{I} \cdot \mathbf{B}_0 = -\gamma(I_x B_{0x} + I_y B_{0y} + I_z B_{0z}) \quad (3.1.4)$$

If the magnetic field is in the z direction the Zeeman Hamiltonian can be written :

$$\hat{H}_Z = -\gamma I_z B_0 \quad (3.1.5)$$

Solving the Schrödinger equation $\hat{H}_Z |m\rangle = E|m\rangle$, where $|m\rangle$ are the nuclear spin levels functions, these levels are distinguished by different quantum number m , then we obtain $2I+1$ values of energy:

$$E = -m\hbar\gamma B_0 \quad (3.1.6)$$

The $2I + 1$ states for spin- I nucleus are equally spaced, with energy gap $\hbar\gamma B$ (Figure 3.1.1).

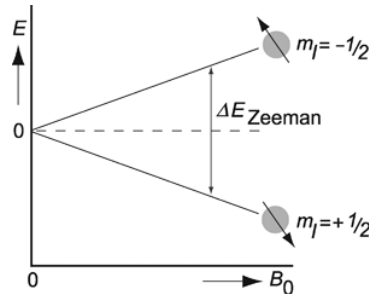


Figure 3.1.1: Energy levels for hydrogen nucleus in a magnetic field B_0 considering the Zeeman interaction.

In the eq. 3.1.3 \hat{H}_Q is the quadrupolar interaction Hamiltonian, \hat{H}_{rf} is the Hamiltonian describing the interaction of radio frequency radiation with the nuclear spins, \hat{H}_D represent the dipolar coupling \hat{H}_{CS} the chemical shift and \hat{H}_J the indirect coupling. Nuclei with a spin $I = \frac{1}{2}$ have a spherical charge distribution and therefore, do not exhibit an electric quadrupole moment Q .

Assuming that an oscillating magnetic field (i.e rf) $2\mathbf{B}_1 \cos(2\pi\nu_1 t)$ is along the x -direction (with radio frequency, ν_1) perpendicular to the static magnetic field \mathbf{B}_0 :

$$\hat{H}_1(t) = \hbar\gamma B_1 I_x \cos(2\pi\nu_1 t) \quad (3.1.7)$$

This Hamiltonian of interaction make known to transitions between the energy levels of spin that have been separated by the Hamiltonian \hat{H}_s . The frequency associated to the transition from the lower energy state to the higher energy state is given by:

$$\nu_0 = \frac{\Delta E}{h} = \frac{B_0}{2\pi} \quad (3.1.8)$$

The relative angular frequency is $\omega_0 = 2\pi\nu_0$ and it is known as the Larmor Frequency. The magnetic field, \mathbf{B}_1 , influences (move) the net magnetization, $M = \sum_i \mu_i$ of the overall sample due to changes in occupancy in the spin state. In other words \mathbf{M} reflects the difference of population between the upper and lower spin levels (for $I = \frac{1}{2}$ nuclei system).

The return of magnetization, \mathbf{M} , to its equilibrium state is known as relaxation. There are three factors that influence the decay of \mathbf{M} : magnetic field inhomogeneity, spin-lattice (longitudinal) T_1 relaxation and spin-spin relaxation (transverse) T_2 relaxation. T_1 relaxation is the mechanism by which the z equilibrium with its surroundings (the “lattice”). T_2 relaxation is the mechanism by which M_{xy} , the transverse component of magnetization vector, exponentially decays towards its equilibrium value of zero.

To observe NMR signals, the spin system must absorb electromagnetic energy (in the radio frequency range) that allows transitions between the energy levels. Equilibrium is achieved through the process of relaxation, which is due to the interaction between the spins and their environment. There are two main types of relaxation: longitudinal or spin-lattice (T_1), and transverse or spin-spin lattice (T_2). If one considers that spin system as isolated thermodynamically, then upon the absorption of energy from the rf pulse, the temperature of the spin system will increase. To restore equilibrium to the system there must be a removal of this excess heat to the lattice bath. Time constant T_1 characterizes the rate of return to equilibrium of the z -component of the magnetization after perturbation. To determine the longitudinal relaxation time for T_1 , the inversion recovery technique is often used. The pulse sequence for this technique is $\pi - \tau - \pi/2$. The time interval τ is varied using approximately 12–15 values. Immediately following the π pulse, the \mathbf{M} is inverted. During the time interval, \mathbf{M} relaxes back to thermal equilibrium at a rate of T_1^{-1} . The application of the $\pi/2$ pulse causes \mathbf{M} to rotate from the z -axis into the x - y plane where the nuclear signal may be picked up by a receiver (see Figure 3.1.2). The time dependence of M_z follows:

$$M_z = M_0(1 - 2\exp^{-\tau/T_1}) \quad (3.1.9)$$

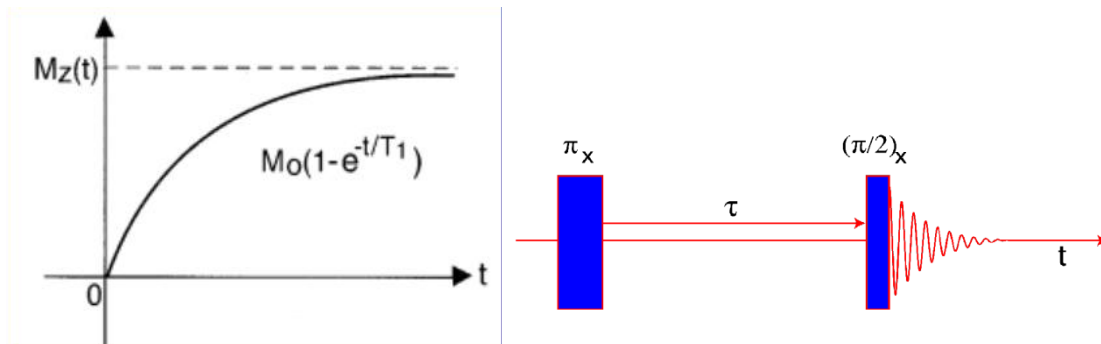


Figure 3.1.2: Inversion recovery sequence.

The time constant T_2 determines the time it takes for the x and y components of the magnetization to equilibrate after perturbation. Whilst there are several more-elaborate techniques for measuring the spin-spin relaxation, T_2 , most are based on the spin-echo pulse sequence, a schematic of which is shown in Figure 5. This technique was first developed by Hahn in 1950¹ and consisted of two rf pulses: one $\pi/2$ and the other π , separated by time $-\tau$. Ideally, in a perfectly homogeneous static magnetic system, the perturbed magnetization returns to equilibrium by a dephasing of the coherences in the x-y plane during a time T_2 , which is related to the spectrum line-width at half height. However, in practice, the static magnetic field is not perfectly homogeneous; this causes nuclei in different regions of the sample to experience different fields and therefore precess at different frequencies. This precession results in additional dephasing of the spins in the x-y plane. In practice, $T_2 \leq T_1$. The initial preparation pulse puts M along the x or y axis (depending on its phase). The difference in the field experienced by the spins results in precession at various frequencies, causing dephasing of M . The slower moving components of M_{xy} appear to move counterclockwise, while those faster moving components appear to move clockwise. At time τ after the π pulse, the magnetization refocuses along the negative x or y axis. The dephasing and rephrasing of the magnetization along the x or y axis are known as spin echoes (see Figure 3.1.3). The intensity of the echo will depend on T_2 according to:

$$M = M_0 \exp^{-\tau/T_2} \quad (3.1.10)$$

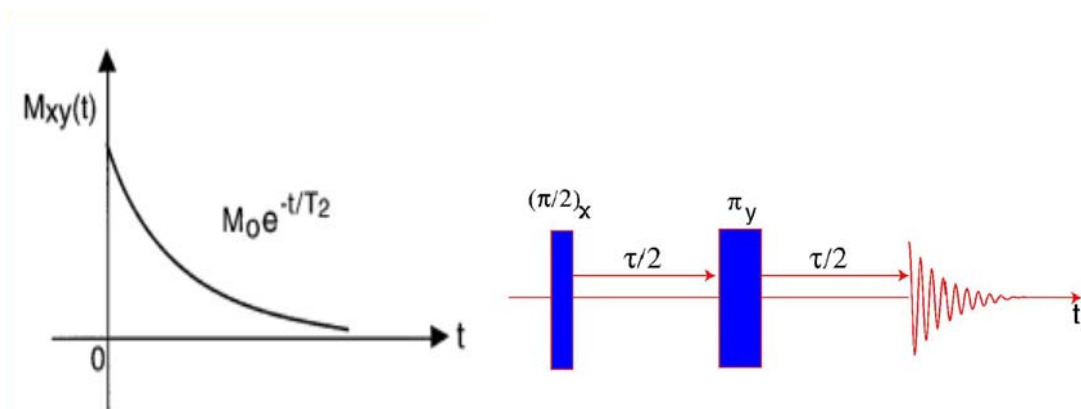


Figure 3.1.3: Spin-echo sequence

3.1.1 Temperature dependence of T_1 and T_2

An NMR state diagram is a curve of NMR relaxation time, be it spin–spin relaxation time (T_2) or spin–lattice relaxation time (T_1), versus temperature. Usually, relaxation times of liquids increase linearly with temperature. However, at very low temperatures or with solid materials, relaxation times behave drastically different. For solids, with rising temperature, T_2 changes little at low temperatures and increases rapidly above certain temperatures, characterized by a mirrored-L shape, while T_1 decreases rapidly to a certain point and rises again rapidly, characterized by a minimum (Figure 3.1.4).

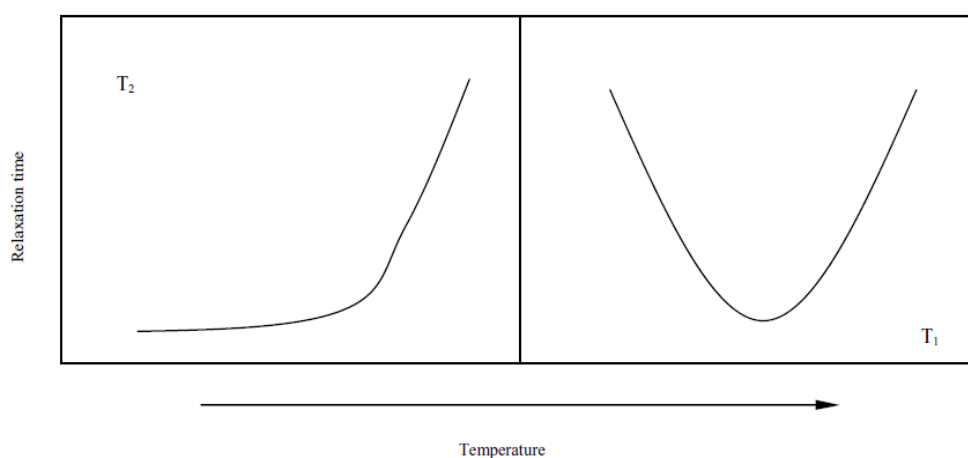


Figure 3.1.4: Schematic diagrams showing relaxation times of a material as a function of temperature.

Let us consider a high molecular weight polymer with side chain segments. When heated, some segments within the long chain of the polymer molecule are mobilized before the whole molecule starts moving. Further heating causes the entire molecule to move and become liquid. Two types of motions can be identified during the gradual heating, that is, segmental motion and molecular motion. At a certain low temperature, both motions are hindered severely or frozen; at higher temperatures, both motions may be activated. These 2 situations correspond to the solid state and liquid state, respectively. When the polymer is placed at a temperature where only the segmental motion is activated while the molecular motion is frozen, the state is called the rubbery state, and such state transition takes place at the glass–rubber transition temperature T_g . On further heating, the polymer in the rubbery state becomes a highly viscous liquid and starts flowing. The polymer moves into the visco-fluid state, and such transition

takes place at the flow temperature T_f . Relaxation time is a function of the spin species and the chemical and physical environments surrounding the spins. Therefore, analysis of T_1 and T_2 of a sample will allow the study of the chemical and physical properties of the sample. A long T_1 or T_2 indicates a slow relaxation and a short T_1 or T_2 value indicates a rapid relaxation.

The dynamic motion of spins can be characterized by a correlation time τ_c , which is, roughly speaking, the minimum time required for the nuclear magnetic moment to rotate 1 radian ($1/2 \pi$ of a complete circle). In general, τ_c for non viscous liquid is very short. With water, for instance, τ_c is about 10^{-12} s. On the other hand, τ_c for solids is very long, about 10^{-5} s. Within limits, the slower the motion, the longer the τ_c , and the faster a perturbed spin system will relax. Thus, the relationship between the motional characteristics and NMR relaxation can be established through the relationship between τ_c and relaxation time, as described in the equations² 3.1.11 and 3.1.12:

$$\frac{1}{T_1} = K \left[\frac{\tau_c}{1+(\omega_0\tau_c)^2} + \frac{4\tau_c}{1+(2\omega_0\tau_c)^2} \right] \quad (3.1.11)$$

$$\frac{1}{T_2} = \frac{K}{2} \left[3\tau_c + \frac{5\tau_c}{1+(\omega_0\tau_c)^2} + \frac{2\tau_c}{1+(2\omega_0\tau_c)^2} \right] \quad (3.1.12)$$

$$K = \frac{3\mu^2}{160\pi^2} \frac{\hbar^2\gamma^4}{r^2}$$

K is a constant that includes a number of nuclear parameters and constants, and ω_0 is the resonance frequency. Figure 3.1.5 is a plot of τ_c versus relaxation time constants T_1 and T_2 . The curves are similar to those in Figure 3.1.4³. This is because, within limits, τ_c is related to temperature. Their relationship can be described by the equation 3.1.13:

$$\tau_c = \tau_{c0} e^{E_{act}/kT} \quad (3.1.13)$$

where E_{act} is the activation energy for rotational motion, k the Boltzmann constant, T the absolute temperature, and τ_{c0} is a constant.

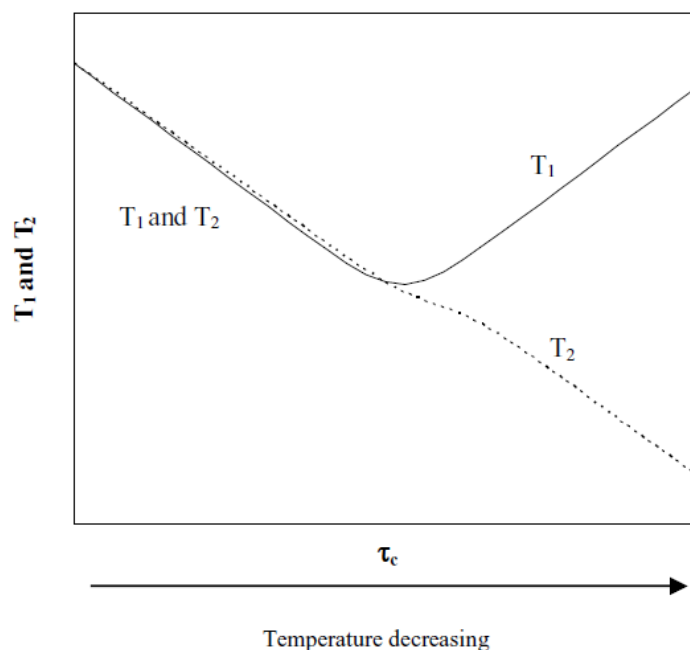


Figure 3.1.5 : A generalized schematic diagram showing the relationship between relaxations time constants and correlation time.

Fundamentally, T_1 , T_2 , and equations 3.1.11 and 12 describe the rotational motions of nuclei. It is suggested that rotation of a probe molecule (e.g., water) in a viscous liquid should be coupled to the structural relaxation of the surroundings, which is largely determined by the translational diffusion properties and the structure of the neighboring molecules⁴. The fact that the product of correlation time and translational diffusion coefficient is a constant indicates that rotational and translational motions are closely related^{4, 5}. Netz and others⁵ (2002) suggest that translational and rotational motions are controlled by a common mechanism. Therefore, T_1 and T_2 are conveniently coupled to molecular mobility; however, the relationship between relaxation times and molecular mobility depends on the nucleus being probed and surrounding systems^{6, 7}.

3.1.2 NMR PGSE Technique

NMR spectroscopy has provided information on the microscopic as well as macroscopic nuclear environments by determination of parameters such as relaxation times (T_1 , T_2), self-diffusion coefficients (D), and structural information. One of its most important uses in the study of PEMs has been to provide mass transport data of

the diffusing ions or molecules through measurement of D by the NMR pulse gradient spin echo (PGSE) and pulse gradient stimulated echo pulse sequences. The schematic for the PGSE technique is shown in Figure 3.1.6. The PGSE technique is a powerful non-invasive method for the determination of D . It can provide very accurate and quick measurement of D in multi-component systems without the need for isotopic labeling based on its chemical shift difference of the diffusing specie. The technique was first developed by Hahn (1950)¹ and originally involved the use of a typical spin-echo-pulse sequence. In addition to this, a constant magnetic gradient was applied along the z axis. This method was later modified by Stejskal and Tanner (1965) in which they replaced the constant magnetic gradient by pulsed magnetic gradients⁸⁻¹⁰. The application of pulsed gradients as opposed to one that is constant eliminates the problem of large broadening of the signal in the presence of the static gradient. The NMR PGSE technique consists of two rf pulses: first $\pi/2$, then π . Following each rf pulse are magnetic gradients of strength g and duration δ , separated by time Δ .

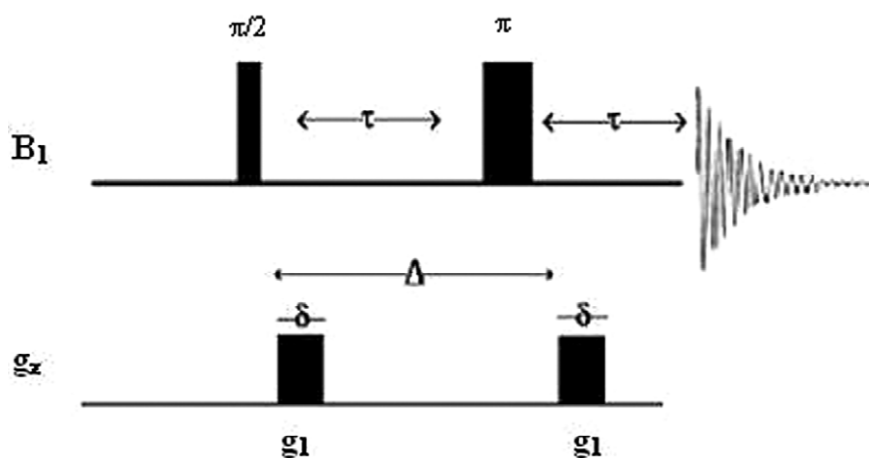


Figure 3.1.6: Schematic of the pulse gradient spin echo technique (PGSE) pulse sequence, which consist of two rf pulses ($\pi/2$ and π), separated by delay time τ , and each followed by a magnetic gradient pulse of magnitude g , duration δ , and separation Δ .

The core of the NMR PGSE technique lies in the fact that in the presence of a magnetic field with superimposed magnetic gradients, a diffusing nucleus will experience changes in the magnetic field it experiences and its resulting phase. This change in

phase results in attenuation of the magnetization M and the resulting attenuation factor is given by⁸:

$$M(g) = \exp(-\gamma^2 g^2 D \delta^2 (\Delta - (\delta/3))) \quad (3.1.14)$$

where D is the self-diffusion coefficient of the diffusing species, g is the gradient strength, and δ and Δ are the gradient pulse width and interval between gradient pulses, respectively. The expression above is for a fixed time between excitation and refocusing pulses. The attenuation of the spin echo versus gradient strength is shown for a representative system in Figure 3.1.7. In order to obtain D , the magnitude of g , Δ , τ , and γ must be known. Typical values of δ are a few milliseconds, whilst Δ ranges from a few milliseconds to a few hundred milliseconds.

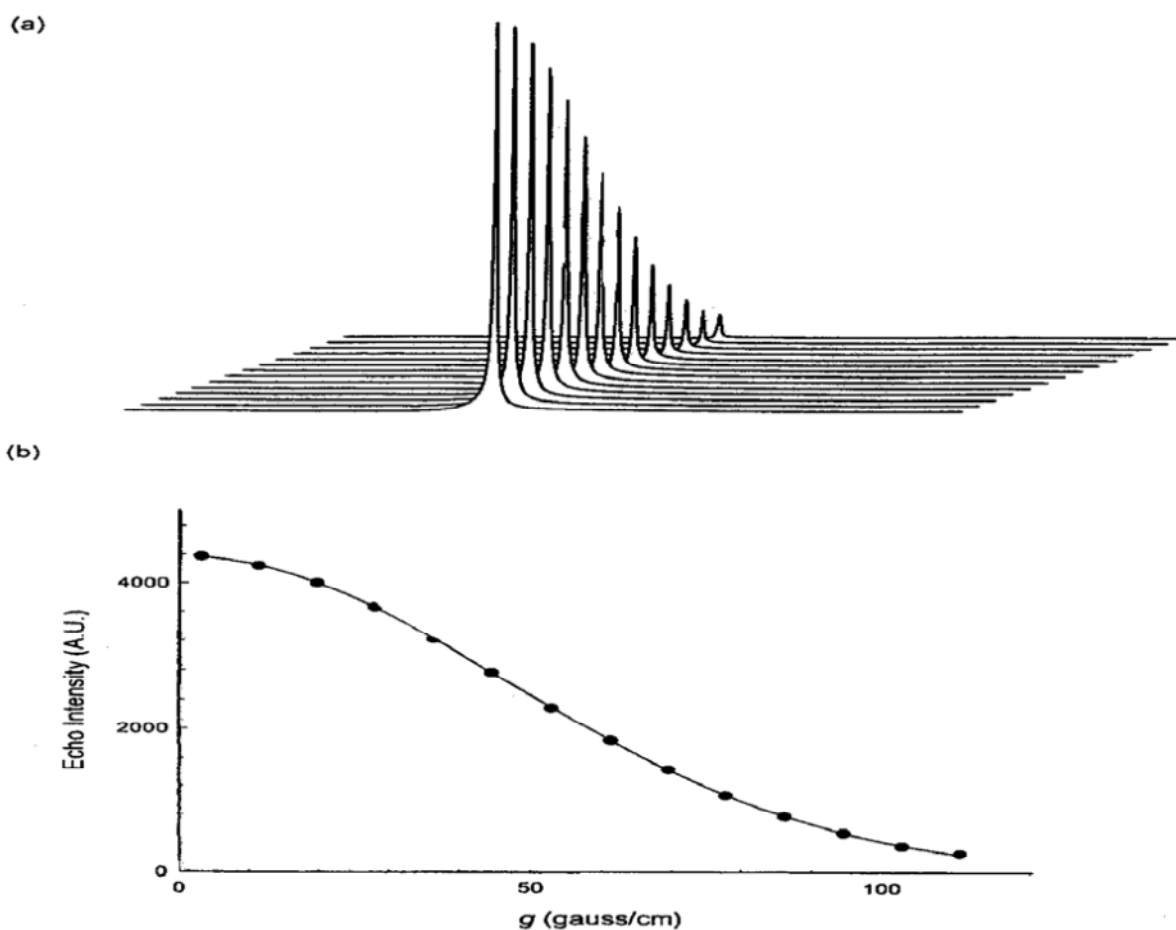


Figure 3.1.7: A representative ^1H PGSE NMR decay profile and plot from which the diffusion coefficient is obtained.⁹

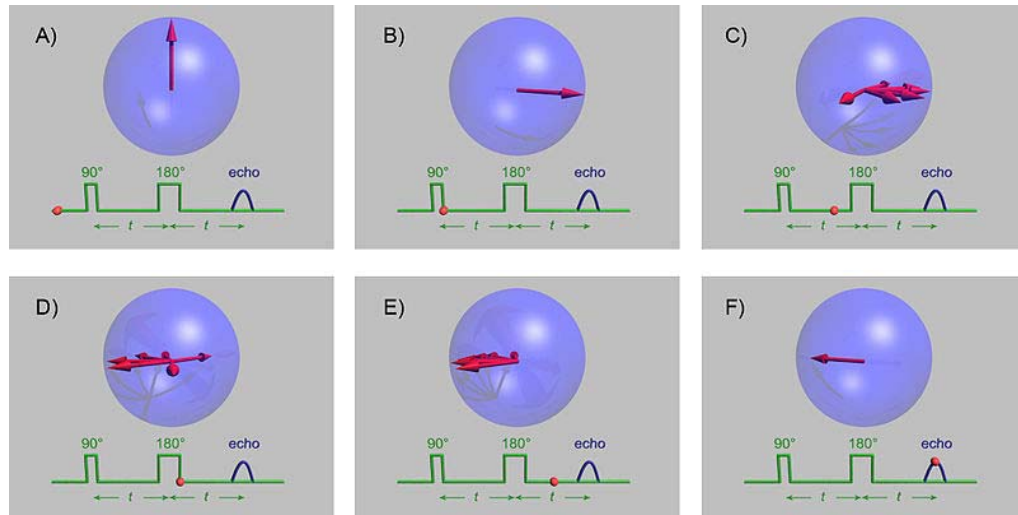


Figure 3.3.3: Spin Echo Pulse.

3.2 Scanning Electron Microscopy

Scanning electron microscope¹¹ is one of the most versatile instruments for examining the microstructural characteristics of solids. High resolution that can go beyond 2,5 nm and three-dimensional view are characteristic principles of this instrument. The variety of the attained signals (x-rays, Auger electrons etc) provides rich information regarding surface's composition and additionally can be studied crystallographic, magnetic and electronic characteristics of the materials. A scanning electron microscope is composed of:

- the luminescence source:
Electron gun;
- the vacuum system;
- the electromagnetic lenses;
- the deflection coil;
- the object's lens;
- the signal detector;
- the signal transformation system to images;
- the sample holder area;

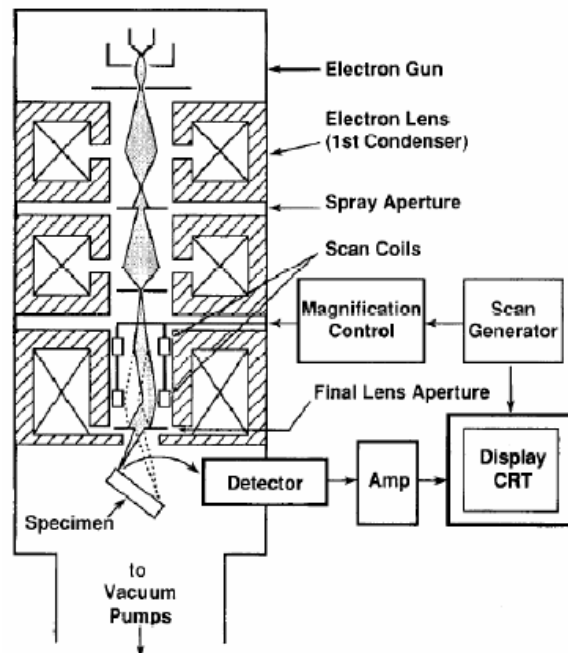


Figure 3.2.1: Schematic presentation of a SEM apparatus.

The scanning procedure takes place through interactions between sample's surface and the electronic beam. Between the produced signals there are: secondary electrons, electrons diffusing inside the surface, a continuum characteristic of the X rays, auger electron emissions and photons of various energies. The resolution of a particular SEM signal is determined primarily by the excitation volume and not by the magnitude of the secondary probe. The energy of the beam electrons lies in between (1 – 30) keV. When the beam arrives in the surface there can be either elastic or inelastic diffusion. The first results from the interactions between the beam electrons and the atoms of the material provoked by significant deviations on the occurring directions.

The second is produced from the inelastic interaction between the beam's electrons and the material's bonds.

The inelastic diffusion is directly responsible for the production of the signals used for the surface's examination. In fact, the interaction with the Coulomb field of the atoms verifies energy loss and emission of characteristic x-rays. Below 10 nm the electrons diffusing from the primary beam get strongly absorbed through recombination with the gap that is created during the diffusion process and in some insulator materials there are produced photons with wave lengths in the visible or the near infrared giving therefore a visible luminescence. The intensity of backscattered electrons can be correlated to the atomic number of the element within the sampling volume. Hence, some qualitative elemental information can be obtained. The analysis of characteristic X-rays emitted from the sample gives more quantitative elemental information. Such X-ray analysis can be confined to analytical volumes as small as 1 cubic micron.

3.3 Dynamic Mechanical Analysis

Dynamic mechanical analysis (abbreviated DMA, also known as dynamic mechanical spectroscopy) is a technique used to study and characterize materials. It is most useful for studying the viscoelastic behavior of the polymers. A sinusoidal stress is applied and the strain in the material is measured allowing one to determine the complex modulus. The temperature of the sample or the frequency of the stress are often varied, leading to variations in the complex modulus; this approach can be used to locate the glass transition temperature of the material, as well as to identify transitions corresponding to other molecular motions. Polymers composed of long molecular chains have unique viscoelastic properties, which combine the characteristics of elastic solids and Newtonian fluids. The classical theory of elasticity describes the mechanical properties of elastic solids where stress is proportional to strain in small deformations. Such response of stress is independent of strain rate. The classical theory of hydrodynamics describes the properties of viscous fluid, for which the response of stress is dependent on strain rate¹². The viscoelastic property of a polymer is studied by dynamic mechanical analysis where a sinusoidal force (stress σ) is applied to a material and the resulting displacement (strain) is measured. For a perfectly elastic solid, the resulting strain and the stress will be perfectly in phase. For a purely viscous fluid, there will be a 90 degree phase lag of strain with respect to stress¹³. Viscoelastic polymers have the characteristics in between where some phase lag will occur during DMA tests¹³.

- Stress : $\sigma = \sigma_0 \sin(t\omega + \delta)$
- Strain: $\varepsilon = \varepsilon_0 \sin t\omega$

Where ω is frequency of strain oscillation, t is time, δ is phase lag between stress and strain.

The storage modulus measures the stored energy, representing the elastic portion, and the loss modulus measures the energy dissipated as heat, representing the viscous portion. The tensile storage and loss moduli are defined as follows:

$$\text{Storage Modulus: } E' = \frac{\sigma_0}{\varepsilon_0} \cos \delta$$

$$\text{Loss Modulus: } E'' = \frac{\sigma_0}{\varepsilon_0} \sin \delta$$

$$\text{Phase angle Tan}(\delta): \quad \tan \delta = \frac{E''}{E'}$$

Similarly are also defined shear storage and loss moduli, G' and G'' .

Complex variables can be used to express the moduli E and G as follows:

$$E = E' + iE'' \qquad G = G' + iG'' \qquad \text{where } i^2 = -1$$

The instrumentation of a DMA consists of a displacement sensor such as a linear variable differential transformer, which measures a change in voltage as a result of the instrument probe moving through a magnetic core, a temperature control system or furnace, a drive motor (a linear motor for probe loading which provides load for the applied force), a drive shaft support and guidance system to act as a guide for the force from the motor to the sample, and sample clamps in order to hold the sample being tested. Depending on what is being measured, samples will be prepared and handled differently. Two major kinds of test modes can be used to probe the viscoelastic properties of polymers: temperature sweep and frequency sweep tests. A common test method involves measuring the complex modulus at low constant frequency while varying the sample temperature. A prominent peak in $\tan \delta$ appears at the glass transition temperature of the polymer. Secondary transitions can also be observed, which can be attributed to the temperature-dependent activation of a wide variety of chain motions¹⁴.

In semi-crystalline polymers, separate transitions can be observed for the crystalline and amorphous sections. Similarly, multiple transitions are often found in polymer blends. A sample can be held to a fixed temperature and can be tested at varying frequency. Peaks in $\tan \delta$ and in E'' with respect to frequency can be associated with the glass transition, which corresponds to the ability of chains to move past each other. Note that this implies that the glass transition is dependent on strain rate in addition to temperature. Secondary transitions may be observed as well.

The Maxwell model provides a convenient, if not strictly accurate, description of viscoelastic materials. Applying a sinusoidal stress to a Maxwell model gives:

$$E'' = \frac{E\tau_0\omega}{\tau_0^2\omega^2 + 1}$$

where $\tau_0 = \frac{\eta}{E}$ is the Maxwell relaxation time.

Thus, a peak in E'' is observed at the frequency $\frac{1}{\tau_0}$.¹⁴

A real polymer may have several different relaxation times associated with different molecular motions. Because glass transitions and secondary transitions are seen in both frequency studies and temperature studies, there is interest in multidimensional studies, where temperature sweeps are conducted at a variety of frequencies or frequency sweeps are conducted at a variety of temperatures. This sort of study provides a rich characterization of the material, and can lend information about the nature of the molecular motion responsible for the transition.

References

- ¹ E. L. Hahn, *Physical Review* **80**, 580 (1950).
- ² T. C. Farrar, Madison: The Farragut Press. p 211 (1989).
- ³ R. R. Ruan and P. L. Chen, Lancaster, Pa.: Technomic Publishing Co (1998).
- ⁴ B. Bagchi, *The Journal of Chemical Physics* **115**, 2207 (2001).
- ⁵ P. A. Netz, F. Starr, M. C. Barbosa, and H. E. Stanley, *Journal of Molecular Liquids* **101**, 159 (2002).
- ⁶ P. S. Belton, I. Delgadillo, A. M. Gil, and G. A. Webb, Cambridge, U.K.: Royal Society of Chemistry (1995).
- ⁷ S. J. Schmidt, *Avances in Food and Nutrition Research* **48**, 1 (2004).
- ⁸ E. O. Stejskal, *The Journal of Chemical Physics* **43**, 3597 (1965).
- ⁹ S. Suarez and S. Greenbaum, *The Chemical Record* **10**, 377 (2010).
- ¹⁰ E. O. Stejskal and J. E. Tanner, *The Journal of Chemical Physics* **42**, 288 (1965).
- ¹¹ J.I.Goldstein and H.Yakovitz, 1rst ed., Plenum Press, New York (1975).
- ¹² J. D. Ferry, (3 ed.). Wiley (1980).
- ¹³ M. A. Meyers and K. K. Chawla, Prentice-Hall (1999).
- ¹⁴ R. J. Young and P. A. Lovell, *Introduction to Polymers* (2 ed.). Nelson Thornes. (1991).

4. Results and Discussion

In this PhD-thesis, a new class of fillers based on swellable smectite clays, Graphite Oxide (GO) and Layered Double Hydroxides, were tested as nanofillers for the creation of Nafion nanocomposites. In addition an alternative to Nafion, a new short side chain perfluorosulfonic membrane (AquivionTM) was used for development of composite membranes comprising inorganic nanoparticles of zirconium phosphate (ZrP). The aim of this study was the creation of novel nanocomposite membranes with high proton conductivity and water retention, even at high temperatures. The solution intercalation method has been successfully applied for incorporation of layered materials into the polymer, while the effect of the solvent, temperature and filler loading were examined in order to determine the optimum conditions for the preparation of highly homogeneous composites. The characteristics of the membranes were studied mainly, in terms of transport properties by NMR spectroscopy, in order to study the water dynamics inside the electrolyte membranes, which is one of the key aspects in the evaluation of these materials.¹⁻⁵ For this purpose the Pulse-Field-Gradient Spin-Echo NMR (PFGSE-NMR) method⁶ (see chapter 3.1) was employed to obtain a direct measurement of water self-diffusion coefficients on the water-swelled membranes in a wide temperature range (25-140 °C). This technique together with the ¹H-NMR spectra have provided a general description of the water behavior: how it is shared in the polymer structure, effects of the nanofillers and their surface modifications, interactions between water molecules and hydrophilic groups present and, finally, a quantitative estimate of the hydration number, i.e. number of water molecules solvating the hydrophilic sites both in the maximum hydration regime and in quasi-dehydration conditions⁷. Spin-lattice relaxation times (T_1) were also taken as a function of temperature and water content. Additionally, both pristine materials (fillers and Nafion) as well as the resulted nanocomposites were characterized by a combination of X-ray diffraction, FTIR and Raman spectroscopies, thermal analysis (DTA/TGA) and scanning electronic microscopy (SEM). The results of these studies have been published on scientific international journals and reported in appendix at this thesis. In this chapter, the most important results are reported and discussed.

4.1 Clays-based nanocomposites for PEMFCs (paper I)

Smectite clays, as have been extensively described in chapter 2.1, are a class of layered aluminosilicate minerals with a unique combination of swelling, intercalation, and ion exchange properties.

One synthetic (Laponite) and two natural clays (Kunipia and SWy-2 montmorillonites) with different structural and physical parameters were chosen as nanofillers: Laponite shows both low layer charge density and particle size (20 nm), SWy-2 has a medium layer charge density and high particle size (200 nm) and, finally, Kunipia has a high layer charge density and particle size also around 200 nm. Table 4.1 summarize the properties of these clay materials and their structural formula.

Table 4.1. - Some physical properties and the structural formula of laponite (Lap) and the two montmorillonites (SWy-2 and Kunipia)

Clay	Particle size (nm)	CEC* (meq/100 g)	Charge density (e ⁻ /unit cell) [‡]	Structural formula
Lap	20	48.1	0.5	Na _{0.56} [Mg _{5.4} Li _{0.4}]Si ₈ O ₂₀ (OH) ₄
SWy-2	200	76.4	0.6	Na _{0.62} [Al _{3.01} Fe(III) _{0.41} Mg _{0.54} Mn _{0.01} Ti _{0.02}](Si _{7.98} Al _{0.02})O ₂₀ (OH) ₄
Kun	200	119	0.9	Na _{0.87} [Al _{3.12} Fe(III) _{0.20} Mg _{0.61} Ti _{0.01}](Si _{7.90} Al _{0.10})O ₂₀ (OH) ₄

* CEC is the cation exchange capacity; [‡] unit cell is the Si₈O₂₀ unit

4.1.1 Structural properties of clays-nanocomposites membranes

Hybrid membranes were synthesized by solution intercalation with different filler loadings: 1, 3, 6 and 9 wt% with respect to the Nafion polymer. Details of the preparation procedure are in the paper in the appendix to the thesis.

Depending on the strength of interfacial interactions between the polymer matrix and the inorganic materials, three different types of nanocomposites are thermodynamically achievable, as shown in Figure 4.1: (1) conventional composites, where packages of silicate layers, keep their stacking, creating a conventional phase separated composite

(microcomposite), (2) intercalated nanocomposites, where the polymer chains are intercalated between the silicate layers, therefore increasing their gallery height but maintaining their layered stacking, resulting in a well ordered multilayer with alternating polymer/silicate layers, (3) exfoliated nanocomposites, in which the individual clay layers lose their stacking and are exfoliated and dispersed in the continuous polymeric matrix⁸. The conventional procedures to prepare these nanocomposites include: i) solution^{9, 10}, ii) melt intercalation¹¹, where the polymer intercalate to the interlayer space from solution or melt respectively and iii) in situ polymerization¹², where the polymerization is started inside of the clay galleries. Melting intercalation is more industrial than the solution; however the exfoliated clays, incorporated into the polymeric matrix, have obtained easily and effectively by solution intercalation¹³.

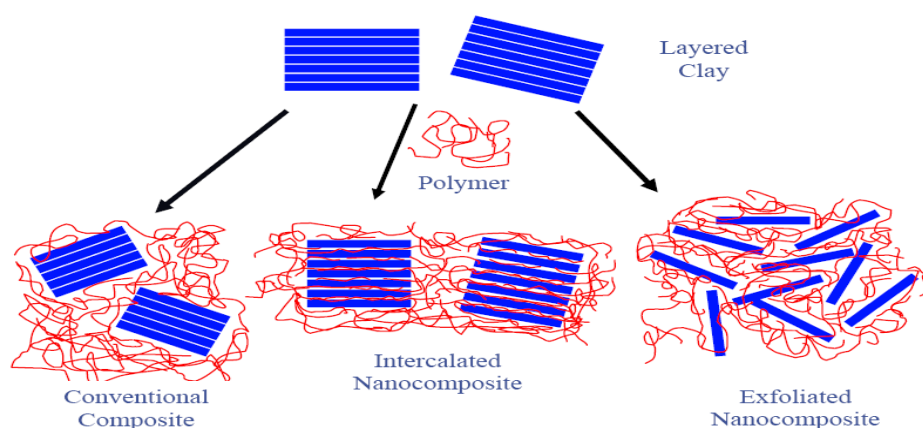


Figure 4.1.1: Image describing the three types of clay-polymer composites: conventional composites (or microcomposites), intercalated nanocomposites and exfoliated nanocomposites

X-ray diffraction (XRD) measurements provide a powerful tool to evaluate the type of composites created after the incorporation of the inorganic layered nanofillers in the Nafion matrix. Figure 4.1.2 shows the XRD patterns of the recast-Nafion and of three nanocomposites with KUN, SWy-2 and Lap at the same filler to polymer loading (3 wt%). In the case of KUN and SWy-2 Nafion nanocomposites, a 001 reflection appeared at 7° due to the presence of packages of ordered aluminosilicate layers in the mass of the polymeric matrix, indicating probably the creation of micro-composites (conventional composites) when using these two montmorillonites as fillers. However, the intensity of the 001 peak in SWy-2 nanocomposite is significant lower than that of

Kunipia nanocomposite, implying that only a small fraction of clay platelets retains its stacking while the majority is existing in fine dispersion between polymer chains (partially exfoliated). On the other hand, in the case of Laponite, the absence of the d_{001} diffraction peak in the pattern of the final nanocomposite, characteristic of the sodium-Laponite, indicates that the ordered structure of the layered mineral is effectively eliminated after mixing with the polymeric mass.

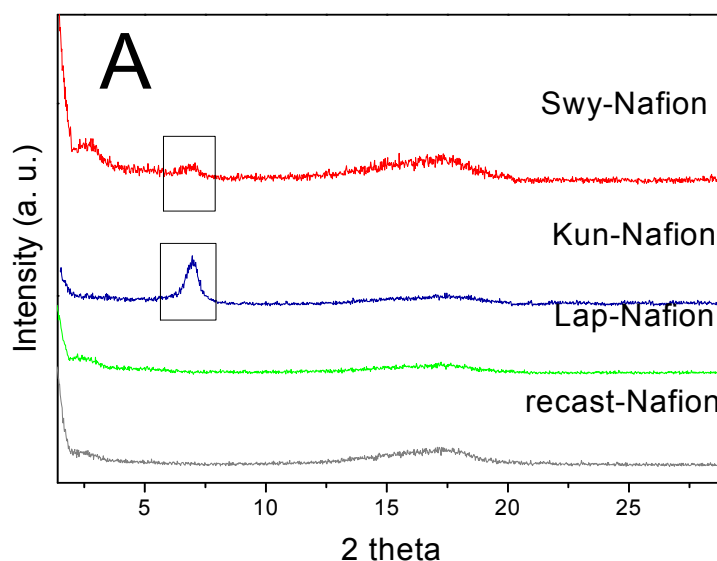


Figure 4.1.2: XRD patterns of recast Nafion and nanocomposites membranes prepared with KUN, SWy-2 and Lap.

4.1.2. Water transport properties in clays-based PEM

The membrane water retention (uptake%) was calculated as:

$$\text{uptake\%} = [(m_{\text{wet}} - m_{\text{dry}}) / m_{\text{dry}}] \times 100.$$

The dry mass (m_{dry}), was measured by drying the sample in a vacuum oven at 80°C for 2 h. The wet mass (m_{wet}) was determined after immersion of the dried sample in distilled water at 30°C for 24 hours. The dimensional variations were calculated at the same conditions of water uptake, by measuring the thickness, the width and the length variation between the dried and wet samples. The transport properties of water molecules confined in the porous structure of the Nafion membrane and the effect of the clay-fillers added was studied by PFG-NMR technique. Figure 4.1.3 displays the

plot of the water self-diffusion coefficients measured on completely swelled membranes (at their maximum water uptake), in the temperature range 25-140 °C. Kunipia composite, similarly to the recast Nafion shows a sudden decrease of the diffusion after 60 – 80 °C, due to loss of water from the membrane. This abrupt drop of the diffusion is hypothesized to be related to the inability of the membrane to retain water at high temperatures jointly with the pore/channel structure of the membrane, where the Kunipia particles, not exfoliated, block part of the hydrophilic polymer channels, through which water molecules migrate. The blocking effect becomes a significant factor just when the water content is low, i.e. when the hydrophilic domains sizes are reduced and therefore, big particles can obstruct the water molecules pathways. On the contrary, Laponite and SWy-2 nanofillers show a significant effect on the water mobility with diffusion values very high and in all temperature range investigated.

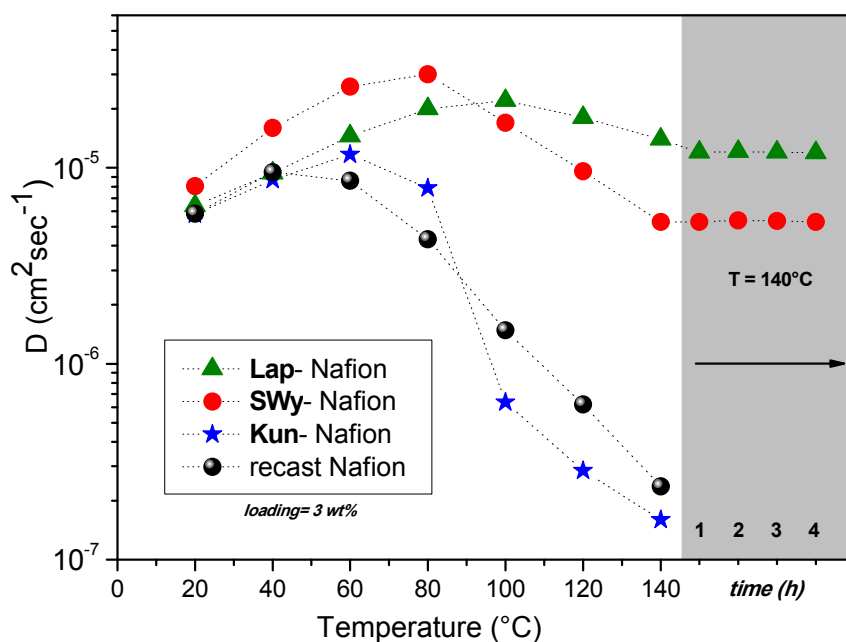


Figure 4.1.3: Self-diffusion coefficients as function of the temperature of the water confined in recast Nafion and in clay composites membranes. The grey part in the graph shows the self-diffusion coefficients measured at 140 °C after each hour for 4 h.

Above 100 °C, the biggest contribution to the diffusion coefficients comes from the hydrated water whereby the mobility is reduced; the obstruction effect causes further reduction of diffusivity, in particular for the SWy-Nafion nanocomposite which, similarly to Kunipia, presents a small amount of big particles not completely exfoliated.

However, the noteworthy result is that both membranes maintain stable water diffusion and unwavering at 140 °C after at least 4 hours and in conditions of not humidification. In fact, for the NMR measurements, the membrane is put in a Pyrex tube and sealed on the top with a Teflon cap, without any further supply of humidification. Obviously, part of the water evaporates from the membrane during the heating (e.g. after cooling we find some little drops on the walls tube), however, the self-diffusion coefficient measured at 140 °C is that of the water remaining in the electrolyte membrane because the water vapor diffuses much more quickly. Therefore, these clay-fillers dispersed in the polymer matrix maintain a certain humidity of the membrane even at rather high temperatures, and this water is responsible for the diffusion revealed by NMR spectroscopy. Further information on the molecular dynamic of the water is provided by measurements of longitudinal relaxation times (T1) (Figure 4.1.4). As described in the experimental section, NMR longitudinal (or spin-lattice) relaxation times (T1), compared to diffusion, reflects more localized motions including both translation and rotation on a time scale comparable to the reciprocal of the NMR angular frequency (~1 ns). As the molecular correlation time τ_c depends on temperature, a minimum in T1 is often observed when $\omega\tau_c \sim 1$, where ω is the NMR frequency. In the temperature range investigated, well above the T1 minimum, i.e., in the so-called extreme narrowing limit ($\omega\tau_c \ll 1$), higher T1 values suggest more facile molecular rotational and translational motion.

Laponite and SWy-2 composites exhibit higher T1 than the recast Nafion and Kunipia composite, quite consistent with the diffusion trends. However, should be underlined once more the exceptional behavior of the Laponite clay that seems favor strongly the local mobility of the water. In fact, even if the water content is less than SWy-Nafion composite, its relaxation times are very high respect both recast Nafion and the other composites and, as saw before, this is reflected on the long-range diffusion properties, i.e. displacements of the order of the micron. In fact, the proton transport process in membranes, such as Nafion, is generally hypothesized (see chapter 1.5) as the contribution of two conduction mechanisms: the *Vehicle mechanism*^{14, 15} that involves the protons diffusion on a vehicle, such as H_3O^+ ions, but disadvantaged in dehydration state, and the *Grotthus mechanism*¹⁶, where proton mobility in water is connected to rotation of water molecules within a constantly changing network of hydrogen bonds (*structural diffusion*). The first one prevails at low temperatures when the water content

is high, while the second mechanism is expected to be predominant at high temperatures in the dehydration state, therefore, it is surely favorite in the Laponite composite that shows the highest longitudinal relaxation times. A last consideration about the T_1 measurements is that the particle blocking effect is less important as T_1 reflects localized motions. This is consistent with the much smaller magnitude of T_1 drop than that of D .

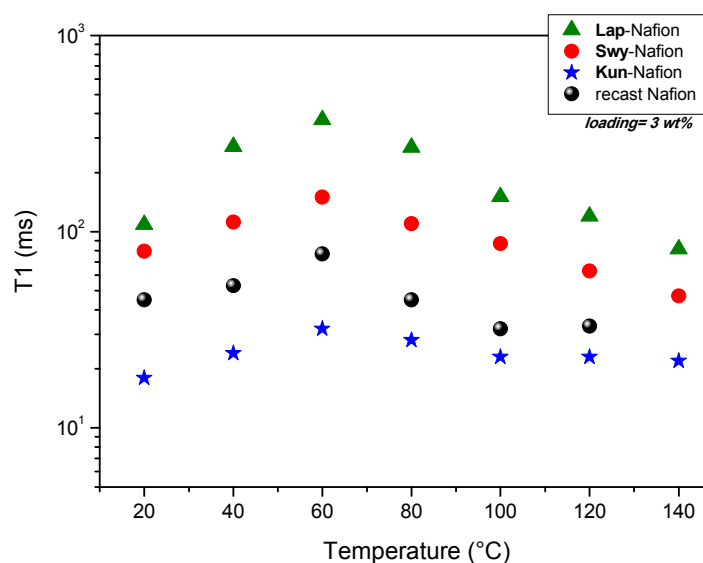


Figure 4.1.4: Plots of water longitudinal relaxation times (T_1) measured in the temperature range from 20 °C up to 140 °C for recast Nafion and composite membranes at the maximum water uptake.

Investigation on the effect of the amount of the filler in the final hybrids (filler loading), suggests, once more, that the microstructure of the composite plays a significant role. In fact, further addition of filler, from one side strengthens the polymeric matrix and thus improves the mechanical properties of the membrane¹⁷, from the other side clearly causes obstruction effects limiting the mobility of the water in the Nafion ionic domains. This optimum loading is in agreement with previous studies on Nafion-clay nanocomposite membranes which showed that the optimal ionic (proton) conductivity, methanol permeability and cell performance is also observed between 2.5 and 5 wt% nanoclay content¹⁸⁻²⁰. This can be explained by the fact that at lower nanoclay loadings, somewhat better intercalation/exfoliation can be expected while at higher loadings, further dispersion of clay platelets is hindered, most probably due to percolation phenomena^{21, 22}.

4.2 Clay-Nanocomposites for direct methanol fuel cells (DMFCs) (paper II)

Hybrid membranes with Laponite and SWy-2, were investigated for their possible use as polymer electrolytes in direct methanol fuel cells (DMFC). In the development of new low temperature PEMs for use in the DMFC, two of the main concerns are proton-ion and methanol-transport through the membrane. The objective is to significantly reduce the methanol transport whilst having and maintaining high proton transport. The research concerning the polymer electrolytes is aimed to the development hybrid morphology in order to promote the *Grotthus*²³ jump proton transport mechanism and minimize the *Vehicle mechanism*^{14, 15}

The electrolyte membranes were swelled by immersion in pure methanol, pure water, and in aqueous methanol solutions at two different alcoholic concentration, 2 M and 4 M. The transport properties of the water and methanol within the electrolyte membranes have been investigated both as a function of methanol concentration and as a function of temperature by NMR methods. Furthermore a preliminary electrochemical characterization was carried out by CNR-ITAE (Messina, Italy), by using ac-impedance spectroscopy and polarization measurements, in order to validate the NMR results.

It is often possible in methanol–water mixtures to resolve spectroscopically the methyl and hydroxyl protons in an NMR experiment which, in principle, should permit the measurement of both water and methanol diffusion. However, in the present case of solvents confined in membranes, due to the linewidth of the ¹H-NMR signals, it is not possible to distinguish, through their chemical shift, methanol and water (see Figure 4.2.1).

In order to discriminate between the NMR signals of methanol and water, the membranes were equilibrated in solutions prepared with deuterated molecules, i.e. mixture of CH₃OD/D₂O and CD₃OD/H₂O. The reason to use CH₃OD instead of CH₃OH is due to the fast rate exchange of hydroxyl groups between water and methanol molecules during the "NMR times", which could affect the measurements. Hence, is used the only NMR signal coming from the methyl groups of methanol. With regard to the deuterium signal, this nucleus has a spin-spin relaxation time (T₂) very

short so it is practically unable to perform measurements of diffusion through the PGSE sequence.

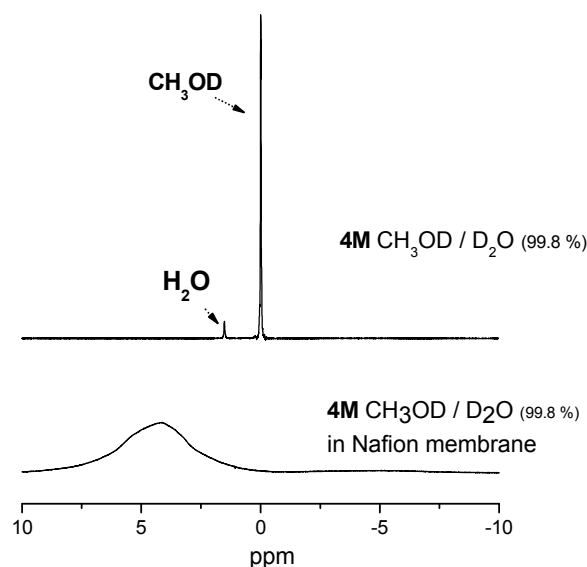


Figure 4.2.1: ¹H-NMR spectra recorded on 4 M aqueous methanol solution (CH₃OD/D₂O) as prepared and confined in Nafion membrane, respectively. The chemical shift variation of the methanol's signal is caused by the different chemical environment and the strong interactions with the polymer backbone.

Table 4.2 reports the solvents and mixtures used to swell the membranes for the NMR study; the solvent marked in bold, is that "seen" to NMR.

Table 4.2. Solvents and solutions used to prepare swollen membranes for the NMR study	
<i>solvents</i>	<i>concentration</i>
CH ₃ OD	pure
H ₂ O	pure
CH ₃ OD / D₂O	2M
CD₃OD / H ₂ O	2M
CH ₃ OD / D₂O	4M
CD₃OD / H ₂ O	4M

The temperature evolution of the diffusion coefficients of pure water and methanol (in 2 M and 4 M solution) inside the swollen membrane of filler-free Nafion are displayed in Figure 4.2.2. The methanol diffusion is slightly lower than water up to 60 °C but,

over this temperature, it remains always higher. This behavior, responsible of the methanol cross-over in the fuel cell operation, can be explained by considering the distribution of the solvents (water and methanol) inside the ionic pores of Nafion membranes and the transport mechanism involved in the water/methanol diffusion. During the swelling, a certain amount of water is involved in the primary hydration shells of the SO_3^- groups, while most of the additional water fills the volumes of pores forming higher order hydration layers and behaves more bulk-like^{24, 25} Methanol molecules are, instead, collected adjacent to the polymer backbone with a less favorable complexation of protons as compared to that by water^{26, 27}. In other words, as reported in other studies^{26, 28}, a micro-phase separation occurs, where water-rich and methanol-rich spatial domains are created, presumably with a characteristic size in the order of the Nafion pore size.

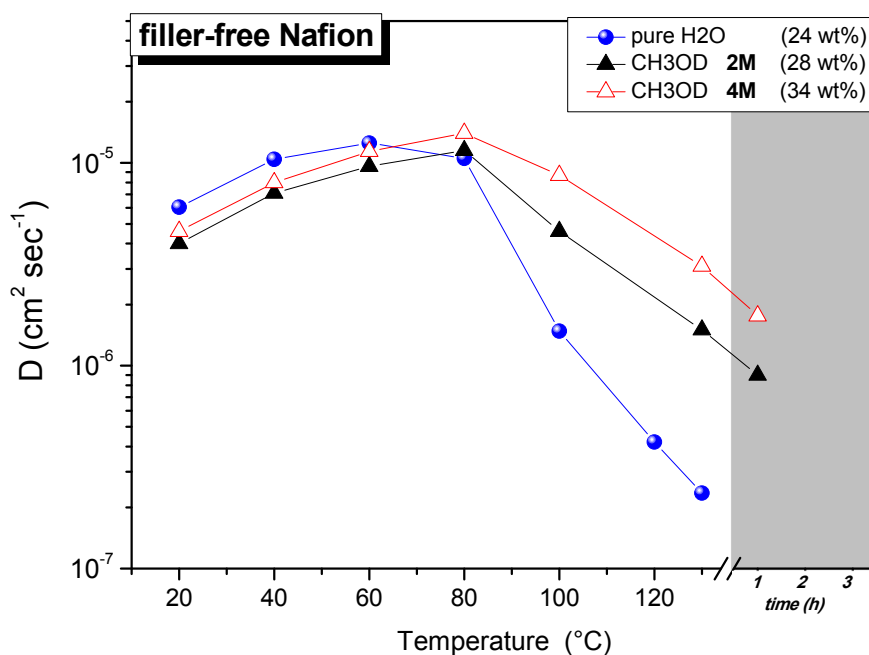


Figure 4.2.2: Self-diffusion coefficients of water and methanol (2 M and 4 M) confined in filler-free Nafion membranes from 20 °C up to 130 °C; the data collected at 130 °C after 1 hour is also plotted. In the legend the water and solution uptakes are indicated.

In this description, as it is schematically presented in Figure 4.2.3, the molecules of methanol interacting with the polymer, and in particular with fluorine atoms on both

the backbone and the side-chains, are distributed on the surface of the pores, while the water molecules are at the center acting, in the maximum swelling conditions, as bulk-like water. This scenario is consistent with: i) the higher methanol diffusion respect to the water at high temperatures; ii) the increase of the swelling (higher uptake of the 4 M solution) and also of the methanol diffusion coefficient with increasing methanol concentration.

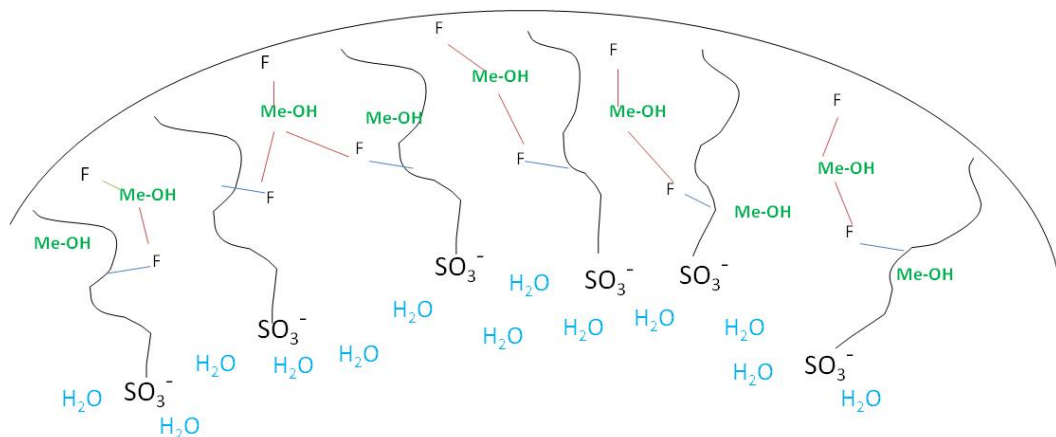


Figure 4.2.3: Schematic illustration of methanol and water molecules distribution inside the ionic pores of the polymer (Nafion).

Figure 4.2.4 shows the diffusion of water and methanol in 2 and 4 M solutions, measured in swollen Swy/Nafion and Lap/Nafion nanocomposite membranes, from 20 °C up to 130 °C. Concerning the Swy/Nafion composite, water diffusion is always higher than methanol in the whole investigated temperature range and for both solution concentrations. Swy montmorillonite particles inside the membrane demonstrate to be a potential physical barrier for methanol cross-over, reducing the methanol diffusion with an evident blocking effect and nevertheless ensuring a high water mobility up to 130 °C and for several hours. Laponite nanocomposite membrane showed a different behavior both for water and methanol with respect to Swy. Basically, the mobility of the methanol is not influenced by the solution concentration and is very similar to that of water and suggests that no relevant obstruction effect from Laponite nanoparticles acts on the methanol transport. The origin of this behavior can be correlated to the lower cationic exchange capacity (CEC) of Laponite clay compared to Swy montmorillonite.

Fewer hydrophilic sites "coordinating" produce the lowering of the retention capacity of the membrane and consequently the water diffusion is reduced. In particular, when we start with lower amount of water (i.e. 4 M solution), what remains at high temperature is strongly linked water.

We obtained more information on the solvents distribution in the membrane (hydration and interactions) as well as on the evaporation dynamics, by analyzing the $^1\text{H-NMR}$ spectra of methanol and water with the temperature increasing. Figure 4.2.5 put in comparison the spectral lines of methanol (on the left) and water (on the right), acquired on Swy/Nafion swollen in 2 M methanol solution, from 20 °C up to 130 °C. Both signals are large and asymmetric, typical of a multiple components configuration, however, the FWHM (full width at half maximum) of the water and methanol spectra are quite different: 675 Hz against 1170 Hz at 20°C, i.e. the line width of methanol is almost double of the water. This implies that, while for the water there is a strong component of bulk which contributes to the "shrinkage" of the spectral line, the molecules of methanol instead are strongly interacting with the polymer (the "complexation" referred above) promoting a broadening of the line, as well as reducing their mobility (diffusion). By heating, the intensity of these peaks decreases because of the solvents evaporation from the membrane, with a pronounced drop above 100 °C; at 130 °C the intensity of the residual signal remains constant for several hours (obviously without any supplying humidity), and this is responsible for both the proton and methanol diffusion that we are able to detect at these high temperatures.

The discussion of the data just analyzed is complex but definitely indicates that the microstructure plays a key role in the mass transport of water and methanol. The microstructure is influenced by the chemical-physical properties of the smectite clays such as the nanoparticles size and the layer charge density. In fact, higher platelets dimensions may promote stronger alterations of the network structure as well as create an obstruction effect, while a high value of surface charge density may facilitate or promote the proton transport through hopping mechanisms.

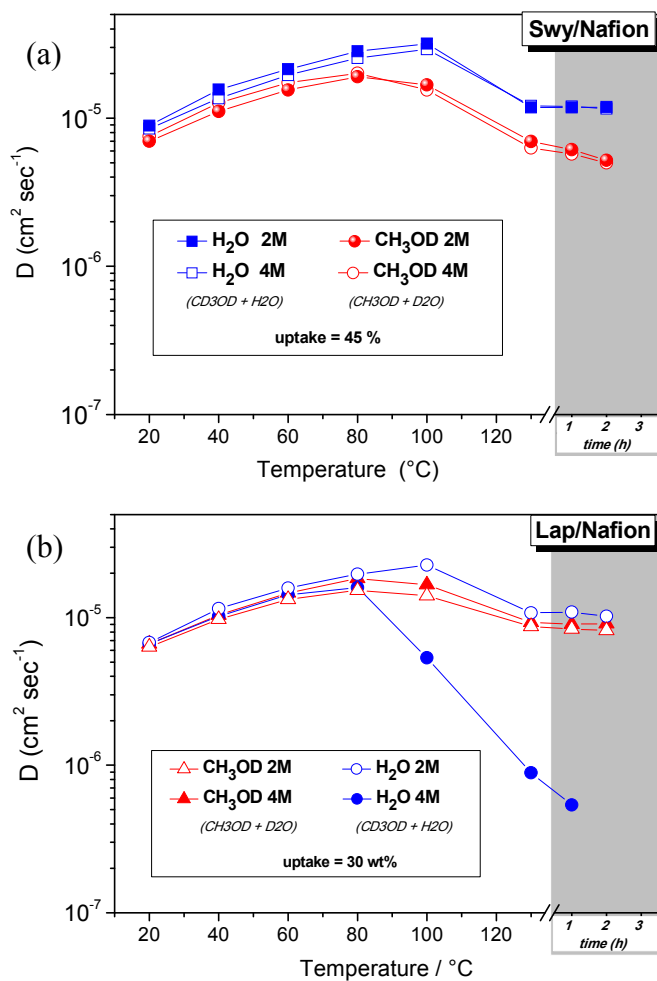


Figure 4.2.4: Self-diffusion coefficients of water and methanol in 2 M and 4 M solutions confined in (a) Swy and (b) Laponite nanocomposite membranes, from 20 $^\circ\text{C}$ up to 130 $^\circ\text{C}$.

In the diffusion graph are also plotted the data collected at 130 $^\circ\text{C}$ after some hours.

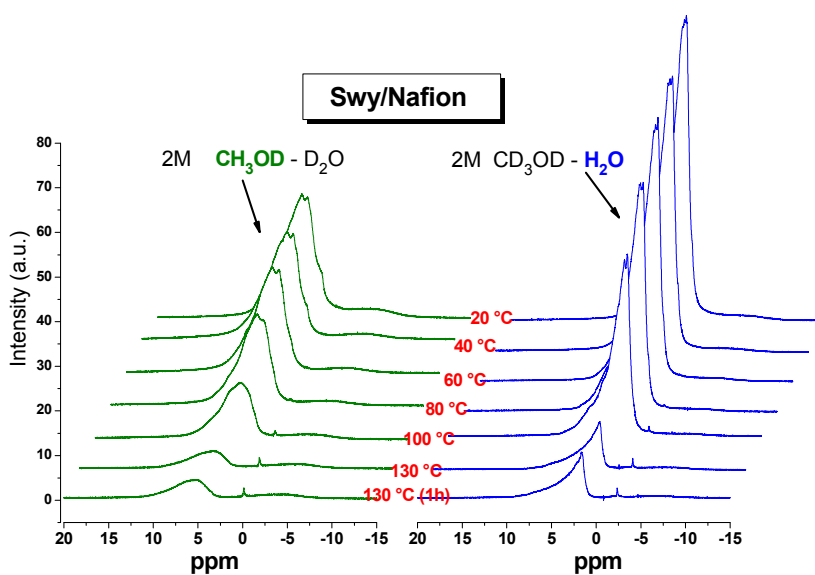


Figure 4.2.5: Evolution of proton spectra from methanol (on the left) and water (on the right) as a function of temperature on Swy/Nafion composite swollen in 2 M methanol solution. The spectra were referenced setting methyl protons and pure water at 0 ppm, respectively.

Concerning the electrochemical investigation, Figure 4.2.6 shows the polarization and power density curves obtained with the different membranes at 90 °C and 110 °C: the filler-free Nafion-based cell showed a drop of performance with the temperature due to water evaporation and the consequent increase of cell resistance.

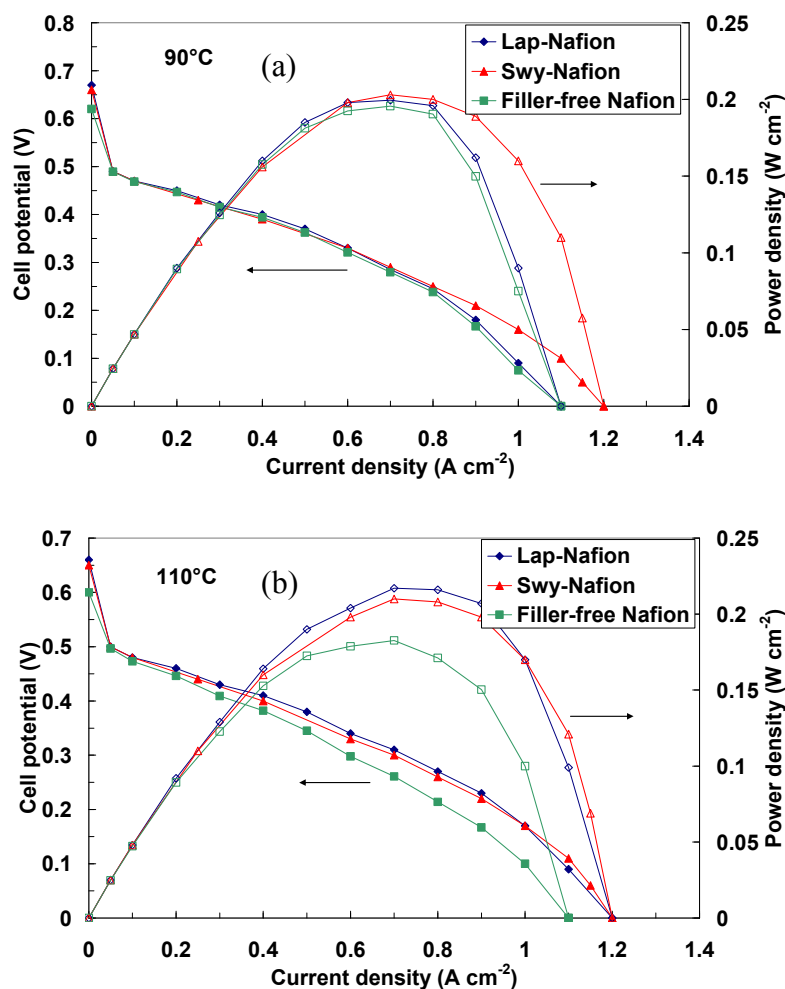


Figure 4.2.6: DMFC polarization and power density curves at (a) 90°C and (b) 110 °C for various membrane-electrode assemblies equipped with composite and filler-free membranes.

We conclude that, despite the obstruction effect due to the dispersion of suitable hydrophilic layered nanoparticles in Nafion, the main contribution to the diffusion of methanol is its high uptake in the polymer. In fact, the solution uptake in Swy-composite (45 wt%) highlight a strong swelling membrane effect demonstrating the high chemical affinity of the methanol towards the polymer that allows a diffusion, even if lower than water, up to temperatures above 100 °C and that increases with increasing methanol solution concentrations. Therefore, to enhance the performance and the efficiency of a DMFC, it is necessary to develop membranes which absorb less methanol while maintaining, however, a high proton conductivity.

4.3 Organo-modified Clays for HT-PEMFCs (paper III)

As a consequence from all the above, the synthetic Laponite and the natural SWy-2 montmorillonite clays, seem the most promising smectite clays that can be used as fillers and thus it could be the base to design, through chemical functionalization, hybrid layered structures such as organically modified clays (organoclays)²⁹ which can be use as nanofillers for the creation of novel polymer nanocomposites (*paper III*).

The monovalent ions located between the clay layers allow the absorption of polar solvent, like water, with good retention capacity so, when incorporated into a polymer membrane, they help to prevent the loss of the hydration water not only at high temperatures but also under low relative humidity environment. The charge on the layers affects many fundamental properties of the clays, including water holding (an important property for the creation of Nafion nanocomposite membrane), cation fixation, swelling ability, cation exchange capacity and high surface area. Moreover, the properties of the smectite nanoclays can be tailored using simple chemical methods such as intercalation with organic or inorganic guest molecules.

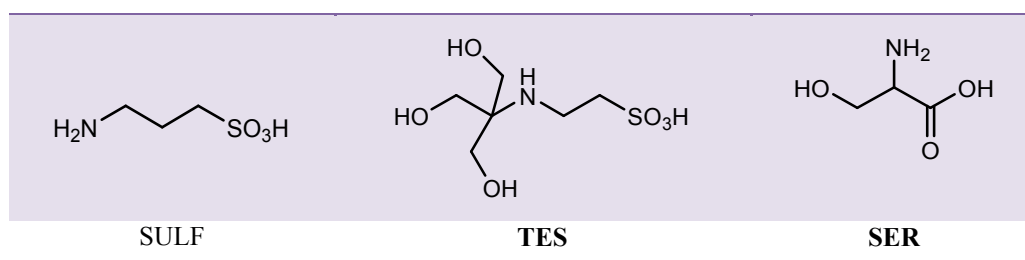
As a result the presence of the surfactant expands the interlayer gallery rendering the nanoclay compatible with hydrophobic media and polymer matrices. Thus a strategy towards the improvement of the water retention of the Nafion membrane is the incorporation in the polymer matrix hybrid nanofillers of modified clays bearing organic functionalities with high affinity for Nafion and increased sites for water trapping.

4.3.1 Preparation of organo-modified clay nanofillers

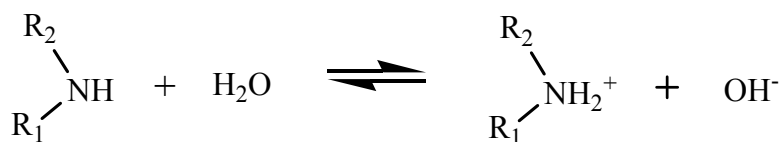
For the chemical modification of the pristine Laponite and SWy clays, three organic molecules were used: 3-amino-1 propanesulfonic acid (**SULF**), 2- {[2-hydroxy-1,1 bis(hydroxymethyl) ethylamino} ethanesulfonic acid (**TES**) and serine (**SER**). Their structural formulas are shown in Table 4.3.

For the preparation of the organoclays, aqueous 1 wt% clay suspensions were reacted under vigorous stirring with aliquots of the above organic molecules solutions in water such that the amount of the cationic molecule added to corresponds three times the CEC of the clay. The mixtures were stirred for 24 h, centrifuged, washed with water, and air-dried by spreading on glass-plates. The products are designated: **SWy/TES**, **SWy/SER**, **SWy/SULF** and **Lap/TES**, **Lap/SER**, **Lap/SULF**.

Table 4.3: Organic molecules used for the chemical modification of SWy and Lap clays.



For the surface modification of the parent smectite clays a simple procedure was followed. Positively charged molecules are introduced into interlayer space of layered clay minerals by ion exchange procedure where charge balancing cations (e.g. Na^+) are replaced by the organic cations. The introduced organic cations are held strongly by electrostatic forces with the negatively charged clay surfaces and the final conformation depends on the shape, size, and total charge of the organic cations and also on the charge density of the clay surface. In our case, the intercalation procedure involves an initial pre-equilibrium reaction the amino groups of the organic molecules are protonated:

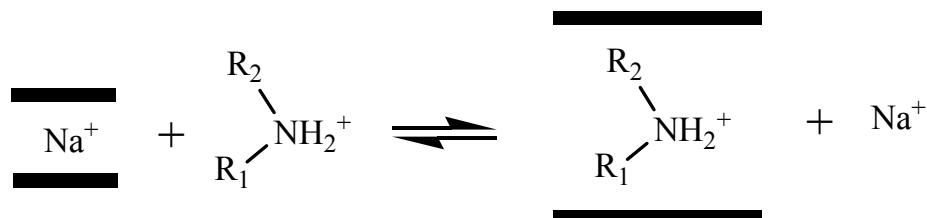


where: (i) for SULF R_1 : $-(\text{CH}_2)_3\text{SO}_3\text{H}$ and R_2 : $-\text{H}$;

(ii) for TES R_1 : $-(\text{CH}_2)_2\text{SO}_3\text{H}$ and R_2 : $-\text{C}(\text{CH}_2\text{OH})_3$

(iii) for SER R_1 : $-\text{C} \begin{array}{l} \text{CH}_2\text{OH} \\ \text{COOH} \end{array}$ and R_2 : $-\text{H}$

The protonated organic molecules were readily adsorbed on the clay surfaces, by ion exchange. The monovalent Na^+ exchangeable cations are replaced easily by the protonated amino molecules according to the reaction:



4.3.2 Properties of SWy-organoclays nanocomposites

SWy-2 montmorillonite and its organoclays demonstrate a considerable effect on the Nafion polymer in terms both of water absorption/retention and water mobility. In fact, if we observe the Figure 4.3.1, the water uptake of the nanocomposites is almost double respect to the recast Nafion, while swelling data (not reported here) show that the dimension is not significantly affected.

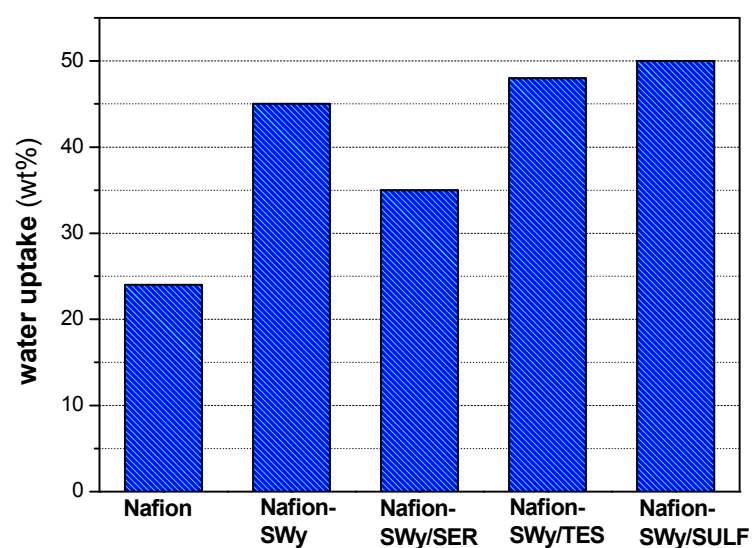


Figure 4.3.1: Histogram of maximum water uptake of filler free Nafion and SWy-composites.

Concerning the water diffusion inside the membranes, data are displayed in Figure 4.3.2. The presence of the clay nanofiller, both with and without surface modification, produces a noteworthy improving of the membranes performances compared to recast Nafion.

In fact, if we observe the water diffusion coefficients of Nafion-SWy/TES and Nafion-SWy/SULF, they increase quasi linearly up to 100 °C reaching values more than one order of magnitude higher than filler free Nafion. At 130 °C is clear a slight decreasing of the diffusivity caused from the water evaporation from the membranes. However, it is extremely significant the behavior of such nanocomposites in this temperature's region since the self-diffusion coefficients remain constants for several hours at quite high values. The reduction of the diffusivity after 100 °C, despite the increase of the temperature, can be explained by considering that the hydrophilic pores of Nafion polymer and the acid nature of the organoclay particles provide numerous proton exchange sites in the polymeric system. Therefore, the water self-diffusion coefficient measured is a weighted average from the different water species coexisting (bounded or hydrated water and bulk water^{30, 31}) in fast exchange rate with respect to the NMR times. In heating, it is reasonable to expect that the evaporation essentially affects the bulk/"free" water, i.e. the most mobile water so, after 100 °C, the biggest contribution to the diffusion comes from the hydrated water resulting in a lower *D*. In any case, stating that in these measurements there is no additional humidification of the membranes, it denotes that this clay material can retain water and thus can maintain a certain level of humidity in the membrane and surface modifications with acid organic molecules significantly improve the performance of the final composite system.

Figure 4.3.3 shows the ¹H-NMR spectra acquired on Nafion-SWy/TES from 20 °C up to 130 °C. The proton's signal is quite large (FWHM is about 1 kHz) and asymmetric, typical of a multiple components configuration, i.e. different "types" of water coexist in the system. Actually, a certain amount of water is involved in the primary hydration "shells" of the SO₃⁻ groups of Nafion^{32, 33} as well as of the organo-modified filler's hydrophilic groups (oxygen and hydroxyl surface groups of clay and hydroxyl, amino and sulfonic groups of TES). The uptake of additional water fills the volumes of membrane's pores forming higher order hydration layers and, experiencing negligible electrostatic interactions, behaves more bulk-like. The different states of water within the hydrophilic pores can be difficult to discern because of the fast rate of

proton exchange in acidic water and for this reason we “see” only one peak. The intensity of this peak decreases with increasing temperature because of the water evaporation from the membrane, with a pronounced drop above 100 °C; when it reaches 130 °C, the intensity of the residual signal remains constant for several hours (obviously without any supplying humidity), and this is responsible for the proton diffusion that we are able to detect at these high temperatures.

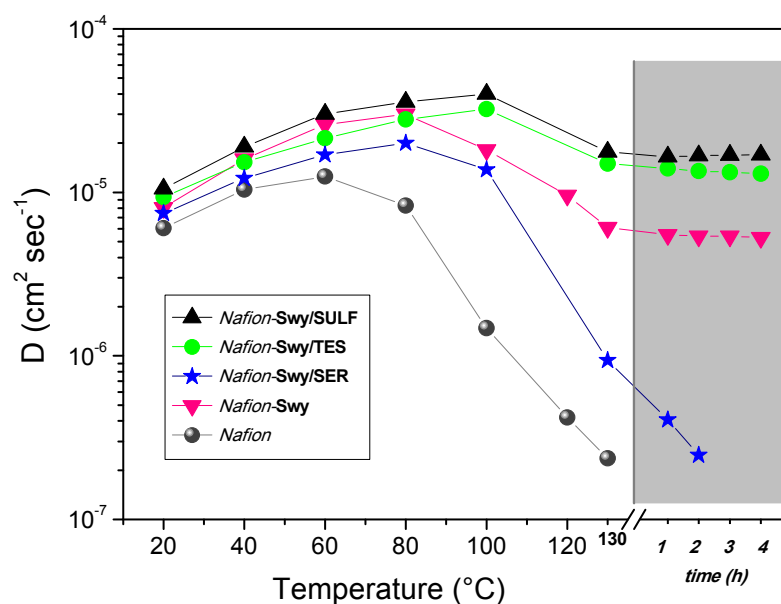


Figure 4.3.2: Self-diffusion coefficients of water confined in Nafion nanocomposite membranes based on SWy pristine clay, SWy/organo-modified clays and filler-free Nafion for comparison, from 20 °C up to 130 °C. In the graph are also plotted the data collected at 130 °C after several hours.

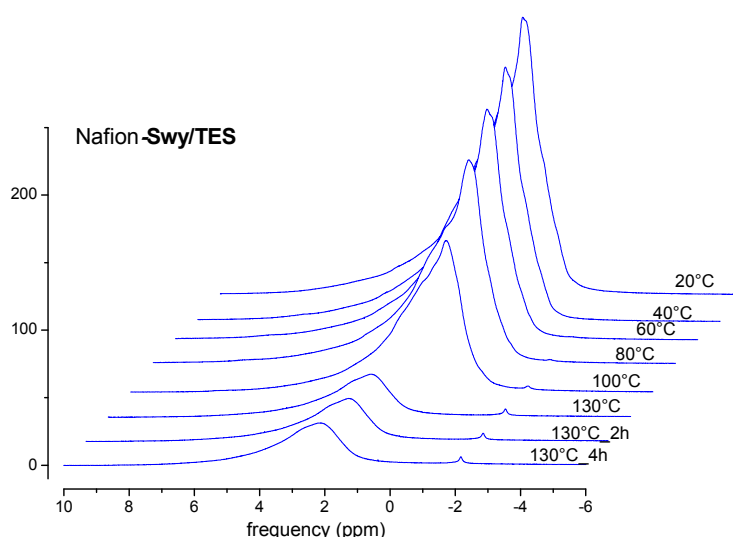


Figure 4.3.3: Temperature evolution of high-resolution ^1H NMR spectra of the water confined in Nafion-Swy/TES nanocomposite acquired from 20 °C up to 130 °C (at this last temperature also after 2 and 4 h).

In all the spectra, until 100 °C, this asymmetrical signal (Figure 4.3.4 A) can be fitted well to the experimental data with three Lorentzian peaks, one narrower (*peak-1*), attributed to the bulk-like water, and two broader (*peak-2* and *peak-3*), assigned to the bound water, i.e. the hydration water to the sulfonic acid groups of both the Nafion and TES molecules, and to the clay's hydrophilic groups, respectively. This peak-picking is argued from the broadness and area of the peaks: at room temperature, the amount of bulk water in completely swelled membranes is surely predominant and having less restricted molecular motions, results in a linewidth reduction. Furthermore, it is obvious that the water evaporation involves mainly the bulk water, in fact, at 130 °C, its contribution to the NMR signal (*peak-1*) disappear while the two broader components are still observed by peak-fitting. By considering the area of these three peaks we estimate that the amount of water lost from the membrane at 100 °C is about 46 wt% of the total water initially absorbed. From this amount, 23 wt% arises from *peak-1*, 17 wt% from the *peak-2* and about 6 wt% from the *peak-3*. At 130 °C only about 18 wt% of water remains in the membrane, shared between the hydration to the SO_3^- groups of the polymer and the hydrophilic clay surfaces (*peak-2* and *peak-3*), while the bulk water is completely evaporated. The variation of the areas of these three peaks as a function of temperature is showed in Figure 4.3.4 B. Up to 100 °C, the area of all signals decreases even if the *peaks 1* and *2* show a greater reduction than *peak-3* (which remains almost unchanged), while at 130 °C the proton spectrum is fitted by only two peaks (*2* and *3*) and their area remains constant for several hours. It is also interesting to show the trend of the chemical shift of the spectral signal, and hence of the three peaks fitting, with the temperature (Figure 4.3.4 C). By comparing with the area's plot, a certain correspondence is noticeable: there is a downfield shift of the resonance during the heating and an abrupt change after 100 °C. This is obviously caused by the strong evaporation of water from the membrane, which in turn causes a structural change of the system (hydrophilic pores size and redistribution of water), but most likely there is also an effect due to the glass transition of the polymer (the T_g of Nafion®-112 membrane is around 110 °C). However, at 130 °C the chemical shift of the signal remains invariable for several hours, indicative of the fact that no important altering, e.g. ulterior water leaking, is happening in the system.

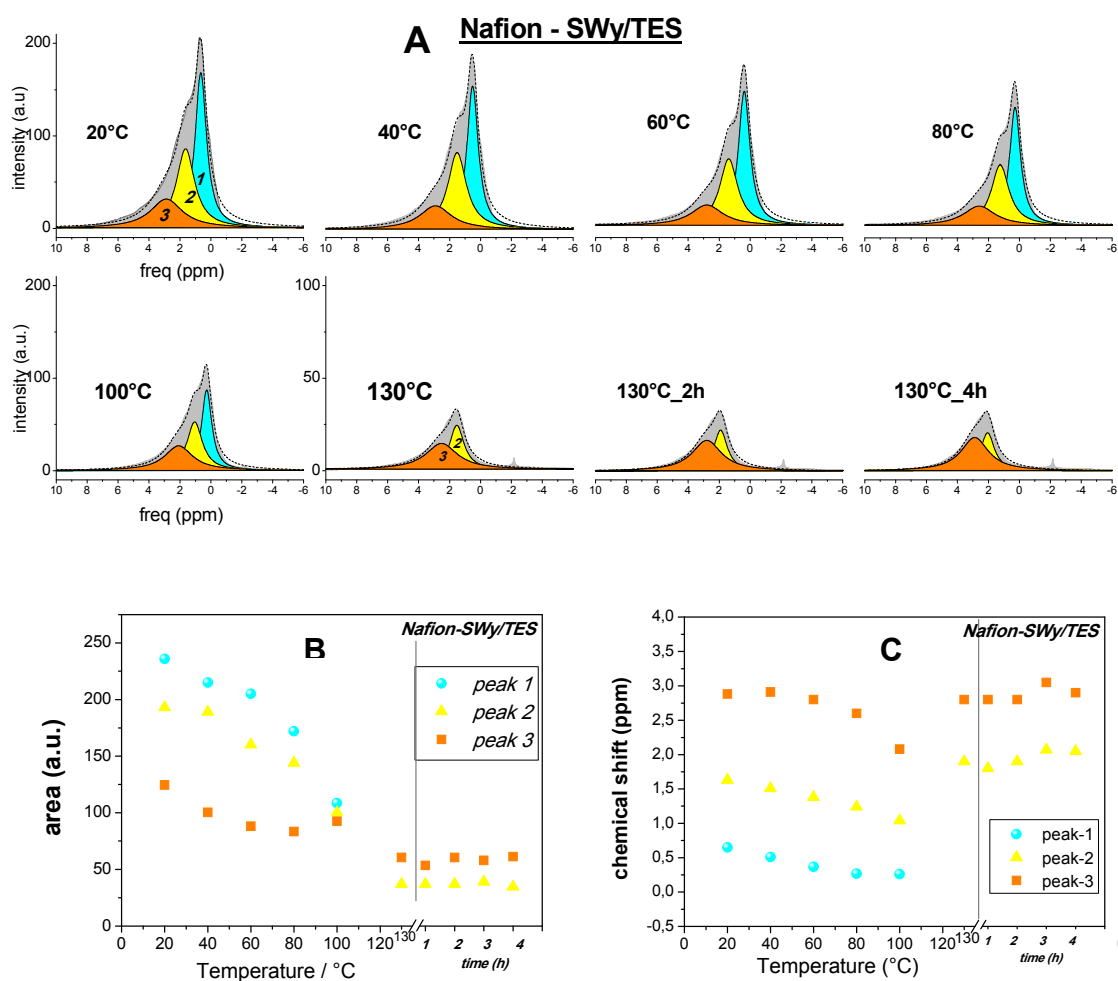


Figure 4.3.4: (A) Peak-fitting of the ^1H NMR spectra of the water confined in Nafion-SWy/TES nanocomposite; (B) plot of the areas of three peaks (resultants from the peak-fitting) vs temperature; (C) chemical shift of the three peaks (resultants from the peak-fitting) vs temperature.

At this point a quantitative analysis was made, starting from these spectral data to estimate the number of water molecules involved in the hydration shell of the sulfonic acid groups of Nafion polymer as well as that absorbed on the organoclay nanoparticles. Taking into account the complexity of the system and to the hydrogen-bonding effects which the protons are subjected, establish the exact chemical shifts is arduous, however, by considering the concepts of electronegativity (of oxygen and sulfur atoms) and proton acidity, the resonance frequency of the protons (of the water) on the clay's surface is expected downfield shift respect to protons hydrating the sulfonic groups. Therefore, we can most likely attribute *peak-2* to the water molecules

hydrating the SO_3^- groups ($h_{SO_3^-}$) and the *peak-3* to the water molecules absorbed on the organo-modified clay particles (h_{clay}). The moles of SO_3^- groups present in the Nafion/Swy-TES system originate almost entirely from Nafion and only for a negligible amount from TES molecules used to functionalize the montmorillonite clay. Even with an overestimation, i.e. by considering that the stoichiometric amount of TES (which corresponds to three times the CEC of the clay) is all intercalated in the clay, and by considering the filler to polymer loading (3 wt%), this quantity is about 6 % of the total moles:

$$mmoles\ of\ SO_3^- = (0.2\ from\ Nafion) + (0.012\ from\ TES\ (3\ wt\%;\ 3\ CEC)) = 0.212$$

Table 3 reports a schematic description of the water distribution in the system taking into account the initial water uptake of the membrane (5.5 mmoles) and the areas ratio of the peaks at 20 °C and then at 130 °C. The hydration numbers obtained by this calculation, about 9 H_2O/SO_3^- mol/mol in the maximum hydration state and 1.8 H_2O/SO_3^- mol/mol in the very low hydration state, are in agreement with the literature,^{34,35} therefore, the peak fitting and the related attributions are appropriate.

Table 3: Water distribution and hydration numbers in Nafion-Swy/TES nanocomposite system

<p><i>Water uptake 48 wt% → 5.5 mmoles</i></p> <p style="text-align: center;"><u>20 °C</u></p>	<p><i>from the areas ratio of the peaks 1, 2 and 3:</i></p> <p><i>bulk 42.6 wt% → 2.34 mmoles</i></p> <p><i>h_{clay} 22.5 wt% → 1.2 mmoles</i></p> <p><i>$h_{SO_3^-}$ 34.8 wt% → 1.9 mmoles ⇒ $\frac{1.9}{0.212} \cong 9\ H_2O/SO_3^-$ mol/mol</i></p>
<p><i>~18 wt% of the initial water uptake remain in the membrane</i></p> <p style="text-align: center;"><u>130 °C</u></p>	<p><i>from the areas ratio of the peaks 2 and 3:</i></p> <p><i>h_{clay} ~ 11 wt% → 0.6 mmoles</i></p> <p><i>$h_{SO_3^-}$ ~ 7 wt% → 0.38 mmoles ⇒ $\frac{0.38}{0.212} \cong 1.8\ H_2O/SO_3^-$ mol/mol</i></p>

4.3.3 Properties of Laponite-organoclays nanocomposites

Concerning the organo-Laponite based nanocomposites, the diffusion coefficients of the water confined in the various membranes are reported in Figure 4.3.5. The introduction of SULF molecules in the clay's interlayers doesn't improve at all the performance of the composite that, in fact, follows exactly the trend of the first one. The result is even worse when Laponite clay is organo-modified with TES and SER molecules: Nafion-Lap/SER has a collapse of the diffusion around to 130 °C, while Nafion-Lap/SES already at lower temperatures begins to show a loss of the water diffusion. This behaviour could be explained taking into account that the cationic exchange capacity (CEC) of Laponite is lower respect to SWy, therefore, the amount of organic molecules attached to the Laponite's surface is considerably lower than the correspondent organo-montmorillonites. For example the small amount of intercalated TES molecules in Laponite does not alter the hydrophilicity of the final organoclay as results from TG data: the adsorbed water which is 11 wt% in the pristine Laponite is reduced to 7.7 wt% in the case of Lap/SES. This reduction in the hydrophilicity of the nanofiller is probably responsible for bad performance of the organo-Laponite Nafion membranes.

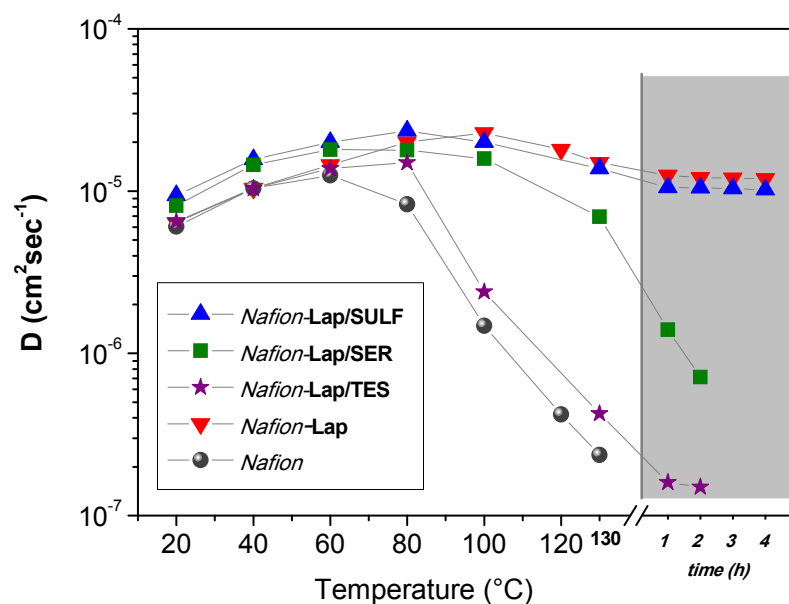


Figure 4.3.5: Self-diffusion coefficients of water confined in Nafion nanocomposite membranes based on Lap pristine clay, Lap/organo-modified clays, and filler-free Nafion for comparison, from 20 °C up to 130 °C. In the graph are also plotted the data collected at 130 °C after several hours.

4.4 Organo-functionalized graphene oxide (GO) – based nanocomposites membranes (**paper IV**)

The development of a nano-dispersion of graphene-based materials in a polymer matrix has opened a new and interesting area in materials science in the recent years.^{36, 37} The pristine graphite is inaccessible in the interlayer space and has a tendency to agglomerate in a polymer matrix³⁸ reducing the use of this material. In order to avoid this problem, the functionalization of graphite by chemical oxidation, creating a hydrophilic graphite derivative with covalently attached oxygen-containing groups (hydroxyl, epoxy and carboxyl) to its layers called graphite or graphene oxide (GO),³⁹ is a particularly attractive solution since it can improve the solubility and processability as well as enhance the interactions with organic and inorganic guest molecules (*paper IV*). GO as well as reduced GO have been used so far as nanoadditives in various polymers such as epoxy resins, polymethylmethacrylate, polypropylene, polyethylene, polystyrene, polyamides but also conductive polymers like polyaniline, poly(styrenesulfonate), Nafion etc, increasing mainly the mechanical, electrical and barrier properties.^{36, 37} At the same time, GO does not exhibit any significant ionic and electronic conductivity⁴⁰ but can be easily converted in a high proton conductor via the intercalation of organic molecules in the interlayer space of GO creating novel hybrid organo-nanofillers with high proton conductivity. This can be implemented by taking advantage of the concept of intercalation chemistry which involves the insertion of suitable and robust organic and/or inorganic species between the layers. Towards this aim, the attachment of organic molecules on the graphene oxide surfaces containing hydrophilic groups such as $-\text{SO}_3\text{H}$, $-\text{COOH}$, $-\text{OH}$ is expected to improve not only the proton conductivity - by increasing the concentration of acidic (hydrophilic) functional groups of GO - of the resulting nanocomposite membranes but also their mechanical, chemical and thermal strength while increases the compatibility with the polymeric membrane.

In my doctoral work, four aliphatic amine derivatives containing various functional groups such as sulfonic, carboxyl and hydroxyl groups were covalently bonded via the amide functionality on the GO surfaces and the resulting organo-modified GO

nanofillers were incorporated in Nafion by solution intercalation (membranes with pristine GO were also synthesized for comparison).

4.4.1 Synthesis of organo-modified GO nanofillers

The first step is the oxidation of graphite powder to aqueous dispersions of graphene oxide by using a modified Staudenmaier's method⁴¹ (details are in the paper IV in appendices). According to elementary analysis data, the C/O atomic ratio of the resulting product was 2.6.⁴²

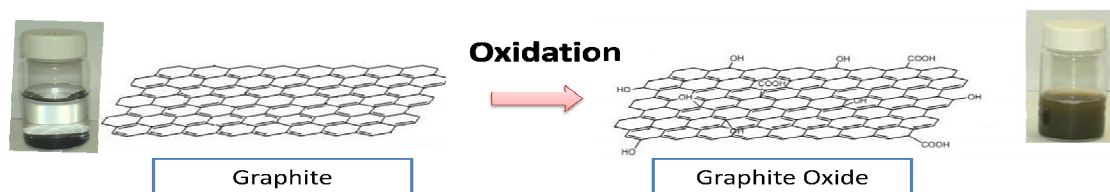


Figure 4.4.1: Chemical oxidation of GO.

Successively, for the preparation of organo-GO nanofillers, we used the same amines utilized for the organo-modification of the clays, reported in Table 4.3. In particular, 100 mg of GO were dispersed in 100 ml water, followed by the addition of aliquots of 300 mg of the above amine derivatives in 40 ml of water. After stirring for 24 h, the organo-modified GO were washed with water, separated by centrifugation and air-dried by spreading on glass plates. A schematic representation of the reactions followed for the organo-modification of GO is presented in Figure 4.4.2. The fillers are denoted as GO-SULF, GO-TES, GO-VAL and GO-SER respectively.

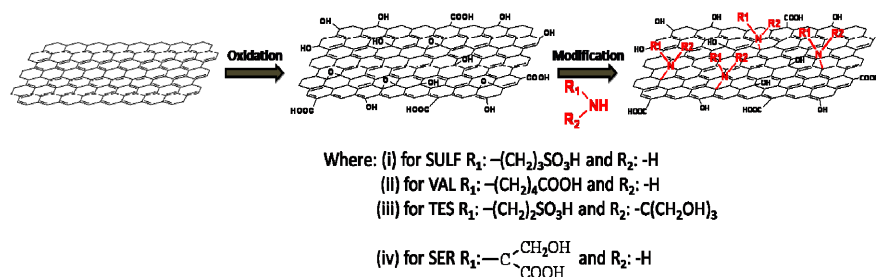


Figure 4.4.2: Schematic representation of the synthetic procedure.

4.4.2 Preparation of organo-GO nanocomposites

The production of a homogeneous colloidal suspension of graphene oxide powder is an important challenge to allow their broad use for both fundamental study and in polymer nanocomposite applications applications.^{3, 40} In this study, the choice of the proper solvent was long and complex but indubitably primary for the preparation of homogeneous and advantageous composite membranes based on this inorganic nanofiller. Organic solvents such as dimethylformamide (DMF) or dimethylacetamide (DMA), which are two of the most widely used solvents for the preparation of nanocomposite electrolyte membranes based on Nafion with various types of fillers, have completely failed in the specific case of graphene oxide materials. Figure 4.4.3 shows characteristic photographs of two GO-based composite membranes prepared by using: (a) DMF (similarly to the clays-composites procedure) and (b) the same solution in which Nafion polymer was dispersed, i.e. a mixture of water and propanol as purchased, to disperse directly the various filler's powders.

As evident, DMF is completely inappropriate to achieve homogeneous dispersion in the polymer matrix, and similar results were obtained by using many other solvents such as DMA, THF, DMSO, acetonitrile, etc but also water. On the contrary, the membranes prepared without any other solvent are quite homogeneous with a uniform dispersion of the nanofiller in the membrane. Likely, this is due to the partially hydrophobic nature of the alcohols that finds greater chemical affinity with the carbon layers of graphene oxide, while the water solvates the hydrophilic groups on the surface. Organo-modified GOs showed the same difficulties, like pristine GO, to be dissolved in these solvents; therefore, all the nanocomposite membranes in this work were prepared by using the method of nanofillers dispersion directly on the alcoholic solution of Nafion.

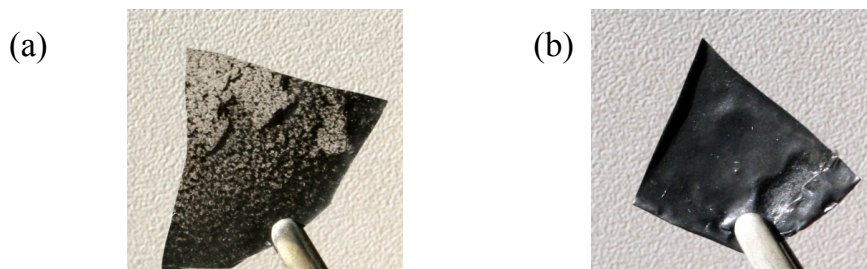


Figure 4.4.3: Photographs of Nafion nanocomposite membranes prepared by dispersing GO in (a) DMF solvent and (b) alcoholic solution of Nafion.

4.4.3 Properties of the organo-GO nanocomposites

First of all, we show the Table 4, with the water uptake values of the prepared nanocomposites, demonstrating the first effect of the fillers.

Table 4

membranes	Water uptake
recast Nafion	24
Nafion/GO	27
Nafion/GO-TES	29
Nafion/GO-SER	29
Nafion/GO-VAL	31
Nafion/GO-SULF	50

Figure 4.4.4 shows the water self-diffusion coefficients of all nanocomposites measured by PFG-NMR technique on completely swelled membranes, in the temperature range 20-140 °C. The presence of unmodified graphene oxide platelets as filler in the polymer doesn't improve at all the performance of the membrane. On the contrary, already at 60 °C almost all the water is lost from the composite and, practically, over this temperature no NMR signal is possible to reveal in order to measure its diffusion coefficient. On the other hand, the benefits from the surface modification of GO sheets with an organic molecule such as the amino propanesulfonic acid (SULF) are evident. Nafion/GO-SULF nanocomposite shows water diffusion coefficients values very high in all temperature range investigated. In fact, the diffusion increases linearly up to 100 °C and soon after, due to the evaporation of a certain amount of water from the membrane, it decreases slightly but remains constant and especially after several hours at 140 °C. This result can be ascribed to two effects: 1) the increment of the number of acid sites in the electrolyte, is reflected in its ability to absorb and hold more water at high temperatures, and, 2) the presence of organic molecules with sulfonic end-groups makes the filler more compatible with the polymer and allows a better dispersion especially within the hydrophilic channels of Nafion. Finally, GO-SER and GO-TES nanocomposites show disappointing results indicative of systems not able to absorb/retain water although both these fillers contain characteristic hydrophilic groups. This behavior is probably due to differences in the size and the stereochemical configuration of the four amine molecules (as shown in the

scheme). The TES and SER molecules occupy more volume, and thus surface, inhibiting the accessibility of water molecules in the remaining hydrophilic acid sites of the graphene oxide layers and thus reduces the insertion of more water molecules in the interlayer space of GO. On the other hand, in the case of primary amines SULF and VAL, which are linear molecules, the hydrophilic sites of the graphene oxide are more easily accessible from water molecules, which, in combination with the additional acidic functional groups of the organic molecules that have been added to the system, is greatly enhance the total amount of adsorbed water.

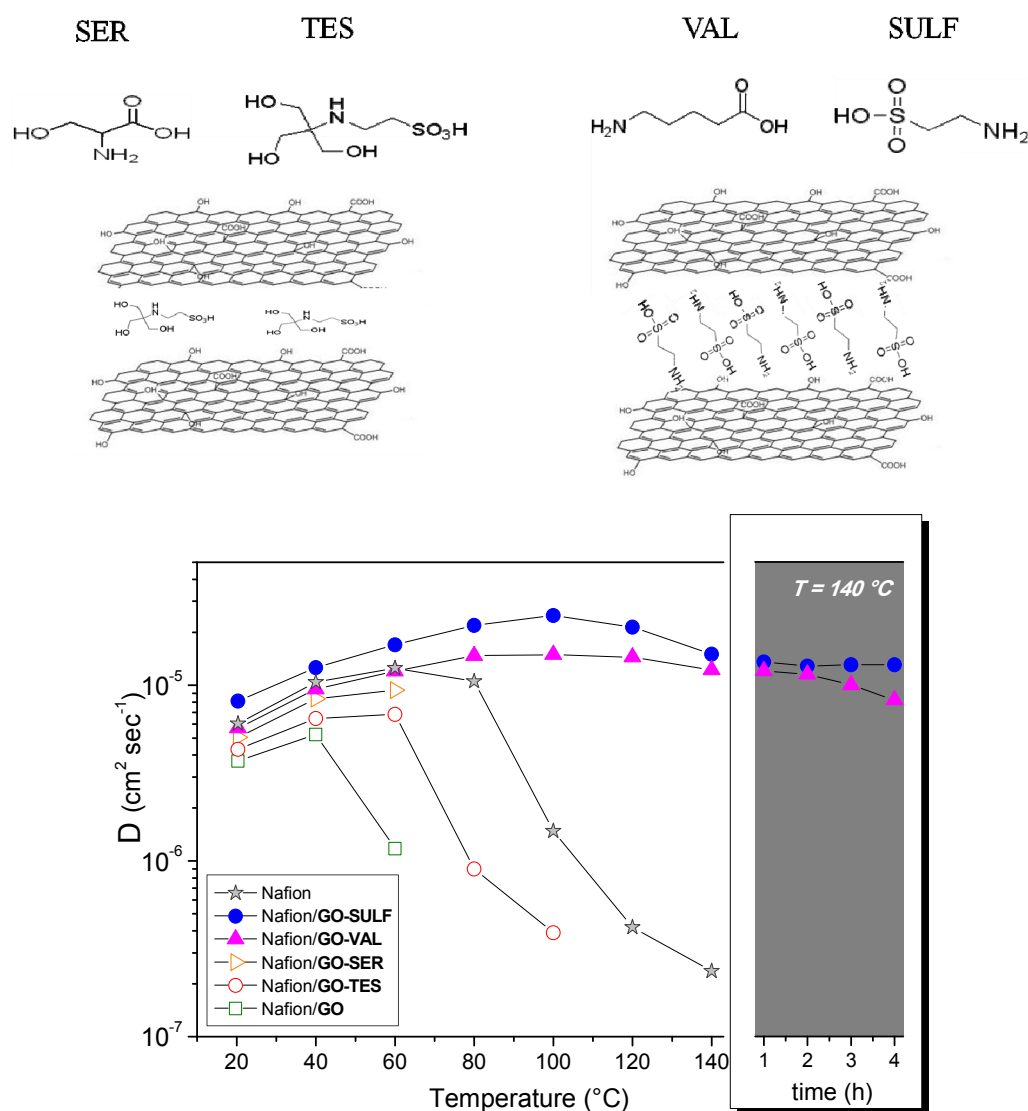


Figure 4.4.4 Self-diffusion coefficients as function of the temperature (from 20 $^{\circ}\text{C}$ up to 140 $^{\circ}\text{C}$) of the water confined in completely swelled membranes of filler free Nafion and nanocomposite membranes with 3 wt% loading of nanofillers (GO, GO-SULF, GO-VAL, GO-SER and GO-TES). In the graph of D are also plotted the data collected at 140 $^{\circ}\text{C}$ after several hours.

Figure 4.4.5 displays the temperature evolution of the ^1H NMR spectra of the GO-SULF, GO-VAL and GO-TES nanocomposites. It is interesting to note is the trend of the chemical shift of the peak vs. temperature (insets in the graphs) and how it is closely related to both the amount of water present in the membrane and the self-diffusion coefficients.

The temperature contributes to the proton resonance variation because it effects on the lifetime of the hydrogen bond. The heating causes a downfield shift of the resonance, and as result a decreasing of the chemical shift is observed. This reduction is more accentuated in the membranes with higher water content (e.g. GO-SULF), at which corresponds the higher chemical shift at room temperature.

From the comparative analysis with

the diffusion data we can assert that before the minimum, the contribution to the chemical shift is mostly that of the bulk-like water. The increasing of the chemical shift

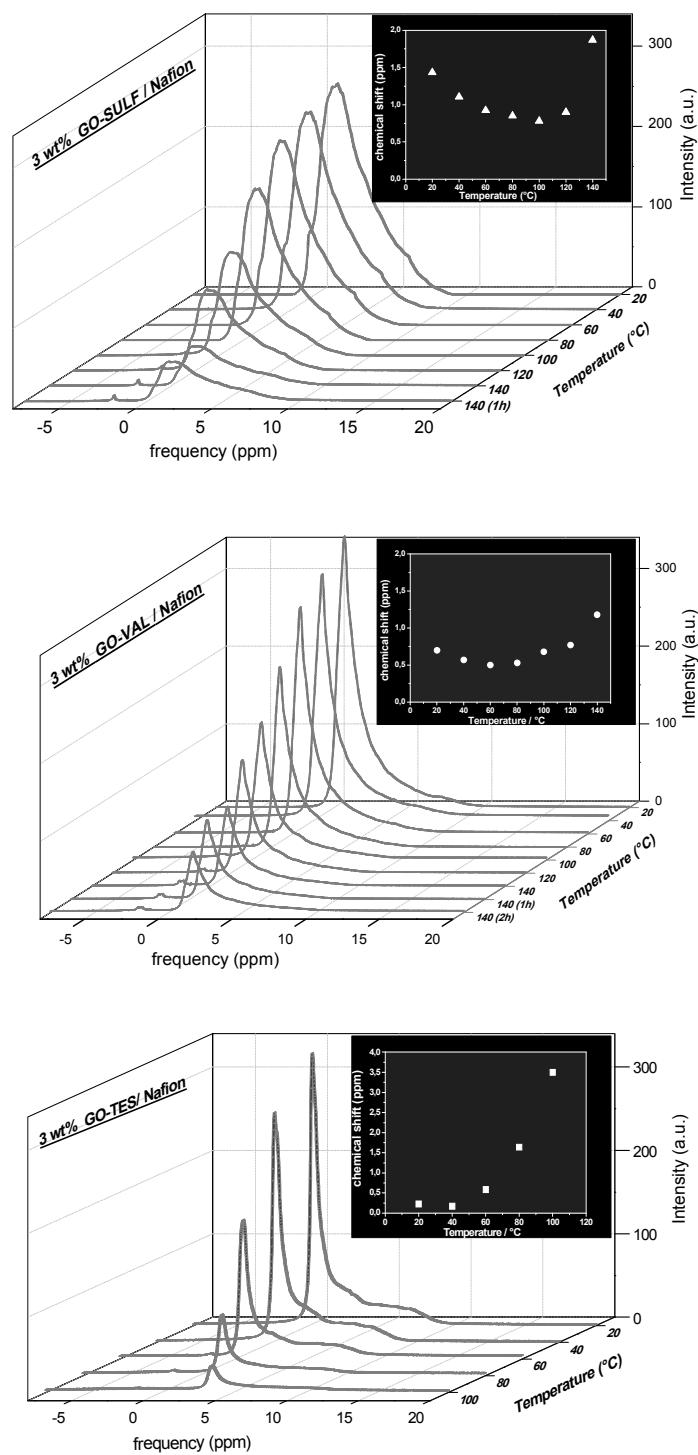


Figure 4.4.5: ^1H -NMR spectra temperature evolution and chemical shift vs. temperature.

soon after is explainable by considering that the residual water remaining in the membranes is the water bound to the hydrophilic groups, consequently the concentration of H^+ ions (acidity of the water is a well-known property of water in Nafion) and the effect of induced fields by the polar groups (sulfonic, hydroxyl, etc.) prevail on the temperature and bring to an upfield shift of the resonance. In a nutshell, the variation of the chemical shift of the water resonance line with temperature might give significant information on the temperature dependence of the liquid water amount as well as on the “states” of the water confined in such membranes. In addition, this NMR data analysis has pointed out a strong correlation between the temperature behavior of the self-diffusion coefficients and of the chemical shift: to an increasing of the diffusion corresponds a decreasing of the chemical shift (and vice versa) with an unexpected symmetry.

Finally, the effect of GO and GO-organo-modified nanofillers on the mechanical properties of the Nafion membrane was studied by DMA measurements, as showed in Figure 4.4.6. These data demonstrate that the presence of the nanofillers within the pores of the Nafion membrane and their interactions with the polymeric chains, creates a membrane with lower flexibility consequently more stiff and can withstand higher temperatures. In fuel cell applications, a nanocomposite membrane with high modulus might permit the employment of a thinner membrane avoiding problems connected with the electrolyte resistance.

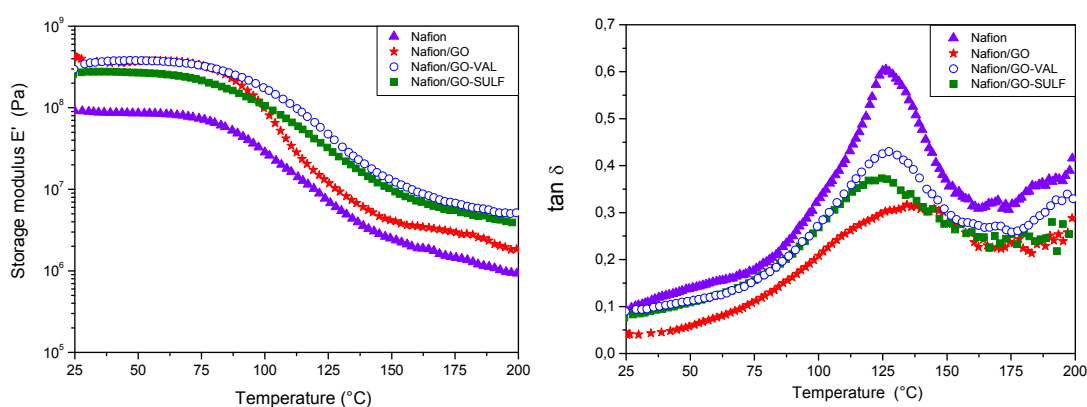


Figure 4.4.6: (left) Storage modulus, E' , and (right) $\tan \delta$ vs. temperature of filler-free Nafion and nanocomposite membranes loaded with 3 wt% GO, GO-SULF and GO-VAL.

4.5 LDH-based nanocomposites for PEMFCs (paper V)

The last layered material studied as nanofiller was the layered double hydroxides (LDHs), this material is detailed described in chapter 2.3. High proton conducting Nafion nanocomposite membranes were developed using Mg^{2+}/Al^{3+} LDH as nanofillers, with two metal ratios (2:1 and 3:1) and various interlayer anions (CO_3^{2-} , ClO_4^- , NO_3^-). Hybrid membranes were synthesized by solution intercalation with 3 wt% LDH loading in Nafion ionomer. In this study we have been compared composites membranes prepared by Nafion with different equivalent weight, i.e. 1000 EW and 1100 EW.

4.5.1 LDH-based nanocomposites by using Nafion 1000 EW as ionomer

Hybrid membranes were prepared with LDH fillers at two metal ratio Mg^{2+}/Al^{3+} , 2:1 and 3:1, and the three anions, CO_3^{2-} , ClO_4^- , and NO_3^- .

From a first screening based on the water absorption analysis (histogram in Figure 4.5.1) of these composite membranes, compared with the recast Nafion membrane, shows a discrete increasing of the uptake. The different Mg^{2+}/Al^{3+} ratio does not substantially affect the water amount absorbed from the membranes, while there is a greater effect related to the type of the intercalated anion. This can be attributed to the higher Anion Exchange Capacity (AEC) of the membranes prepared with the metals ratio 2:1, than the 3:1, as a consequence the presence of more anions in the material interlayer space.

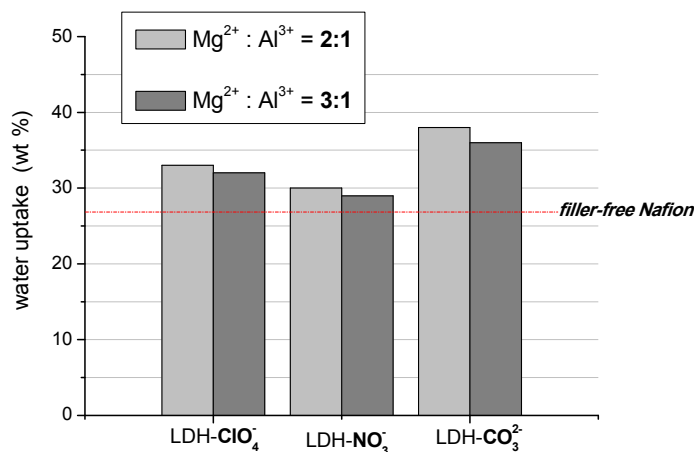


Figure 4.5.1: Maximum water uptake of the filler free Nafion and of the LDH nanocomposites (3% wt) prepared with different $Mg^{2+}:Al^{3+}$ ratios (2/1 and 3/1) and with the different anions (CO_3^{2-} , ClO_4^- , and NO_3^-).

The water self-diffusion coefficients measured in these composites reveal, instead, a strong effect of the metal ratio and anions (Figure 4.5.2 a and b).

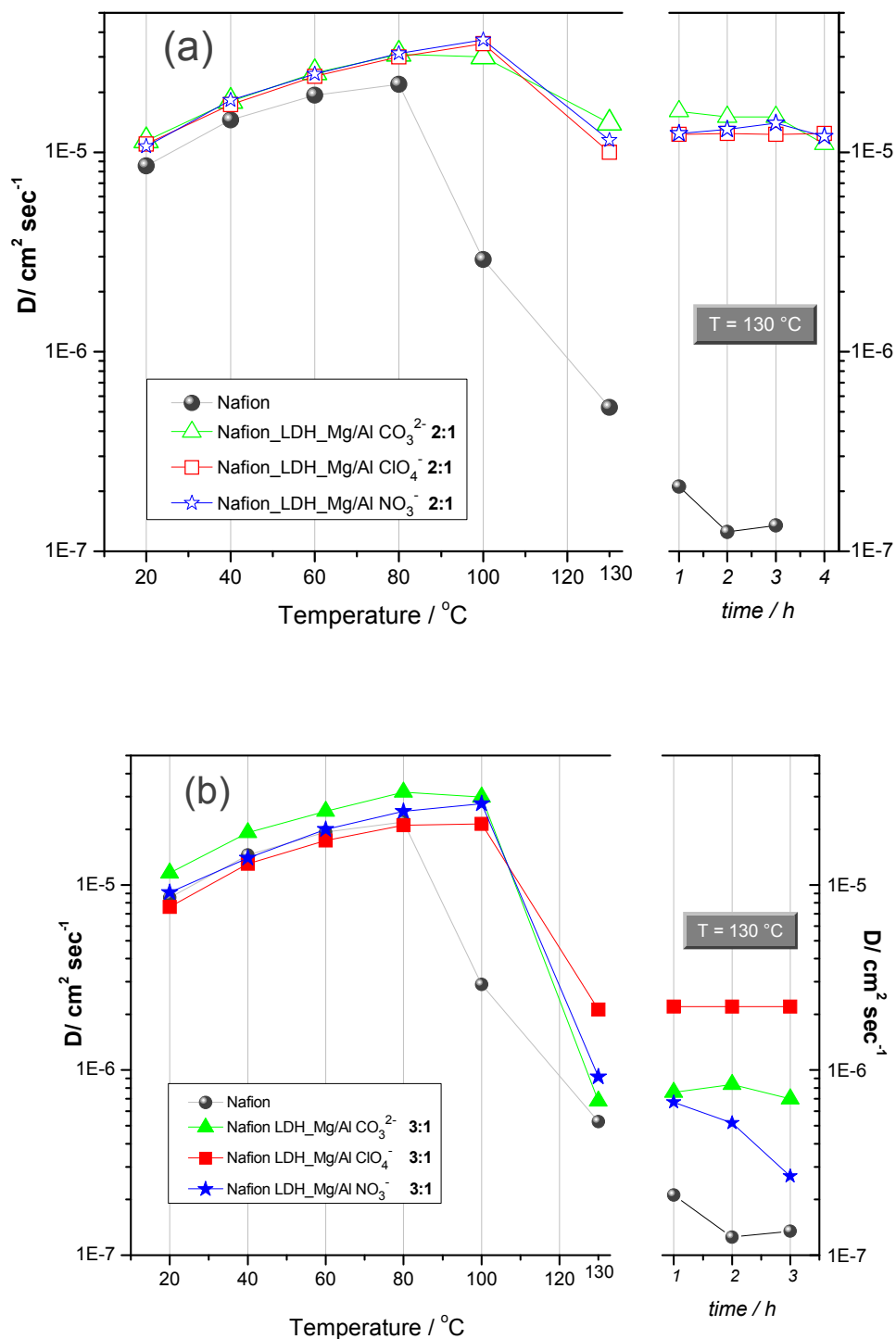


Figure 4.5.2: Water self-diffusion coefficients vs. temperature of the water confined in completely swelled LDH composites with (a) 2:1 and (b) 3:1 metal ratios. In both two graphs are presented also and the diffusion coefficients of pure Nafion for comparison and the data collected at 130°C after several hours.

Membranes with 2/1 ratio showed that the water diffusion after the slightly decrease, remains constant and especially after several hours at 130 ° C. Instead the Mg-LDH membranes with 3/1 metal ratio is observed a significant decreasing to the water diffusion coefficients, even two orders of magnitude, respect to the first. This can be attributed to the higher positive charge of Mg-LDH layers in the nanocomposites with 2/1, which results at first, to a bigger amount of anions intercalated in the interlayer space of the Mg-LDH, in order to neutralize the charge and therefore more water molecules, and secondly the positively charged Mg-LDH nanoplatelets interact with the negatively charged sulfonic groups in Nafion polymer chains, resulting to a strong interactions between the Mg-LDH layers and the hydrophilic groups of the polymer, facilitating the water mobility. However, it is extremely significant the behavior of such nanocomposites in the high temperature's region since the water self-diffusion coefficients remain constant for several hours at quite high values.

Therefore, further electrochemical study on these systems is in progress.

4.5.2 LDH ($Mg^{2+}:Al^{3+} = 2:1$) -- based nanocomposites by using Nafion 1100 EW as ionomer

The above results provide evidence that presence of the Mg-LDH nanofillers with metal ratios 2:1, produces a noteworthy improving of the membranes performances. Based on this, LDHs at this ratio and various interlayer anions (CO_3^{2-} , ClO_4^- , NO_3^-) were prepared and incorporated in Nafion 1100 EW, and all the results of the experimental study are discussed in the **paper V**, recently submitted, and reported in the appendix to the thesis.

Here we report only the NMR data, diffusion and T1, showed in Figure 4.5.3 and 4.5.4, respectively. It is evident that the equivalent weight of the ionomer have a strong influence on the final performance of the composites. Actually, lower EW denotes a higher number of sulfonic groups, so higher water absorption but also higher swelling. Additionally, the mechanical properties of Nafion 1000 are poorer than the same ionomer at 1100 EW.

However, even if the diffusion at higher temperatures decreases, leaving the membranes for 1 hour at 130 °C, on the filler-free Nafion there is no any proton signal

while two of the three composites have a weak signal but sufficient for the measurement; even NLDH- NO_3^- after 2 hours there is still mobile water in the membrane with a coefficient D unaltered. Nitrate and carbonate anions show to have a superior ability to retain water than perchlorate anion, probably due to its greater charge delocalization that, as a consequence, affects the microstructure of the complex system “filler-polymer”.

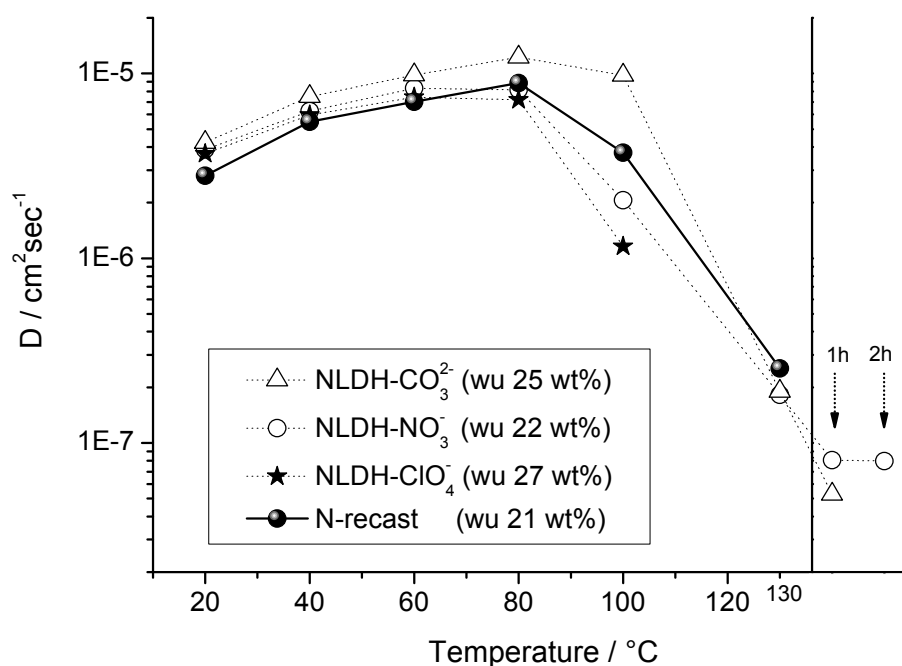


Figure 4.5.2: Self-diffusion coefficients of water confined in the LDH-composite membranes with different interlayer anions, NO_3^- , CO_3^{2-} , ClO_4^- , from 20 °C up to 130 °C. Filler-free Nafion (1100 EW) is also reported for comparison.

The relaxation times of water in the composites are longer compared to the polymer recast and this is related to the greater hydration due to the presence of a larger number of hydrophilic sites. The nitrates and perchlorates ions are not only larger in size than the carbonates, but they have a lower valence⁴³ resulting in weaker interactions with the interlayer water molecules, additionally, the divalent anions are more strongly held in the interlayer than the monolayer anions⁴⁴. This entails higher roto-translational degrees of freedom of the molecules of water in composites nitrates and perchlorates, while the double negative charge of the carbonate stiffens the molecular conformations

and makes movements slower lowering the T_1 . Above 100 °C the composite with the perchlorate shows a more drastic reduction of the T_1 associated with a significant loss of hydration water.

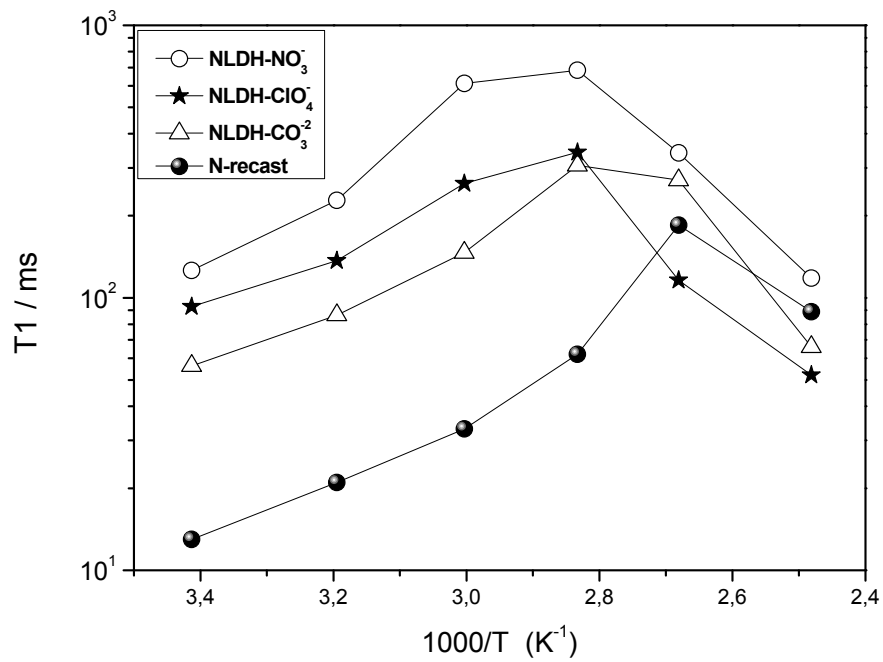


Figure 4.5.3: Arrhenius plot of water longitudinal relaxation times (T_1) measured in the temperature range from 20 °C up to 130 °C for recast Nafion and Mg/Al-LDH composite membranes at the maximum water uptake.

4.6 Aquivion™ - ZrP composite membranes

Despite their outstanding stabilities and their excellent electrochemical-physicochemical properties, Perfluorosulfonic acid (PFSA) membranes show many drawbacks as high methanol permeability (in DMFC), loss of proton conductivity at high temperatures and low humidity, as well as their high cost, impeding its further applications⁴⁶. Recent progress has been made in the design and development of a broad range of polymers and membranes as “alternatives” to the conventional PFSA type. Low equivalent weight PFSA membranes with shorter pendant side-chains developed by Dow, 3 M, Gore, Asahi glass, Solvay-Solexis, etc⁴⁷⁻⁴⁹ have recently received attention as promising membrane materials for PEM fuel cells operating at elevated temperatures^{50, 51}. Solvay-Solexis has recently developed a new short side chain perfluorosulfonic membrane with the trade name Aquivion™ (Figure. 4.6.1)⁵⁰. Normally, the equivalent weight of these membranes ranges from about 750-850 g eq⁻¹. These types of materials have considerably higher concentration of sulfonic acid groups compared with the conventional Nafion® membrane, known as a long-side-chain (LSC) ionomer. Short side chain ionomers are characterized by both larger crystallinity and higher glass transition temperature than LSC polymers at a given equivalent weight (EW)^{52, 53}. Both characteristics are promising in terms of mechanical stability and conductivity for operation in the high temperature range. Furthermore the higher degree of crystallinity, prevents the membranes from completely dissolving in water as the equivalent weight is reduced⁴⁷. It has also been demonstrated that the short side chain PFSA membranes exhibit significantly better water retention characteristics thus higher proton conductivity under dehydrating conditions compared with the conventional PFSA membranes, which should further facilitate the PEM fuel cell operation at elevated temperatures⁵⁰. However PEMs based on these membranes suffer from excessive swelling, loss of proton conductivity at high temperatures due to degradation of sulfonic acid groups⁵⁴⁻⁵⁹. Up to now several studies reported a consistent of fuel cell performance of composite membranes, at temperatures above 80°C, by development of composite membranes comprising inorganic nanoparticles such as metal oxides⁶⁰⁻⁶⁴ or zirconium phosphate (ZrP)^{23, 45, 56, 58, 65-73}. Jones and Rozière^{74, 75}, Alberti and Casciola⁷⁶ have reviewed the development and applications of inorganic-organic

membranes for fuel cells. The presence of inorganic phase is effective in enhancing interactions between components, in limiting dimensional changes and improving fuel cell performance under high temperature and low relative humidity conditions. In addition improvements in mechanical properties are also expected. Since mechanical fragility is one of the principal reasons for membrane failure in in-long term *in situ* fuel cell. The use of ZrP as inorganic components is attractive for its good thermal and chemical stability, its solid acid properties, and its high proton conductivity.

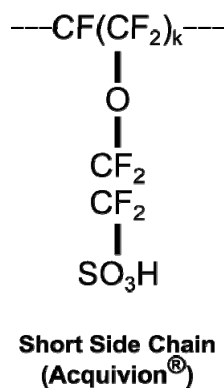


Figure 4.6.1: Chemical structure of SSC-PFSA ionomer (AcquivionTM).

4.6.1 Zirconium Phosphate

Zirconium phosphate hydrated (ZrP, $\text{Zr}(\text{HPO}_4)_2 \cdot \text{H}_2\text{O}$ for the α -form, abbreviated as a α -ZrP) has the layered structure shown in figure ⁶⁵ the latter of α -form⁷⁷ has a basal spacing of 7.6 Å (4.6.2). The layers are considered to be weakly held together by Van der Waals forces as well as long hydrogen bonds from the layer to the water molecules located at interlayer positions. These hosted water molecules in the interlayer zeolitic cavities are responsible for the high hygroscopicity and the water retention of the material. Zirconium phosphate shows some additional properties defining it as an attractive component in inorganic-organic composite membranes such as good thermal and chemical stability; higher proton conductivity than many metal oxides nanoparticles with high aspect ratio ^{78, 79} that are effective to reduce the membrane permeability ⁸⁰. Moreover has the potential to: enhance elastic modulus;

keep water at higher temperature and increase glass transition temperature of membranes.

General approaches for the preparation of inorganic-organic membranes have been reviewed^{76, 81}. PFSA/ZrP composite membranes can be prepared according two main procedures: (1) Dispersion of ZrP particles in PFSA solution followed by film casting; (2) in situ formation of ZrP in preformed PFSA membranes.

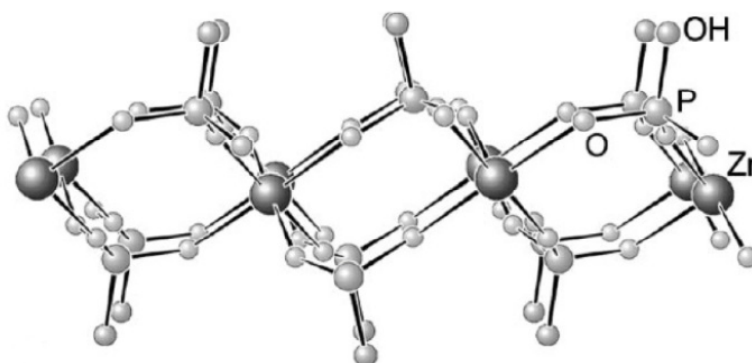


Figure 4.6.2: Schematic representation of the single lamella structure of α -ZrP.⁷⁶

4.6.2 Preparation of Composite Membrane

Two methods are generally followed to prepare nanocomposites based on ZrP: (i) dispersion of preformed zirconium phosphate particles in PFSA solution followed by film casting and (ii) in situ formation of ZrP in preformed PFSA membranes.

The first method^{76, 82, 83}, used to prepare the other composites described in this thesis, is very simple, however is usually difficult to avoid the formation of particle agglomerates inside the polymeric matrix.

For this work I used the in situ procedure to prepare homogeneous composites based on AquivionTM membrane as template for α -type ZrP inorganic particle growth.

PFSA ionomer membranes can act as a morphological template for growth of the inorganic phase. Their distinct morphology arises from self-organisation into hydrophobic and hydrophilic regions. The preparation of nanocomposite membranes by intra-membrane growth within a proton exchange membrane was first described by Mauritz et al..^{85, 86} The group made use of the hydrophilic ionic clusters regions of

Nafion for confined, sulfonic acid group catalyst, hydrolysis/condensation reactions of impregnated alkoxides. Nafion membranes were first swollen in ethanol/water, then tetraethoxysilane (or aluminium, titanium and zirconium alkoxides) was permeated from one side of the membrane. In situ formation of ZrP in preformed PFSA membranes usually carried out in two steps: (i) incorporation of an ionic zirconium species in the polymer matrix by ion exchange reaction and (ii) subsequent treatment of the membrane with H_3PO_4 to convert the precursor into ZrP. The exchangeable nature of H^+ ions on the sulfonated group in PFSA membranes allows the synthesis of nanoparticles through a simple ion exchange reaction. The PFSA structure is composed of numerous hydrophilic ionic clusters (pores) interconnected by channels within the hydrophobic perfluorocarbon matrix⁸⁷. Such hydrophilic pores make it quite suitable as host matrix for the encapsulation of guest species. In SSC-PFSA ionomer matrix, Zr(IV) was loaded through cation exchange within the confines of the hydrophilic regions of the membrane. The ZrP was subsequently precipitated *in situ* by treatment in dilute phosphoric acid. The resulting membranes were characterized by measurement of water uptake and dimensional change, determination of proton conductivity as a function of relative humidity, observation of structure by SEM and TEM, ^{31}P NMR spectroscopy, and X-ray diffraction. The differences of the characteristics of the SSC-PFSA-ZrP nanocomposite membrane compared to the pure SSC-PFSA membrane were investigated.

The general procedure for preparation of SSC-PFSA-ZrP composite membranes in this work was by ion exchange reaction in ZrOCl_2 solution and precipitation in phosphoric acid (H_3PO_4) solution. The membranes were immersed in an aqueous solution of ZrOCl_2 of concentration in the range 0.1-2.5 mol/L at 80°C for 2h. They were then removed, washed 3 times by deionized water at room temperature to eliminate the excess of zirconium oxychloride solution and immersed in phosphoric acid (concentration 1 mol/L) at 80°C for 15h. The procedure for preparation of SSC-PFSA/ ZrP composite membranes is shown Figure 4.6.3. The content of zirconium phosphate was controlled by the ion exchange time and the concentration of aqueous ZrOCl_2 solution.

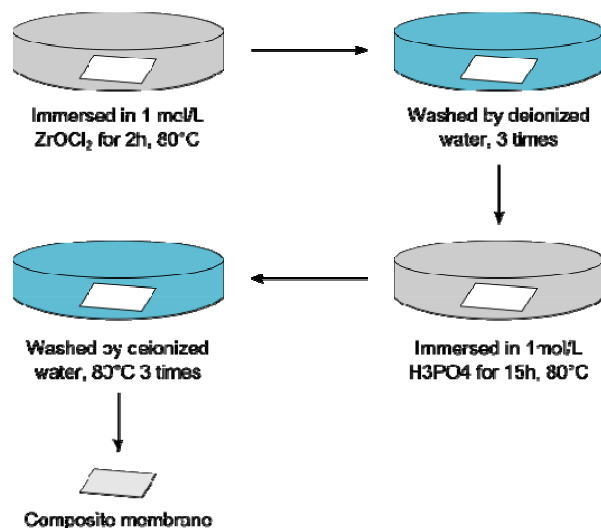
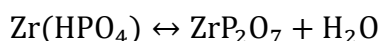


Figure 4.6.3: Procedure for preparation of SSC-PFSA-ZrP-26% membrane by ion exchange/precipitation.

4.6.3 Structural and Morphological Characterization

The content of zirconium phosphate in SSC-PFSA-ZrP membrane was determined from thermogravimetric analysis by a heating rate 10 °C/min with air flow to 1000°C. At this temperature the remaining solid was zirconium pyrophosphate, assuming that the zirconium phosphate was compressed to zirconium pyrophosphate⁸⁸, according to:



The amount of ZrP inside the membrane is 26 wt% respect to the polymer.

The cross section of SSC-PFSA-ZrP-26 % composite membrane was observed using SEM (Figures 4.6.4) and TEM (Figure 4.6.5) microscopy, while the structural features of the ZrP in the membrane was investigated by X-ray diffraction (Figure 4.6.7).

Concerning the SEM images, no ZrP particles are visible at 20 µm and 5 µm scales, while at higher magnification with TEM more dispersed particles located in the amorphous region of the polymer are detected. These particles are seen to comprise agglomerates of individual nanometric particles (4-7 nm). The agglomerates give roughly spherical or oblate spheroid domains of size 0.1-0.5 µm in the composite membrane. These observations propose that sites most favorable to ion exchange are distributed homogeneously throughout the membrane and are consumed rapidly on immersion of the membranes in ZrOCl₂. Thereafter is presumed that when the

membranes are immersed in phosphoric acid, the protons exchange with the zirconium cations, which are then free to diffuse through the membrane until they form the nucleus of a ZrP particle. For short reaction times, ZrP particles form in the hydrophilic regions, which limits the particle size. For longer reaction times, ZrP particles migrate to further distances, into the non-hydrophilic, interbundle regions and grow to larger sizes^{89, 90}. Nevertheless, the observation of oblate spheroid type clusters of ZrP is not fully consistent with this assumption. The possibility of filling a second type of ion-exchange site, the distribution of which leads to a cluster like appearance seems to be more compatible, however a further investigation of the microstructure by detailed small angle scattering, is required for supporting this hypothesis.

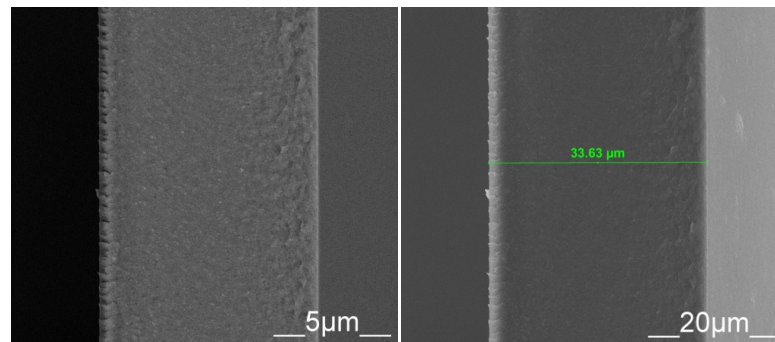


Figure 4.6.4: SEM images of the cross section of SSC-PFSA-ZrP (26%) membrane.

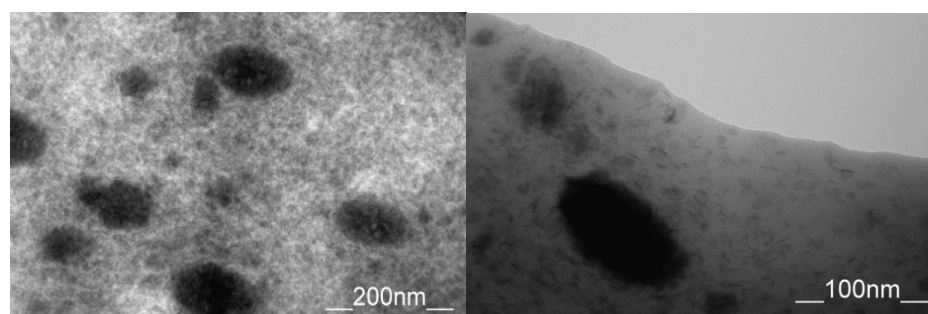


Figure 4.6.5: TEM photos of SSC-PFSA-ZrP (26%) composite membrane.

SEM-EDX provides information about the elemental composition on a micrometer scale and was used to determine the presence and distribution of

phosphorous and zirconium in the membrane. Figure 4.6.6 illustrates the elemental distribution over the cross-section of the zirconium phosphate composite membrane, a homogeneous distribution of zirconium and phosphorous is revealed throughout the entire cross section of the membrane.

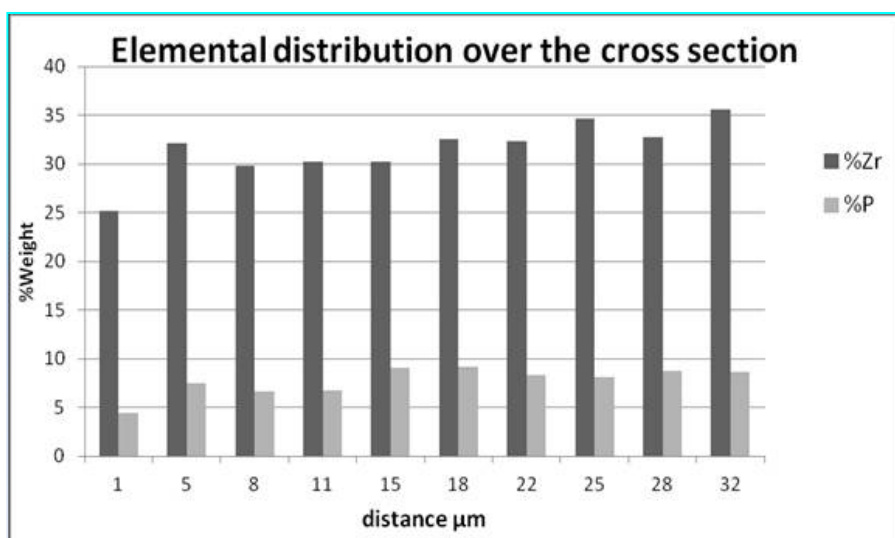


Figure 4.6.6: Elemental distribution over the cross-section of the SSC-PFSA-ZrP-26% membrane.

In the X-ray diffraction patterns of the composite membrane (Figure 4.6.7), the broad reflections located at $2\theta = 16.21^\circ$ and 40° are attributed to the crystalline perfluorinated backbone, $-\text{[CF}_2\text{-CF}_2\text{]}-$, of PFSA membrane⁶⁸. The peaks at $2\theta = 8.15, 19.6, 33.9$ are characteristics of the 002, 200, and 020 crystallographic planes of $\alpha\text{-ZrP}$ ^{68, 73, 91}. The 002 diffraction line is shifted to lower angle, indicating higher interlayer spacing, probably due to a greater degree of hydration and less crystalline character of ZrP particles. According the literature has been suggested that an exfoliated amorphous or semi-crystalline phase of ZrP is formed within the confines of the hydrophilic regions during the in situ precipitation of ZrP in PFSA. Moreover at such high concentrations zirconium phosphate is significantly enriched in the surface near region of the membrane and shields the inner parts of the membrane⁶⁸. Diffraction peak width of the line at 34° was used to estimate the particle size of the zirconium phosphate by using the Scherrer formula with Warren correction for instrumental effects. The domain size

in the fully dried membranes the zirconium phosphate particles is estimated to be 6.5 ± 1 nm in size.

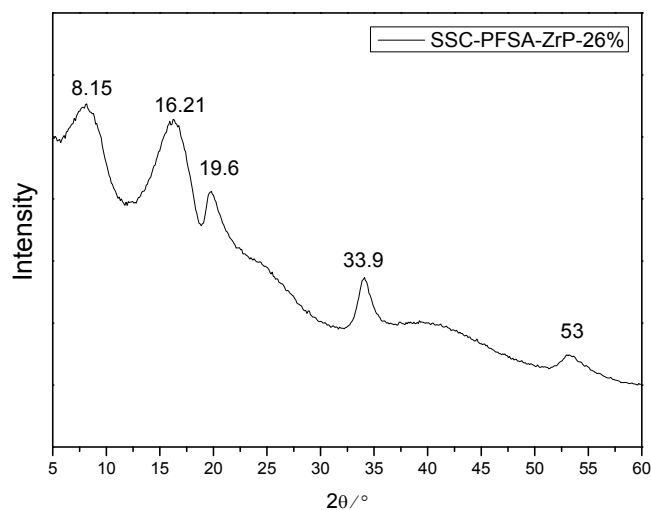


Figure 4.6.7: X-ray diffraction pattern for SSC-PFSA-ZrP (26%) composite membrane.

Further structural information on the phosphorous environment was obtained by ^{31}P MAS NMR (Figure 4.6.8). It is observed a strong peak at -22 ppm assigned to monohydrogen phosphate groups (HPO_4) bonded to Zr(IV) atoms in α -ZrP layer^{45, 92}. In addition, a medium intensity resonance peak at -28 ppm characteristic of PO_4 groups sharing four oxygen atoms with Zr(IV) and a minor contribution from H_2PO_4 (-14ppm) sharing two oxygen with zirconium^{45, 73, 93}. The XRD and the NMR data are consistent with the formation of α -ZrP inside SSC PFSA polymeric matrix.

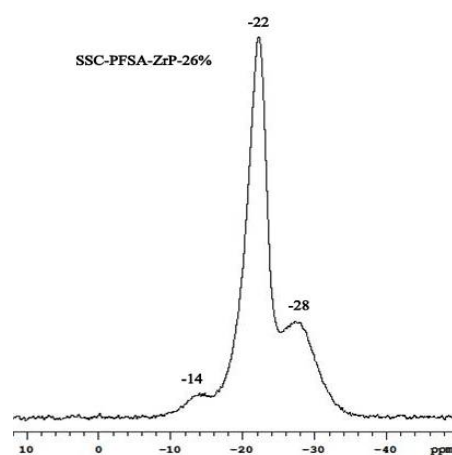


Figure 4.6.8: ^{31}P MAS NMR spectrum of composite SSC-PFSA-ZrP membrane with 26 wt % ZrP.

4.6.4 Physicochemical Characterization and Proton Conductivity

Water uptake and dimensional changes (volume %, area %, thickness %) of SSC-PFSA and SSC-PFSA-ZrP-26% membranes were determined from immersion in water at 25 °C and 80 °C. The results are shown in the Figure 4.6.9. The results show that the presence of the inorganic ZrP component in the SSC-PFSA-ZrP-26% membrane lowered the water uptake and dimensional change, comparing with that of the pristine SSC-PFSA membrane. Water uptake was decreased from 55 % to 40 % at ambient temperature and from 57% to 42 at 80°C, at the same time the area was decreased from 55 % to 40 % at 25°C and from 57 to 61 at 42 °C. These results indicate that a solid content of around 26 wt % ZrP, enhance the dimensional stability, thus reduce the tendency of the membrane to swell. Despite the high hygroscopicity of ZrP, the lower water uptake on the composite membrane SSC-PFSA-ZrP-26% compared to pristine SSC-PFSA, is more likely a consequence of morphological or structural changes induced by the *in situ* precipitation of the inorganic filler⁸⁹.

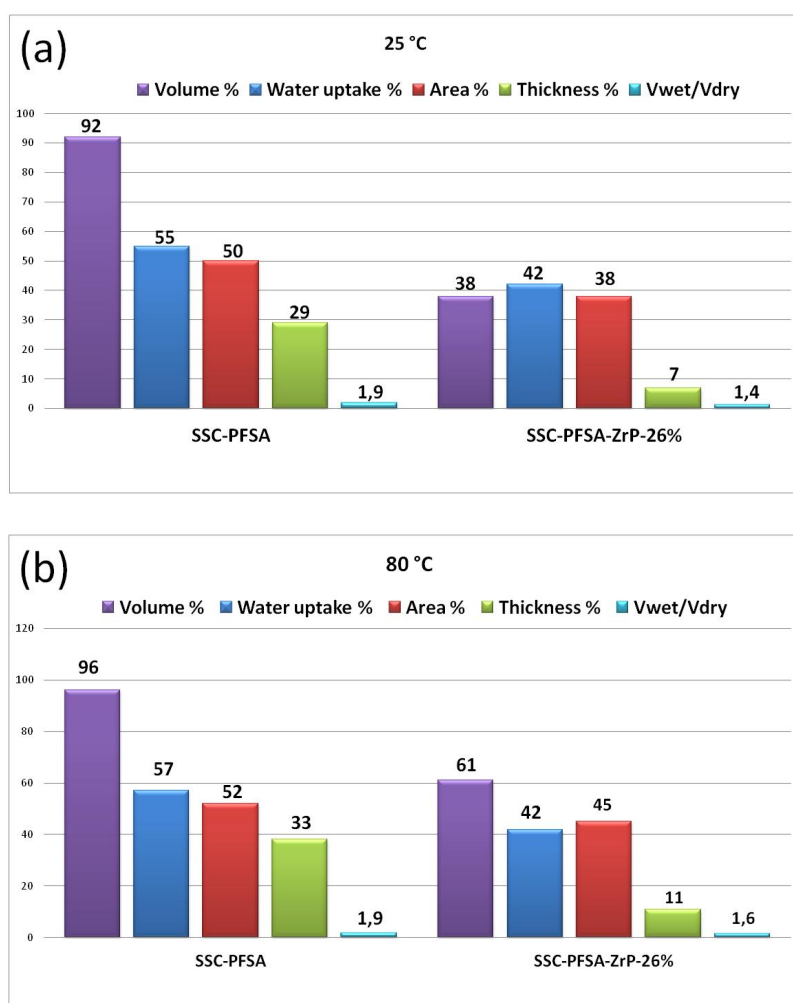


Figure 4.6.9: Histograms of water uptake and dimensional change (volume %, area %, thickness %) of SSC-PFSA and SSC-PFSA-ZrP-26% membranes at (a) 25°C and (b) 80°C.

In plane proton conductivity of membranes was measured in a Beck-Tech instrument. The data were collected at 80°C and 120°C as function of relative humidity, which was varied between 50 to 90 %. The results are plotted to graphs presented in Figure 4.6.10. The conductivities of both membranes decreased with decreasing the relative humidity from 95 % to 50 %. Compared to the pure SSC-PFSA membrane, the inorganic component of ZrP in SSC-PFSA.-ZrP membrane decreased its proton conductivity at 80 °C, this is mainly the consequence of the fact that ZrP is less conductive than PFSA, even in the amorphous form⁷⁰. These results are consistent with other results in literature^{62, 66, 69, 70, 73, 76}. Nevertheless the effect of zirconium phosphate on the conductivity stability is observed at 120°C. The proton conductivity of the composite membrane increasing the temperature, remain stable, compared to SSC-PFSA its self. The composite membrane for 80 % 65 % and 50 % RH reach almost the same values of the pure SSC-PFSA membrane, where its conductivity decrease at elevated temperature, and close to glass transition temperature (127 °C). These results agree with the work of Alberti et al⁴⁵ on Nafion-ZrP, reporting that the enhanced stability of the conductivity is associated with higher values of the elastic modulus in the presence of the filler, thus confirming the positive effect of ZrP particles on the dimensional stability of Nafion membranes. However in this thesis the mechanical properties of the membranes were not investigated and will be the topic of future work.

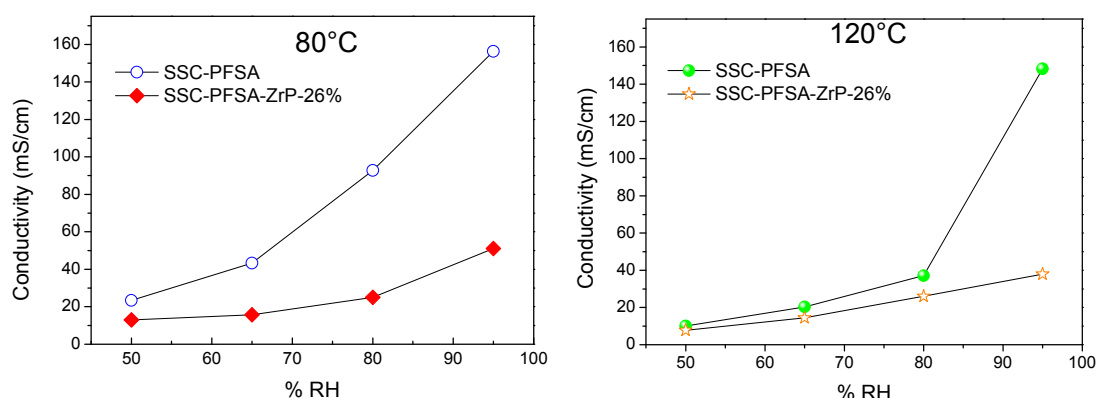


Figure 4.6.10: Plots of, in plane proton conductivity, of SSC-PFSA and SSC-PFSA-ZrP -26% membranes, at 80°C (left) and 120°C (right), as a function of relative humidity.

In conclusions composite membrane, based on short-side-chain PFSA with low EW, has been developed by modification, with zirconium phosphate, up to 26 wt. % filler loading. The inorganic component was produced *in situ* by ion-exchange and precipitation process. The formation of α -ZrP inside the SSC-PFSA polymeric matrix is proved by the ^{31}P -MAS-NMR spectrum and X-ray pattern, of the composite membrane. Two levels of organisation are observed in the composite membrane: (i) a first level at the nanometer scale, as detected by TEM and XRD – more dispersed particles located in the amorphous region of the polymer; (ii) a second level detected by SEM, having organization at the sub-micron level - located in the crystalline regions of the polymer. The existence of oblate spheroid, agglomerates of individual nanometric particles, has been observed also in other SSC-PFSA composite membranes, in a work carried out in the same laboratory. The origin of this observation most probably lies in a specific characteristic microstructure. Further investigation of these arrangements and the composite membrane microstructure is required.

ZrP, as inorganic component in composite SSC-PFSA membrane, increased the dimensional stability, lowered the water uptake as well as the swelling of the membrane. Moreover the presence of ZrP enhanced the stability of the proton conductivity at medium temperature and high relative humidity. The major perspective of this work lies in the development of composite membranes with ZrP particles, capable to reduce the methanol permeability, and improve the fuel cell performance. On this route fuel cell tests of the membranes and a detailed study on the effect of different filler loading on composite membranes properties are in progress.

References

- 1 T. A. J. Zawodzinski, M. Neeman, L. O. Sillerud, and S. Gottesfeld, *J. Phys. Chem. A* **95**, 6040 (1991).
- 2 J. J. Fontanella, M. G. McLin, M. C. Wintersgill, and S. G. Greenbaum, *Solid State Ionics* **66**, 1 (1993).
- 3 I. Nicotera, T. Zhang, A. Bocarsly, and S. Greenbaum, *Journal of Electrochemical Society* **154**, B466 (2007).
- 4 I. Nicotera, L. Coppola, C. O. Rossi, M. Youssry, and G. A. Ranieri, *J Phys Chem B* **113**, 13935 (2009).
- 5 J. R. P. Jayakody, P. E. Stallworth, E. S. Mananga, J. F. Zapata, and S. G. Greenbaum, *J. Phys. Chem. B* **108** 4260 (2004).
- 6 E. O. Stejskal and J. E. Tanner, *The Journal of Chemical Physics* **42**, 288 (1965).
- 7 K. T. Adjemian, S. Srinivasan, J. Benziger, and A. B. Bocarsly, *Journal of Power Sources* **109**, 356 (2002).
- 8 S. S. Ray and M. Okamoto, *Progr Polym Sci* **28**, 1539 (2003).
- 9 J. M. Thomassin, C. Pagnouille, G. Caldarella, A. Germain, and R. Jerome, *Polymer* **46**, 11389 (2005).
- 10 V. Georgakilas, A. Bourlinos, D. Gournis, T. Tsoufis, C. Trapalis, A. Mateo-Alonso, and M. Prato, *J. Am. Chem. Soc.* **130**, 8733 (2008).
- 11 D. H. Jung, S. Y. Cho, D. H. Peck, D.R.Shin, and J. S. Kim, *Journal of Power Sources* **118**, 205 (2003).
- 12 Y. S. Kim, L. M. Dong, M. A. Hickner, B. S. Pivovar, and J. E. McGrath, *Polymer* **44**, 5729 (2003).
- 13 N. Cele and S. S. Ray, *Macromolecular Materials and Engineering* **294**, 719 (2009).
- 14 M. Eikerling, A. A. Kornyshev, A. M. Kuznetsov, J. Ulstrup, and S. Walbran, *J. Phys. Chem. B* **105**, 3646 (2001).
- 15 K. D. Kreuer, *Solid State Ionics* **94**, 55 (1997).
- 16 B. Cohen and D. Huppert, *J. Phys. Chem. A* **107**, 3598 (2003).
- 17 E. Burgaz, H. Lian, R. H. Alonso, L. Estevez, A. Kellarakis, and E. P. Giannelis, *Polymer* **50**, 2384 (2009).
- 18 R. H. Alonso, L. Estevez, H. Q. Lian, A. Kellarakis, and E. P. Giannelis, *Polymer* **50**, 2402 (2009).
- 19 Y. Kim, J. S. Lee, C. H. Rhee, H. K. Kim, and H. Chang, *Journal of Power Sources* **162**, 180 (2006).
- 20 Y.-F. Lin, C.-Y. Yen, C.-H. Hung, Y.-H. Hsiao, and C.-C. M. Ma, *Journal of Power Sources* **168**, 162 (2007).
- 21 A. Ladhari, H. Ben Daly, H. Belhadjsalah, K. C. Cole, and J. Denault, *Polymer Degradation and Stability* **95**, 429 (2010).
- 22 S. Pavlidou and C. D. Papaspyrides, *Progress in Polymer Science(Oxford)* **33**, 1119 (2008).
- 23 G. Alberti, M. Casciola, U. Costantino, and G. Levi, *Journal of Membrane Science* **3**, 179 (1978).
- 24 G. Gebel, *Polymer* **41**, 5829 (2000).
- 25 S. J. Paddison and R. Paul, *Phys. Chem. Chem. Phys.* **4**, 1158 (2002).
- 26 F. Hallberg, T. Vernersson, E. T. Pettersson, S. V. Dvinskikh, G. Lindbergh, and I. Furó, *Electrochim Acta* **55** 3542 (2010).
- 27 X. Ji, L. Yan, S. Zhu, L. Zhang, and W. Lu, *J. Phys. Chem. B* **112** 15616 (2008).
- 28 I. Adamovic and M. S. Gordon, *J. Phys. Chem. A* **110** 10267 (2006).
- 29 B. K. G. Theng, *The Chemistry of Clay Organic Reactions* (Adam Hilger, London, 1974).
- 30 G. Gebel and P. Atkins, *Polymer* **41**, 5829 (2000).
- 31 S. J. Paddison and R. Paul, *Phys. Chem. Chem. Phys.* **4**, 1158 (2002).

- 32 F. Salles, J. M. Douillard, R. Denoyel, O. Bildstein, M. Jullien, I. Beurroies, and H. Van
Damme, *J. Colloid Interface Sci.* **333**, 510 (2009).
- 33 G. Gompper, M. Hauser, and A. A. Kornyshev, *J. Chem. Phys.* **101**, 3378 (1994).
- 34 K. A. Mauritz and R. B. Moore, *Chem. Rev.* **104**, 4535 (2004).
- 35 M. Falk, *Can. J. Chem.* **58**, 1495 (1980).
- 36 T. Kuilla, S. Bhadra, D. Yao, N. H. Kim, S. Bose, and J. H. Lee, *Progress in Polymer
Science (Oxford)* **35**, 1350 (2010).
- 37 J. R. Potts, D. R. Dreyer, C. W. Bielawski, and R. S. Ruoff, *Polymer* **52**, 5 (2011).
- 38 Y. Geng, S. J. Wang, and J. K. Kim, *J. Colloid Interface Sci.* **336**, 592 (2009).
- 39 A. B. Bourlinos, D. Gournis, D. Petridis, T. Szabo, A. Szeri, and I. Dekany, *Langmuir* **19**,
6050 (2003).
- 40 S. Ansari, A. Kelarakis, L. Estevez, and E. P. Giannelis, *Small* **6**, 205 (2010).
- 41 L. Staudenmaier and B. Dtsch., *Chem. Ges* **31**, 1484 (1898).
- 42 D. V. Stergiou, E. K. Diamanti, D. Gournis, and M. I. Prodromidis, *Electrochemistry
Communications* **12**, 1307.
- 43 J. T. Klopogge, D. Wharton, L. Hickey, and R. L. Frost, *American Mineralogist* **87**
(2002).
- 44 S. Miyata, *Clays and Clay Minerals*, 1983).
- 45 G. Alberti, M. Casciola, D. Capitani, A. Donnadio, R. Narducci, M. Pica, and M.
Sganappa, *Electrochimica Acta* **52**, 8125 (2007).
- 46 B. P. Tripathi and V. K. Shahi, *Journal of Colloid and Interface Science* **316**, 612 (2007).
- 47 A. Ghielmi, P. Vaccarone, C. Troglia, and V. Arcella, *Journal of Power Sources* **145**, 108
(2005).
- 48 V. Arcella, C. Troglia, and A. Ghielmi, *Industrial & Engineering Chemistry Research* **44**,
7646 (2005).
- 49 A. S. Arico, V. Baglio, A. Di Blasi, V. Antonucci, L. Cirillo, A. Ghielmi, and V. Arcella,
Desalination **199**, 271 (2006).
- 50 A. S. Arico, et al., *Fuel Cells* **10**, 1013 (2010).
- 51 K. D. Kreuer, M. Schuster, B. Obliers, O. Diat, U. Traub, A. Fuchs, U. Klock, S. J.
Paddison, and J. Maier, *Journal of Power Sources* **178**, 499 (2008).
- 52 M. R. Tant, K. D. Lee, K. P. Darst, and C. W. Martin, *Polymeric Materials: Science and
Engineering* **58**, 1074 (1988).
- 53 R. B. Moore and C. R. Martin, **22**, 3594 (1989).
- 54 V. K. Shahi, *Solid State Ionics* **177**, 3395 (2007).
- 55 G. Alberti and M. Casciola, *Solid State Ionics* **145**, 3 (2001).
- 56 Y.-i. Park and M. Nagai, *Solid State Ionics* **145**, 149 (2001).
- 57 M.-S. Kang, J. H. Kim, J. Won, S.-H. Moon, and Y. S. Kang, *Journal of Membrane
Science* **247**, 127 (2005).
- 58 M. L. Hill, Y. S. Kim, B. R. Einsla, and J. E. McGrath, *Journal of Membrane Science* **283**,
102 (2006).
- 59 S. Zhong, C. Liu, Z. Dou, X. Li, C. Zhao, T. Fu, and H. Na, *Journal of Membrane Science*
285, 404 (2006).
- 60 D. J. Jones, E. Wortham, J. Rozière, F. d. r. Favier, J.-L. Pascal, and L. Monconduit,
Journal of Physics and Chemistry of Solids **65**, 235 (2004).
- 61 D. J. Jones and J. Rozière, *Adv. Polymer. Sci.* **215**, 219 (2008).
- 62 C. Yang, P. Costamagna, S. Srinivasan, J. Benziger, and A. B. Bocarsly, *Journal of Power
Sources* **103**, 1 (2001).
- 63 G. Alberti and M. Casciola, *Annu. Rev. Mater. Res.* **33**, 129 (2003).
- 64 G. Alberti, M. Casciola, and R. Palombi, *Journal of Membrane Science* **172**, 233 (2000).
- 65 L. Tchicaya-Bouckary, D. J. Jones, and J. Rozière, *Fuel Cells* **2**, 40 (2002).
- 66 P. Costamagna, C. Yang, A. B. Bocarsly, and S. Srinivasan, *Electrochimica Acta* **47**, 1023
(2002).

- 67 S. P. Nunes, B. Ruffmann, E. Rikowski, S. Vetter, and K. Richau, *Journal of Membrane Science* **203**, 215 (2002).
- 68 F. Bauer and M. Willert-Porada, *Journal of Membrane Science* **233**, 141 (2004).
- 69 C. Yang, S. Srinivasan, A. B. Bocarsly, S. Tulyani, and J. B. Benziger, *Journal of Membrane Science* **237**, 145 (2004).
- 70 F. Bauer and M. Willert-Porada, *Journal of Power Sources* **145**, 101 (2005).
- 71 F. Bauer and M. Willert-Porada, *Fuel Cells* **6**, 261 (2006).
- 72 V. S. Silva, S. Weisshaar, R. Reissner, B. Ruffmann, S. Vetter, A. Mendes, L. M. Madeira, and S. Nunes, *Journal of Power Sources* **145**, 485 (2005).
- 73 M. Casciola, D. Capitani, A. Comite, A. Donnadio, V. Frittella, M. Pica, M. Sganappa, and A. Varzi, *Fuel Cells* **8**, 217 (2008).
- 74 D. Jones, J. Rozière, and G. Scherer, (*Springer Berlin / Heidelberg*, 2008), Vol. 215, p. 219.
- 75 D. J. Jones and J. Rozière, *Inorganic/organic composite membranes*, in *Handbook of fuel cells- Fundamentals, Technology and Applications*; Wiley **3** (2003).
- 76 G. Alberti and M. Casciola, *Annual Review of Materials Research* **33**, 129 (2003).
- 77 G. Alberti and M. Casciola, *Solid State Ionics* **97**, 177 (1997).
- 78 M. Casciola, G. Alberti, A. Donnadio, M. Pica, F. Marmottini, A. Bottino, and P. Piaggio, *Journal of Materials Chemistry* **15**, 4262 (2005).
- 79 M. Casciola, A. Donnadio, M. Pica, V. Valentini, and P. Piaggio, *Macromolecular Symposia* **230**, 95 (2005).
- 80 H.-C. Kuan, C.-S. Wu, C.-Y. Chen, Z.-Z. Yu, A. Dasari, and Y.-W. Mai, (2006), Vol. 9, p. A76.
- 81 D. Jones and J. Rozière, in *Fuel Cells I*, edited by G. Scherer (*Springer Berlin Heidelberg*, 2008), Vol. 215, p. 219.
- 82 E. Peled, T. Duvdevani, and A. Melman, *Electrochem. Solid-State Lett.* **1** (1998).
- 83 M. Casciola, G. Alberti, A. Ciarletta, A. Cruccolini, P. Piaggio, and M. Pica, *Solid State Ionics* **176**, 2985 (2005).
- 84 G. Alberti, M. Casciola, M. Pica, D. J. Jones, J. Rozière, and B. Bauer, *Italian Patent No. PG2002A0013* (2002).
- 85 K. A. Mauritz, *Materials Science and Engineering: C* **6**, 121 (1998).
- 86 R. V. Gummaraju, R. B. Moore, and K. A. Mauritz, *Journal of Polymer Science Part B: Polymer Physics* **34**, 2383 (1996).
- 87 W. Y. Hsu and T. D. Gierke, *Journal of Membrane Science* **13**, 307 (1983).
- 88 F. Chen, Q. Shen, J. M. Schoenung, and L. Zhang, *Journal of the American Ceramic Society* **91**, 3173 (2008).
- 89 M. P. Rodgers, Z. Shi, and S. Holdcroft, *Fuel Cells* **9**, 534 (2009).
- 90 D. Truffier-Boutry, A. De Geyer, L. Guetaz, O. Diat, and G. Gebel, *Macromolecules* **40**, 8259 (2007).
- 91 G. Alberti, U. Costantino, R. Millini, G. Perego, and R. Vivani, *Journal of Solid State Chemistry* **113**, 289 (1994).
- 92 D. J. MacLachlan and K. R. Morgan, *The Journal of Physical Chemistry* **94**, 7656 (1990).
- 93 N. J. Clayden, *Journal of the Chemical Society, Dalton Transactions*, 1877 (1987).

CONCLUSIONS

In this thesis, inorganic layered structures such as (i) smectite clays synthetic and natural (Laponite and two montmorillonites: Kunipia and SWy-2) with different structural and physical parameters, (ii) graphite oxide (GO) and (iii) layered double hydroxides (LDHs) with different compositions (various combinations of metal cations, interlayer anions and molar ratios of divalent to trivalent cations), were tested as 2D nanofillers in order to create Nafion nanocomposites. Furthermore, functionalization of clays and GO with organo-surfactants bearing different hydrophilic groups (-NH₂, -OH, -SO₃H) was also performed in order to increase the number of acid sites and consequently the water retention of the produced nanocomposites membranes. Solution intercalation was followed for the synthesis of the above hybrid membranes. The type of solvent and the temperature for membrane preparation were examined in order to determine the optimum conditions for the preparation of highly homogeneous nanocomposite membranes.

Results showed that highly homogeneous exfoliated nanocomposites were created in most cases where the individual layered nanofillers are uniformly dispersed in the continuous polymeric matrix. The study of the water transport mechanism, consequently of the H⁺ ions within the electrolyte membrane, is one of the key aspects in the evaluation of these materials. The Pulse Field Gradient (PFG) NMR technique was used in this work to obtain a direct measurement of the water self-diffusion coefficients in a wide temperature range (20-130 °C) either in pure Nafion membrane or in the final nanocomposites.

For the clay nanocomposites the transport mechanism appears to be influenced from the dimensions of the dispersed platelets and mainly from the type of nanocomposites formed upon mixing the clay particles with the polymer matrix. A remarkable behaviour at high temperature (above 100 °C) is observed for the smectite clays Laponite and SWy-2, where composite membranes maintain stable and unwavering diffusion for many hours and in conditions of not humidification, proving the exceptional water retention property of these materials. Moreover, Swy-2 clays

particles demonstrate to be a potential physical barrier for methanol cross-over, reducing the methanol diffusion with an evident blocking effect and nevertheless ensuring a high water mobility up to 130 °C. The electrochemical behavior investigated by cell resistance and polarization measurements on these membranes show that the addition of clay materials to recast Nafion decreases the ohmic losses at high temperatures extending in this way the operating range of a direct methanol fuel cell. The organo-functionalizations of Lap and SWy clays materials have showed no particular effect on the first, while a considerable outcome in terms both of water absorption/retention and water mobility for the second one: some organo-SWy –based composite membrane shows an exceptional behavior above 100 °C where the membranes retained a small amount of "still mobile" water for several hours without any further humidification, denoting that the surface modifications of this clay with acid organic molecules significantly improve the performance of the final composite membrane. Diffusion's data together with $^1\text{H-NMR}$ spectral analysis has allowed a general description of the water distribution in the nanoporous membranes and has resulted in an estimation of the number of water molecules involved in the hydration shell of the sulfonic groups as well as that absorbed on the organoclay particles.

Concerning the graphite oxide filler, the organo-functionalization with two linear amino-acids, SULF and VAL, resulted in composite membranes with very high performance over a wide range of temperatures. On the contrary, by using branched organo-surfactants, such as TES and SER, the respective composite membranes have very poor retention/diffusion properties, most probably due to their size and stereochemical configuration. In any case, the mechanical investigation of all the nanocomposites indicates that the organo modification of the GO produces membranes more structured and with higher stiffness than the filler-free Nafion.

High proton conducting Nafion nanocomposite membranes were developed using $\text{Mg}^{2+}/\text{Al}^{3+}$ layered double hydroxides as nanofillers. LDHs with different $\text{Mg}^{2+}/\text{Al}^{3+}$ metal ratios (2:1 and 3:1) and various interlayer anions (CO_3^{2-} , ClO_4^- , NO_3^-) were prepared and incorporated in Nafion polymers with different equivalent weight, 1000 EW and 1100 EW. The transport mechanism appears to be affected of the different interlayer anions but mainly of the $\text{Mg}^{2+}/\text{Al}^{3+}$ metal ratios. A further electrochemical investigation has demonstrated that some composite membranes show better

performance than recast Nafion, indicating that the filler introduction has a beneficial effect in a drastic operative conditions of the cell.

Perspective future of this work will be to deepen some aspects and properties of the best nanocomposites here exposed, e.g. by testing them in fuel cells, i.e. in real operating conditions.

Acknowledgements

This work would not have been possible without the extensive and precious support from a great number of people. I would like to express my deep thanks to all of them!

First of all, I deeply thank my supervisor Dr. Isabella Nicotera for believing in me and giving me the opportunity to join the scientific community. I am extremely grateful to her for the continuous support, guidance and for sharing all her practical and theoretical knowledge with me. All her advices have been invaluable on both an academic and a personal level.

I am thankful to Prof. Giuseppe A. Ranieri for providing me the opportunity to work in the Physical Chemistry Soft Matter Laboratory “Mario Terenzi” (PC_SM Mario Terenzi) of the Department of Chemistry in the University of Calabria. I also thank the members of my group, Prof. Luigi Coppola and Dr. Luigi Gentile.

Special thanks to Prof. Dimitrios Gournis from the Department of Materials Science & Engineering (University of Ioannina, Greece) for his excellent collaboration, continuous encouragement and assistance to me.

I am very grateful to Dr. Apostolos Enotiadis for his significant support, advice, many insightful discussions and suggestions. I also want to thank Dr. Maria Baikousi for her assistance.

Dr. Alessandra Carbone and Dr. Vincenzo Baglio from CNR-ITAE Institute (Messina, Italy) are acknowledged for their great collaboration and for providing me with the electrochemical data.

I want to thank Dr. Noemi Baldino from the Department of Engineering Modeling (University of Calabria, Italy) for supporting me with mechanical characterization of materials.

Many thanks to Prof. Raffaele Giuseppe Agostino from the Department of Physics (University of Calabria, Italy) for his significant help with the SEM measurements.

I am particularly thankful to Dr. Deborah Jones and Prof. Jacque Rozière for providing me the opportunity to have my stage in their group, in the Institute Charles Gerhardt ICGM – AIME, CNRS - University of Montpellier II, in France. Working in such a nice environment has been a pleasure for me. I also thank very much all the members of the group, Dr. Surya Subianto, Dr. Sara Cavaliere for their assistance and productive discussions, the Ph.D. students, Aurélien Fraise Kreis, Vincent Goellner, Julia Savich, Marta Zaton, Nicolas Sephane, Anita Skulimowska, Elia Giannoti, Alvaro Reyes, Gautie Meunassol and Dr. Nicolas Donzel for their limitless support during my sojourn in the group and especially for their friendship.

I am grateful to International Doctoral School of Science and Technology “Bernadino Telesio” for the financial support during these three years.

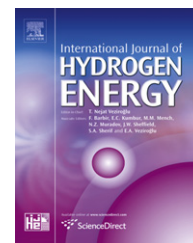
I deeply thank my friends Myrsini, Katerina, Massimiliano, Costanza, Francesca, Debora, Georgios, Ali, and Amir that have been a wonderful company these years.

Many thanks to all my best friends in Greece, Efi, Daphne, Rania, Nikos, Eleni, klairi because they are sincerely, always here for me, despite the distance. Special thanks to Pierre-Luc for his endless support, patience and for standing by me all this time.

I really thank my beloved grandfather, Ilias, who always believed in me, I wish he could still be here to see me reaching the end.

Last but definitely not least I would like to thank my parents, Miranda and Savas, and my sister Marianna, for supporting, encouraging and helping me to overcome every difficulty all these years.

Thank you all!!!

Available at www.sciencedirect.comjournal homepage: www.elsevier.com/locate/he

Evaluation of smectite clays as nanofillers for the synthesis of nanocomposite polymer electrolytes for fuel cell applications

Isabella Nicotera^{a,*}, Apostolos Enotiadis^b, Kristina Angjeli^a, Luigi Coppola^a,
Dimitrios Gournis^b

^a Department of Chemistry, University of Calabria, 87036 Rende, Cosenza, Italy

^b Department of Material Science and Engineering, University of Ioannina, 45110 Ioannina, Greece

ARTICLE INFO

Article history:

Received 8 March 2011

Received in revised form

27 May 2011

Accepted 9 June 2011

Available online 13 July 2011

Keywords:

Self-diffusion

NMR

PEMFC

Nanocomposite membranes

Clays

ABSTRACT

Synthetic and natural smectite clays, with different structural and physical parameters, were tested as nanofillers for the creation of Nafion nanocomposites. The solution intercalation method has been successfully applied for incorporation of layered materials into the polymer, while the effect of the solvent, temperature and filler loading were examined in order to determine the optimum conditions for the preparation of highly homogeneous composites.

NMR methods, including pulsed-field-gradient spin-echo (PFGSE) and spin-lattice relaxation time (T₁) were used to investigate behavior of water confined in recast Nafion and in Nafion–clay hybrids membranes.

The transport mechanism appears to be influenced from the dimensions of the dispersed platelets and mainly from the type of nanocomposites formed upon mixing the clay particles with the polymer matrix. Compared to pure Nafion, the water uptake and the water diffusion of the hybrid membranes are increased, with the exception of the Kunipia–Nafion composite. A remarkable behaviour at high temperature is observed, where composite membranes maintain stable and unwavering diffusion for many hours and in conditions of not humidification, proving the exceptional water retention property of these materials. Finally the hybrid membranes are much stiffer and can withstand higher temperatures compared to pure Nafion, hence both these characteristics are highly desirable for use in fuel cell applications.

Copyright © 2011, Hydrogen Energy Publications, LLC. Published by Elsevier Ltd. All rights reserved.

1. Introduction

The fuel cell technology has increased rapidly during the last two decades. PEMFCs operating in the typical 60–80 °C temperature range face problems including poor carbon monoxide tolerance and heat rejection. These drawbacks can be overcome by increasing the operating temperature range up to 120–130 °C. In this temperature two opposite effects come into play: i) improved electro-catalytic kinetics and ii) decreased proton

conductivity of the electrolyte. Furthermore, high temperature operation will reduce the complexity of the reforming reactor employed for PEMFC [1–3]. PEMFC performance is critically dependent on the membrane water content. However, too much humidification causes flooding of the electrodes and consequently, the diffusion overpotential increases due to insufficient oxygen and hydrogen supply. In order to reduce these overpotentials, properties such as stable water uptake and high proton conductivity are essential for the electrolyte.

* Corresponding author. Tel.: +39 0984 492021; fax: +39 0984 492044.

E-mail address: isabella.nicotera@unical.it (I. Nicotera).

Composite perfluorosulfonic membranes based on Nafion containing hygroscopic ceramic oxides (such as titania nanotubes [4] and particles [5,6], $Zr(HPO_4)_2$ [7,8], ZrO_2 [9], Fe_2O_3 [10], SiO_2 [11–14], etc) have been demonstrated to operate up to about 150 °C both in direct methanol [15] and hydrogen–air [14,16,17] polymer electrolyte fuel cells with reduced preheating temperature for the reactants (85 °C). As opposite, Nafion membranes without ceramic fillers may operate only up to 130 °C [2] under elevated pressures (4 atm abs) and with higher reactants preheating temperature (120–140 °C). Additionally, the inclusion of inorganic fillers improves the mechanical properties and the membrane water management.

In this study we propose a new class of fillers based on swellable smectite clays [18]. Smectite clays are a class of layered aluminosilicate minerals with a unique combination of swelling, intercalation, and ion exchange properties. They consist of an octahedral alumina layer fused between two tetrahedral silica layers (about 1 nm). Such clays have a cation exchange capacity, which depends on the substitution of low valent atoms, e.g., Mg^{2+} for Al^{3+} in the octahedral sheet and Al^{3+} for Si^{4+} in the tetrahedral sites. As a consequence, the 1 nm thick aluminosilicate platelets have a fixed negative charge and neutrality is obtained, for example, by hydrated cations present in the galleries. The intercalation process in these systems is equivalent to ion exchange, and unlike the intercalation compounds of graphite, it does not involve necessarily charge transfer between the guest and host species. The charge on the layers affects many fundamental properties of the clays, including water holding (an important property for the creation of Nafion nanocomposite membrane), cation fixation, swelling ability, cation exchange capacity and high specific surface area.

Depending on the strength of interfacial interactions between the polymer matrix and the inorganic materials, three different types of nanocomposites are thermodynamically achievable, as shown in Fig. 1: (1) conventional composites, where packages of silicate layers, keep their stacking, creating a conventional phase separated composite (microcomposite), (2) intercalated nanocomposites, where the polymer chains are intercalated between the silicate layers, therefore increasing their gallery height but maintaining their layered stacking, resulting in a well ordered multilayer with

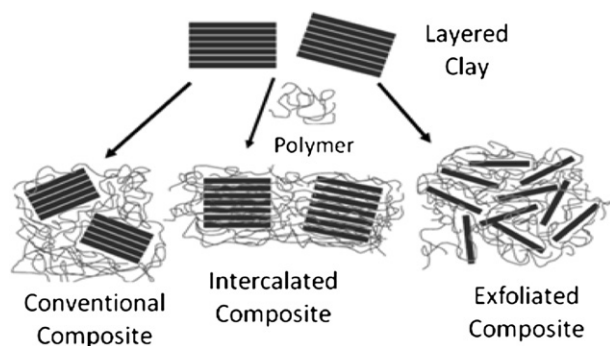


Fig. 1 – Image describing the three types of clay-polymer composites: conventional composites (or micro-composites), intercalated nanocomposites and exfoliated nanocomposites.

alternating polymer/silicate layers, (3) exfoliated nanocomposites, in which the individual clay layers lose their stacking and are exfoliated and dispersed in the continuous polymeric matrix [19].

The conventional procedures to prepare these nanocomposites include: i) solution [20,21], ii) melt intercalation [22], where the polymer intercalate to the interlayer space from solution or melt respectively and iii) in situ polymerization [23], where the polymerization is started inside of the clay galleries. Melting intercalation is more industrial than the solution; however the exfoliated clays, incorporated into the polymeric matrix, have obtained easily and effectively by solution intercalation [24].

Over the last decade, many efforts have been made for the development of Nafion composite membranes using swellable clays as nanofillers [25]. The presence of two dimensional platelike silicate layers in the Nafion matrix showed significant gains in thermal [26], mechanical [26] and methanol barrier [20] properties while reduces the methanol permeability [27–29] and increases the water retention [29] and the power density [22,26] of the resulting nanocomposite membranes.

In this work, one synthetic (Laponite) and two natural clays (Kunipia and SWy-2 montmorillonites) with different structural and physical parameters were chosen as nanofillers: Laponite shows both low layer charge density and particle size (20 nm), SWy-2 has a medium layer charge density and high particle size (200 nm) and, finally, Kunipia has a high layer charge density and particle size also around 200 nm.

Hybrid membranes were synthesized by solution intercalation with different filler loadings (1, 3, 6 and 9 wt% with respect to the polymer) in order to create Nafion nanocomposites with improved water retention properties, stability in temperature and good water mobility performance. The choice of the solvent during the preparation procedure of the membranes and its effect on the clay-fillers were also examined with the aim to determine the optimum conditions for the preparation of highly homogeneous nanocomposite membranes.

The study of the water transport mechanism is one of the key aspects in the evaluation of these materials and the Pulse-Field-Gradient Spin-Echo NMR (PFGSE-NMR) method [30] was employed in this work to obtain a direct measurement of the water self-diffusion coefficients in recast Nafion and Nafion composite membranes. This technique has been shown to provide valuable information on water transport in PEM materials [31]. NMR spin-lattice relaxation times (T_1) were also taken as a function of temperature and water content. Additionally, both pristine materials (clay and Nafion) as well as the resulted nanocomposite membranes were characterized by a combination of powder X-ray diffraction, FTIR spectroscopy and thermogravimetric analysis.

2. Experimental section

2.1. Materials

Three different smectites clays with different structural and physical parameters (structural formula, particle size and

cation exchange capacity) were used. The first was a natural Wyoming montmorillonite (SW_y-2) obtained from the Source Clay Minerals Repository, University of Missouri, Columbia, with a cation exchange capacity (CEC) measured by the Co(II) procedure equal to 80 mequiv per 100 g clay and particle size around 200 nm. The second clay, was also a natural sodium-saturated montmorillonite Kunipia (KUN) purchased from Kunimine Industries Co (Japan), with higher CEC than the SW_y-2 (120 mequiv per 100 g clay) and with the same particle size like SW_y-2. Finally, the third smectite was a synthetic trioctahedral hectorite, Laponite (Lap), produced by Laporte Industries Ltd with the lowest CEC 48 mequiv per 100 g clay and the smallest particle size (20 nm). Table 1 summarize the properties of these clay materials and their structural formula. Montmorillonites were fractionated to <2 μm by gravity sedimentation and purified by well-established procedures in clay science [32]. Sodium-exchanged samples (Na⁺-SW_y-2) were prepared by immersing the clay into 1 N solution of sodium chloride. Cation exchange was complete by washing and centrifuging four times with dilute aqueous NaCl. The samples were finally washed with distilled-deionized water and transferred into dialysis tubes in order to obtain chloride-free clays and then dried at room temperature.

Finally, Nafion solution (20 wt% in mixture of lower aliphatic alcohols and water) and the solvents (isopropyl alcohol (IPA) and *N,N*-dimethylformamide (DMF)) were purchased from Aldrich and used as received.

2.2. Composites membranes preparation

The composite membranes were prepared from 20 wt% Nafion[®] solution according to the following processes: i) 1g of Nafion solution was heated at about 60 °C to remove all the solvents (water, isopropanol, etc.); ii) Nafion resin was redissolved with 10 ml of the desired solvent (DMF or IPA) until become a clear solution; iii) the filler was dispersed in the same solvent under stirring for 1 day and added slowly to the solution of Nafion; iv) the final solution was ultra-sonicated for 1 h and then stirred at 60 °C to ensure complete mixing; finally v) casting on a petridisk at about 50 °C for the suspension with IPA and between 100 and 110 °C for DMF overnight, was performed in order to obtain a homogeneous membrane. The hybrid membrane was removed from the petridisk by immersing the glass plate in deionised water for several minutes. In order to reinforce the membrane, this was sandwiched and pressed between two Teflon plates and put in oven at 150 °C for about 15 min. All composite membranes

produced by casting were subsequently treated by rinsing in: (i) boiling HNO₃ solution (1 M) for 1 h to oxidize the organic impurities, (ii) boiling H₂O₂ (3 vol %) for 1 h in order to remove all the organic impurities, (iii) boiling deionized H₂O for 40 min three times, (iv) boiling H₂SO₄ (0.5 M) for 1 h to remove any metallic impurities, and again (v) boiling deionized H₂O for 40 min twice to remove excess acid. According to McMillan et.al [33], an ulterior purification procedure was performed in order to ensure the removal of paramagnetic contaminants which are particularly damaging an n.m.r. experiment, such as the presence of copper that we found by Electron Paramagnetic Resonance analysis. By this procedure membranes were soaked in EDTA solution (0.001M) for 1 day after followed by a thorough rinse. Then soaked in 2 M HCl at a temperature of 80 °C for 2 h followed by boiling in fresh distilled–deionized water to remove any residual acids and again repeated the treatment with EDTA. Finally, rinsing in boiled deionized water three times to remove residual EDTA and stored at room temperature at fully hydrated state.

2.3. Characterization

The X-ray powder diffraction data were collected on a D8 Advanced Bruker diffractometer by using CuK_α (40 kV, 40 mA) radiation and a secondary beam graphite monochromator. The patterns were recorded in a 2-theta range from 2° to 40°, in steps of 0.02° and counting time 2 s per step. Infrared spectra were measured with an FT-IR 8400 spectrometer, in the region of 400–4000 cm⁻¹, equipped with a DTGS detector. Each spectrum was the average of 32 scans collected at 2 cm⁻¹ resolution. Membrane samples were measured as prepared. Thermogravimetric (TGA) analysis was performed using a Perkin Elmer Pyris Diamond TG/DTA. Fully dried and hydrated samples of approximately 5 mg were heated under nitrogen from 25 to 850 °C, at a rate of 10 °C/min.

NMR measurements were performed using a Bruker AVANCE 300 wide bore NMR spectrometer working at 300 MHz on 1H. Spectra were obtained by transforming the resulting free-induction decay (FID) of single π/2 pulse sequences. Self-diffusion coefficients of water were performed with a Diff30 NMR probe by using the pulsed field gradient spin-echo (PFGSE) method [30] with a gradient pulse length of 1 ms, a delay time for diffusion of Δ of 10 ms, and varying the gradient amplitude from 10 to 700 G/cm. Uncertainties in D measurements are ~3%. Finally, longitudinal relaxation times (T₁) of water were measured on the same spectrometer by the inversion-recovery sequence (π–τ–π/2). Both self-diffusion

Table 1 – Some physical properties and the structural formula of laponite (Lap) and the two montmorillonites (SW_y-2 and Kunipia).

Clay	Particle size (nm)	CEC ^a (meq/100 g)	Charge density (e ⁻¹ /unit cell) ^b	Structural formula
Lap	20	48.1	0.5	Na _{0.56} [Mg _{5.4} Li _{0.4}]Si ₈ O ₂₀ (OH) ₄
SW _y -2	200	76.4	0.6	Na _{0.62} [Al _{3.01} Fe(III) _{0.41} Mg _{0.54} Mn _{0.01} Ti _{0.02}](Si _{7.98} Al _{0.02})O ₂₀ (OH) ₄
Kun	200	119	0.9	Na _{0.87} [Al _{3.12} Fe(III) _{0.20} Mg _{0.61} Ti _{0.01}](Si _{7.90} Al _{0.10})O ₂₀ (OH) ₄

a CEC is the cation exchange capacity.

b Unit cell is the Si₈O₂₀ unit.

and T_1 measurements were conducted by increasing temperature step by step from 20 to 140 °C, with steps of 10 °C, and leaving the sample to equilibrate for about 20 min.

Prior to the NMR measurements, membranes were dried in oven, weighed and then immersed in distilled water at room temperature. Upon being removed from the water they were quickly blotted dry with a paper tissue (to eliminate most of the free surface liquid). The water content value was determined using a microbalance and recorded as: uptake % = $[(m_{\text{wet}} - m_{\text{dry}}) / m_{\text{dry}}] \times 100$.

At this point the membranes were loaded into a 5 mm NMR Pyrex tube and hermetically sealed. In order to minimize the evaporation of the solvent from the membrane with increased temperature, a “cap” of Teflon was placed just above the membrane. Thus, the free volume available to the evaporated water was minimized.

3. Results and discussion

X-ray diffraction (XRD) measurements provide a powerful tool to evaluate the type of composites created after the incorporation of the inorganic layered nanofillers in the Nafion matrix. Fig. 2 shows the XRD patterns of the recast-Nafion and of three nanocomposites prepared using DMF as solvent (see experimental part) with KUN, SWy-2 and Lap at the same filler to polymer loading (3 wt%). All XRD patterns show clearly the existence of the characteristic peaks of Nafion structure: the first one is observed at 2–3° corresponding to a Bragg spacing of 3–5 nm, which is typical of a system containing ionic clusters [34], while a broad band centered at 18° is also distinctive of the polymer arrangement (crystalline peak scattering from the polyfluorocarbon chains of Nafion) [22,35]. In the case of KUN and SWy-2 Nafion nanocomposites, a 001 reflection appeared at 7° due to the presence of packages

of ordered aluminosilicate layers in the mass of the polymeric matrix. This peak corresponds to an intersheet separation of $L = (12.6 \text{ \AA} - 9.6 \text{ \AA}) = 3.0 \text{ \AA}$, where 9.6 Å is the thickness of the clay layer [32], indicating probably the creation of micro-composites (conventional composites) when using these two montmorillonites as fillers. In fact, XRD patterns (Fig. 2B) of both montmorillonites, treated several times with DMF and dried at room temperature, show a d_{001} -spacing of 12.6 Å, the same to that observed in the patterns of montmorillonite-Nafion composites. However, the intensity of the 001 peak in SWy-2 nanocomposite is significant lower than that of Kuni-pia nanocomposite, implying that in the case of Wyoming montmorillonite a small fraction of clay platelets retains its stacking while the majority is existing in fine dispersion between polymer chains (partially exfoliated). On the other hand, in the case of Laponite, the absence of the d_{001} diffraction peak in the pattern of the final nanocomposite, characteristic of the sodium-Laponite, indicates that the ordered structure of the layered mineral is effectively eliminated after mixing with the polymeric mass. The stronger interaction of DMF molecules with Laponite platelets compared with the two montmorillonites is confirmed from the XRD measurements (Fig. 2B). Laponite treated with DMF solvent, shows an increase in basal spacing (d_{001}), from 12.6 Å in the pristine clay to $d_{001} = 14.4 \text{ \AA}$ ($L = 14.4 \text{ \AA} - 9.6 \text{ \AA} = 4.8 \text{ \AA}$), indicative of the intercalation of a high amount of DMF molecules into the clay interlayers. This confirms the strong interaction of DMF with the siloxane surfaces of Laponite [36] and is probably responsible, in conjunction to the small size of Laponite platelets (20 nm), for the creation of fully exfoliated nanocomposites.

The presence of the clay nanofiller in the final Nafion composites is revealed also from FTIR spectra. Fig. 2C shows the FTIR spectra in the region between 400 and 900 cm^{-1} of pristine Nafion and Lap-Nafion membranes, while the

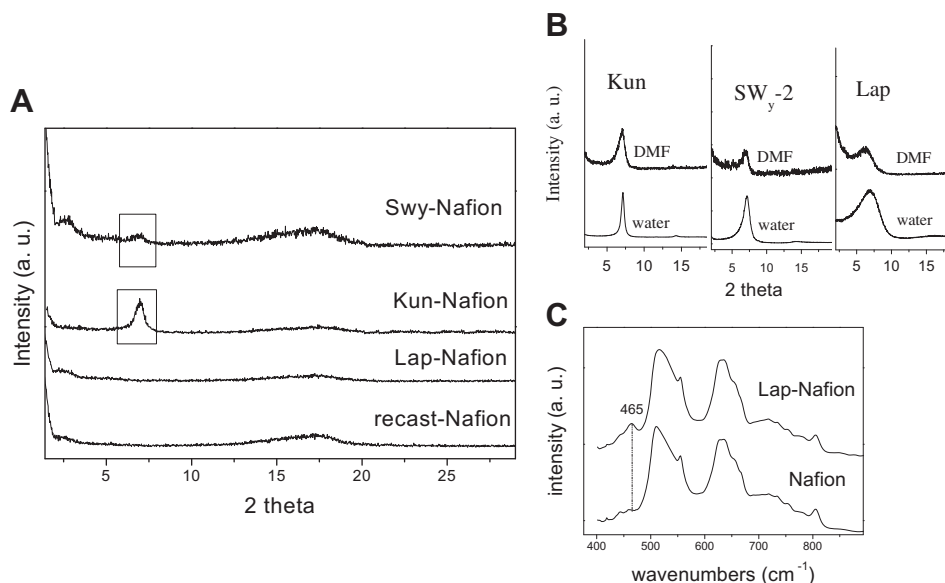


Fig. 2 – A) XRD patterns of recast Nafion and nanocomposites membranes prepared with KUN, SWy-2 and Lap, at the same loading (3 wt% respect to the Nafion polymer) using DMF as solvent, **B)** XRD patterns of pristine clays (Lap, SWy-2 and KUN) before and after treatment with DMF for several times and **C)** FTIR spectra of the recast Nafion and the nanocomposite membrane with Laponite in 3 wt% loading.

correlative attribution of vibrational peaks detected is summarized in Table 2 [37,38]. The spectrum of Laponite hybrid membrane shows all the characteristic bands of Nafion, while the peak at 463 cm^{-1} , corresponding to Si–O vibration of the clay lattice, is indicative of the existence of the phyllosomorphous nanomaterial in the final composite. Furthermore, TGA results of dried membranes (Fig. 3) shows that in the case of nanocomposite loaded with 3 wt% Laponite, the decomposition of Nafion was shifted to higher temperatures. The higher thermal resistance of the nanocomposite than that of pure Nafion membrane is due to the strong interaction of polymer main chains with Laponite which in fact provides evidence for the homogeneous dispersion of the silicate platelets in the polymeric matrix [30]. Similar results were observed for all the series of nanocomposites (not shown here) indicating that all clay nanofillers distributed homogeneously on the polymer matrix. On the other hand, thermogravimetric measurements on hydrated membranes (Fig. 3 inset) were also performed for pristine Nafion and Lap-Nafion (3 wt%). From the weight loss up to $120\text{ }^{\circ}\text{C}$ the percentage water uptake was calculated from the equation: % water uptake = (mass hydrated – mass dried)/mass dried $\times 100\%$ [39]. The percentage water uptake was estimated 25% for pristine Nafion and 37% for Lap-Nafion membrane, indicating that nanocomposite membrane adsorbs significant higher amount of water compared to recast Nafion.

NMR technique was applied in this study to investigate the transport properties of water molecules confined in the porous structure of the Nafion membrane and in order to check the effect of the clay-fillers added. Fig. 4 displays the plot of the water self-diffusion coefficients measured by PFG-NMR method on completely swelled membranes, in the temperature range $25\text{--}140\text{ }^{\circ}\text{C}$. In this graph the self-diffusion coefficients of the three hybrid composites, Lap-Nafion, SWy-Nafion and Kun-Nafion, are compared with the recast Nafion.

As expected, recast Nafion shows a sudden decrease of the diffusion after $60\text{ }^{\circ}\text{C}$, due to loss of water from the membrane. Similar behavior is also displayed by the Kun-Nafion

Table 2 – FTTR assignments if the recast Nafion and the nanocomposite membrane with Laponite in 3 wt% loading.

Frequencies of bands		Band assignments ^a
Nafion	Lap-Nafion	
	463	$\nu(\text{Si-O})$
514	511	$\delta(\text{CF}_2)$
554	555	$\nu(\text{CF}_2)$
631	632	$\omega, \delta(\text{CF}_2)$
655	657	
718	718	$\nu_s(\text{CF}_2)$
804	804	$\nu(\text{C-S})$
970	968	$\nu_s(\text{C-O-C})$
981	927	$\nu_{as}(\text{C-O-C})$
1056	1056	$\nu_s(\text{SO}_3^-)$

a ν : stretching; δ : bending; ω : wagging; ν : twisting; r : rocking; ν_{as} : antisymmetric mode; ν_s , symmetric mode.

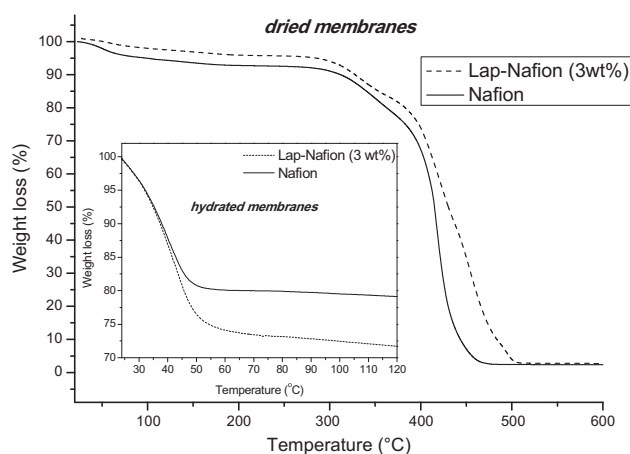


Fig. 3 – TGA curves of dried recast Nafion and nanocomposite membrane with Laponite in 3 wt% loading. Inset: TGA curves of the same hydrated membranes.

composite, whose diffusion decreases drastically after $80\text{ }^{\circ}\text{C}$, reaching values even lower than the recast Nafion.

This abrupt drop of the diffusion is hypothesized to be related to the inability of the membrane to retain water at high temperatures jointly with the pore/channel structure of the membrane, where the Kunipia particles, not exfoliated, block part of the hydrophilic polymer channels, through which water molecules migrate. The blocking effect becomes a significant factor just when the water content is low, i.e. when the hydrophilic domains sizes are reduced and therefore, big particles can obstruct the water molecules pathways.

On the contrary, Laponite and SWy-2 nanofillers show a significant effect on the water mobility with diffusion values very high and in all temperature range investigated.

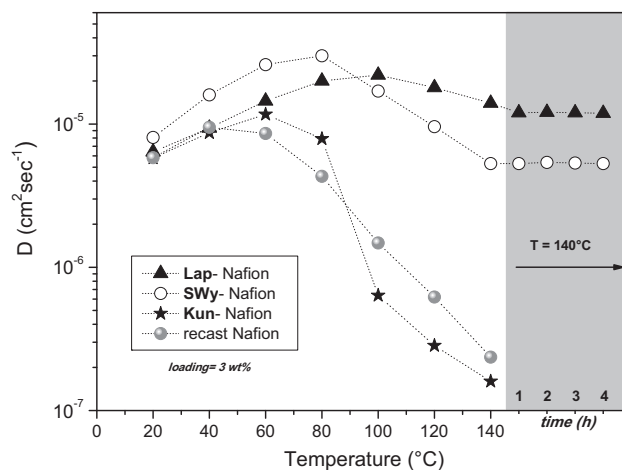


Fig. 4 – Self-diffusion coefficients as function of the temperature (from $20\text{ }^{\circ}\text{C}$ up to $140\text{ }^{\circ}\text{C}$) of the water confined in recast Nafion and in clay composites membranes (3 wt% loading) and at the maximum water uptake. The grey part in the graph shows the self-diffusion coefficients measured at $140\text{ }^{\circ}\text{C}$ after each hour for 4 h.

The temperature evolution of the diffusion coefficients displays a regular increasing up to 80–100 °C and then decrease, slightly for Lap composite, appreciably for SWy composite. In order to clarify why despite the increasing of the water molecules thermal energy, the diffusion decreases, we need to consider the distribution of the water inside the ionic pores of Nafion membranes: a certain amount of water is involved in the primary hydration shells of the SO_3^- groups as well as of the clays hygroscopic surfaces, while most of the additional water fills the volumes of pores forming higher order hydration layers and behaves more bulk-like [40,41]. Discriminate between these different environments can be difficult because of the fast rate of proton exchange in acidic water, so we see only one ^1H NMR signal and the diffusion coefficient is the average result from different water species. In heating, the proton signal intensity decreases due to the water evaporation, which mostly involves the bulk water. Therefore, above 100 °C, the biggest contribution to the diffusion coefficients comes from the hydrated water whereby the mobility is reduced. The obstruction effect causes further reduction of diffusivity, in particular for the SWy-Nafion nanocomposite which, similarly to Kunipia, presents a small amount of big particles not completely exfoliated.

However, the noteworthy result is that both membranes maintain stable water diffusion and unwavering at 140 °C after at least 4 h and in conditions of not humidification. As described in the experimental section, for the NMR measurements the membrane is put in a Pyrex tube and sealed on the top with a cap, without any further supply of humidification. Obviously, part of the water evaporates from the membrane during the heating (e.g. after cooling we find some little drops on the walls tube), however, the self-diffusion coefficient measured at 140 °C is that of the water remaining in the electrolyte membrane because the water vapor diffuses much more quickly. Therefore, these clay-fillers dispersed in the polymer matrix maintain a certain humidity of the membrane even at rather high temperatures, and this water is responsible for the diffusion revealed by NMR spectroscopy.

It is well-known [7,8,12] the strong relationship between water uptakes of the electrolyte and the self-diffusion coefficients that is, the systems which absorb more water, exhibit higher diffusivity at room temperature or, usually, up to 60–80 °C (above these, the water retention ability of the membrane is crucial). The histogram in Fig. 5 illustrates the maximum water uptake reached from each membrane. All the nanocomposites can absorb more water than recast Nafion (24 wt%) in agreement with TGA results: Kun-Nafion is around 28 wt%, Lap-Nafion is 35 wt% while SWy-Nafion absorbs up to 45 wt% of water.

These differences in the water uptakes can be explained by considering the combination of at least three factors: CEC and particle size of the clay as well as exfoliation degree of the clay nanoplatelets in the polymeric matrix. SWy-2 and Kunipia have similar dimensions and high CEC but the first is able to exfoliate almost totally - only a small fraction of clay platelets retains its stacking - therefore a bigger amount of hydrophilic sites on the layers are available for hydration. Moreover, the dimensions of each platelet can promote stronger alterations of the network structure, e.g. creating larger cavities where the water molecules can be hosted in cluster form. Laponite is

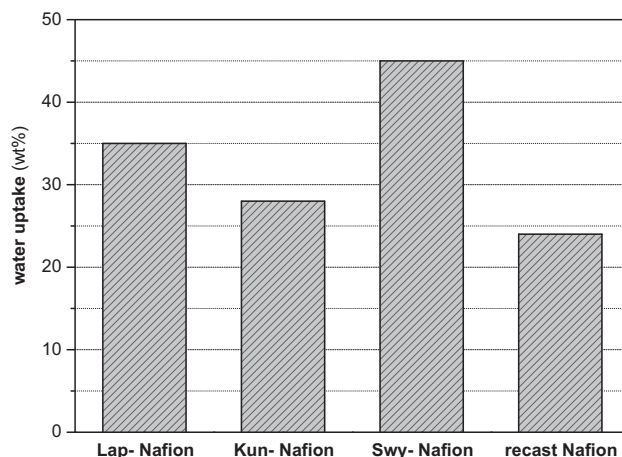


Fig. 5 – Histogram of the maximum water uptake value reached from recast Nafion and from the composite membranes.

a compromise between the two montmorillonites because it is completely exfoliated but has the smaller CEC and particle size.

In spite of this last data, self-diffusion coefficients reported in Fig. 4 put in evidence a better performance of the Laponite nanocomposite than SWy-2, in particular above 100 °C. This suggests that, the amount of water absorbed from the electrolyte prevails at lower temperatures, while at higher temperatures, when the amount of water is low, is important to consider the structure of the complex “filler-polymer” and the blocking effect of the nanoparticles.

Further information on the molecular dynamic of the water is provided by measurements of longitudinal relaxation times (T_1) (Fig. 6). T_1 reflects more localized motions, including both translation and rotation, on a time scale comparable to the reciprocal of the NMR angular frequency (~ 1 ns); higher T_1 values indicate more facile water molecular motion. The graph shows the temperature dependence of T_1 of the water

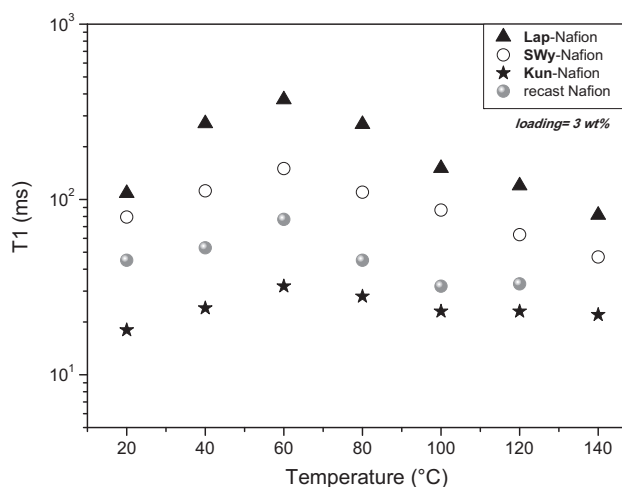


Fig. 6 – Plots of water longitudinal relaxation times (T_1) measured in the temperature range from 20 °C up to 140 °C for recast Nafion and composite membranes at the maximum water uptake.

confined in recast Nafion and hybrid membranes. Laponite and SWy-2 composites exhibit higher T_1 than the recast Nafion and Kunipia composite, quite consistent with the diffusion trends observed in Fig. 4. However, we should underline once more the exceptional behavior of the Laponite clay that seems favor strongly the local mobility of the water. In fact, even if the water content is less than SWy-Nafion composite, its relaxation times are very high respect both recast Nafion and the other composites and, as saw before, this is reflected on the long-range diffusion properties, i.e. displacements of the order of the micron.

In fact, the proton transport process in membranes, such as Nafion, is generally hypothesized as the contribution of two conduction mechanisms: the *Vehicle mechanism* [42,43] that involves the protons diffusion on a vehicle, such as H_3O^+ ions, but disadvantaged in dehydration state, and the *Grotthuss mechanism* [44], where proton mobility in water is connected to rotation of water molecules within a constantly changing network of hydrogen bonds (*structural diffusion*). The first one prevails at low temperatures when the water content is high, while the second mechanism is expected to be predominant at high temperatures in the dehydration state, therefore, it is surely favorite in the Laponite composite that shows the highest longitudinal relaxation times.

A last consideration about the T_1 measurements is that the particle blocking effect is less important as T_1 reflects localized motions. This is consistent with the much smaller magnitude of T_1 drop than that of D .

From the above data, the synthetic Laponite seems the most promising smectite clay that can be used as filler and thus it could be the base to design, through chemical functionalization, hybrid layered structures such as organically modified clays (organoclays) [45] which can be used as nano-fillers for the creation of novel polymer nanocomposites.

However, in this preliminary study on clays, two basic issues must be further investigated: (1) the method of preparation of the membranes, and especially the solvent used to dissolve both polymer and filler; (2) the optimum filler loading with respect to the polymer. The first one comes from the XRD results shown in Fig. 2 on the interaction/intercalation of solvent molecules in the interlayer space of the Laponite; the second is related to the goodness of the structural modifications of Nafion resulting from the dispersion of clay material since it is clear that the mass transport in the electrolyte deeply depend on the molecular-level structure.

In order to evaluate the type of solvent used during the membrane preparation, Lap-Nafion nanocomposite membranes, at the same clay/polymer loading (3 wt%), were synthesized using DMF (*N,N*-dimethylformamide) and IPA (isopropyl alcohol) as solvents. The XRD patterns (Fig. 7) of the composites membranes (patterns c and d) do not present the characteristic d_{001} diffraction peak due to sodium-clay, indicating in both cases the creation of fully exfoliated structures. However, NMR results (Fig. 8) show a different behavior between Laponite composite prepared by using DMF and that prepared by using IPA.

The loading of the filler in the polymer was fixed at 3% in mass and we compare two water uptake values, about 27 wt% and 15 wt%, respectively. The choose of the uptake value at about 27 wt% was imposed from the maximum absorption of

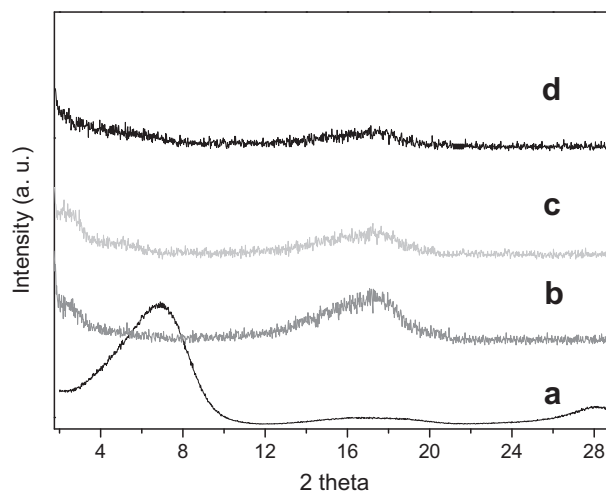


Fig. 7 – XRD patterns of a) pristine Laponite, b) recast Nafion, c) Nafion-Laponite nanocomposite (3 wt%) prepared using DMF solvent and d) Nafion-Laponite nanocomposite (3 wt%) prepared using IPA solvent.

water reached from the composite prepared by IPA, showing already a first significant difference with the sample prepared by DMF which can absorb, as mentioned above, around 35 wt % of water.

The membrane prepared by IPA shows a decrease of the water mobility at temperature above 80 °C, differently from the membrane prepared by DMF that maintains self-diffusion coefficients almost constant up to 140 °C and for several hours. However, when the initial uptake of the membrane is at the maximum value, also the membrane by IPA has a good trend at high temperatures even if the diffusion is lowered of

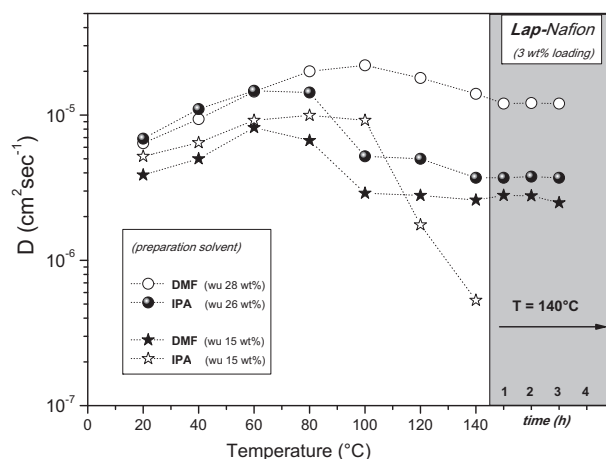


Fig. 8 – Self-diffusion coefficients as function of temperature (from 20 °C up to 140 °C) of the water confined in composites membranes of Lap-Nafion (3 wt% loading) prepared by DMF and by IPA solvents. For comparison, two water uptake (wu) values, high uptake (about 27 wt%) and low uptake (15 wt%), are presented. The grey part in the graph shows the self-diffusion coefficients measured at 140 °C after each hour for 4 h.

at least half order of magnitude after 80 °C. On the contrary, above 100 °C the collapse of the diffusion is net when the membrane by IPA has a low initial humidification grade, i.e. this system cannot anymore retain water inside. The electrolyte obtained by DMF, also at low humidification condition, manifests a very high diffusion performance.

Therefore, although from XRD data reported above we have seen that both the preparation by IPA and by DMF produces composites completely exfoliated, the final membranes are not the same as regard uptake, mobility and water retention at high temperatures. This could be attributed to:

- 1) The difference between the dielectric constant of these two solvents. In fact, DMF has a dielectric constant (36.7) almost double with respect to IPA (19.92). A higher value of dielectric constant favors Coulomb forces between the ionic sites of the system, imparting the right ionic dissociation grade. This property of the solvents, so, is expected to influence the microstructure of the hybrids during the preparation.
- 2) The combined effect of temperature and solvent on the polymer chains mobility. Basically, the preparation procedure of the membrane with DMF permits higher casting temperatures than IPA, due to its higher boiling point. Thermal excitation and plasticizing effect of the solvent imparts mobility to the polymer chains, consequently the size of the lamellar crystallites increases, their internal order probably improves, and a long-range order develops [46,47]. Instead, if the polymer chains are immobile, crystallization cannot occur and low-quality solution-cast films are obtained. Therefore, such reorganization of the polymeric structure and the probable presence of residual solvent in the hydrophobic phase, that acts as plasticizer, makes the polymeric matrix more elastic, facilitating the segmental motions and, consequently, water absorption and mobility.

Regarding the effect of the amount of the filler in the final hybrids, Fig. 9 shows the XRD patterns of the parent materials and the Lap-Nafion composites in different loadings. In particular we prepared four samples at 1, 3, 6 and 9 mass percentage loadings with respect to the Nafion polymer. Also here, even when the percentage of Laponite is increased, the absence of the d_{001} diffraction peak, characteristic of the sodium-clay, in the patterns of all the final hybrid composites indicates that the ordered structure of the layered mineral is effectively destroyed, leading to creation of exfoliated nanocomposites. The later proves the high affinity of Nafion polymer with the siloxane surfaces of Laponite clay.

Finally, Fig. 10 shows the diffusion data collected on membranes prepared at different Laponite clay loadings. The initial water uptake of the membranes with 1 and 3% of filler is around 35 wt%, while the membranes at 6 and 9% of loading can reach uptake values up to 40–42 wt%. In spite of this, the general behavior of the self-diffusion coefficients shows that the increasing of mobility is not at all proportional to the amount of clay in the system. On the contrary, the composite at higher loading is the most instable and loses water after 60 °C. At lower loading (1%) there is a discrete effect of the filler on the Nafion matrix while the best loading seems to be between 3 and 6%. This suggests, once more, that the microstructure of the

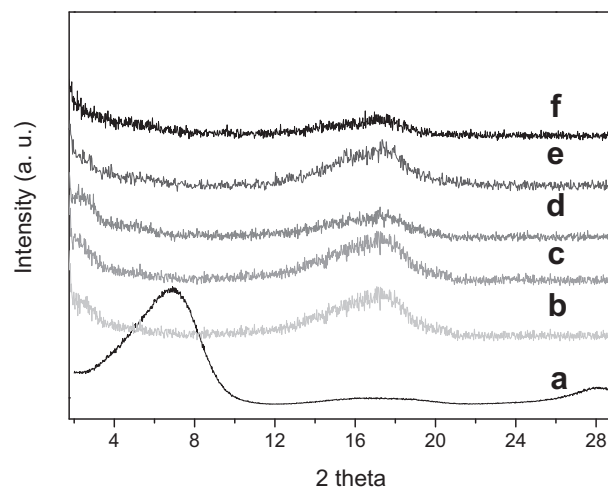


Fig. 9 – XRD patterns of a) pristine Laponite, b) recast Nafion and nanocomposites with synthetic Laponite at different loadings: c) 1 wt%, d) 3 wt%, e) 6 wt% and f) 9 wt%.

composite plays a significant role. In fact, further addition of filler, from one side strengthens the polymeric matrix and thus improves the mechanical properties of the membrane [48], from the other side clearly causes obstruction effects limiting the mobility of the water in the Nafion ionic domains. This optimum loading is in agreement with previous studies on Nafion-clay nanocomposite membranes which showed that the optimal ionic (proton) conductivity, methanol permeability and cell performance is also observed between 2.5 and 5 wt% nanoclay content [18,49,50]. This can be explained by the fact that at lower nanoclay loadings, somewhat better intercalation/exfoliation can be expected while at higher loadings, further dispersion of clay platelets is hindered, most probably due to percolation phenomena [51,52].

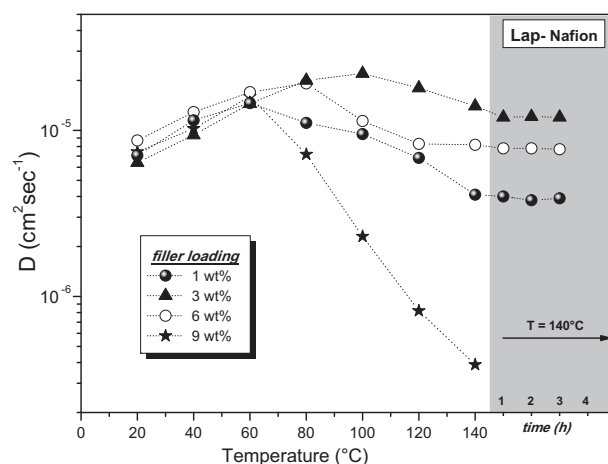


Fig. 10 – Self-diffusion coefficients as function of temperature (from 20 °C up to 140 °C), of the water confined in composites membranes of Laponite-Nafion prepared by DMF solvent and with four different filler loading: 1, 3, 6 and 9 wt%. The grey part in the graph shows the self-diffusion coefficients measured at 140 °C after each hour for 4 h.

4. Conclusion

Nafion hybrid membranes based on smectite clays were synthesized by solution intercalation and characterized by different techniques. One synthetic (Laponite) and two natural (Kunipia and Swy-2) layered aluminosilicate minerals with different physical and structural properties were tested as fillers in order to understand how basic parameters of the clays, such as particles size and layer charge density, can influence the final properties of the nanocomposite membranes.

XRD measurements reveal that SWy-2 and Kunipia montmorillonites produce conventional composites where the clay layers keep -in higher or less extend- their stacking, while exfoliated nanocomposites are created using Laponite.

The dynamic behavior of water confined in the recast Nafion and hybrid nanocomposites, in the temperature range 25–140 °C, was studied by NMR (self-diffusion and T_1) technique. With the exception of the Kunipia, both Laponite and SWy-2 show important effects both on water uptake and on transport properties. In fact, self-diffusion coefficients and T_1 have showed that the mobility of water molecules is favorite in these composites systems with respect to the recast Nafion. However, remarkable outcome is the behavior of these hybrids at high temperature: water diffusion remains stable and unwavering at 140 °C after at least 4 h and in conditions of not humidification, confirming the excellent ability of these clay-polymer complexes to retain water.

The effect of the filler loading and the type of solvent used for the membranes preparation were also investigated. We found that the optimum amount of Laponite clay incorporated into the polymer is between 3 and 6 mass percentage with respect to the Nafion, while a higher loading causes obstruction effects which effectively reduces the mobility of water.

Finally, the choice of the solvent used for the preparation of the composite membranes is not a negligible parameter. Hybrids prepared by using DMF as solvent have exhibited better performance than that prepared by IPA. We imputed this difference at: i) the higher dielectric constant of DMF than IPA and ii) the effect on the polymeric structure of the casting temperature of the membrane together with the plasticizer effect of DMF.

Acknowledgments

Apostolos Enotiadis gratefully acknowledges the Academy of Athens for a Ph.D. fellowship.

REFERENCES

- [1] Adjemian KT, Srinivasan S, Benziger J, Bocarsly AB. Investigation of PEMFC operation above 100 °C employing perfluorosulfonic acid silicon oxide composite membranes. *Journal of Power Sources* 2002;109(2):356–64.
- [2] Arico AS, Creti P, Antonucci PL, Antonucci V. Comparison of ethanol and methanol oxidation in a liquid-feed solid polymer electrolyte fuel cell at high temperature. *Electrochemical and Solid-State Letters* 1998;1:66.
- [3] Alberti G, Casciola M. Layered metalIV phosphonates, a large class of inorgano-organic proton conductors. *Solid State Ionics* 1997;97:177.
- [4] Jun Y, Zarrin H, Fowler M, Chen Z. Functionalized titania nanotube composite membranes for high temperature proton exchange membrane fuel cells. *International Journal of Hydrogen Energy* 2011;36(10):6073–81.
- [5] Amjadi M, Rowshanzamir S, Peighambaroust SJ, Hosseini MG, Eikani MH. Investigation of physical properties and cell performance of Nafion/TiO₂ nanocomposite membranes for high temperature PEM fuel cells. *International Journal of Hydrogen Energy* 2010;35(17):9252–60.
- [6] Jian-hua T, Peng-fei G, Zhi-yuan Z, Wen-hui L, Zhong-qiang S. Preparation and performance evaluation of a Nafion-TiO₂ composite membrane for PEMFCs. *International Journal of Hydrogen Energy* 2008;33(20):5686–90.
- [7] Nicotera I, Zhang T, Bocarsly A, Greenbaum S. NMR characterization of composite polymer membranes for low-humidity PEM fuel cells. *Journal of Electrochemical Society* 2007;154:B466–BB473.
- [8] Nicotera I, Coppola L, Rossi CO, Youssry M, Ranieri GA. NMR investigation of the dynamics of confined water in Nafion-based electrolyte membranes at subfreezing temperatures. *Journal of Physical Chemistry B* 2009;113(42):13935–41.
- [9] Pan J, Zhang H, Chen W, Pan M. Nafion-zirconia nanocomposite membranes formed via in situ sol-gel process. *International Journal of Hydrogen Energy* 2010;35(7):2796–801.
- [10] Sun L, Wang S, Jin W, Hou H, Jiang L, Sun G. Nano-sized Fe₂O₃-SO₄²⁻ solid superacid composite Nafion® membranes for direct methanol fuel cells. *International Journal of Hydrogen Energy* 2010;35(22):12461–8.
- [11] Ke C-C, Li X-J, Shen Q, Qu S-G, Shao Z-G, Yi B-L. Investigation on sulfuric acid sulfonation of in-situ sol-gel derived Nafion/SiO₂ composite membrane. *International Journal of Hydrogen Energy* 2010;36(5):3606–13.
- [12] Nicotera I, Khalfan A, Goenaga G, Zhang T, Bocarsly A, Greenbaum S. NMR investigation of water and methanol mobility in nanocomposite fuel cell membranes. *Ionics* 2008;14:243–53.
- [13] Baglio V, Arico AS, Antonucci V, Nicotera I, Oliviero C, Coppola L, et al. An NMR spectroscopic study of water and methanol transport properties in DMFC composite membranes: influence on the electrochemical behaviour. *Journal of Power Sources* 2006;163:52–5.
- [14] Arico AS, Baglio V, Antonucci V, Nicotera I, Oliviero C, Coppola L, et al. An NMR and SAXS investigation of DMFC composite recast Nafion membranes containing ceramic fillers. *Journal of Membrane Science* 2006;270(1–2):221–7.
- [15] Kreuer KD. On the development of proton conducting polymer membranes for hydrogen and methanol fuel cells. *Journal Membrane Science* 2001;185(1):29–39.
- [16] Costamagna P, Yang C, Bocarsly AB, Srinivasan S. Nafion (R) 115/zirconium phosphate composite membranes for operation of PEMFCs above 100 degrees C. *Electrochimica Acta* 2002;47(7):1023–33.
- [17] Alberti G, Casciola M. Composite membranes for medium-temperature PEM fuel cells. *Annual Review of Materials Research* 2003;33:129–54.
- [18] Alonso RH, Estevez L, Lian HQ, Kelarakis A, Giannelis EP. Nafion-clay Nanocomposite Membranes: Morphology and Properties *Polymer* 2009;50(11):2402–10.
- [19] Ray SS, Okamoto M. Polymer/layered silicate nanocomposites: a review from preparation to processing. *Progress in Polymer Science* 2003;28(11):1539–641.

- [20] Thomassin JM, Pagnouille C, Caldarella G, Germain A, Jerome R. Impact of acid containing montmorillonite on the properties of Nafion® membranes. *Polymer* 2005;46(25):11389–95.
- [21] Georgakilas V, Bourlinos A, Gournis D, Tsoufis T, Trapalis C, Mateo-Alonso A, et al. Multipurpose organically modified carbon nanotubes: from functionalization to nanotube composites. *Journal of the American Chemical Society* 2008;130(27):8733–40.
- [22] Jung DH, Cho SY, Peck DH, Shin DR, Kim JS. Preparation and performance of a Nafion (R)/montmorillonite nanocomposite membrane for direct methanol fuel cell. *Journal of Power Sources* 2003;118(1–2):205–11.
- [23] Kim YS, Dong LM, Hickner MA, Pivovar BS, McGrath JE. Processing induced morphological development in hydrated sulfonated poly(arylene ether sulfone) copolymer membranes. *Polymer* 2003;44(19):5729–36.
- [24] Cele N, Ray SS. Recent Progress on Nafion-based nanocomposite membranes for fuel cell applications. *Macromolecular Materials and Engineering* 2009;294(11):719–38.
- [25] Peighambaroust SJ, Rowshanzamir S, Amjadi M. Review of the proton exchange membranes for fuel cell applications. *International Journal of Hydrogen Energy* 2010;35(17):9349–84.
- [26] Song M-K, Park S-B, Kim Y-T, Kim K-H, Min S-K, Rhee H-W. Characterization of polymer-layered silicate nanocomposite membranes for direct methanol fuel cells. *Electrochimica Acta* 2004;50(2–3):639–43.
- [27] Silva RF, Passerini S, Pozio A. Solution-cast Nafion®/montmorillonite composite membrane with low methanol permeability. *Electrochimica Acta* 2005;50(13):2639–45.
- [28] Kim DW, Choi H-S, Lee C, Blumstein A, Kang Y. Investigation on methanol permeability of Nafion modified by self-assembled clay-nanocomposite multilayers. *Electrochimica Acta* 2004;50(2–3):659–62.
- [29] Gosalawit R, Chirachanchai S, Shishatskiy S, Nunes SP. Krytox-Montmorillonite-Nafion® nanocomposite membrane for effective methanol crossover reduction in DMFCs. *Solid State Ionics* 2007;178(29–30):1627–35.
- [30] Stejskal EO, Tanner JE. Spin diffusion measurements: spin echoes in the presence of a time-dependent field gradient. *The Journal of Chemical Physics* 1965;42(1):288–92.
- [31] Zawodzinski TA, Derouin C, Radzinski S, Sherman RJ, Smith VT, Springer TE, et al. Water-uptake by and transport through Nafion 117 membranes. *Journal of the Electrochemical Society* 1993;140(4):1041–7.
- [32] Gournis D, Lappas A, Karakassides MA, Tobbens D, Moukarika A. A neutron diffraction study of alkali cation migration in montmorillonites. *Physics and Chemistry of Minerals* 2008;35(1):49–58.
- [33] MacMillan B, Sharp AR, Armstrong RL. An NMR investigation of the dynamical characteristics of water absorbed in Nafion. *Polymer* 1999;40(10):2471–80.
- [34] Herrera Alonso R, Estevez L, Lian H, Kelarakis A, Giannelis EP. Nafion-clay nanocomposite membranes: morphology and properties. *Polymer* 2009;50(11):2402–10.
- [35] Mauritz KA, Moore RB. State of understanding of Nafion. *Chemical Reviews* 2004;104:4535–85.
- [36] Xie XL, Hayashi S. NMR study of kaolinite intercalation compounds with formamide and its derivatives. 1. structure and orientation of guest molecules. *Journal of Physical Chemistry B* 1999;103(29):5949–55.
- [37] Di Noto V, Gliubizzi R, Negro E, Pace G. Effect of SiO₂ on relaxation phenomena and mechanism of ion conductivity of [Nafion/(SiO₂)_x] composite membranes. *The Journal of Physical Chemistry B* 2006;110(49):24972–86.
- [38] Gruger A, Regis A, Schmatko T, Colomban P. Vibrational Spectroscopy 2001;26:215.
- [39] Moster AL, Mitchell BS. Mechanical and hydration properties of Nafion®/ceramic nanocomposite membranes produced by mechanical attrition. *Journal of Applied Polymer Science* 2009;111(2):1144–50.
- [40] Gebel G, Atkins P. *Polymer* 2000;41:5829–38.
- [41] Paddison SJ, Paul R. *Physical Chemistry Chemical Physics* 2002;4:1158–63.
- [42] Eikerling M, Kornyshev AA, Kuznetsov AM, Ulstrup J, Walbran SJ. *Journal of Physical Chemistry B* 2001;105:3646–62.
- [43] Kreuer KD. *Solid State Ionics* 1997;94:55–62.
- [44] Cohen B, Huppert DJ. *Journal of Physical Chemistry A* 2003;107:3598.
- [45] Theng BKG. *The Chemistry of Clay Organic Reactions*. London: Adam Hilger; 1974.
- [46] Moore RB, Martin CR. Chemical and morphological properties of solution-cast perfluorosulfonate ionomers. *Macromolecules* 1988;21:1334–9.
- [47] Gebel G, Aldebert P, Pineri M. *Macromolecules* 1987;20:1425.
- [48] Burgaz E, Lian H, Alonso RH, Estevez L, Kelarakis A, Giannelis EP. Nafion-clay hybrids with a network structure. *Polymer* 2009;50(11):2384–92.
- [49] Kim Y, Lee JS, Rhee CH, Kim HK, Chang H. Montmorillonite functionalized with perfluorinated sulfonic acid for proton-conducting organic-inorganic composite membranes. *Journal of Power Sources* 2006;162(1):180–5.
- [50] Lin Y-F, Yen C-Y, Hung C-H, Hsiao Y-H, Ma C-CM. A novel composite membranes based on sulfonated montmorillonite modified Nafion® for DMFCs. *Journal of Power Sources* 2007;168(1):162–6.
- [51] Ladhari A, Ben Daly H, Belhadjsalah H, Cole KC, Denault J. Investigation of water absorption in clay-reinforced polypropylene nanocomposites. *Polymer Degradation and Stability* 2010;95(4):429–39.
- [52] Pavlidou S, Papaspyrides CD. A review on polymer-layered silicate nanocomposites. *Progress in Polymer Science(Oxford)* 2008;33(12):1119–98.

Article

NMR and Electrochemical Investigation of the Transport Properties of Methanol and Water in Nafion and Clay-Nanocomposites Membranes for DMFCs

Isabella Nicotera ^{1,*}, Kristina Angjeli ¹, Luigi Coppola ¹, Antonino S. Aricò ² and Vincenzo Baglio ²

¹ Department of Chemistry, University of Calabria, 87036 Rende (CS), Italy;
E-Mails: kristina.angjeli@unical.it (K.A.); lg.coppola@unical.it (L.C.)

² CNR-ITAE Institute, via Salita S. Lucia sopra Contesse, 5, 98126 Messina, Italy;
E-Mails: arico@itaecnr.it (A.S.A.); baglio@itaecnr.it (V.B.)

* Author to whom correspondence should be addressed; E-Mail: isabella.nicotera@unical.it;
Tel.: +39-0984-493379; Fax: +39-0984-492044.

Received: 18 May 2012; in revised form: 8 June 2012 / Accepted: 12 June 2012 /

Published: 20 June 2012

Abstract: Water and methanol transport behavior, solvents adsorption and electrochemical properties of filler-free Nafion and nanocomposites based on two smectite clays, were investigated using impedance spectroscopy, DMFC tests and NMR methods, including spin-lattice relaxation and pulsed-gradient spin-echo (PGSE) diffusion under variable temperature conditions. Synthetic (Laponite) and natural (Swy-2) smectite clays, with different structural and physical parameters, were incorporated into the Nafion for the creation of exfoliated nanocomposites. Transport mechanism of water and methanol appears to be influenced from the dimensions of the dispersed platelike silicate layers as well as from their cation exchange capacity (CEC). The details of the NMR results and the effect of the methanol solution concentration are discussed. Clays particles, and in particular Swy-2, demonstrate to be a potential physical barrier for methanol cross-over, reducing the methanol diffusion with an evident blocking effect yet nevertheless ensuring a high water mobility up to 130 °C and for several hours, proving the exceptional water retention property of these materials and their possible use in the DMFCs applications. Electrochemical behavior is investigated by cell resistance and polarization measurements. From these analyses it is derived that the addition of clay materials to recast Nafion decreases the ohmic losses at high temperatures extending in this way the operating range of a direct methanol fuel cell.

Keywords: self-diffusion; NMR; DMFC; nanocomposites; clays; transport properties; methanol

1. Introduction

The direct methanol fuel cell (DMFC) is a promising alternative power source [1,2] that combines the merits of direct hydrogen/air fuel cells with the advantages of a liquid fuel, such as convenient handling and high energy density. Despite these advantages, technical barriers still need to be overcome for their large scale commercialization of DMFCs [3]. One of such technical barriers is the methanol crossover, or the direct transport of methanol from anode to cathode via the proton exchange membrane. Methanol crossover will not only lead to reduced energy conversion efficiency because of the direct chemical oxidation of methanol in the cathodic half-cell that hence drastically degrades fuel cell performance but also cause fuel cell operational failures. It is essential to investigate the mechanisms of the methanol transport through the electrolyte in order to gain a better understanding of the crossover mechanism.

In recent years, increasing interest has been devoted to the development of high temperature PEMFC systems. In fact, most of the key issues and shortcomings of the PFSA-based PEMFC technology, such as water management, CO poisoning, cooling and heat recovery, can be solved or avoided by developing alternative membranes with suitable ionic conductivity and stability up to 120–130 °C. Polymer membranes able to operate above 120 °C could benefit from both enhanced carbon monoxide (CO) tolerance and improved heat removal. The most significant barrier to running a polymer electrolyte fuel cell at elevated temperatures is maintaining the proton conductivity of the membrane. Higher temperature increases the water vapour pressure required to keep a given amount of water in the membrane, thereby increasing the likelihood that water loss will occur and significantly reduce proton conductivity. The conductivity of a dry membrane is several orders of magnitude lower than a fully saturated membrane. A number of alternative strategies [4–7] have been proposed to satisfy these requirements and to maintain membrane conductivity in a dehydrating environment (*i.e.*, elevated temperature and reduced relative humidity), such as composite membranes containing finely dispersed hygroscopic inorganic oxides [8–12] or heteropolyacids [13]. The properties of these composite membranes not only depend on the nature of the ionomer and the solid used but also on the amount, homogeneous dispersion, size, and orientation of the solid particles dispersed in the polymeric matrix. Additionally, the introduction of inorganic materials into the polymeric matrix can be considered as a good approach to improve the proton transport, the retention to the swelling and the resistance to the methanol cross-over in DMFC working conditions (membrane in equilibrium with liquid water-methanol mixture).

Recent studies have shown that polymer nanocomposites based on layered clay nanoparticles exhibit reduced gas permeability due to the presence of impermeable clay platelets as well as structural changes in the polymer induced by the clay nanofillers [14–16]. Additionally, our recent study [11] has demonstrated as such smectite clays materials dispersed in Nafion significantly improve the water retention and mobility at temperatures above 100 °C of the nanocomposite membrane.

Clay minerals are among the most important soil constituents. The structure, chemical composition, exchangeable ion type and small crystal size of smectite clays are responsible for several unique properties, including a large chemically active surface area, a high cation exchange capacity, interlamellar surfaces having unusual hydration characteristics, and sometimes the ability to strongly affect the flow behaviour of liquids. These materials demonstrate high chemical and thermal stability; in fact, they are very attractive for numerous industrial applications such as adsorbents, ion exchangers, pharmaceutical additives, fertilizers, *etc.* Concerning the polymer nanocomposites, the first practical application of a nanocomposite was the nylon-montmorillonite clay system that displayed a large increase in tensile strength, modulus, and heat distortion temperature without loss of impact resistance [17]. Since then, the field has rapidly expanded using different polymer/clay systems, giving rise either to exfoliated or to intercalated systems [15,18,19].

Smectite clays are a class of layered aluminosilicate minerals and consist of an octahedral alumina layer fused between two tetrahedral silica layers (about 1 nm) [20,21]. The monovalent ions located between the clay layers allow the absorption of polar solvent, like water, with good retention capacity so, when incorporated into a polymer membrane, they help to prevent the loss of the hydration water not only at high temperatures but also under low relative humidity environment. Moreover, the properties of the smectite nanoclays can be tailored using simple chemical methods such as intercalation with organic or inorganic guest molecules. Their surface properties, for example, can be easily modified through treatment with an organic surfactant. As a result the presence of the surfactant expands the interlayer gallery rendering the nanoclay compatible with hydrophobic media and polymer matrices.

Typical preparation methods of these nanocomposites include solution, melt intercalation, and *in situ* polymerization [22], from which we can obtain conventional, intercalated or exfoliated nanocomposites. We have verified that the solution intercalation method is very effective in incorporating exfoliated clays into Nafion polymer, in which the individual clay layers lose their stacking and are uniformly dispersed in the continuous polymeric matrix. In this study, we want to verify if, as soon as exfoliated nanocomposites are formed, the barrier properties of polymer are increased (due to less surface area and longer pathway) leading not only to low gas (O₂, air) permeability but, reducing the fuel crossover. In fact, in the development of new low temperature PEMs for use in the DMFC, two of the main concerns are proton-ion and methanol-transport through the membrane. The objective is to significantly reduce the methanol transport whilst having and maintaining high proton transport. The research concerning the polymer electrolytes is aimed to the development hybrid morphology in order to promote the Grotthus [23] jump proton transport mechanism and minimize the Vehicle mechanism [24,25].

In this work, one synthetic (Laponite) and one natural clay (SWy-2 montmorillonite) with different structural and physical parameters were chosen as nanofillers: Laponite shows both low layer charge density (CEC = 48 molar equiv/100 g) and particle size (20 nm), SWy-2 has a high layer charge density (CEC = 76.4 molar equiv/100 g) and particle size (200 nm). Composite membranes were synthesized by solution intercalation with 3% of filler loading with respect to the polymer.

We have investigated the transport properties of the water and methanol within the electrolyte membranes both as a function of methanol concentration and as a function of temperature by NMR methods. The aim is to understand the molecular dynamics and the mechanisms that are at the basis for ionic conduction and how these are influenced by polymeric structure and by nanofillers added to the

polymer, through direct measurement of the self-diffusion coefficients (D) and relaxation times (T_1). The explored temperature range was from 20 °C up to 130 °C and for two methanol-water solution concentrations, 2 M and 4 M.

A preliminary electrochemical characterization was carried out on the filler-free and composite membranes by using ac-impedance spectroscopy and polarization measurements, in order to validate the NMR results.

2. Results and Discussion

2.1. Uptake and Swelling Properties of the Nafion and Nanocomposites Membranes

The electrolyte membranes were swelled by immersion in pure methanol, pure water, and in aqueous methanol solutions at two different alcoholic concentration, 2 M and 4 M.

The swelling properties of the membranes show marked differences with respect to used solvents, with an increasing of the uptake, consequently of the swelling, as the solution concentration increases, up to reach an uptake of over 150% by mass and a doubling of the membrane size if we use pure methanol. This implies a significant limit to utilizing high concentrations of methanol solutions in the DMFCs. Table 1 shows some data concerning the saturation (maximum) uptake values of the filler-free Nafion and the clay-nanocomposites membranes. It is evident that the effect of the nanofillers is to promote an increase of the membrane water uptake (from 24 wt % of Nafion up to 45 wt % of the Swy-composite), but there is also a big effect on the methanol solutions, in fact, membranes can reach an uptake of 60 wt % when swelled in 4 M methanol solution.

Table 1. Methanol solution and water uptake (wt %) of the membranes at room temperature.

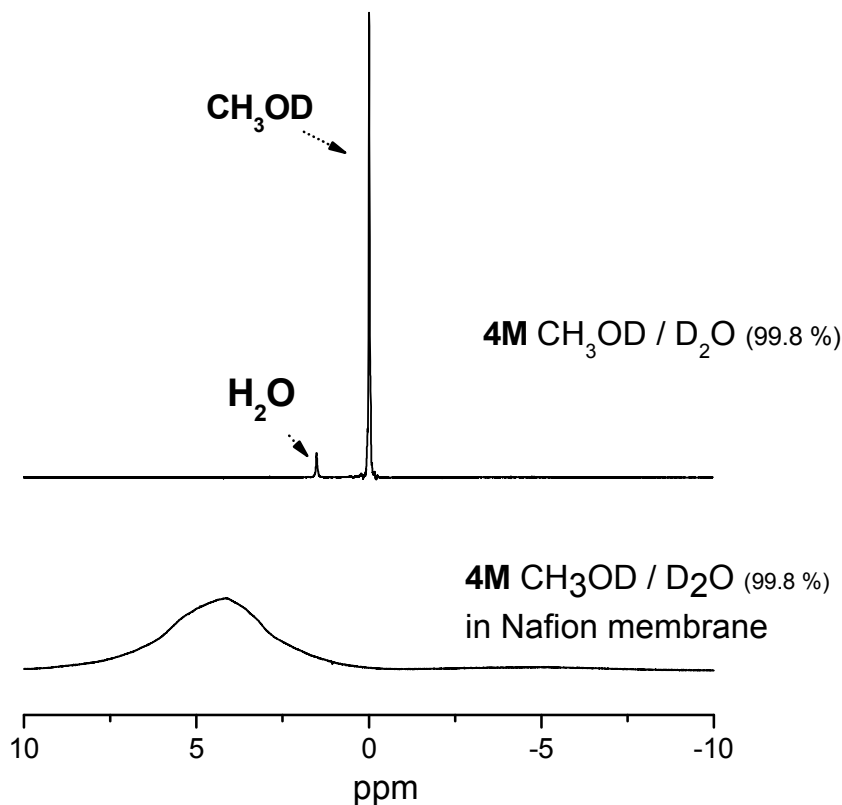
Membranes	Uptake (wt %) 4M solution	Uptake (wt %) 2M solution	Uptake (wt %) pure H ₂ O
filler-free Nafion	34	28	24
Lap/Nafion	60	46	30
Swy/Nafion	60	56	45

2.2. ¹H-NMR Study: D , T_1 and Spectra Lineshapes

In this study we used NMR methods to investigate the transport properties of water and methanol molecules confined in the porous structure of Nafion and composite membranes and in order to check the effect of the clay-fillers added.

It is often possible in methanol–water mixtures to resolve spectroscopically the methyl and hydroxyl protons in an NMR experiment which, in principle, should permit the measurement of both water and methanol diffusion. However, in the present case of solvents confined in membranes, due to the linewidth of the ¹H-NMR signals, it is not possible to distinguish, through their chemical shift, methanol and water (see Figure 1).

Figure 1. ^1H -NMR spectra recorded on 4 M aqueous methanol solution ($\text{CH}_3\text{OD}/\text{D}_2\text{O}$) as prepared and confined in Nafion membrane, respectively. The chemical shift variation of the methanol's signal is caused by the different chemical environment and the strong interactions with the polymer backbone.



In order to discriminate between the NMR signals of methanol and water, the membranes were equilibrated in solutions prepared with deuterated molecules, *i.e.*, mixture of $\text{CH}_3\text{OD}/\text{D}_2\text{O}$ and $\text{CD}_3\text{OD}/\text{H}_2\text{O}$. The reason to use CH_3OD instead of CH_3OH is due to the fast rate exchange of hydroxyl groups between water and methanol molecules during the “NMR times”, which could affect the measurements.

Hence, we used the only available signal coming from the methyl groups to perform the NMR diffusometry and relaxometry measurements of methanol confined inside the electrolytes films. With regard to the deuterium signal, this nucleus has a spin-spin relaxation time (T_2) which is very short, so it is practically impossible to perform measurements of diffusion through the PGSE sequence. For this reason, in order to achieve complete information on the solvents mobility (both water and methanol in mixture), membranes were also swollen in solutions of $\text{CD}_3\text{OD}-\text{H}_2\text{O}$, to have only the proton's signal from the water molecules.

In summary, Table 2 reports the solvents and mixtures used to swell the membranes for the NMR study; the solvent marked in bold, is that “seen” by NMR.

Table 2. Solvents and solutions used to prepare swollen membranes for the NMR study.

solvents	concentration
CH ₃ OD	pure
H ₂ O	pure
CH ₃ OD/D ₂ O	2M
CD ₃ OD/H ₂ O	2M
CH ₃ OD/D ₂ O	4M
CD ₃ OD/H ₂ O	4M

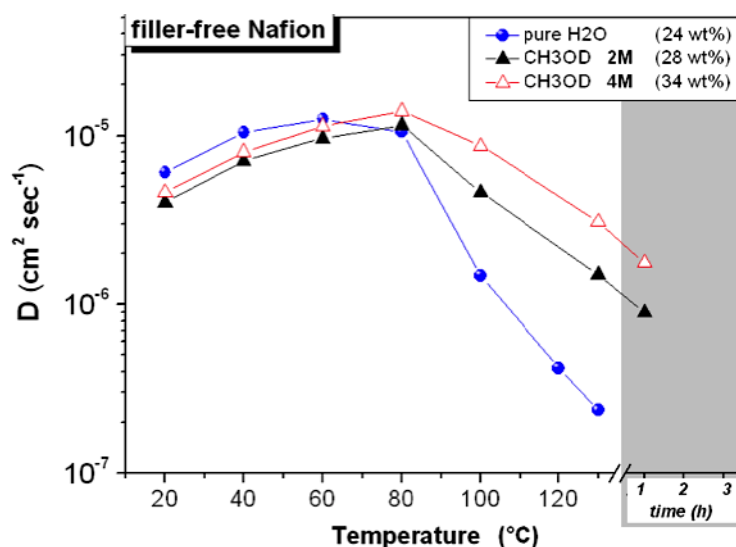
Figure 2. Self-diffusion coefficients of water and methanol (2 M and 4 M solution concentration) confined in filler-free Nafion membranes from 20 °C up to 130 °C; the data collected at 130 °C after 1 h is also plotted. In the legend, the water and solution uptakes are indicated.

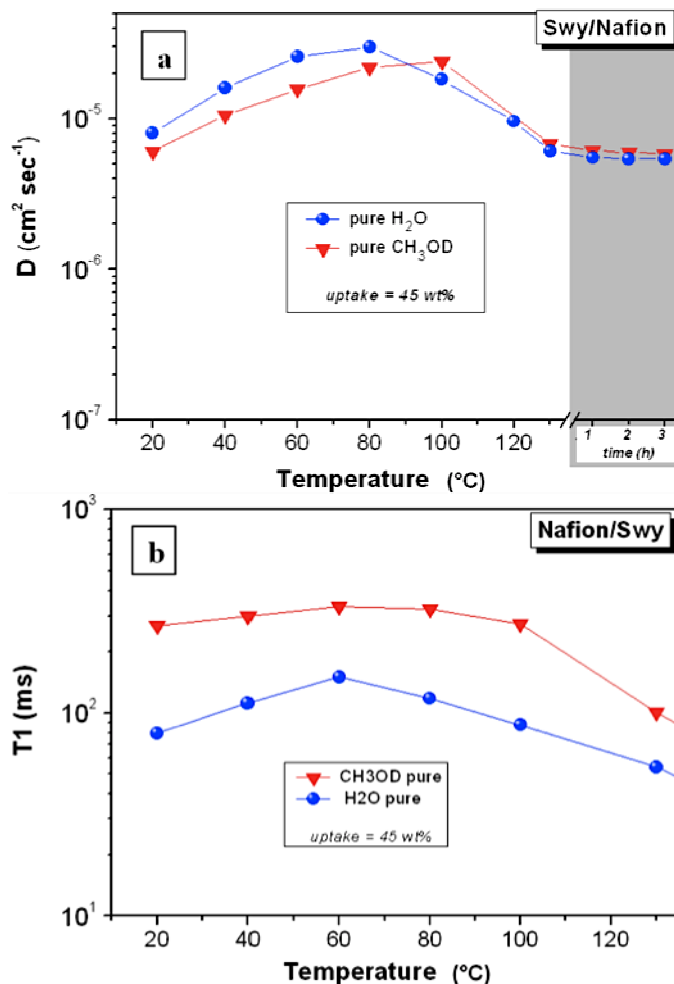
Figure 2 displays the diffusion coefficients of water and methanol (in 2 M and 4 M solutions) measured in the swollen membrane of filler-free Nafion, in the range 20–130 °C. Concerning the water diffusion, as expected, at temperatures over 60–80 °C, it decreases rapidly due to the water evaporation from the membrane, which is the main limitation of Nafion in order to work at high temperatures. The methanol diffusion is slightly lower than water up to 60 °C, both at 2 and 4 M concentration but, over this temperature, it remains always higher. For instance, at 130 °C, while the water signal and diffusion are very low, the methanol maintains both NMR signal and diffusion coefficients fairly well, even after 1 h at the same temperature (without any external humidification). We groped to explain this result by considering the distribution of the solvents (water and methanol) inside the ionic pores of Nafion membranes and the transport mechanism involved in the water/methanol diffusion. During the swelling, a certain amount of water is involved in the primary hydration shells of the SO₃⁻ groups, while most of the additional water fills the volumes of pores forming higher order hydration layers and behaves more bulk-like [26,27] Methanol molecules are, instead, collected adjacent to the polymer backbone with a less favorable complexation of protons as compared to that by water [28,29]. In other words, as reported in other studies [28,30], a micro-phase separation occurs, where water-rich and methanol-rich spatial domains are created, presumably with a characteristic size in the order of the

Nafion pore size. In this description, the molecules of methanol interacting with the polymer, and in particular with fluorine atoms on both the backbone and the side-chains, are distributed on the surface of the pores, while the water molecules are at the center acting, in the maximum swelling conditions, as bulk-like water. This scenario is consistent with: (i) the higher methanol diffusion respect to the water at high temperatures; (ii) the increase of the swelling (higher uptake of the 4 M solution) and also of the methanol diffusion coefficient with increasing methanol concentration.

Differently from the membrane of Nafion recast, that is completely soluble in pure methanol, the composite membrane obtained by Swy-nanoclay at 3 wt % of filler loading with respect to the polymer, shows a greater stiffness, even if it gets a maximum of 200 wt % of uptake and a swelling which causes at least a doubling of the size of the film. The same membrane in pure water reaches 45% of uptake and low swelling.

In order to compare the data of diffusion of water and methanol in this membrane, we left to dry the piece of membrane swollen in pure methanol until it reached a weight corresponding to 45 wt % methanol uptake, and therefore it was put in the NMR tube. Figure 3 displays the diffusion coefficients and the relaxation times (T_1) of the pure water and pure methanol measured on the swollen Swy/Nafion membrane in the temperature range 20–130 °C.

Figure 3. (a) Self-diffusion coefficients and (b) longitudinal relaxation times (T_1) of pure water and pure methanol confined in Swy/Nafion nanocomposite membrane from 20 °C up to 130 °C. Data collected at 130 °C after some hours are also plotted in the diffusion graph.



The first noticeable difference with the recast Nafion is that the water mobility in the Swy/Nafion composite is very high in all temperature ranges investigated. In fact, the diffusion increases linearly up to 80 °C and soon after, due to the evaporation of a certain amount of water, it decreases slightly but remains constant and especially after several hours at 130 °C. Methanol diffusion follows the same behavior (also part of the methanol over the 80–100 °C evaporates from the membrane) even if, at lower temperatures, its diffusion is lower than water.

NMR longitudinal (or spin-lattice) relaxation times (T_1), compared to diffusion, reflects more localized motions including both translation and rotation on a time scale comparable to the reciprocal of the NMR angular frequency (~ 1 ns). As the molecular correlation time τ_c depends on temperature, a minimum in T_1 is often observed when $\omega\tau_c \sim 1$, where ω is the NMR frequency [31]. In the temperature range investigated, well above the T_1 minimum, *i.e.*, in the so-called extreme narrowing limit ($\omega\tau_c \ll 1$), higher T_1 values suggest more facile molecular rotational and translational motion.

If we observe the temperature dependence of the T_1 of water and methanol in the Swy-nanocomposite membrane (Figure 3b), we find a much different behavior with respect to the diffusion: methanol relaxes slower than water and the T_1 values are almost constant in the temperature range 20–100 °C. This implies a greater local mobility (more translational and rotational degrees of freedom) of the methanol molecules, probably due to the weaker electrostatic interactions with the polymer matrix respect to the water molecules: methanol forms a less extensive network of hydrogen bonds in Nafion compared to water.

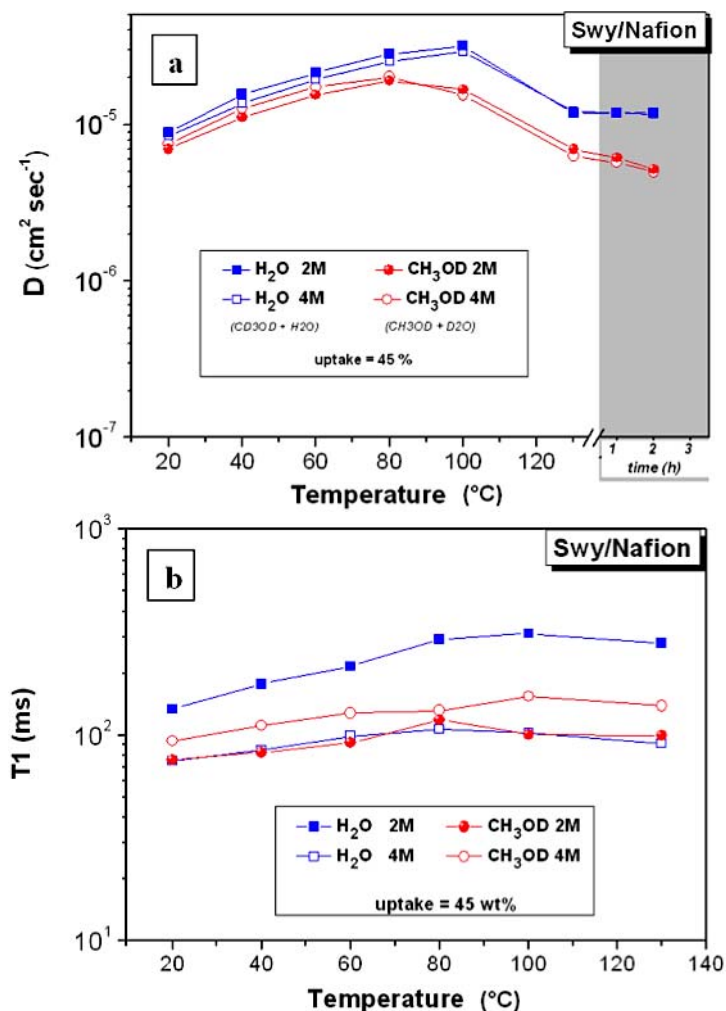
As a result, the lower diffusion of methanol at temperatures below 100 °C (before a significant evaporation), when a large amount of water and methanol is present, may be explained through the blocking effect of the layered nanoclays dispersed in the polymer matrix. In this temperature range, the *Vehicle mechanism* [24,25], where molecules associated with the proton are dragged along, overrides the *Grotthus mechanism* [23], where proton mobility is connected to rotation of the molecules within a constantly changing network of hydrogen bonds.

Above 100 °C, it is reasonable to expect that the evaporation essentially affects the bulk/“free” solvents, so the biggest contribution to the diffusion comes from the solvent molecules strongly interacting with hydrophilic groups and the polymer backbone, for water and methanol, respectively, resulting in a lower D . In such conditions the structural transport mechanism (*Grotthus*) should be predominant for both solvents, therefore the effect of obstruction by the nanoparticles is less effective. The result is that, despite the local motions of molecules of methanol are faster (higher T_1), since it fails to form an extensive network of hydrogen bonds, the diffusion is practically equal to that of water.

From these results, certainly the use of pure methanol is not a practicable choice in the DMFCs because the solvent cross-over is not sufficiently reduced, and there is excessive swelling of the membrane. However, it is important to underline the different water retention behavior of the filler-free Nafion and this composite membrane at high temperatures which suggests that a significant proton conductivity can be ensured by electrolytic membranes in high temperatures and low humidity conditions. Therefore, it would be of great interest to investigate the water and methanol diffusion changing the boundary condition from pure methanol to a methanol/water mixture.

Figure 4 shows the diffusion and relaxation times of water and methanol in 2 and 4 M solutions, measured in swollen Swy/Nafion nanocomposite membrane, from 20 °C up to 130 °C.

Figure 4. (a) Self-diffusion coefficients and (b) longitudinal relaxation times (T1) of water and methanol in 2 M and 4 M solutions confined in Swy/Nafion nanocomposite membrane from 20 °C up to 130 °C. Data collected at 130 °C after some hours are also plotted in the diffusion graph.



As mentioned previously, two mixtures of deuterated solvents were used: CH₃OD + D₂O and CD₃OD + H₂O, to perform the NMR experiments on methanol and water, respectively. In such a way we can compare the mobility of water and methanol confined in membrane at the same solution concentration and, for the same reason, we used the same solution uptake value, 45 wt %.

Water diffusion is always higher than methanol in the whole investigated temperature range and for both solution concentrations. Up to 100 °C the diffusion coefficients of water in 2 M solution are slightly higher than 4 M, accordingly to the water surplus available in the first solution which increases the bulk-like water fraction. When most of this “free” water evaporates, the diffusion coefficients of the “bounded” water (hydrated water) are similar for both concentrations.

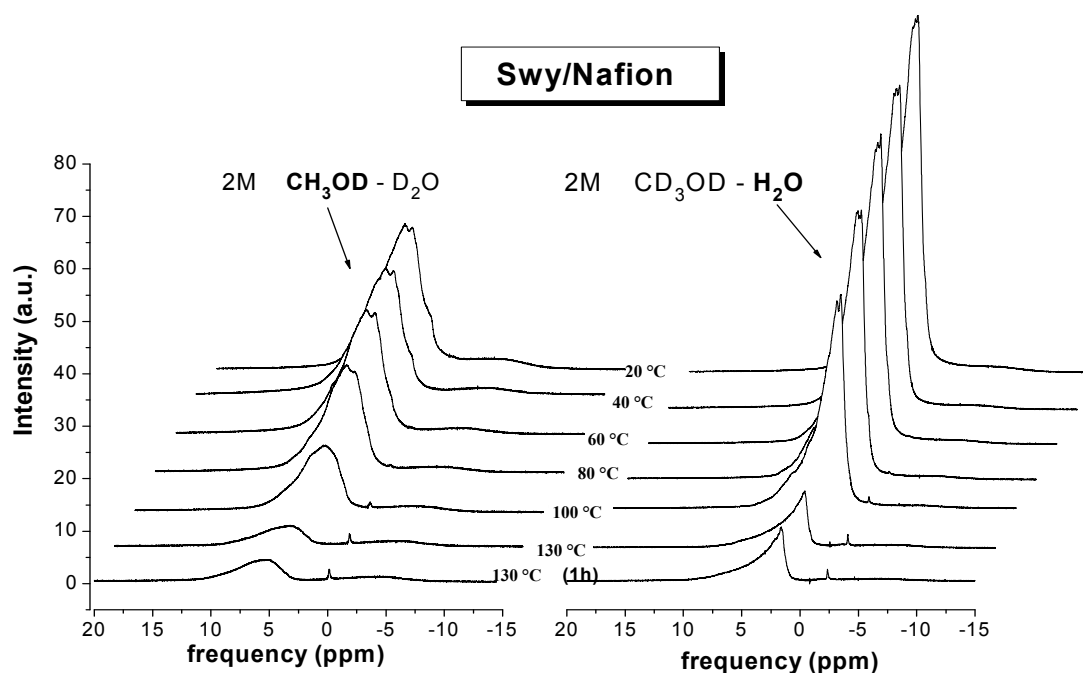
Concerning the methanol diffusion at 4 M concentration, initially it is very close to that of water but, with the increasing of the temperature, it becomes gradually smaller and moves far from water with a significant fall after 80 °C. This abrupt drop is still related to the blocking effect, that becomes a significant factor just when the solution content is low (due to evaporation), *i.e.*, when the hydrophilic domains sizes are reduced and therefore, big particles can obstruct the methanol molecules pathways.

The comparison with the methanol diffusion in 2 M solution describes a similar trend, however already starting from the low temperatures, the diffusion is much lower than water at the same concentration. This is consistent with the vehicular transport mechanism and with the molecular interactions of the methanol molecules with the polymeric sites, the first one increases the water mobility, the second effect reduces the methanol diffusion because molecules are “complexed” on the clusters surface.

The molecular complexation is also visible from the relaxation times (Figure 4b): methanol T_1 in 2 M solution are lower than 4 M, *i.e.*, the local motions are more impeded and inhibited in the first solution.

The analysis of the ^1H -NMR spectra of methanol and water with the temperature increasing can give further information on the solvents distribution in the membrane (hydration and interactions) as well as on the evaporation dynamics. Figure 5 shows the temperature evolution of the proton spectra acquired on Swy/Nafion swollen in 2 M methanol solution, from 20 °C up to 130 °C (spectrum recorded at 130 °C after 1 h is also reported). In the figure, we compare the spectral lines of methanol (on the left) and water (on the right). Both signals are large and asymmetric, typical of a multiple components configuration, however, the FWHM (full width at half maximum) of the water and methanol spectra are quite different: 675 Hz against 1,170 Hz at 20 °C, *i.e.*, the line width of methanol is almost double of the water.

Figure 5. Evolution of proton spectra from methanol (on the left) and water (on the right) as a function of temperature on Swy/Nafion composite swollen in 2 M methanol solution. The spectra were referenced setting methyl protons and pure water at 0 ppm, respectively.



This implies that, while for the water there is a strong component of bulk which contributes to the “shrinkage” of the spectral line, the molecules of methanol instead are strongly interacting with the polymer (the “complexation” referred to above) promoting a broadening of the line, as well as reducing their mobility on both short and long range (T_1 and diffusion).

By heating, the intensity of these peaks decreases because of the solvents evaporation from the membrane, with a pronounced drop above 100 °C; at 130 °C the intensity of the residual signal remains constant for several hours (obviously without any supplying humidity), and this is responsible for both the proton and methanol diffusion that we are able to detect at these high temperatures.

The discussion of the data just analyzed is complex but definitely indicates that the microstructure plays a key role in the mass transport of water and methanol.

The microstructure is influenced by the chemical-physical properties of the smectite clays such as the nanoparticles size and the layer charge density. In fact, higher platelets dimensions may promote stronger alterations of the network structure as well as create an obstruction effect, while a high value of surface charge density may facilitate or promote the proton transport through hopping mechanisms.

These assumptions are corroborated by the experimental results obtained on the hybrid membrane based on Laponite nanoclay. This synthetic clay is completely exfoliated in the Nafion polymer but has both smaller CEC and particle size with respect to Swy.

In Figure 6 diffusion coefficients and relaxation times of water and methanol in 2 M and 4 M solutions in the swollen Lap/Nafion nanocomposite membrane (uptake 30 wt %), from 20 °C up to 130 °C, are reported. Basically, the mobility of the methanol is not influenced by the solution concentration and is very similar to that of water and suggests that no relevant obstruction effect from Laponite nanoparticles acts on the methanol transport.

In order to achieve a complete framework on this membrane and analyze the various differences, we show in Figure 7 the plots of the spectral area vs. temperature, of water and methanol in both 2 M and 4 M solutions confined in Lap/Nafion nanocomposite. An evident evaporation of both water and methanol after 60 °C is evident in these graphs producing a remarkable reduction of the NMR signals. The water at 4 M concentration shows a decrease of the peak area which is slightly different because, rather than a net head between 60 °C and 80 °C, there is a clear and constant reduction of the intensity of the proton signal starting at 40 °C.

Figure 6. (a) Self-diffusion coefficients and (b) longitudinal relaxation times (T1) of water and methanol in 2 M and 4 M solutions confined in lap/Nafion nanocomposite membrane from 20 °C up to 130 °C. Data collected at 130 °C after some hours are also plotted in the diffusion graph.

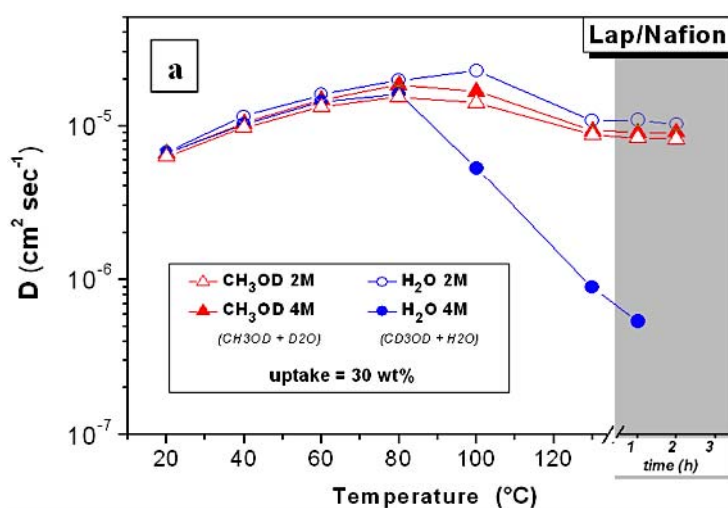


Figure 6. Cont.

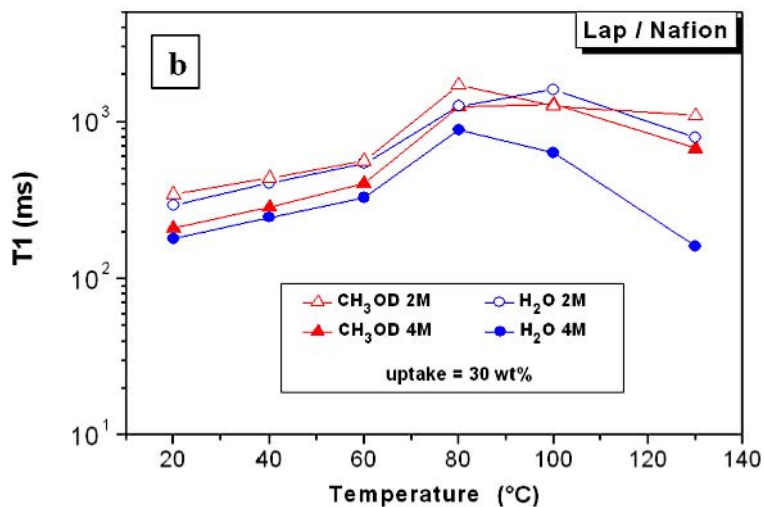
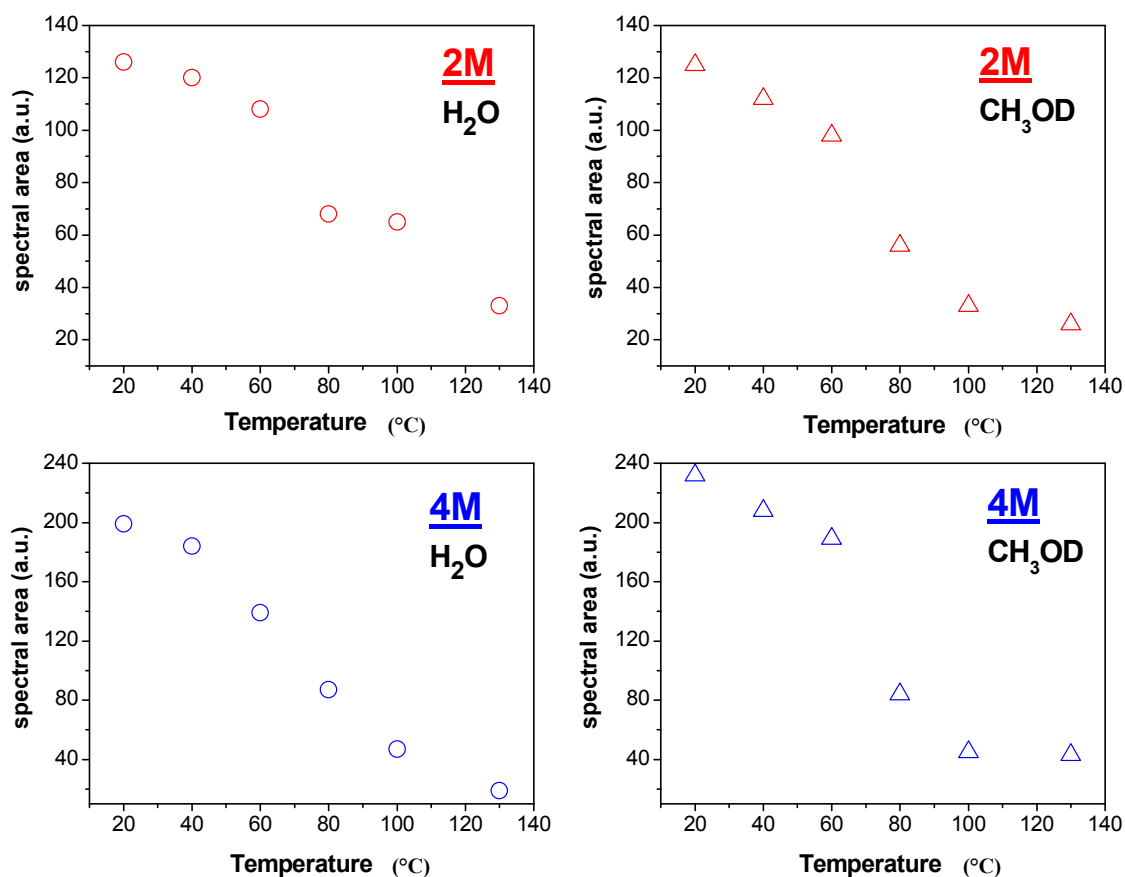


Figure 7. Plots of the spectral area vs. temperature of water and methanol in both 2 M and 4M solutions confined in Lap/Nafion nanocomposite.



The behavior of Lap/Nafion membrane is quite different with respect to Swy/Nafion and a comparison of all NMR data sheds light on the following main differences:

(1) The relaxation times of Lap-composite are higher over the whole temperature range, which implies higher local motions (rotations and translations) and therefore, weaker interactions with the filler;

(2) significant evaporation on Lap-composite at 80 °C, evidenced by the strong reduction of the spectra integrals; in Swy-composite, this drop is found at 130 °C;

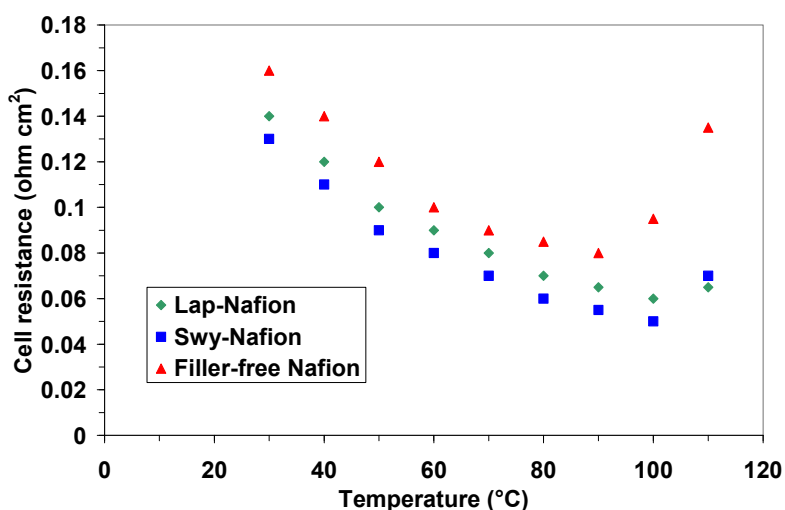
(3) in Lap-composite, water for the 4 M solution shows a decrease of both diffusion and T1 after 80 °C, while for the 2 M solution, water and methanol diffusion is similar.

The origin of these three outcomes can be correlated to the lower cationic exchange capacity (CEC) of Laponite clay compared to Swy montmorillonite. Fewer hydrophilic “coordinating” sites produce the lowering of the retention capacity of the membrane and, consequently, the water diffusion is reduced. In particular, when we start with a lower amount of water (*i.e.*, 4 M solution), what remains at high temperature is strongly linked water. However, further investigations are necessary to clarify this issue.

2.3. Electrochemical Investigation

The electrochemical investigation was carried out in a single cell by recording the ac-impedance spectra at different temperatures (from 30 °C to 110 °C) and the polarization curves in the temperature range from 90 °C to 110 °C, feeding a 2 M methanol solution at the anode and oxygen at the cathode. The series resistance (high frequency intercept on the real axis in the Nyquist plot) was plotted as a function of temperature as shown in Figure 8. Obviously, the fuel cell conditions are completely different from that of the NMR experiments. However, there are some analogies with the NMR results; in fact, the decrease of cell resistance in the composite membranes indicates an increase of water retention caused by the fillers, in particular for the Swy-based membrane. The introduction of these clays thus produces an extension of the operating temperature of a direct methanol fuel cell.

Figure 8. Cell resistance values as a function of temperature for the cells equipped with the different membranes.



In Figures 9 and 10 the polarization and power density curves obtained with the different membranes at 90 °C and 110 °C, respectively, are reported. As can be observed, the maximum power density of the DMFC equipped with the composite membranes increases as the temperature increases, although the methanol solution is fed under atmospheric pressure and thus subjected to evaporation. Unfortunately, these operating conditions (atmospheric pressure) did not reach higher temperatures

than 110 °C. However, from this analysis the effect of the water retention properties of the fillers is clear. In fact, the filler-free Nafion-based cell showed a drop of performance with the temperature due to water evaporation and the consequent increase of cell resistance (see Figure 8).

Figure 9. DMFC polarization and power density curves at 90 °C for various membrane-electrode assemblies equipped with composite and filler-free membranes.

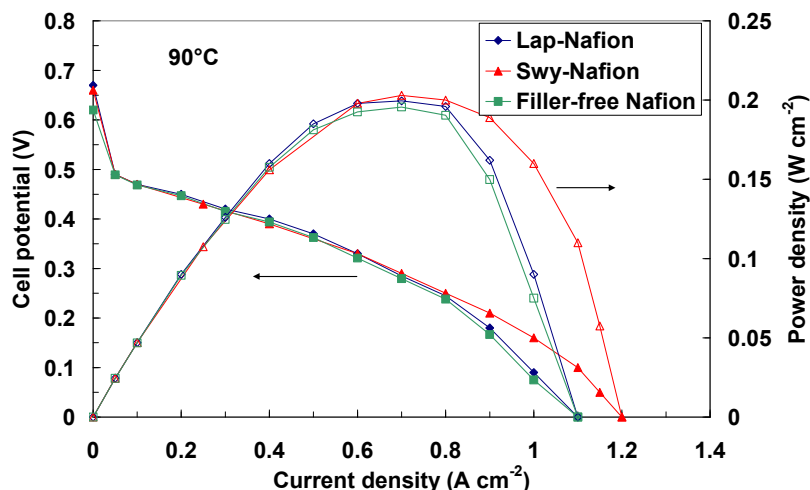
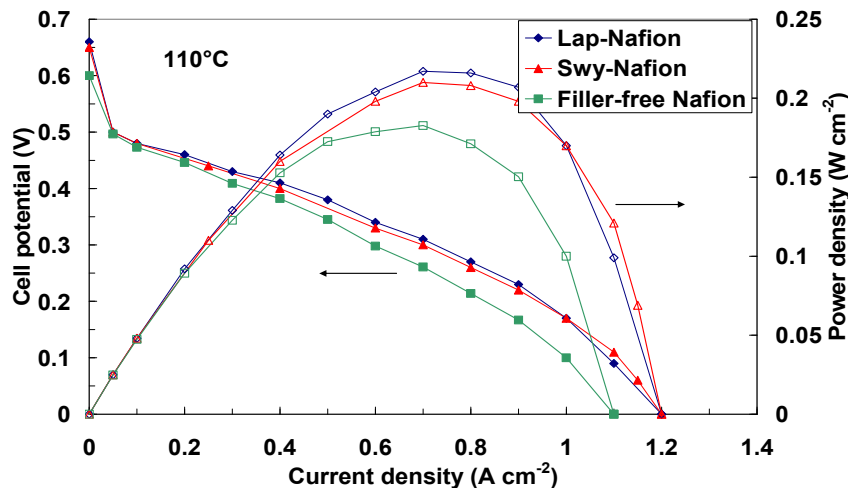


Figure 10. DMFC polarization and power density curves at 110 °C for various membrane-electrode assemblies equipped with composite and filler-free membranes.



The performance at 90 °C (Figure 9) is very similar for all the membranes and superior compared to previously investigated composite membranes at this temperature [32–36].

However, we have to take into account that different catalysts were used in the present analysis; also the thickness of the membranes was different compared to the composite membranes previously developed by our group [32–36] using various inorganic oxides as fillers. Increasing the temperature up to 110 °C (Figure 10), under atmospheric pressure at the anode, water evaporation produces an increase of cell resistance (see Figure 8) with a consequent decrease of the performance for the filler-free Nafion membrane. Whereas, a slight increase of power density is recorded with the clays-nanocomposites under these conditions, confirming the higher water affinity of these membranes as shown by NMR experiments.

The remarkable behavior of smectite clays-based nanocomposites at high temperatures is reported in our two recent studies [11,12] where the exceptional water retention and mobility property of composites systems with respect to the recast Nafion is proven. This suggests that a significant proton conductivity can be ensured by electrolytic membranes in high temperatures and, therefore, highly promising also in PEMFCs applications.

Finally, Table 3 shows the variation of the open circuit potential (OCP) as a function of temperature for the various membranes. The OCP is an important parameter in a DMFC in order to assess the methanol permeability of a membrane. The DMFCs based on Lap/Nafion and Swy/Nafion membranes showed similar behavior in the temperature range from 90 °C to 110 °C, whereas the cell equipped with the filler-free membrane evidenced a lower value of OCP. This is a clear indication of the blocking effect of the composite membranes towards methanol cross-over, as already evidenced from NMR results.

Table 3. Open circuit potential (OCP) values at the different temperatures for the various membranes.

Membranes	Open Circuit Potential (V) @ 90 °C	Open Circuit Potential (V) @ 100 °C	Open Circuit Potential (V) @ 110 °C
filler-free Nafion	0.62	0.61	0.60
Lap/Nafion	0.67	0.66	0.66
Swy/Nafion	0.66	0.66	0.65

As a result, such composite membranes, capable of extending the operating temperature of Nafion membranes, would be a potential solution to some of the drawbacks presently affecting direct methanol fuel cells (DMFCs) as well as reformate-fuelled polymer electrolytes (PEMFCs). Fuel cell operation at elevated temperatures will limit the effects of electrode poisoning by adsorbed CO molecules, increase both methanol oxidation and oxygen reduction kinetics and simplify water and thermal management. Recently, composite Nafion membranes have been also proposed for PEM electrolyzers with good results [37,38], demonstrating the high potentiality of these composite materials and the need to understand the water transport mechanism inside them for a further improvement of their properties.

3. Experimental Section

3.1. Materials

Two smectites clays with different structural and physical parameters (structural formula, particle size and cation exchange capacity) were used. The first was a natural Wyoming montmorillonite (SWy-2) obtained from the Source Clay Minerals Repository, University of Missouri, Columbia, with a cation exchange capacity (CEC) measured by the Co(II) procedure equal to 80 mequiv per 100 g clay and particle size around 200 nm. The second clay was a synthetic trioctahedral hectorite, Laponite (Lap), produced by Laporte Industries Ltd with the lowest CEC 48 mequiv per 100 g clay and the smallest particle size (20 nm). SWy-2 montmorillonite was fractionated to <2 µm by gravity sedimentation and purified by well-established procedures in clay science [39]. Sodium-exchanged

samples (Na⁺-SWy-2) were prepared by immersing the clay into 1 M solution of sodium chloride. Cation exchange was complete by washing and centrifuging four times with dilute aqueous NaCl. The samples were finally washed with distilled deionized water and transferred into dialysis tubes in order to obtain chloride-free clays and then dried at room temperature.

Finally, Nafion solution (20 wt % in mixture of lower aliphatic alcohols and water) were purchased from Aldrich.

3.2. Composites Membranes Preparation

The composite membranes were prepared from 20 wt % Nafion[®] solution according to the following processes: (i) 1 g of Nafion solution was heated at about 60 °C to remove all the solvents (water, isopropanol, *etc.*); (ii) Nafion resin was redissolved with 10 mL DMF until become a clear solution; (iii) the filler was dispersed in the same solvent under stirring for 1 day and added slowly to the solution of Nafion; (iv) the final solution was ultra-sonicated for 1 h and then stirred at 60 °C to ensure complete mixing; finally (v) casting on a petridisk at 80 °C overnight was performed in order to obtain a homogeneous membrane. The hybrid membrane is removed from the petridisk by immersing the glass plate in deionised water for several minutes. In order to reinforce the membrane, this was sandwiched and pressed between two Teflon plates and put in oven at 150 °C for about 15 min. Composite membranes produced by casting were subsequently treated by rinsing in: (i) boiling HNO₃ solution (1 M) for 1 h to oxidize the organic impurities, (ii) boiling H₂O₂ (3 vol.%) for 1 h in order to remove all the organic impurities, (iii) boiling deionized H₂O for 40 min three times, (iv) boiling H₂SO₄ (0.5 M) for 1 h to remove any metallic impurities, and again (v) boiling deionized H₂O for 40 min twice to remove excess acid. According to McMillat *et al.*, [40] an ulterior purification procedure was performed in order to ensure the removal of paramagnetic contaminants which are particularly damaging to an NMR experiment, such as the presence of copper that we found by Electron Paramagnetic Resonance analysis. By this procedure membranes were soaked in EDTA solution (0.001 M) for 1 day after followed by a thorough rinse. Then soaked in 2 M HCl at a temperature of 80 °C for 2 h followed by boiling in fresh distilled-deionized water to remove any residual acids and again repeated the treatment with EDTA. Finally, rinsing in boiled deionized water three times to remove residual EDTA and stored at room temperature at fully hydrated state.

3.3. Characterization Techniques

NMR measurements were performed using a Bruker AVANCE 300 wide bore NMR spectrometer working at 300 MHz on ¹H and the spectra were obtained by transforming the resulting free-induction decay (FID) of single $\pi/2$ pulse sequences. Self-diffusion coefficients of water were performed with a Diff30 NMR probe by using the pulsed gradient spin-echo (PGSE) method [41]. This technique consists of two rf pulses, Hahn-echo sequence $\pi/2 - \tau - \pi$ with two identical pulsed-gradients, the first applied between the 90° and 180° rf pulse (during the dephasing) and the second after the 180° rf pulse (during the rephasing) but before the echo. Following the usual notation, the gradients have magnitude g , duration δ , time delay Δ , and the factor $(\Delta - (\delta/3))$ is the diffusion time over which the molecular displacements are monitored. The attenuation of the echo amplitude is represented by the Stejskal-Tanner equation:

$$A = \exp[-\gamma^2 g^2 D \delta^2 (\Delta - (\delta/3))]$$

where D is the self-diffusion. For the investigated samples, the experimental parameters, Δ and δ , are 10 and 1 ms, respectively. The gradient amplitude, g , varied from $10 \text{ G}\cdot\text{cm}^{-1}$ to $600 \text{ G}\cdot\text{cm}^{-1}$. All PGSE data were well described by a single exponential and, for accurate treatment of experimental error, D was determined by regressing the theoretical echo-attenuation onto the experimental data (*i.e.*, resonance integrals). Finally, longitudinal relaxation times (T_1) of water were measured on the same spectrometer by the inversion-recovery sequence ($\pi - \tau - \pi/2$). Both self-diffusion and T_1 measurements were conducted by increasing temperature step by step from $20 \text{ }^\circ\text{C}$ to $140 \text{ }^\circ\text{C}$, with steps of $10 \text{ }^\circ\text{C}$, and leaving the sample to equilibrate for about 20 min.

Prior to the NMR measurements, membranes were dried in oven, weighed and then immersed in the various aqueous methanol solutions, in pure water and in pure methanol, at room temperature (in the results section it will be explicated the different kind of solutions prepared and the motivations). Upon being removed from the solutions they were quickly blotted dry with a paper tissue (to eliminate most of the free surface liquid). The liquid content value was determined using a microbalance and recorded as: $\text{uptake}\% = [(m_{\text{wet}} - m_{\text{dry}})/m_{\text{dry}}] \times 100$.

At this point the membranes were loaded into a 5 mm NMR Pyrex tube and sealed. In order to minimize the evaporation of the solvent from the membrane with increased temperature, a “cap” of Teflon was placed just above the membrane. Thus, the free volume available to the evaporated solvent was minimized.

For the electrochemical characterization, the electrodes used were composed of commercial gas-diffusion layer-coated carbon cloth for high temperature (HT-ELAT, E-TEK) and low temperature operation (LT-ELAT, E-TEK) at the anode and cathode, respectively. Unsupported Pt-Ru (Johnson-Matthey) and Pt (Johnson-Matthey) catalysts were mixed under ultrasounds with 15 wt % Nafion ionomer (Ion Power, 5 wt % solution) and deposited by a doctor blade technique onto the diffusion media for the anode and cathode, respectively. A Pt loading of $2 \text{ mg}\cdot\text{cm}^{-2}$ was used for all MEAs, both at the anode and cathode. The MEAs were obtained by a hot pressing method between electrodes and the different membranes (filler-free recast Nafion, Lap-Nafion and SWy-Nafion composite membranes) at $130 \text{ }^\circ\text{C}$ and $30 \text{ kg}\cdot\text{cm}^{-2}$ for 1.5 min. The thickness of the membranes used for the electrochemical tests was about $50 \text{ }\mu\text{m}$. The MEAs were tested in a 5 cm^2 single cell (Fuel Cell Tech., Inc.) connected with an Autolab PGSTAT 302 Potentiostat/Galvanostat (Metrohm) equipped with a frequency response analyzer (FRA) module of impedance. The impedance measurements were performed under potentiostatic control in a frequency range between 20 kHz and 0.1 Hz by frequency sweeping in the single sine mode. The amplitude of the sinusoidal excitation signal was 0.01 V. The series resistance was determined from the high frequency intercept on the real axis in the Nyquist plot. A 2 M methanol solution was fed at the anode under atmospheric pressure with a flow rate of $3 \text{ mL}\cdot\text{min}^{-1}$, whereas oxygen was fed at the cathode at a flow rate of $100 \text{ mL}\cdot\text{min}^{-1}$ under 1.5 bar of pressure. The performance of each MEA was measured under steady-state conditions in the temperature range $90 \text{ }^\circ\text{C}$ – $110 \text{ }^\circ\text{C}$.

4. Conclusions

PGSE and relaxometry in NMR are powerful methods that allow for the measurement of multicomponent diffusion and mobility on a molecular scale. Using this technique, self-diffusion coefficients and spin-lattice relaxation times of methanol and water in Nafion and nanocomposite membranes were measured as a function of methanol solution concentration and temperature. In order to discriminate between the NMR signals of methanol and water, the membranes were equilibrated in solutions CH₃OD/D₂O and CD₃OD/H₂O, at 2 M and 4 M concentrations.

The results achieved on the filler-free Nafion and on two hybrid membranes based on smectic clays, Laponite and Swy-2, with different particle size and cation exchange capacity (CEC), have been analyzed and compared.

In the filler-free Nafion, the methanol diffusion, both at 2 M and 4 M concentration, is higher than water and, at high temperature (100–130 °C), when the water signal almost disappears, the methanol still maintains a discrete mobility.

Swy montmorillonite particles inside the membrane demonstrate being a physical barrier for methanol cross-over, reducing the methanol diffusion with an evident blocking effect yet, nevertheless ensuring a high water mobility up to 130 °C and over several hours. However, the solution uptake data highlight a strong swelling membrane effect demonstrating the high chemical affinity of the methanol towards the polymer that allows a diffusion, even if lower than water, up to temperatures above 100 °C and that increases with increasing methanol solution concentrations.

Nanocomposite membrane based on the Laponite clay showed a different behavior both for water and methanol with respect to Swy. The smaller CEC and particle size of this synthetic clay result in both lower water retention capacity of the membrane and obstruction toward the methanol, respectively. This is confirmed by the slightly higher cell resistance of the cell based on this membrane compared to Swy-based membrane by using 2 M methanol concentration.

We conclude that, despite the obstruction effect due to the dispersion of suitable hydrophilic layered nanoparticles in Nafion, the main contribution to the diffusion of methanol is its high uptake in the polymer. Therefore, to enhance the performance and the efficiency of a DMFC, it is necessary to develop membranes which absorb less methanol while maintaining, however, a high proton conductivity.

Acknowledgments

The authors gratefully acknowledge D. Gournis (Department of Material Science and Engineering, University of Ioannina) for his scientific support on the clay materials.

References

1. Wasmus, S.; Kuver, A. Methanol oxidation and direct methanol fuel cells: A selective review. *J. Electroanal. Chem.* **1999**, *461*, 14–31.
2. Aricò, A.S.; Srinivasan, S.; Antonucci, V. DMFCs: From fundamental aspects to technology development. *Fuel Cells* **2001**, *2*, 133–161.
3. Han, J.; Liu, H. Real time measurements of methanol crossover in a DMFC. *J. Power Sources* **2007**, *164*, 166–173.

4. Alberti, G.; Casciola, M. Composite membranes for medium-temperature PEM fuel cells. *Annu. Rev. Mater. Res.* **2003**, *33*, 129–154.
5. Steele, B.C.H.; Heinzel, A. Materials for fuel-cell technologies. *Nature* **2001**, *414*, 345–352.
6. Perry, M.L.; Fuller, T.F. A historical perspective of fuel cell technology in the 20th century. *J. Electrochem. Soc.* **2002**, *149*, S59–S67.
7. Yang, C.; Costamagna, P.; Srinivasan, S.; Benziger, J.; Bocarsly, A.B. Approaches and technical challenges to high temperature operation of proton exchange membrane fuel cells. *J. Power Sources* **2001**, *103*, 1–9.
8. Navarra, M.A.; Abbati, C.; Croce, F.; Scrosati, B. Temperature-dependent performances of a fuel cell using a superacid zirconia-doped Nafion polymer electrolyte. *Fuel Cells* **2009**, *9*, 222–225.
9. Nicotera, I.; Zhang, T.; Bocarsly, A.; Greenbaum, S. NMR characterization of composite polymer membranes for low-humidity PEM fuel cells. *J. Electrochem. Soc.* **2007**, *154*, B466–B473.
10. Baglio, V.; Aricò, A.S.; Antonucci, V.; Nicotera, I.; Oliviero, C.; Coppola, L.; Antonucci, P.L. An NMR spectroscopic study of water and methanol transport properties in DMFC composite membranes: Influence on the electrochemical behaviour. *J. Power Sources* **2006**, *163*, 52–55.
11. Nicotera, I.; Enotiadis, A.; Angjeli, K.; Coppola, L.; Gournis, D. Evaluation of smectite clays as nanofillers for the synthesis of nanocomposite polymer electrolytes for fuel cell applications. *Int. J. Hydrog. Energy* **2011**, *37*, 6236–6245.
12. Nicotera, I.; Enotiadis, A.; Angjeli, K.; Coppola, L.; Ranieri, G.A.; Gournis, D. Effective improvement of water-retention in nanocomposite membranes using novel organo-modified clays as fillers for high temperature PEMFCs. *J. Phys. Chem. B* **2011**, *115*, 9087–9097.
13. Tazi, B.; Savadogo, O. Effect of various heteropolyacids (HPAs) on the characteristics of Nafion[®]-HPAS membranes and their H₂/O₂ polymer electrolyte fuel cell parameters. *J. New Mater. Electrochem. Syst.* **2001**, *4*, 187–196.
14. Yano, K.; Usuki, A.; Okada, A.; Kurauchi, T.; Kamigaito, O. Synthesis and properties of polyimide-clay hybrid. *J. Polym. Sci. Part A Polym. Chem.* **1993**, *31*, 2493–2498.
15. Giannelis, E.P. Polymer layered silicate nanocomposites. *Adv. Mater.* **1996**, *8*, 29–35.
16. Paul, D.R.; Robeson, L.M. Polymer nanotechnology: Nanocomposites. *Polymer* **2008**, *49*, 3187–3204.
17. Kojima, Y.; Usuki, A.; Kawasumi, M.; Okada, A.; Kurauchi, T.; Kamigaito, O. Synthesis of nylon-6-clay hybrid by montmorillonite intercalated with epsilon-caprolactam. *J. Polym. Sci. Part A Polym. Chem.* **1993**, *31*, 983–986.
18. Gournis, D.; Floudas, G. “Hairy” Plates: Poly(ethylene oxide)-b-polyisoprene copolymers in the presence of laponite clay. *Chem. Mater.* **2004**, *16*, 1686–1692.
19. Gournis, D.; Jankovic, L.; Maccallini, E.; Benne, D.; Rudolf, P.; Colomer, J.F.; Sooambar, C.; Georgakilas, V.; Prato, M.; Fanti, M.; Zerbetto, F.; Sarova, G.H.; Guldi, D.M. Clay-fulleropyrrolidine nanocomposites. *J. Am. Chem. Soc.* **2006**, *128*, 6154–6163.
20. Wang, J.; Merino, J.; Aranda, P.; Galvan, J.C.; Ruiz-Hitzky, E. Reactive nanocomposites based on pillared clays. *J. Mater. Chem.* **1998**, *9*, 161–168.
21. Bébin, P.; Caravanier, M.; Galiano, H. Nafion[®]/clay-SO₃H membrane for proton exchange membrane fuel cell application. *J. Membr. Sci.* **2006**, *278*, 35–42.

22. Ray, S.S.; Okamoto, M. Polymer/layered silicate nanocomposites: A review from preparation to processing. *Prog. Polym. Sci.* **2003**, *28*, 1539–1641.
23. Cohen, B.; Huppert, D. Connection between proton abnormal conductivity in water and dielectric relaxation time. *J. Phys. Chem. A* **2003**, *107*, 3598–3605.
24. Eikerling, M.; Kornyshev, A.A.; Kuznetsov, A.M.; Ulstrup, J.; Walbran, S. Mechanisms of proton conductance in polymer electrolyte membranes. *J. Phys. Chem. B* **2001**, *105*, 3646–3662.
25. Kreuer, K.D. Fast proton conductivity: A phenomenon between the solid and the liquid state? *Solid State Ionics* **1997**, *94*, 55–62.
26. Gebel, G. Structural evolution of water swollen perfluorosulfonated ionomers from dry membrane to solution. *Polymer* **2000**, *41*, 5829–5838.
27. Paddison, S.J.; Paul, R. The nature of proton transport in fully hydrated Nafion[®]. *Phys. Chem. Chem. Phys.* **2002**, *4*, 1158–1163.
28. Hallberg, F.; Vernersson, T.; Pettersson, E.T.; Dvinskikh, S.V.; Lindbergh, G.; Furó, I. Electrokinetic transport of water and methanol in Nafion membranes as observed by NMR spectroscopy. *Electrochim Acta* **2010**, *55*, 3542–3549.
29. Ji, X.; Yan, L.; Zhu, S.; Zhang, L.; Lu, W. Methanol distribution and electroosmotic drag in hydrated poly(perfluorosulfonic) acid membrane. *J. Phys. Chem. B* **2008**, *112*, 15616–15627.
30. Adamovic, I.; Gordon, M.S. Methanol–water mixtures: A microsolvation study using the effective fragment potential method. *J. Phys. Chem. A* **2006**, *110*, 10267.
31. Slichter, C.P. *Principles of Magnetic Resonance*, 3rd ed.; Springer Series in Solid State Science: New York, NY, USA, 1990.
32. Hu, J.; Baglio, V.; Tricoli, V.; Aricò, A.S.; Antonucci, V. PEO-PPO-PEO triblock copolymer/Nafion blend as membrane material for intermediate temperature DMFCs. *J. Appl. Electrochem.* **2008**, *38*, 543–550.
33. Baglio, V.; Di Blasi, A.; Aricò, A.S.; Antonucci, V.; Antonucci, P.L.; Nannetti, F.; Tricoli, V. Investigation of the electrochemical behaviour in DMFCs of chabazite and clinoptilolite-based composite membranes. *Electrochim Acta* **2005**, *50*, 5181–5188.
34. Baglio, V.; di Blasi, A.; Aricò, A.S.; Antonucci, V.; Antonucci, P.L.; Trakanprapai, C.; Esposito, V.; Licoccia, S.; Traversa, E. Composite mesoporous Titania Nafion-based membranes for direct methanol fuel cell operation at high temperature. *J. Electrochem. Soc.* **2005**, *152*, A1373–A1377.
35. Staiti, P.; Aricò, A.S.; Baglio, V.; Lufrano, F.; Passalacqua, E.; Antonucci, V. Hybrid Nafion-silica membranes doped with heteropolyacids for application in direct methanol fuel cells. *Solid State Ionics* **2001**, *145*, 101–107.
36. Yang, C.; Srinivasan, S.; Aricò, A.S.; Cretì, P.; Baglio, V.; Antonucci, V. Composite Nafion/zirconium phosphate membranes for direct methanol fuel cell operation at high temperature. *Electrochem. Solid State Lett.* **2001**, *4*, A31–A34.
37. Baglio, V.; Ornelas, R.; Matteucci, F.; Martina, F.; Ciccarella, G.; Zama, I.; Arriaga, L.G.; Antonucci, V.; Aricò, A.S. Solid polymer electrolyte water electrolyser based on Nafion-TiO₂ composite membrane for high temperature operation. *Fuel Cells* **2009**, *9*, 247–252.

38. Antonucci, V.; Di Blasi, A.; Baglio, V.; Ornelas, R.; Matteucci, F.; Ledesma-Garcia, J.; Arriaga, L.G.; Aricò, A.S. High temperature operation of a composite membrane-based solid polymer electrolyte water electrolyser. *Electrochim Acta* **2008**, *53*, 7350–7356.
39. Gournis, D.; Lappas, A.; Karakassides, M.A.; Tobbens, D.; Moukarika, A. A neutron diffraction study of alkali cation migration in montmorillonites. *Phys. Chem. Miner.* **2008**, *35*, 49–58.
40. MacMillan, B.; Sharp, A.R.; Armstrong, R.L. An n.m.r. investigation of the dynamical characteristics of water absorbed in Nafion. *Polymer* **1999**, *40*, 2471–2480.
41. Stejskal, E.O.; Tanner, J.E. Spin diffusion measurements: Spin echoes in the presence of a time-dependent field gradient. *J. Chem. Phys.* **1965**, *42*, 288–292.

© 2012 by the authors; licensee MDPI, Basel, Switzerland. This article is an open access article distributed under the terms and conditions of the Creative Commons Attribution license (<http://creativecommons.org/licenses/by/3.0/>).

Effective Improvement of Water-Retention in Nanocomposite Membranes Using Novel Organo-Modified Clays as Fillers for High Temperature PEMFCs

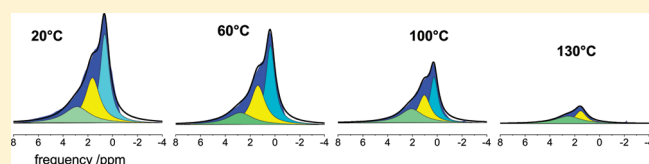
Isabella Nicotera,^{*,†} Apostolos Enotiadis,[‡] Kristina Angjeli,[†] Luigi Coppola,[†] Giuseppe A. Ranieri,[†] and Dimitrios Gournis[‡]

[†]Department of Chemistry, University of Calabria, 87036 Rende, Cosenza, Italy

[‡]Department of Material Science and Engineering, University of Ioannina, 45110 Ioannina, Greece

S Supporting Information

ABSTRACT: Toward an enhanced water-retention of polymer electrolyte membranes at high temperatures, novel organo-modified clays were prepared and tested as fillers for the creation of hybrid Nafion nanocomposites. Two smectite clays (Laponite and montmorillonite), with different structural and physical parameters, were loaded with various cationic organic molecules bearing several hydrophilic functional groups ($-\text{NH}_2$, $-\text{OH}$, $-\text{SO}_3\text{H}$) and incorporated in Nafion by solution intercalation. The resulted hybrid membranes were characterized by a combination of powder X-ray diffraction, FTIR spectroscopy, and thermal analysis (DTA/TGA) showing that highly homogeneous exfoliated nanocomposites were created where the individual organoclay layers are uniformly dispersed in the continuous polymeric matrix. In this paper, water-transport properties were investigated by NMR spectroscopy, including pulsed-field-gradient spin-echo diffusion and spectral measurements conducted under variable temperature. Organo-montmorillonite nanofillers demonstrate a considerable effect on the Nafion polymer in terms both of water absorption/retention and water mobility with a remarkable behavior in the region of high temperatures (100–130 °C), denoting that the surface modifications of this clay with acid organic molecules significantly improve the performance of the final composite membrane. ^1H NMR spectral analysis allowed a general description of the water distribution in the system and an estimation of the number of water molecules involved in the hydration shell of the sulfonic groups as well as that absorbed on the organoclay particles.



1. INTRODUCTION

Proton exchange membrane fuel cells (PEMFCs) are promising candidates for both vehicle applications and local on-site power generation system in the future, due to their high energy efficiency as well as high power density, even at relatively low operation temperatures. The electrolyte in these systems is a proton conducting polymer membrane. The development of high-performance electrolyte membrane is critical to achieve the optimal power density and efficiency of a PEMFC. In fact, the ohmic loss of the membrane is one of the most significant cause of overpotential in the fuel cell operational current range. PEMFCs operating in the typical 60–80 °C temperature range face problems including poor carbon monoxide (from reformed hydrogen or methanol as fuels) tolerance and heat rejection. These drawbacks can be overcome by increasing the operation temperature range up to 110–130 °C,^{1,2} but this leads to an unacceptable decrease in the proton conductivity of the electrolyte due to water loss.³ As a rule, the following properties of polymeric membranes need to be optimized for use in fuel cells: (1) high proton conduction; (2) good mechanical, chemical and thermal strength requiring the selection of suitable polymer backbone;

(3) low gas permeability, which is dependent on material and thickness of the membrane.

Nafion (a registered trademark of E. I. du Pont de Nemours and Co.) is the electrolyte that has been most extensively studied in PEMFC applications. However, the most significant barrier to run such polymer electrolyte fuel cell at elevated temperatures is maintaining the proton conductivity of the membrane, which depends critically on the presence of water: the conductivity of a dry membrane is several orders of magnitude lower than that of a fully saturated membrane. According to the literature several membrane properties may benefit from the presence of homogeneously dispersed organic/inorganic fillers such as hygroscopic inorganic oxide (SiO_2 , TiO_2 , ZrO_2), zeolite, heteropoly acids, and zirconium hydrogen phosphate to enhance the water retention property.^{3–13}

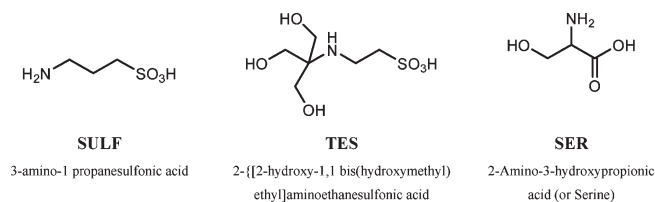
Recent studies have shown that polymer nanocomposites based on layered clay nanoparticles exhibit reduced gas permeability due to the presence of impermeable clay platelets as well as

Received: March 30, 2011

Revised: June 8, 2011

Published: June 14, 2011

Table 1. Organic Molecules Used for the Chemical Modification of SWy and Lap Clays



structural changes in the polymer induced by the clay nanofillers.^{14–16} Among layered silicates, smectite clays are attractive candidates as Nafion additives because of their nanometer size, proton conductivity, good thermal stability and potential to reduce fuel (e.g., methanol) permeability.^{17,18} Smectite clays are a class of layered aluminosilicate minerals with a unique combination of swelling, intercalation, and ion exchange properties. They consist of an octahedral alumina layer fused between two tetrahedral silica layers (about 1 nm).^{19,20} The monovalent ions located between the clay layers allow the absorption of polar solvent, like water, with good retention capacity so, when incorporated into a polymer membrane, they help to prevent the loss of the hydration water not only at high temperatures but also under low relative humidity environment. The charge on the layers affects many fundamental properties of the clays, including water holding (an important property for the creation of Nafion nanocomposite membrane), cation fixation, swelling ability, cation exchange capacity, and high surface area. Moreover, the properties of the smectite nanoclays can be tailored using simple chemical methods such as intercalation with organic or inorganic guest molecules. Their surface properties, for example, can be easily modified through treatment with an organic surfactant. As a result the presence of the surfactant expands the interlayer gallery rendering the nanoclay compatible with hydrophobic media and polymer matrices. Because of their distinctive structure and properties, these organic–inorganic hybrid materials (so-called “organo-clays”) can be utilized in a wide variety of applications including, construction of modified electrodes, biosensors or biocatalysts,^{21–23} adsorbents for environmental remediation (e.g., removal of heavy metal ions for water²⁴) but also as nanofillers for polymer reinforcement.^{25–27} Thus, a strategy toward the improvement of the water retention of the Nafion membrane is the incorporation in the polymer matrix hybrid nanofillers of modified clays bearing organic functionalities with high affinity for Nafion and increased sites for water trapping.

In the present work, various organo-modified clays were prepared and tested as nanofillers for the creation of novel hybrid Nafion composites. The clays used were a synthetic clay (Laponite) with low layer charge density and small particle size (20 nm), and a natural montmorillonite (SWy-2) with medium layer charge density and high particle size (200 nm). Three cationic organic molecules, 3-amino-1-propanesulfonic acid, 2-[[2-hydroxy-1,1-bis(hydroxymethyl) ethyl]amino]ethanesulfonic acid and serine, were used for the clay modification and the resulting organo-modified derivatives were incorporated in Nafion by solution intercalation (membranes with pristine clays were also synthesized for comparison). The modification is based on the functionalization of the clay surfaces by various functional groups ($-\text{NH}_2$, $-\text{OH}$, $-\text{SO}_3\text{H}$) that can effectively (1) increase the concentration of acidic (hydrophilic) functional groups

(sulfonic, hydroxyl, etc.) on the surfaces of the clay minerals and thus improve the proton conductivity through the membrane and, (2) enhance their compatibility with polymeric materials, since silicate clays are hydrophilic and have little affinity for hydrophobic polymers like the hydrophobic phase of Nafion.

The organofillers and the nanocomposite membranes were investigated by a combination of powder X-ray diffraction, FTIR spectroscopy and thermal analysis (DTA/TGA) while the characteristics of the membranes were studied in terms of morphological analysis by scanning electronic microscopy (SEM), and, mainly, in terms of transport properties by NMR spectroscopy, in order to study of the water dynamics inside the electrolyte membranes, which is one of the key aspects in the evaluation of these materials.^{10,28–31} For this purpose the pulse-field-gradient spin–echo NMR (PFGSE-NMR) method³² was employed in this work to obtain a direct measurement of water self-diffusion coefficients on the water-swelled membranes in a wide temperature range (25–130 °C). This technique together with the ¹H NMR spectra have provided a general description of the water behavior: how it is shared in the polymer structure, effects of the nanofillers and their surface modifications, interactions between water molecules and hydrophilic groups present and, finally, a quantitative estimate of the hydration number, i.e., number of water molecules solvating the hydrophilic sites both in the maximum hydration regime and in quasi-dehydration conditions.

2. EXPERIMENTAL SECTION

2.1. Materials. Two smectite clays with different structural and physical parameters (structural formula, particle size and cation exchange capacity) were used.^{33,34} The first was a natural Wyoming montmorillonite (SWy-2) obtained from the Source Clay Minerals Repository, University of Missouri (Columbia), with a cation exchange capacity (CEC) measured by the Co(II) procedure equal to 80 mequiv per 100 g of clay and particle size around 200 nm. The second clay was a synthetic trioctahedral hectorite, Laponite (Lap), produced by Laporte Industries Ltd. with a CEC of 48 mequiv per 100 g clay and a particle size of 20 nm. SWy-2 montmorillonite was fractionated to $<2\ \mu\text{m}$ by gravity sedimentation and purified by well-established procedures in clay science.³⁵ Sodium-exchanged samples ($\text{Na}^+\text{-SWy-2}$) were prepared by immersing the clay into 1 N solution of sodium chloride. Cation exchange was complete by washing and centrifuging four times with dilute aqueous NaCl. The samples were finally washed with distilled deionized water and transferred into dialysis tubes in order to obtain chloride-free clays and then dried at room temperature.

For the chemical modification of the pristine clays three organic molecules were used: 3-amino-1-propanesulfonic acid (SULF), 2-[[2-hydroxy-1,1-bis(hydroxymethyl) ethyl]amino]ethanesulfonic acid (TES) and serine (SER). Their structural formulas are shown in Table 1.

Finally, Nafion solution (20 wt % in mixture of lower aliphatic alcohols and water) and *N,N*-dimethylformamide (DMF) were purchased from Aldrich and used as received.

2.2. Preparation of Organo-Modified Clay Nanofillers. For the preparation of the organoclays, aqueous 1 wt % clay suspensions were reacted under vigorous stirring with aliquots of the above organic molecules solutions in water such that the amount of the cationic molecule added corresponds three times the CEC of the clay. The mixtures were stirred for 24 h, centrifuged, washed with water, and air-dried by spreading on glass-plates. The products are designated as follows: SWy/TES, SWy/SER, and SWy/SULF and Lap/TES, Lap/SER, and Lap/SULF.

2.3. Composites Membranes Preparation. The composite membranes were prepared from 20 wt % Nafion solution according to the following processes: (i) 1 g of Nafion solution was heated at about 60 °C to remove all the solvents (water, 2-propanol, etc.); (ii) Nafion resin was redissolved with 10 mL of DMF until become a clear solution; (iii) the filler was dispersed in the same solvent under stirring for 1 day and then added slowly to the solution of Nafion; (iv) the final solution was ultrasonicated for 1 h and then stirred at 60 °C to ensure complete mixing; finally (v) casting on a Petri dish at 80 °C overnight was performed in order to obtain a homogeneous membrane. The hybrid membrane is removed from the petri dish by immersing the glass plate in deionized water for several minutes. In order to reinforce the membrane, this was sandwiched and pressed between two Teflon plates and put in oven at 150 °C for about 15 min. All composite membranes produced by casting were subsequently treated by rinsing in: (i) boiling HNO₃ solution (1 M) for 1 h to oxidize the organic impurities, (ii) boiling H₂O₂ (3 vol %) for 1 h in order to remove all the organic impurities, (iii) boiling deionized H₂O for 40 min three times, (iv) boiling H₂SO₄ (0.5 M) for 1 h to remove any metallic impurities, and again (v) boiling deionized H₂O for 40 min twice to remove excess acid. According to McMillan et al.³⁶ an ulterior purification procedure was performed in order to ensure the removal of paramagnetic contaminants which are particularly damaging to an NMR experiment, such as the presence of copper that we found by electron paramagnetic resonance analysis. By this procedure membranes were soaked in EDTA solution (0.001 M) for 1 day after followed by a thorough rinse. Then soaked in 2 M HCl at a temperature of 80 °C for 2 h followed by boiling in fresh distilled–deionized water to remove any residual acids and again repeated the treatment with EDTA. Finally, rinsing in boiled deionized water three times to remove residual EDTA and stored at room temperature at fully hydrated state.

2.4. Characterization Techniques. The X-ray powder diffraction data were collected on a D8 Advanced Bruker diffractometer by using Cu K α (40 kV, 40 mA) radiation and a secondary beam graphite monochromator. The patterns were recorded in a 2θ range from 2° to 40°, in steps of 0.02° and counting time 2 s per step. Infrared spectra were measured with a FT-IR 8400 spectrometer, in the region of 400–4000 cm⁻¹, equipped with a DTGS detector. Each spectrum was the average of 32 scans collected at 2 cm⁻¹ resolution. Samples were in the form of KBr pellets containing ca. 2 wt % samples while membranes measured as received. Thermogravimetric (TGA) and differential thermal (DTA) analysis were performed using a Perkin-Elmer Pyris Diamond TG/DTA. Samples of approximately 5 mg were heated under air from 25 to

850 °C, at a rate of 10 °C/min. The morphological studies were performed by using a QUANTA FEG 400 F7, FEI microscope operating in the e-SEM mode. The SEM images were acquired collecting the backscattered electrons induced by using 10 keV electron beam and 0.4 mbar of water humidity.

NMR measurements were performed on a Bruker NMR spectrometer AVANCE 300 Wide Bore working at 300 MHz on ¹H. The employed probe was a Diff30 Z-diffusion 30 G/cm/A multinuclear with substitutable RF inserts. The spectra were obtained by a single $\pi/2$ pulse sequence. The NMR pulsed field gradient spin–echo (PFG-SE) method³² was used to measure self-diffusion coefficients. This technique consists of two rf pulses, Hahn-echo sequence ($\pi/2-\tau-\pi$), with two identical pulsed-field gradients, the first applied between the 90° and 180° rf pulse (during the dephasing) and the second after the 180° rf pulse (during the rephasing) but before the echo. Following the usual notation, the pulsed-field gradients have magnitude g , duration δ , and time delay Δ (different from the degree of ionic association). The attenuation of the echo amplitude is represented by the Stejskal-Tanner equation:

$$A(g) = A(0) \exp[-\gamma^2 g^2 D \delta^2 (\Delta - (\delta/3))]$$

where D is the self-diffusion coefficient and γ is the nuclear gyromagnetic ratio and $A(0)$ is the amplitude of the echo at $g = 0$. Note that the exponent in the equation is proportional to the mean-squared displacement of the molecules over an effective time scale ($\Delta - (\delta/3)$). For the investigated samples, the experimental parameters, Δ and δ , are 10 and 1 ms, respectively. The gradient amplitude, g , varied from 10 to 600 G cm⁻¹. In this condition the uncertainty in the self-diffusion measurements is ~3%. It is worth noting that a Gaussian self-diffusion of water (i.e., not restricted diffusion) has been observed also for a diffusion time (Δ) longer than 40 ms. (See the Supporting Information, Figure S1).

Both self-diffusion and spectra measurements were conducted by increasing temperature step by step from 20 to 130 °C, with steps of 20 K, and leaving the sample to equilibrate for about 20 min.

Prior to the NMR measurements, membranes were dried in oven, weighed and then immersed in distilled water at room temperature. Upon being removed from the water they were quickly blotted dry with a paper tissue (to eliminate most of the free surface liquid). The water content value was determined using a microbalance and recorded as:

$$\text{uptake \%} = [(m_{\text{wet}} - m_{\text{dry}})/m_{\text{dry}}] \times 100$$

At this point, the membranes were loaded into a 5 mm NMR Pyrex tube and hermetically sealed.

3. RESULTS AND DISCUSSION

3.1. Structural Investigation. For the surface modification of the parent smectite clays a simple procedure was followed. Positively charged molecules are introduced into interlayer space of layered clay minerals by ion exchange procedure where charge balancing cations (e.g., Na⁺) are replaced by the organic cations. The introduced organic cations are held strongly by electrostatic forces with the negatively charged clay surfaces and the final conformation depends on the shape, size, and total charge of the organic cations and also on the charge density of the clay surface. In our case, the intercalation procedure involves

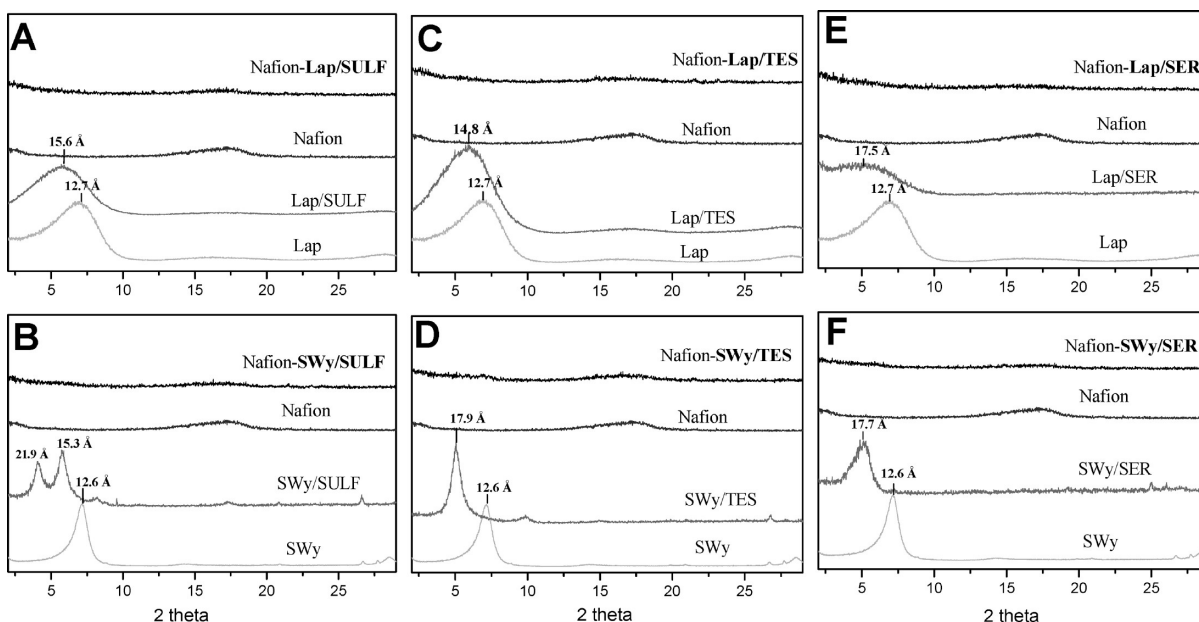


Figure 1. XRD patterns of pristine clays, organo-modified clays, filler-free Nafion and nanocomposite membranes with 3 wt % organoclay nanofillers.

an initial pre-equilibrium reaction in which the primary (SULF and SER) or secondary (TES) amino groups of the organic molecules are protonated:



where: (i) for SULF R_1 : $-(\text{CH}_2)_3\text{SO}_3\text{H}$ and R_2 : $-\text{H}$;
 (ii) for TES R_1 : $-(\text{CH}_2)_2\text{SO}_3\text{H}$ and R_2 : $-\text{C}(\text{CH}_2\text{OH})_3$
 (iii) for SER R_1 : $-\text{C}(\text{CH}_2\text{OH})_2\text{COOH}$ and R_2 : $-\text{H}$

The protonated organic molecules were readily adsorbed on the clay surfaces, by ion exchange. The monovalent Na^+ exchangeable cations are replaced easily by the protonated amino molecules according to the following reaction:



where the bold lines represent the clay platelets.

X-ray diffraction (XRD) measurements provide a powerful tool to understand not only the changes in the interior of the clay microenvironment, and thus reveal the successful modification of the parents nanoclays, but also to evaluate the type of composites created after the incorporation of the hybrid layered fillers in the Nafion matrix. Figure 1 shows in comparison the XRD patterns of pristine clays before and after the intercalation of the organic molecules as well as the filler-free Nafion and the nanocomposites prepared with the organoclays at 3 wt % filler to polymer loading. The XRD data show an increase of the basal spacing (d_{001}) of both clays after insertion of the three guest materials. More specifically, in the case of Laponite samples, the basal spacing d_{001} , which is 12.7 Å in the pristine clay, becomes 15.6,

14.8, and 17.5 Å in the modified clays with SULF, TES, and SER, respectively. If we consider that the thickness of a clay layer is 9.6 Å,³⁷ these values correspond to intersheet separations (L) of 6.0, 5.2, and 7.9 (where $L = d_{001} - 9.6$ Å) for Lap/SULF, Lap/TES, and Lap/SER, respectively. This increment in the interlayer space is indicative of the intercalation of the three cationic molecules into the Laponite interlayers where the guest molecules adopts an inclined orientation (at a certain angle) between the clay surfaces. The XRD results for the other organoclays with SWy-2 montmorillonite are analogous with the increment in the d -spacing to be more pronounced. XRD patterns of SWy/TES and SWy/SER show d_{001} spacings of 17.9 and 17.7 Å, which corresponds to intersheet separations of 8.3 and 8.1 Å, respectively. These higher d -spacings of the montmorillonite organoclays implying that the organic cations are lying in the interlayer space of the mineral in a more upward position (higher angle) compared with the corresponding organoclays with Laponite. This is probably due to the higher CEC of montmorillonite compared to Laponite which designates that the amount of intercalated molecules is much higher in the case of montmorillonite leading to higher d -spacings compared to Laponite samples. Finally, when the montmorillonite clay was treated with SULF solution (SWy/SULF), two d_{001} spacings are observed at 21.6 Å ($\Delta = 12.0$ Å) and 15.5 Å ($\Delta = 5.9$ Å) arising from two different conformations of the SULF cations within the clay layers. The intersheet separation of 12.0 Å is probably due to the formation of a double-layer arrangement of the SULF molecules in the interlayer space while the value of 5.9 Å—which is almost half of the previous one—arises from the formation of a single layer arrangement. Similar mixed phases have been observed during the intercalation of organic surfactants (alkylammonium derivatives)^{38,39} or other polar molecules such as ethylene glycol.⁴⁰

Moreover, the XRD patterns (Figure 1) of all nanocomposite membranes show clearly a broad band centered at 17° distinctive of the Nafion polymer arrangement.^{41,42} The absence of the d_{001} diffraction peak, characteristic of the

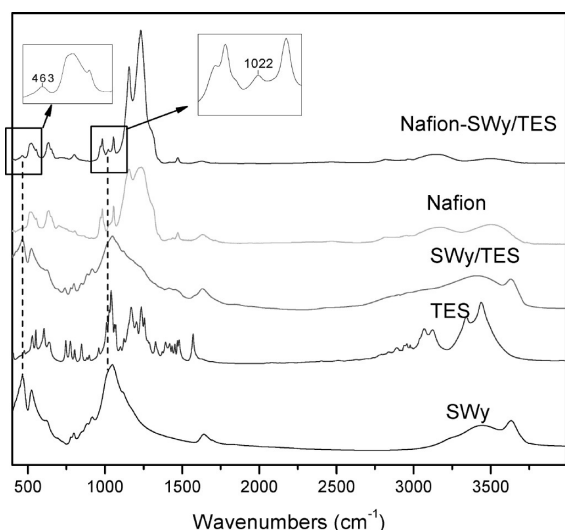


Figure 2. FT-IR spectra of pristine (SWy) clay, TES surfactant, SWy/ TES organoclay, filler-free Nafion, and nanocomposite membrane with 3 wt % SWy/ TES.

modified clays, in the patterns of the final nanocomposites indicates that the ordered structure of the layered mineral is effectively eliminated after mixing with the polymeric mass. This means that the use of all the organo-modified clays lead to the creation of exfoliated nanocomposites where the individual clay layers loose their stacking and are uniformly dispersed in the continuous polymeric matrix. Furthermore, the broad band around 17° loose its intensity in the XRD patterns of all the nanocomposite membranes indicating changes in morphological features of the Nafion due to differences in crystallinity of the perfluorocarbon backbone. In fact, as shown in Figure S2 of the Supporting Information, this broad band can be fitted to the experimental data using two distinct diffraction peaks: a large amorphous halo centered at ca. 16° , and a superimposed Bragg peak centered at 17.5° corresponding to the crystalline fraction of the perfluorocarbon backbone.¹⁸ The ratio between these two peaks provides a measure of the amount of crystallinity in the membrane. The crystallinity of all nanocomposite membranes is lower than that of pristine Nafion membrane indicating that the presence of modified clay nanoplatelets leads to membranes with essentially more amorphous structure.

The presence of nanofiller in the final composites was revealed also with FT-IR spectroscopy. Figure 2 shows the FT-IR spectra of Nafion–SWy/ TES membrane in comparison with the filler-free Nafion, modified clay (SWy/ TES), pristine clay (SWy) and TES molecule. Initially, the spectrum of the SWy/ TES presents the characteristic bands of SWy and TES cations confirming the presence of organic molecules in the modified nanofiller. In addition, the pattern of Nafion–SWy/ TES presents all the characteristic bands of the Nafion and the modified clay, without significant changes, confirming the presence of the organoclay (SWy/ TES) in the final composite membrane. More specifically, the appearance of the peaks at 463 and 1022 cm^{-1} which correspond to Si–O and Si–O–Si vibrations of the clay lattice are indicative of the existence of the phyllosilicate mineral in the final composite. Similar spectra were observed for all nanocomposites membranes prepared using the other organo-modified clays.

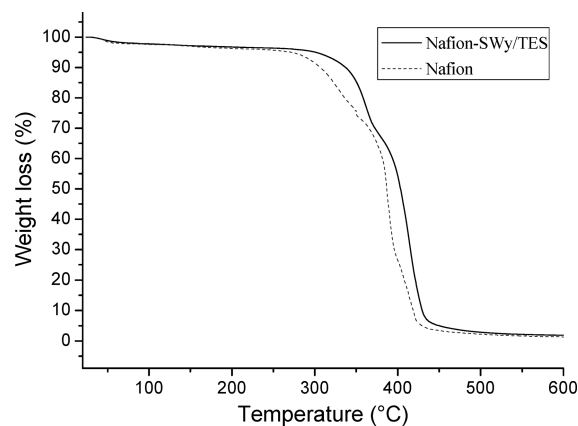


Figure 3. TGA curves of filler-free Nafion and nanocomposite membrane with 3 wt % SWy/ TES.

The thermo-gravimetric curves, derived from TGA measurements, were used to determine the amount of adsorbed water in the organoclays. From the weight loss up to 120°C , the percentage of adsorbed water was calculated for all organo-modified clays. The adsorbed water was found 7.7, 8.9, and $9.2\text{ wt } \%$ for Lap/ TES, Lap/ SER, and Lap/ SULF, respectively, while lower values were estimated for organo-montmorillonites, 2.5, 3.0, and $5.9\text{ wt } \%$ for SWy/ TES, SWy/ SER, and SWy/ SULF, respectively. The higher water content of organo-Laponite samples originates from the different structural and the physico-chemical properties of the two parent clays. In general, it is well-known⁴³ that Laponite clay adsorbs more water than montmorillonite (or other smectite clays) due to multilayer water adsorption on the external surface of this high surface area material. Furthermore, TGA was used also to reveal the homogeneous distribution of the organoclay platelets in the Nafion matrix. TGA results (Figure 3) show that in the case of Nafion–SWy/ TES loaded with 3 wt % nanofiller, the decomposition of Nafion was shifted to higher temperatures. The higher thermal resistance of the nanocomposite than that of pure Nafion membrane is due to the strong interaction of polymer main chains with modified nanofiller which in fact provides evidence for the homogeneous dispersion of the organo-modified silicate platelets in the polymeric matrix.^{42,44} Similar results were observed for all the series of nanocomposites (not shown here) indicating that all organoclay nanofillers are distributed homogeneously in the polymer matrix.

3.2. Morphological Analysis. In this study, SEM was used to observe the surface morphology of the nanocomposite membranes (Figure 4) based on both SWy and Lap organoclays. Starting from Nafion–SWy (Figure 4a), the first observation concerns the difference between the superior and inferior edges (first image) as well as the two surfaces of the membrane (second image shows the superior surface): one side is smooth, compact and uniform while the other side is particularly wrinkled and spongy even if, no aggregates or agglomerates are visible inside the polymeric matrix but rather a porous structure typical of the clays. This result is imputable to the casting procedure used to prepare the membranes where, during the 8–10 h of the solvent evaporation process, the filler particles tend to settle on the substrate. In general, it is known that the preparation procedure of composite membranes by dispersion of preformed particles followed by film casting is a very simple method, but it is usually

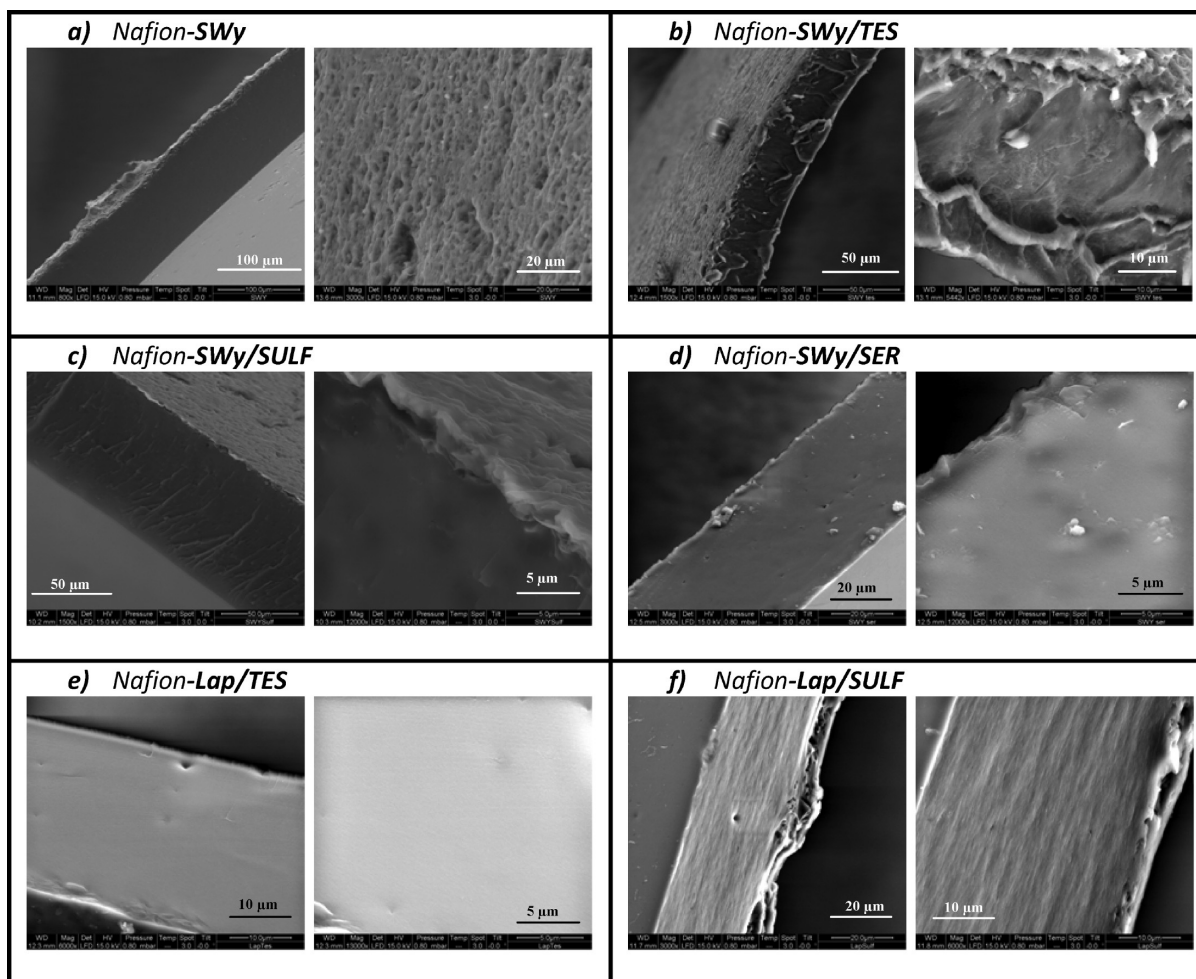


Figure 4. SEM images of the Nafion–organoclays composite membranes.

difficult to avoid the formation of particle agglomerates inside the polymeric matrix and, consequently, membranes containing nonhomogeneous dispersions of microsized particles are usually obtained.⁵

The organo-modification of the smectite clays produces some modest morphological changing in the composite membranes. In particular, SWy/TES (Figure 4b) shows a spongy structure on the entire section of the film and on both surfaces which are wrinkled even if with different intensity. Instead, SWy/SULF and SWy/SER nanocomposites show less significant changes (Figure 4, parts c and d, respectively) and have a morphology more similar to Nafion–SWy composite, with one side smooth and featureless, the other side spongy. However, going in detail, both these two nanocomposites present a structure less compact and in Nafion–SWy/SER some particles are also visible. Finally, Laponite composites show a quite different structure also by considering that the particles size is about ten times smaller than montmorillonite. Nafion–Lap/TES (Figure 4e) is uniform, smooth and homogeneous on the whole volume without pores or agglomerates, hence there is a very good dispersion of the clay platelets in the polymeric matrix. Nafion–Lap/SULF (Figure 4f), instead, shows more spongy texture with a well evident weaving and with a little deposit of clay sheets on the substrate. However,

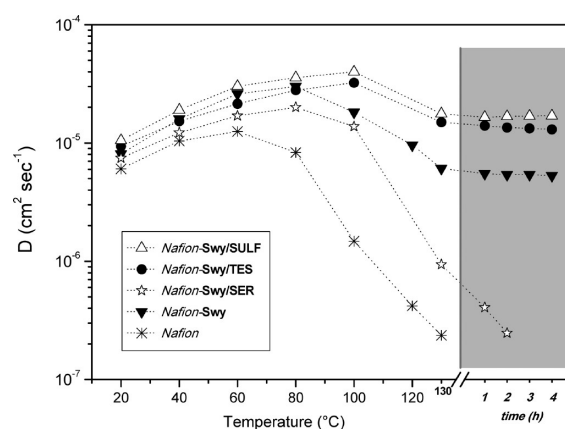


Figure 5. Self-diffusion coefficients of water confined in Nafion nano-composite membranes based on SWy pristine clay, SWy/organo-modified clays and filler-free Nafion for comparison, from 20 °C up to 130 °C. In the graph are also plotted the data collected at 130 °C after several hours.

TGA measurements, discussed previously, have provide an evidence for the homogeneous dispersion of the organo-modified silicate platelets in the polymer, therefore, although

Table 2. Maximum Water Uptake of Filler-Free Nafion and SWy-Composites

membrane	maximum water uptake (wt %)
Nafion–SWy/SULF	50
Nafion–SWy/TES	48
Nafion–SWy/SER	35
Nafion–SWy	45
Nafion	24

a certain amount of nanofiller is deposited on the substrate (depending on the type of organoclay), the rest is evenly distributed and this will allow a vast improvement of the nanocomposite's performance compared to the filler-free Nafion.

3.3. NMR Study on SWy–Organoclays Nanocomposites.

NMR self-diffusion coefficients of water confined in organo-montmorillonite composite membranes are showed in Figure 5; diffusion data of filler-free Nafion are also reported for comparison. The measurements were collected in the temperature range 20–130 °C on membranes completely swelled in pure water up to reach their maximum uptake values (these values are reported in the Table 2 for each membrane).

SWy-2 montmorillonite and its organoclays demonstrate a considerable effect on the Nafion polymer in terms both of water absorption/retention and water mobility. It is well-known, and it is corroborated also from the Figure 5, that filler-free Nafion membrane starts to lose water at about 80 °C so, at temperatures above 100 °C the conductivity go down to values no longer useful to permit the ordinary working of the cell. The presence of the clay nanofiller, both with and without surface modification, produces a noteworthy improving of the membranes performances. In fact, if we observe the water diffusion coefficients of Nafion–SWy/TES and Nafion–SWy/SULF, they increase quasi linearly up to 100 °C reaching values more than 1 order of magnitude higher than filler-free Nafion. At 130 °C is clear a slight decreasing of the diffusivity caused from the water evaporation from the membranes. However, it is extremely significant the behavior of such nanocomposites in this temperature's region since the self-diffusion coefficients remain constants for several hours at quite high values.

The reduction of the diffusivity after 100 °C, despite the increase of the temperature, can be explained by considering that the hydrophilic pores of Nafion polymer and the acid nature of the organoclay particles provide numerous proton exchange sites in the polymeric system. Therefore, the water self-diffusion coefficient measured is a weighted average from the different water species coexisting (bounded or hydrated water and bulk water^{45,46}) in fast exchange rate with respect to the NMR times (see Figure S1 in the Supporting Information regarding the diffusion decay lines). In heating, it is reasonable to expect that the evaporation essentially affects the bulk/"free" water, i.e., the most mobile water so, after 100 °C, the biggest contribution to the diffusion comes from the hydrated water resulting in a lower *D*.

In any case, stating that in these measurements there is no additional humidification of the membranes, it denotes that this clay material can retain water and thus can maintain a certain level of humidity in the membrane and surface modifications with acid organic molecules significantly improve the performance of the final composite system.

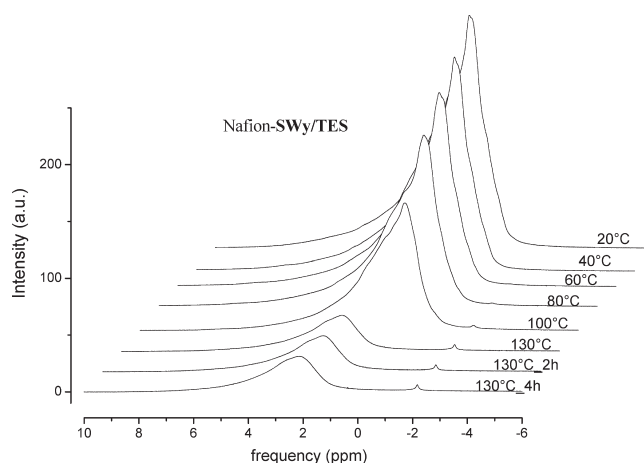


Figure 6. Temperature evolution of high-resolution ¹H NMR spectra of the water confined in Nafion–SWy/TES nanocomposite acquired from 20 °C up to 130 °C (at this last temperature also after 2 and 4 h).

In order to investigate on the water distribution in the membranes (hydration and bulk waters) as well as on the evaporation dynamics, we show the ¹H NMR spectra acquired on Nafion–SWy/TES from 20 °C up to 130 °C (Figure 6). In the graph are also reported the spectra acquired at 130 °C after 2 and 4 h, respectively. Spectra were referenced against pure water set at 0 ppm and were acquired with the same number of scans to compare their intensities. As can be seen, the proton's signal is quite large (fwhm is about 1 kHz) and asymmetric, typical of a multiple components configuration, i.e., different "types" of water coexist in the system. Actually, a certain amount of water is involved in the primary hydration "shells" of the SO₃[−] groups of Nafion^{47,48} as well as of the organo-modified filler's hydrophilic groups (oxygen and hydroxyl surface groups of clay and hydroxyl, amino and sulfonic groups of TES). The uptake of additional water fills the volumes of membrane's pores forming higher order hydration layers and, experiencing negligible electrostatic interactions, behaves more bulk-like. The different states of water within the hydrophilic pores can be difficult to discern because of the fast rate of proton exchange in acidic water and for this reason we "see" only one peak. The intensity of this peak decreases with increasing temperature because of the water evaporation from the membrane, with a pronounced drop above 100 °C; when it reaches 130 °C, the intensity of the residual signal remains constant for several hours (obviously without any supplying humidity), and this is responsible for the proton diffusion that we are able to detect at these high temperatures.

In all the spectra, until 100 °C, this asymmetrical signal (Figure 7A) can be fitted well to the experimental data with three Lorentzian peaks, one narrower (*peak-1*), attributed to the bulk-like water, and two broader (*peak-2* and *peak-3*), assigned to the bound water, i.e. the hydration water to the sulfonic acid groups of both the Nafion and TES molecules, and to the clay's hydrophilic groups, respectively. This peak-picking is argued from the broadness and area of the peaks: at room temperature, the amount of bulk water in completely swelled membranes is surely predominant and having less restricted molecular motions, results in a line width reduction. Furthermore, it is obvious that the water evaporation involves mainly the bulk water, in fact, at 130 °C, its contribution to the NMR signal (*peak-1*) disappear while the two broader components are still observed by peak-fitting.

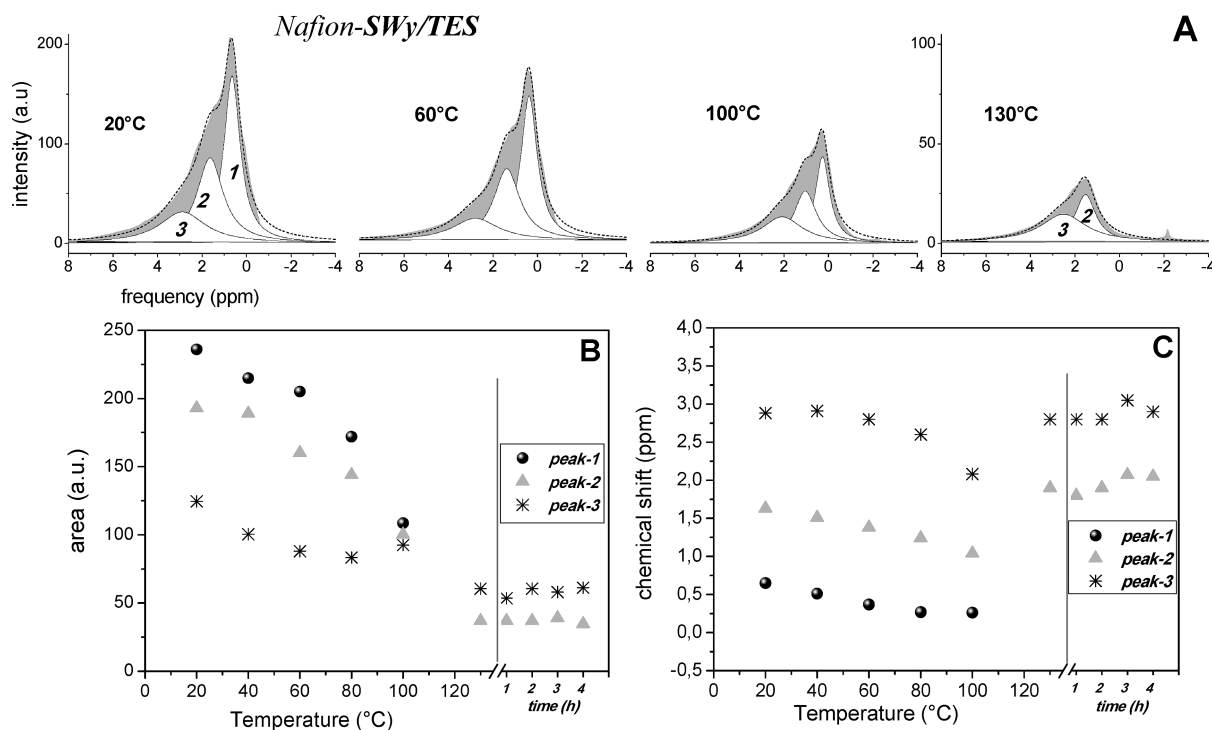


Figure 7. (A) Peak-fitting of the ^1H NMR spectra of the water confined in Nafion–SWy/TES nanocomposite; (B) plot of the areas of three peaks (resultants from the peak-fitting) vs temperature; (C) chemical shift of the three peaks (resultants from the peak-fitting) vs temperature.

By considering the area of these three peaks we estimate that the amount of water lost from the membrane at 100 °C is about 46 wt % of the total water initially absorbed. From this amount, 23 wt % arises from *peak-1*, 17 wt % from the *peak-2* and about 6 wt % from the *peak-3*. At 130 °C only about 18 wt % of water remains in the membrane, shared between the hydration to the SO_3^- groups of the polymer and the hydrophilic clay surfaces (*peak-2* and *peak-3*), while the bulk water is completely evaporated. The variation of the areas of these three peaks as a function of temperature is showed in Figure 7B. Up to 100 °C, the area of all signals decreases even if the *peaks 1* and *2* show a greater reduction than *peak-3* (which remains almost unchanged), while at 130 °C the proton spectrum is fitted by only two peaks (*2* and *3*) and their area remains constant for several hours. It is also interesting to show the trend of the chemical shift of the spectral signal, and hence of the three peaks fitting, with the temperature (Figure 7C). The reported chemical shift values were referenced to the distilled water shifts at the same temperature as the membrane. By comparing with the area's plot, a certain correspondence is noticeable: there is a downfield shift of the resonance during the heating and an abrupt change after 100 °C. This is obviously caused by the strong evaporation of water from the membrane, which in turn causes a structural change of the system (hydrophilic pores size and redistribution of water), but most likely there is also an effect due to the glass transition of the polymer (the T_g of Nafion-112 membrane is around 110 °C). However, at 130 °C the chemical shift of the signal remains invariable for several hours, indicative of the fact that no important altering, e.g., ulterior water leaking, is happening in the system.

At this point, we groped to make a quantitative analysis starting from these spectral data to estimate the number of water molecules involved in the hydration shell of the sulfonic acid

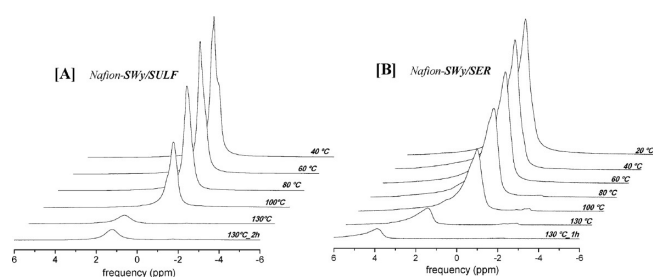
groups of Nafion polymer as well as that absorbed on the organoclay nanoparticles. Taking into account the complexity of the system and to the hydrogen-bonding effects which the protons are subjected, establish the exact chemical shifts is arduous, however, by considering the concepts of electronegativity (of oxygen and sulfur atoms) and proton acidity, the resonance frequency of the protons (of the water) on the clay's surface is expected downfield shift respect to protons hydrating the sulfonic groups. Therefore, we can most likely attribute *peak-2* to the water molecules hydrating the SO_3^- groups ($h_{\text{SO}_3^-}$) and the *peak-3* to the water molecules absorbed on the organo-modified clay particles (h_{clay}). The moles of SO_3^- groups present in the Nafion/Swy-*TES* system originate almost entirely from Nafion and only for a negligible amount from *TES* molecules used to functionalize the montmorillonite clay. Even with an overestimation, i.e. by considering that the stoichiometric amount of *TES* (which corresponds to three times the CEC of the clay) is all intercalated in the clay, and by considering the filler to polymer loading (3 wt %), this quantity is about 6% of the total moles:

$$\begin{aligned} \text{mmol of } \text{SO}_3^- &= (0.2 \text{ from Nafion}) + (0.012 \text{ from TES}_{(3\text{wt}\%;3\text{CEC})}) \\ &= 0.212 \end{aligned}$$

Table 3 reports a schematic description of the water distribution in the system taking into account the initial water uptake of the membrane (5.5 mmol of absorbed water) and the areas ratio of the NMR peaks at 20 °C and then at 130 °C. The hydration numbers obtained by this calculation, about 9 $\text{H}_2\text{O}/\text{SO}_3^-$ mol/mol in the maximum hydration state and 1.8 $\text{H}_2\text{O}/\text{SO}_3^-$ mol/mol in the very low hydration state, are in agreement with the literature;^{49,50} therefore, the peak fitting and the related attributions are appropriate.

Table 3. Water Distribution and Hydration Numbers in the Nafion–SWy/TES Nanocomposite System

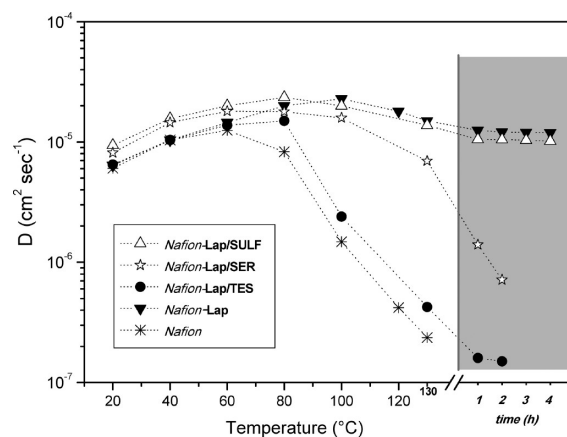
20 °C
water uptake 48 wt % → 5.5 mmol
from the areas ratio of the peaks 1, 2 and 3:
bulk 42.6 wt % → 2.34 mmol
h_{clay} 22.5 wt % → 1.2 mmol
$h_{\text{SO}_3^-}$ 34.8 wt % → 1.9 mmol ⇒ $(1.9/0.212) \cong 9\text{H}_2\text{O}/\text{SO}_3^-$ mol/mol
130 °C
~18 wt % of the initial water uptake remain in the membrane
from the areas ratio of the peaks 2 and 3:
$h_{\text{clay}} \sim 11$ wt % → 0.6 mmol
$h_{\text{SO}_3^-} \sim 7$ wt % → 0.38 mmol ⇒ $(0.38/0.212) \cong 1.8\text{H}_2\text{O}/\text{SO}_3^-$ mol/mol

**Figure 8.** Temperature evolution of high-resolution ^1H NMR spectra of the water confined in (A) Nafion–SWy/SULF and (B) Nafion–SWy/SER nanocomposite membranes, acquired from 20 °C up to 130 °C (at this last temperature also after 2 and 4 h).

Temperature evolution of the spectra of water confined in Nafion–SWy/SER and Nafion–SWy/SULF membranes are shown in Figure 8. Once again it is visible at high temperatures, above 100 °C, the residual signal of the protons of the hydrating water the hydrophilic groups which, thanks to an appreciable mobility, can ensure the ionic transport in the membrane through, for example, the *Grotthus* mechanism, where proton mobility in water is connected to rotation of water molecules within a constantly changing network of hydrogen bonds (*structural diffusion*).^{51,52}

Nafion–SWy/SULF presents the higher water uptake together with the higher self-diffusion coefficients. This excellent performance may be due, among other things, to: (i) the formation of a double-layer arrangement of the SULF molecules in the interlayer space (by XRD spectra) allowing to have a greater number of hydrophilic sites inside the polymeric system and (ii) this SWy-organofiller showed the highest capacity to absorb water (see TGA results).

The same data analysis procedure used for the spectra of Nafion–SWy/TES, gave approximately similar results in terms of hydration water to the sulfonic groups even if, in the case of SWy/SER nanocomposite we find an inferior hydration number than SWy/SULF certainly imputable to the higher water loss at 130 °C. This outcome is reflected on the diffusion and in general on the performance of the electrolyte membrane as saw in Figure 5. In fact, the rapid drop of the diffusion is hypothesized to be related to a blocking effect (the particles can obstruct the hydrophilic polymer channels) that becomes a significant factor when the water content in the membrane is very low, i.e., when the hydrophilic domains sizes are reduced.

**Figure 9.** Self-diffusion coefficients of water confined in Nafion nanocomposite membranes based on Lap pristine clay, Lap/organo-modified clays, and filler-free Nafion for comparison, from 20 °C up to 130 °C. In the graph are also plotted the data collected at 130 °C after several hours.

3.4. NMR study on Laponite–Organoclays Nanocomposites. Concerning the organo-Laponite-based nanocomposites, the diffusion coefficients of the water confined in the various membranes are reported in Figure 9. The water uptake of all these membranes is about 30 wt % and, therefore, definitely lower than the organo-montmorillonite based membranes even if, as we reported in the TGA measurements, the water absorption of the Laponite organoclays is higher than the montmorillonites. In our view, the exfoliation that the clay platelets undergo when dispersed in the polymer matrix not only modifies their characteristic properties, but also induces an alteration on the polymeric structure. This result strengthens the idea that the structure of the composite plays a key role in the membrane performance and that the enhanced absorption is not merely a consequence of the fact that the filler's nanoparticles are more or less hygroscopic, but is also attributable to their effect on the porous structure of the polymer. However, even with a relatively low water content, the membrane prepared with pristine Laponite clay without any modification shows a good diffusion behavior in all the temperature range and it is able to preserve an excellent performance at 130 °C for several hours without any further humidification. The introduction of SULF molecules in the clay's interlayers does not improve at all the performance of the composite that, in fact, follows exactly the trend of the first one. The result is even worse when Laponite clay is organo-modified with TES and SER molecules: Nafion–Lap/SER has a collapse of the diffusion around to 130 °C, while Nafion–Lap/TES already at lower temperatures begins to show a loss of the water diffusion. Above 100 °C, practically, this reaches values comparable to those of the Nafion, although maintains a minimum water content on which we can still measure the diffusion after 2 h that it was at 130 °C. This behavior could be explained taking into account that the cationic exchange capacity (CEC) of Laponite is lower respect to SWy, therefore, the amount of organic molecules attached to the Laponite's surface is considerably lower than the correspondent organo-montmorillonites. For example the small amount of intercalated TES molecules in Laponite does not alter the hydrophilicity of the final organoclay as results from TG data: the adsorbed water which is 11 wt % in the pristine Laponite is reduced to 7.7 wt % in the case of Lap/TES. This reduction in the hydrophilicity of the nanofiller is probably

responsible for bad performance of the organo-Laponite Nafion membranes.

4. CONCLUSIONS

Nafion hybrid membranes based on organo-modified smectite clays were synthesized by solution intercalation and characterized by different techniques. One synthetic (Laponite) and one natural (montmorillonite) layered aluminosilicate minerals with different physical and structural properties were modified with various organic acid molecules in order to increase the concentration of hydrophilic functional groups and the compatibility with the polymeric matrix. XRD results show that fully exfoliated nanocomposites were created, where the individual organoclay layers are uniformly dispersed in the continuous polymeric matrix.

SEM analysis showed two main morphologies of the nanocomposites depending on the clay-filler used: one more smooth, compact and uniform even if there is a small deposit of filler on the substrate, the other with more wrinkled and spongy texture with a well evident weaving; however, in both case no aggregates or agglomerates are visible inside the polymeric matrix. The nanocomposite membranes with the second type of morphology showed both better diffusion performance and water retention at high temperatures.

The dynamic behavior of water confined in the nanocomposite membranes, in a wide temperature range (20–130 °C), was studied by NMR (self-diffusion and ^1H spectra). It was pointed out the noteworthy improving of the water retention and mobility when the organo-montmorillonites are used as fillers in the Nafion polymer. This result derives from a synergy between the hydrophilicity of the organoclays and the capacity to induce an alteration on the polymeric structure. But, the most important feature is the behavior above 100 °C: these nanocomposites can retain a small amount of "still mobile" water for several hours without any further humidification, which suggests that a significant proton conductivity can be ensured by electrolytic membranes in high temperatures condition.

Organo-Laponite fillers do not improve the electrolyte performance respect to the pristine clay without any organo-modification, this is probably due to very low amount of organic molecules able to be intercalated in this clay.

Finally, an accurate analysis of the ^1H NMR spectra put in evidence the different "types" of water coexisting in a composite membrane: water filling the pore volumes which behaves more bulklike, hydration water to the sulfonic acid groups of the polymer and the water absorbed on the organoclay nanoparticles. The hydration numbers obtained from these spectral data are about $9 \text{H}_2\text{O}/\text{SO}_3^-$ mol/mol in the maximum hydration state and $1.8 \text{H}_2\text{O}/\text{SO}_3^-$ mol/mol in the very low hydration state.

■ ASSOCIATED CONTENT

Supporting Information. Decay lines of $-\ln[A(g)/A(0)]$ vs g^2 which are used to calculate the self-diffusion coefficients (D), for all the temperature range explored and for the most representative membranes studied (Figure S1) and representative examples of deconvolution of the XRD diffractograms at $2\theta = 10\text{--}24^\circ$ of Nafion membranes (Figure S2). This material is available free of charge via the Internet at <http://pubs.acs.org>.

■ AUTHOR INFORMATION

Corresponding Author

*Telephone: +39 0984 492021. Fax: +39 0984 492044. E-mail: isabella.nicotera@unical.it.

■ REFERENCES

- (1) Adjemian, K. T.; Srinivasan, S.; Benziger, J.; Bocarsly, A. B. *J. Power Sources* **2002**, *109*, 356.
- (2) Aricò, A. S.; Creti, P.; Antonucci, P. L.; Antonucci, V. *Electrochem. Solid-State Lett.* **1998**, *1*, 66.
- (3) Adjemian, K. T.; Lee, S. J.; Srinivasan, S.; Benziger, J.; Bocarsly, A. B. *J. Electrochem. Soc.* **2002**, *149*, A256.
- (4) Yang, C.; Costamagna, P.; Srinivasan, S.; Benziger, J.; Bocarsly, A. B. *Power Sources* **2001**, *103* (1), 1.
- (5) Alberti, G.; Casciola, M. *Annu. Rev. Mater. Res.* **2003**, *33*, 129.
- (6) Arico, A. S.; Baglio, V.; Antonucci, V.; Nicotera, I.; Oliviero, C.; Coppola, L.; Antonucci, P. L. *J. Membr. Sci.* **2006**, *270*, 221.
- (7) Saccà, A.; Carbone, A.; Passalacqua, E.; D'Epifanio, A.; Licocchia, S.; Traversa, E.; Sala, E.; Traini, F.; Ornelas, R. *Power Sources* **2005**, *152*, 16.
- (8) Baglio, V.; Aricò, A. S.; Antonucci, V.; Nicotera, I.; Oliviero, C.; Coppola, L.; Antonucci, P. L. *J. Power Sources* **2006**, *163*, 52.
- (9) Navarra, M. A.; Abbati, C.; Scrosati, B. *J. Power Sources* **2008**, *183*, 109.
- (10) Nicotera, I.; Zhang, T.; Bocarsly, A.; Greenbaum, S. *J. Electrochem. Soc.* **2007**, *154*, B466.
- (11) Antonucci, V.; Di Blasi, A.; Baglio, V.; Ornelas, R.; Matteucci, F.; Ledesma-García, J. *Electrochim. Acta* **2008**, *53* (24), 7350.
- (12) Alberti, G.; Casciola, M.; Massinelli, L.; Bauer, B. *Membr. Sci.* **2001**, *185* (1), 73.
- (13) Kongkachuichay, P.; Pimprom, S. *Chem. Eng. Res. Des.* **2010**, *88*, 496.
- (14) Yano, K.; Usuki, A.; Okada, A.; Kurauchi, T. *J. Polym. Sci., Part A: Polym. Chem. Rev.* **1993**, *31*, 2493.
- (15) Giannelis, E. P. *Adv. Mater.* **1996**, *8*, 29.
- (16) Paul, D. R.; Lim, R. *Polymer* **2008**, *49*, 3187.
- (17) Chang, J.-H.; Park, J. H.; Park, G.-G.; Kim, C.-S.; O.-O., P. *J. Power Sources* **2003**, *124*, 18.
- (18) Alonso, R. H.; Estevez, L.; Lian, H. Q.; Kelarakis, A.; Giannelis, E. P. *Polymer* **2009**, *50*, 2402.
- (19) Wang, J.; Merino, J.; Aranda, P.; Galvan, J.-C.; E., H.-R. *J. Mater. Chem.* **1998**, *9*, 161.
- (20) Bébin, P.; Caravanier, M.; H., G. *J. Membr. Sci.* **2006**, *278*, 35.
- (21) Mbouguen, J. K.; Ngameni, E.; Walcarius, A. *Anal. Chim. Acta* **2006**, *578*, 145.
- (22) Tziaila, A. A.; Kalogeris, E.; Enotiadis, A.; Taha, A. A.; Gournis, D.; Stamatis, H. *Mater. Sci. Eng. B-Adv. Funct. Solid-State Mater.* **2009**, *165*, 173.
- (23) Tziaila, A. A.; Pavlidis, I. V.; Felicissimo, M. P.; Rudolf, P.; Gournis, D.; Stamatis, H. *Bioresour. Technol.* **2010**, *101*, 1587.
- (24) Stathi, P.; Litina, K.; Gournis, D.; Giannopoulos, T. S.; Deligiannakis, Y. *J. Colloid Interface Sci.* **2007**, *316*, 298.
- (25) Pinnavaia, T. J.; Beall, G. W. *Polymer-clay nanocomposites*; J. Wiley & Sons: New York, 2001.
- (26) Giannelis, E. P. *Adv. Mater.* **1996**, *8*, 29.
- (27) LeBaron, P. C.; Wang, Z.; Pinnavaia, T. J. *Appl. Clay Sci.* **1999**, *15*, 11.
- (28) Zawodzinski, T. A. J.; Neeman, M.; Sillerud, L. O.; Gottesfeld, S. *J. Phys. Chem. A* **1991**, *95*, 6040.
- (29) Fontanella, J. J.; McLin, M. G.; Wintersgill, M. C.; Greenbaum, S. G. *Solid State Ionics* **1993**, *66*, 1.
- (30) Nicotera, I.; Coppola, L.; Rossi, C. O.; Youssry, M.; Ranieri, G. A. *J. Phys. Chem. B* **2009**, *113*, 13935.
- (31) Jayakody, J. R. P.; Stallworth, P. E.; Mananga, E. S.; Zapata, J. F.; Greenbaum, S. G. *J. Phys. Chem. B* **2004**, *108*, 4260.
- (32) Stejskal, E. O.; Tanner, J. E. *J. Chem. Phys.* **1965**, *42*, 288.

- (33) Gournis, D.; Mantaka, A. M.; Karakassides, M. A.; Petridis, D. *Phys. Chem. of Miner.* **2001**, *28*, 285.
- (34) Gournis, D.; Jankovič, L.; Maccallini, E.; Benne, D.; Rudolf, P.; Colomer, J.-F.; Sooambar, C.; Georgakilas, V.; Prato, M.; Fanti, M.; Zerbetto, F.; Sarova, G. H.; Guldi, D. M. *J. Am. Chem. Soc.* **2006**, *128*, 6154.
- (35) Gournis, D.; Lappas, A.; Karakassides, M. A.; Tobbens, D.; Moukarika, A. *Phys. Chem. Miner.* **2008**, *35*, 49.
- (36) MacMillan, B.; Sharp, A. R.; Armstrong, R. L. *Polymer* **1999**, *40*, 2471.
- (37) Theng, B. K. G. *The Chemistry of Clay Organic Reactions*; Adam Hilger: London, 1974.
- (38) de Paiva, L. B.; Morales, A. R.; Diaz, F. R. V. *Appl. Clay Sci.* **2008**, *42*, 8.
- (39) Vaia, R. A.; Teukolsky, R. K.; Giannelis, E. P. *Chem. Mater.* **1994**, *6*, 1017.
- (40) Gournis, D.; Mantaka-Marketou, A. E.; Karakassides, M. A.; Petridis, D. *Phys. Chem. Miner.* **2000**, *27*, 514.
- (41) Mauritz, K. A.; Moore, R. B. *Chem. Rev.* **2004**, *104*, 4535–4585.
- (42) Jung, D. H.; Cho, S. Y.; Peck, D. H.; Shin, D. R.; Kim, J. S. *J. Power Sources* **2003**, *118*, 205.
- (43) Kaviratna, P. D.; Pinnavaia, T. J.; Schroeder, P. A. *J. Phys. Chem. Solids* **1996**, *57*, 1897.
- (44) Goslawit, R.; Chirachanchai, S.; Shishatskiy, S.; Nunes, S. P. *Solid State Ionics* **2007**, *178*, 1627.
- (45) Gebel, G.; Atkins, P. *Polymer* **2000**, *41*, 5829.
- (46) Paddison, S. J.; Paul, R. *Phys. Chem. Chem. Phys.* **2002**, *4*, 1158.
- (47) Salles, F.; Douillard, J. M.; Denoyel, R.; Bildstein, O.; Jullien, M.; Beurroies, I.; Van Damme, H. *J. Colloid Interface Sci.* **2009**, *333*, 510.
- (48) Gompper, G.; Hauser, M.; Kornyshev, A. A. *J. Chem. Phys.* **1994**, *101*, 3378.
- (49) Mauritz, K. A.; Moore, R. B. *Chem. Rev.* **2004**, *104*, 4535.
- (50) Falk, M. *Can. J. Chem.* **1980**, *58*, 1495.
- (51) Cohen, B.; Huppert, D. *J. Phys. Chem. A* **2003**, *107*, 3598.
- (52) Saito, M.; Hayamizu, K.; Okada, T. *J. Phys. Chem. B* **2005**, *109*, 3112.

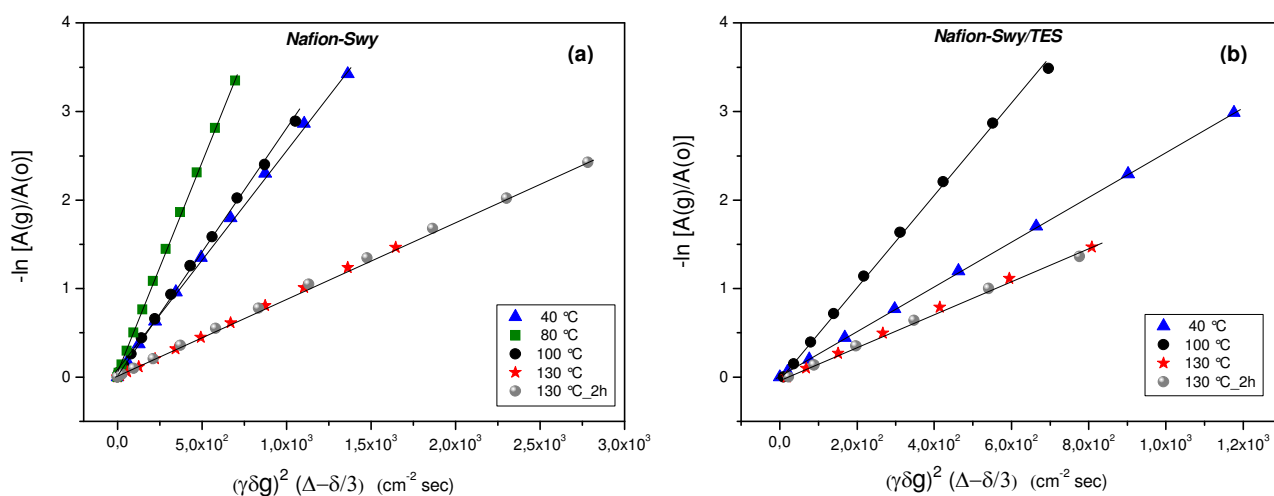
SUPPORTING INFORMATION

As described in the experimental section, the NMR pulsed field gradient spin-echo (PFG-SE) method was used to measure the water self-diffusion coefficients in the Nafion and composites membranes. The attenuation of the echo amplitude in this sequence is represented by the Stejskal-Tanner equation:

$$-\ln \frac{A(g)}{A(0)} = (\gamma g \delta)^2 D (\Delta - \delta/3)$$

Figure S1 shows the decay lines of $-\ln[A(g)/A(0)]$ vs. g^2 (the other parameters are constants) which are used to calculate the self-diffusion coefficients (D), for all the temperature range explored and for the most representative membranes studied.

We can observe that the decay lines are straight for all the systems and, mainly, for all the investigated temperatures. This feature is very important in order to use the above equation to calculate D, and to confirm the Gaussian self-diffusion behaviour of the water confined in the hydrophilic pores of the membranes. Furthermore, it supports the consequence that in such complex systems, with a multiple-component water configuration, we measure only one diffusion value which is a weighted average from the different water species in fast rate of proton exchange.



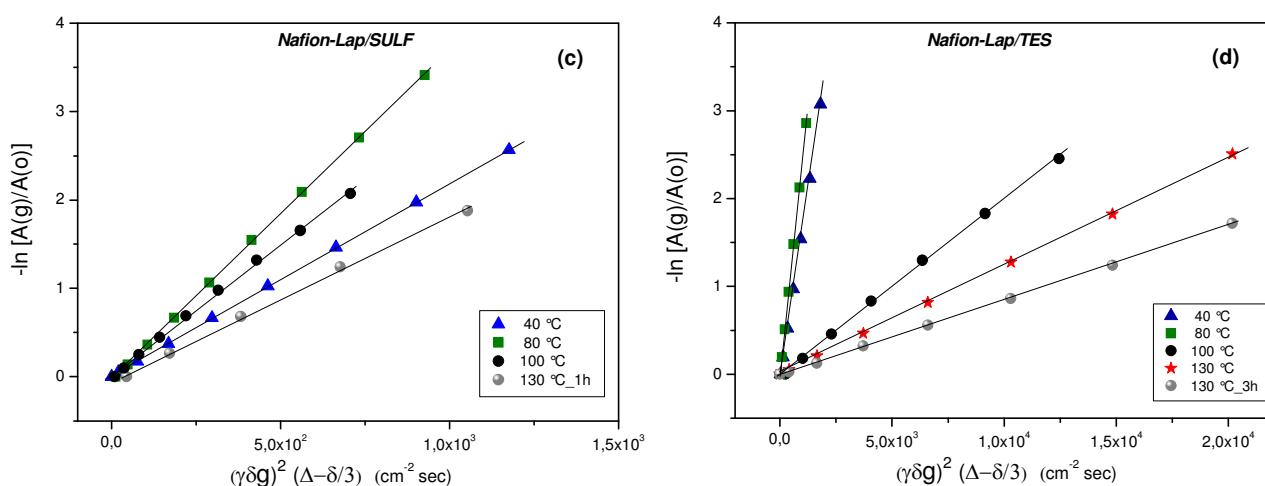


Figure S1. Decay lines of $-\ln[A(g)/A(0)]$ vs. $(\gamma\delta g)^2(\Delta-\delta/3)$ for various temperatures of four Nafion composite membranes: a) Nafion-Swy, b) Nafion-Swy/TES, c) Nafion-Lap/Sulf and d) Nafion-Lap-TES.

Figure S2 shows a representative examples of deconvolution of the XRD diffractograms at $2\Theta = 10-24^\circ$ of Nafion membranes. Fit curves of experimental data are deconvoluted into an amorphous (16°) and crystalline (17.5°) scattering peaks.

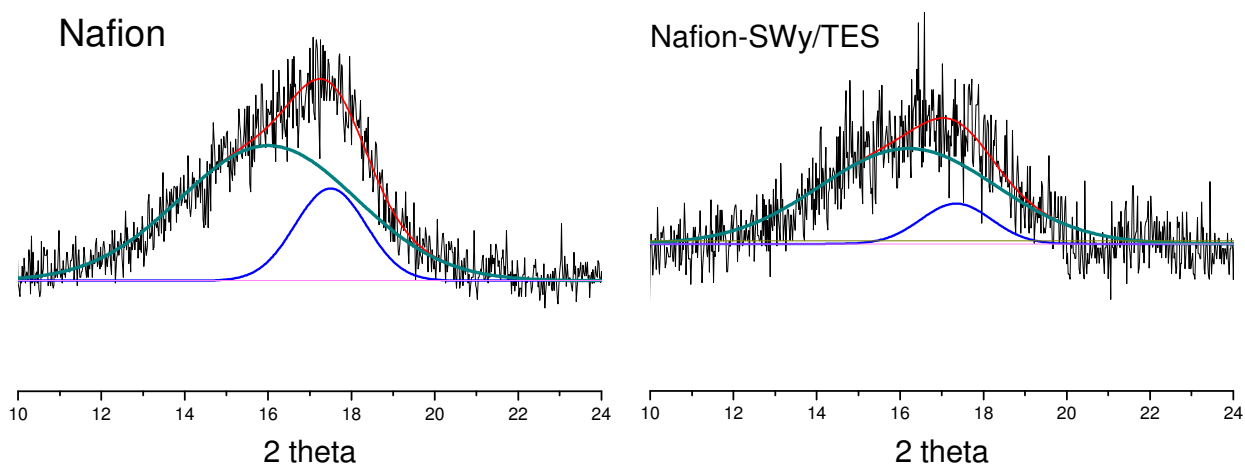


Figure S2. X-ray diffraction patterns of recast Nafion (A) and composite membrane Nafion-SWy/TES (B).

<i>Fitting results</i>		<i>Position</i>	<i>Width</i>	<i>Area</i>	
Nafion	1 st Peak	17.50012	2.02801	35.5565	(21.4687%)
	2 nd Peak	16.00320	4.99467	130.064	(78.5313%)
Nafion-SWy/TES	1 st Peak	17.3458	2.00027	29.1648	(14.4862%)
	2 nd Peak	16.1948	4.99001	172.163	(85.5138%)

Graphene-Based Nafion Nanocomposite Membranes: Enhanced Proton Transport and Water Retention by Novel Organo-functionalized Graphene Oxide Nanosheets

Apostolos Enotiadis, Kristina Angjeli, Noemi Baldino, Isabella Nicotera, and Dimitrios Gournis**

Novel nanostructured organo-modified layered materials based on graphene oxide carrying various hydrophilic functional groups ($-NH_2$, $-OH$, $-SO_3H$) are prepared and tested as nanofillers for the creation of innovative graphene-based Nafion nanocomposites. The hybrid membranes are characterized by a combination of analytical techniques, which show that highly homogeneous exfoliated nanocomposites are created. The pulsed field gradient NMR technique is used to measure the water self-diffusion coefficients. Remarkable behavior at temperatures up to 140 °C is observed for some composite membranes, thereby verifying the exceptional water retention property of these materials. Dynamic mechanical analysis shows that hybrid membranes are much stiffer and can withstand higher temperatures than pure Nafion.

1. Introduction

It is well known that carbon materials such as amorphous carbon, nanotubes, fibers, and graphite can be used as sorbents/sieves, catalytic substrates, and nanofillers due to their low mass in combination with very high ($2500 \text{ m}^2 \text{ g}^{-1}$) and easily modified (chemically) surface area, thermal stability,

and mechanical properties.^[1] On the other hand, the main attention in polymer research over the last two decades has been focused on the development of novel composites to enhance several properties of neat polymeric matrices using molecular or nanoscale reinforcement.^[2] Homogeneous dispersion of the nanoadditives and utilization of their high available surface area (per unit mass) for interaction with the polymer are key objectives for the preparation of polymer nanocomposites with improved mechanical, thermal, electrical, and barrier properties. Inorganic layered structures, such as nanoclays,^[3] layered double hydroxides,^[4] carbon-based nanofillers (e.g., carbon nanotubes),^[5] and hybrid fillers such as carbon nanotubes rooted on smectite clays,^[6] have been successfully applied to numerous potential applications in the automotive, aerospace, construction, and electronic industries.^[7] In this regard, the development of a nanodispersion of graphene-based materials in a polymer matrix has opened a new and interesting area in materials science in recent years.^[7,8] The pristine graphite is inaccessible in the interlayer space and has a tendency to agglomerate in a polymer matrix,^[9] thus reducing the use of this material. To avoid this problem, the functionalization of graphite by chemical oxidation, thereby creating a hydrophilic graphite

Dr. A. Enotiadis, Prof. D. Gournis
Department of Material Science and Engineering
University of Ioannina
45110 Ioannina, Greece
E-mail: dgourni@cc.uoi.gr

K. Angjeli, Dr. I. Nicotera
Department of Chemistry
University of Calabria
87036 Rende, Cosenza, Italy
E-mail: isabella.nicotera@unical.it

Dr. N. Baldino
Department of Engineering Modeling
University of Calabria
87036 Rende, Cosenza, Italy

DOI: 10.1002/sml.201200609



derivative with covalently attached oxygen-containing groups (hydroxy, epoxy, and carboxy) on its layers, called graphite or graphene oxide (GO),^[10] is a particularly attractive solution since it can improve the solubility and processability as well as enhance the interactions with organic and inorganic guest molecules. GO and reduced GO have been used so far as nanoadditives in various polymers, such as epoxy resins, poly(methyl methacrylate), polypropylene, polyethylene, polystyrene, and polyamides, and also in conductive polymers like polyaniline, poly(styrenesulfonate), Nafion etc., thereby increasing the mechanical, electrical, and barrier properties.^[7,8,11–13]

Nafion (a registered trademark of E. I. du Pont de Nemours and Co.) is a perfluorosulfonic polymer that shows significant properties, such as high ionic conductivity, ion-exchange capacity, and stable structure, thus making possible its use in numerous applications (fuel cells, electrochemical devices, sensors etc.). Nafion is a common electrolyte that has been most extensively studied in proton exchange membrane fuel cells (PEMFCs) for both vehicle applications and local on-site power generation systems in the future. The most significant barrier of polymer electrolytes at elevated temperatures is the proton conductivity of the membrane, which depends critically on the presence of water. In fact, PEMFCs operating in the typical 60–80 °C temperature range face problems including poor carbon monoxide (from reformed hydrogen or methanol as fuels) tolerance and heat rejection. These drawbacks can be overcome by increasing the operation temperature range up to 120–130 °C, but this leads to an unacceptable decrease in the proton conductivity of the electrolyte due to water loss. To enhance the water retention property, hydrophilic nanofillers, such as titania,^[14] zirconia,^[14,15] silica,^[16] alumina,^[16] clays (organo-modified or not),^[17] zeolites,^[18] and carbon nanotubes,^[19] have been successfully applied for the creation of Nafion nanocomposite membranes. At the same time, GO does not exhibit any significant ionic or electronic conductivity^[11a] but can be easily converted in a high proton conductor via the intercalation of organic molecules in the interlayer space of GO, thereby creating novel hybrid organo nanofillers with high proton conductivity. This can be implemented by taking advantage of the concept of intercalation chemistry, which involves the insertion of suitable robust organic and/or inorganic species between the layers. Towards this aim, the attachment of organic molecules on the GO surfaces containing hydrophilic groups such as $-\text{SO}_3\text{H}$, $-\text{COOH}$, and $-\text{OH}$ is expected to improve not only the proton conductivity of the resulting nanocomposite membranes—by increasing the concentration of acidic (hydrophilic) functional groups of GO—but also their mechanical, chemical, and thermal strength while increasing the compatibility with the polymeric membrane. Recently, by synthesizing sulfonated GOs through a microwave-assisted sulfonation method (introduction of sulfonic acid groups directly on GO layers) and incorporation into a Nafion matrix, Choi et al.^[20] showed that these 2D

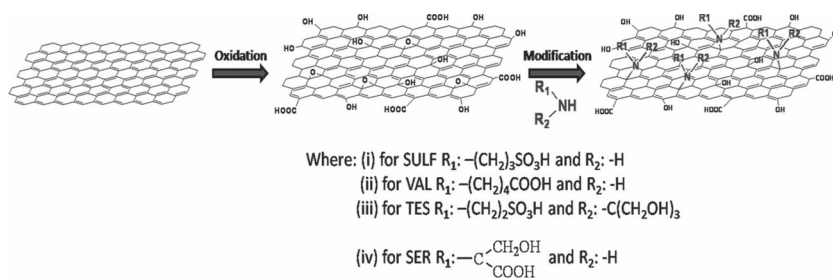
nanofillers controlled the state of water confined in nanoscale ionic channels of Nafion. As a result, nanocomposite membranes showed high proton conductivity and low methanol permeability at high temperature.

Based on the above, in this work a series of novel nanostructured organo-modified layered materials based on GO were prepared and tested as nanofillers for the creation of novel hybrid Nafion nanocomposites. Four aliphatic amine derivatives containing various functional groups, such as sulfonic, carboxy, and hydroxy groups, were covalently bonded via the amide functionality on the GO surfaces and the resulting organo-modified GO nanofillers were incorporated in Nafion by solution intercalation (membranes with pristine GO were also synthesized for comparison). The nanocomposites as well as the modified nanofillers were characterized by a combination of powder X-ray diffraction (XRD), Raman and Fourier transform infrared (FTIR) spectroscopies, differential thermal analysis (DTA)/thermogravimetric analysis (TGA), and scanning electron microscopy (SEM) while the transport properties of the membranes were investigated by NMR spectroscopy. Finally, the mechanical properties of the polymeric films were tested by dynamic mechanical analysis in a wide temperature range.

2. Results and Discussion

2.1. Characterization of the Organo-Modified GO Nanofillers

Organo derivatives of GO were prepared and tested as nanofillers in Nafion polymer to increase the water retention properties, and thus the proton conductivity, of the final nanocomposite membranes, as well as to improve their mechanical, chemical, and thermal properties. Our starting material was produced by oxidizing powdered graphite to obtain exfoliated hydrophilic single-layer flakes of GO. The GO was then reacted with the corresponding acidic amine derivatives, which were covalently bonded to the GO surfaces resulting in the formation of organo-modified GO nanofillers. Interaction of primary or secondary aliphatic amines with GO takes place mainly through chemical grafting of the amine end groups to the GO surfaces via nucleophilic substitution reactions on the epoxy groups of GO.^[10,21a,b] A schematic representation of the reactions for the organo modification of GO is presented in **Scheme 1**.



Scheme 1. Schematic representation of the synthetic procedure. SULF = 3-amino-1-propanesulfonic acid, VAL = 5-aminovaleric acid, TES = 2-[[2-hydroxy-1,1-bis(hydroxymethyl)ethyl]amino]ethanesulfonic acid, SER = 2-amino-3-hydroxypropanoic acid or serine.

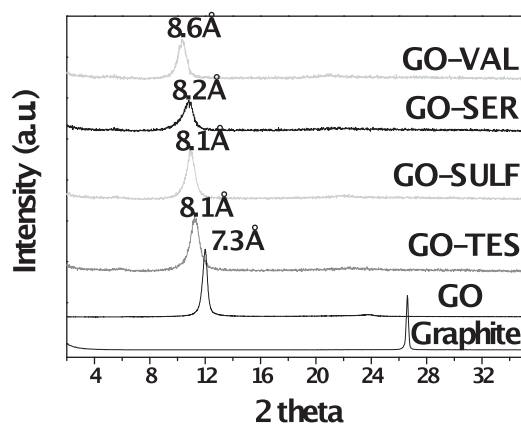


Figure 1. XRD patterns of pristine graphite, GO and organo-modified GOs.

The XRD patterns of the pristine graphite, the oxidized GO, and the final organo-modified GO using the four different amines are shown in **Figure 1**. The pattern of pure graphite exhibits a peak at 26.6° with a basal spacing $d_{002} = 3.34 \text{ \AA}$ while in the case of GO a 001 reflection peak appears at 12.0° with a basal spacing of $d_{001} = 7.3 \text{ \AA}$. Treatment of GO with the four amine derivatives increases the d_{001} spacing of GO due to the successful insertion of the guest molecules in the interlayer space of the layered material. More specifically, in the case of GO-TES, the basal spacing d_{001} , which is 7.3 \AA in the pristine GO, becomes 8.1 \AA corresponding to an intersheet separation of $\Delta = 8.1 - 6.1 = 2.0 \text{ \AA}$, where 6.1 \AA is the thickness of the GO monolayer.^[10,21c,d] This is indicative of the successful intercalation of the TES molecules into the graphene interlayers. A similar increment is observed for GO-SER ($d_{001} = 8.2 \text{ \AA}$) while in the case of the two linear primary amines (SULF and VAL) the d_{001} spacings were found to be 8.1 and 8.6 \AA for GO-SULF and GO-VAL, respectively. For these two linear amine derivatives the intersheet separation is calculated to 2.0 \AA for GO-SULF and 2.5 \AA for GO-VAL, thus indicating that the two guest molecules adopt a slightly inclined orientation between the GO surfaces. By using the following equation,^[10] $d_{001} = 6.1 + L \times \sin\theta$ (where L is the length of the linear amine molecule and θ the hydrocarbon chain inclination), which refers to an interdigitated

configuration of the organic molecules within the GO layers, for SULF and VAL with molecule lengths 6.63 and 7.20 \AA (calculated through minimization of energy using Chem3D Ultra v. 8.0.1 for XRD patterns of pristine graphite, GO, and organo-modified GOs) the chain inclination is calculated as $\theta = 18$ and 21° , respectively. On the other hand, by considering a bilayer formation of the organic molecules in the interlayer space of GO, the inclination of SULF and VAL molecules is estimated to be $\theta = 8.7$ and 10° , respectively, using a similar formula to the above ($d_{001} = 6.1 + 2 \times L \times \sin\theta$).

The FTIR spectra of the pristine materials and the organo-modified derivatives are shown in **Figure 2** (left). The pure graphite is an IR-inactive solid in all the frequency range while the GO exhibits the following characteristic IR features: a weak band at 1620 cm^{-1} assigned to the C=O stretching vibrations of the COOH groups, a strong band at 1396 cm^{-1} assigned to the O—H deformations of the C—OH groups, a strong band at 1062 cm^{-1} attributed to C—O stretching vibrations, and a weak band at 1230 cm^{-1} assigned to asymmetric stretching of C—O—C bridges in epoxy groups and/or to deformation vibrations of O—H in the carboxylic acid groups.^[10,22] The presence of all these characteristic vibrations confirms the successful oxidation of the pristine graphite. In the case of organo-GO samples, the same bands are also present while the intensity of the band at 1230 cm^{-1} decreases due to the nucleophilic substitution reactions between the amine end groups of the organic molecules and the epoxy groups of the GO, thus confirming the successful functionalization of this material. Moreover, at high frequencies (Figure 2 inset), the organo-GO derivatives exhibit two extra bands at 2927 and 2856 cm^{-1} due to asymmetric and symmetric stretching vibrations of CH_2 groups, respectively, thus revealing the presence of the amine derivatives in the solid nanofillers. Furthermore, Raman spectroscopy is a widely used tool for the characterization of carbon products. As shown in Figure 2 (right), the Raman spectrum of pristine graphite displays a prominent G band at 1580 cm^{-1} corresponding to the first-order scattering of the tangential stretching (E_{2g}) mode, while the D band at 1353 cm^{-1} is very weak and originates from disorder in the sp^2 -hybridized carbon atoms, characteristic of lattice distortions in the graphene sheets.^[23a] In the Raman spectrum of GO the G band is broadened and shifted to 1594 cm^{-1}

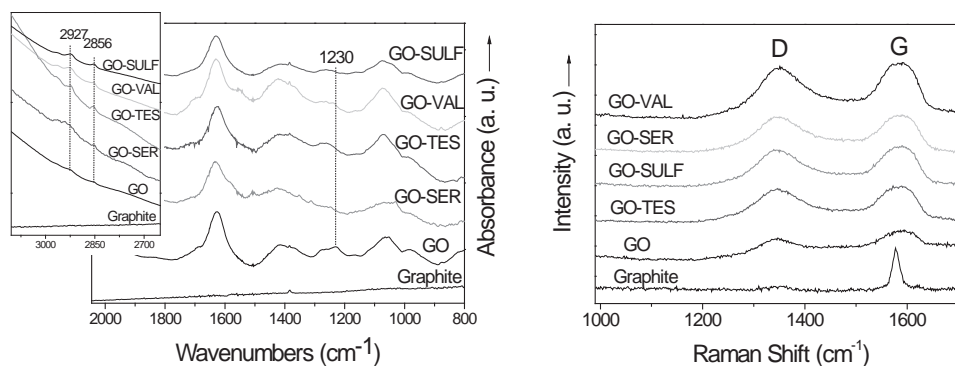


Figure 2. FTIR (left) and Raman (right) spectra of pristine graphite, GO, and organo-modified GOs.

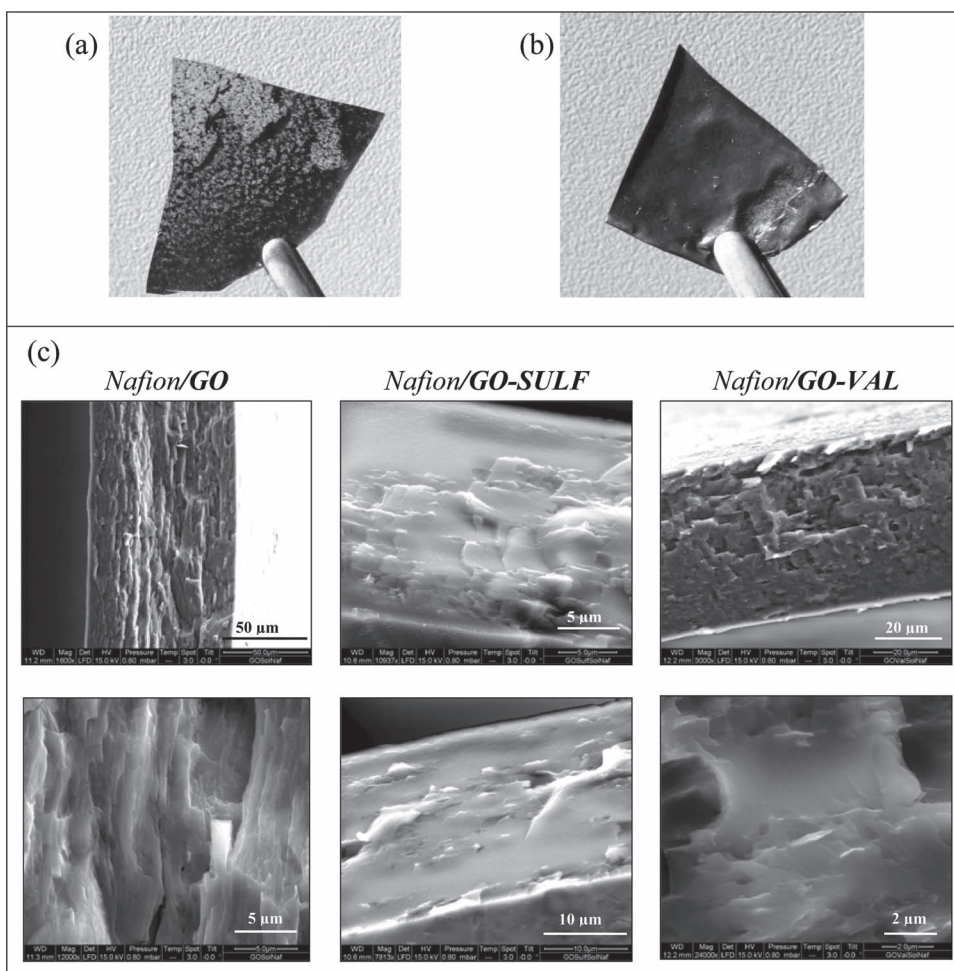


Figure 3. Photographs of Nafion nanocomposite membranes prepared by dispersing GO in a) DMF solvent and b) alcoholic solution of Nafion. c) SEM images of Nafion nanocomposite membranes loaded with 3 wt% GO, GO-SULF, and GO-VAL.

whereas the D band at 1363 cm^{-1} becomes the prominent feature in the spectrum, which testifies the creation of sp^3 domains due to the extensive oxidation.^[23a] The intensity ratio of the D and G bands is a measure of the disorder, as expressed by the sp^2/sp^3 carbon ratio. The $I_{\text{D}}/I_{\text{G}}$ intensity ratio was found to be 0.90 in the case of GO while the ratios of the final hybrid fillers have similar values in the range of 0.94–0.98. These findings indicate that the graphitized structure of GO remains unaffected by the covalent attachment of amine molecules on the graphene layers.

To estimate the amounts of aliphatic amine derivatives introduced in GO, thermal analysis (DTA/TGA) measurements were performed (see Supporting Information, Figure S1) on all the organo-GOs (GO-SULF, GO-TES, GO-VAL, and GO-SER) as well as the pristine GO. Based on these data, the weight loss observed in the temperature range 280–400 °C is attributed to the thermal decomposition of the aliphatic amine molecules^[23b] and is calculated to be 22.2, 18.1, 14.5, and 18 wt% for GO-SULF, GO-TES, GO-VAL, and GO-SER, respectively. Furthermore, data analysis elucidates the increased hydrophilic nature of these novel nanofillers. The thermogravimetric curves, derived from TGA measurements, were also used to determine the amount of adsorbed water

in the organo-GOs. From the weight loss up to 120 °C, the percentage of adsorbed water was calculated for all organo-modified GOs. The adsorbed water was 15, 17, 17.5, and 19 wt% for GO-VAL, GO-TES, GO-SULF, and GO-SER, respectively, while a lower value (11 wt%) was observed for pristine GO.

2.2. Characterization of the Hybrid Nanocomposite Membranes

2.2.1. Preparation and Morphology

The production of a homogeneous colloidal suspension of GO powder is an important challenge to allow its broad use for both fundamental studies and in polymer nanocomposite applications.^[11a,24] In this study, the choice of the proper solvent was long and complex but indubitably primary for the preparation of homogeneous and advantageous composite membranes based on this inorganic nanofiller. Organic solvents such as dimethylformamide (DMF) and dimethylacetamide (DMA), which are two of the most widely used solvents for the preparation of nanocomposite electrolyte membranes based on Nafion with various types of fillers, completely failed in the specific case of GO materials. **Figure 3a** and **b** shows

characteristic photographs of two GO-based composite membranes prepared using DMF and an alcoholic solution of the Nafion, respectively, as described in the Experimental Section. As evident, DMF is completely inappropriate to achieve homogeneous dispersion in the polymer matrix, and similar results were obtained by using many other solvents such as DMA, tetrahydrofuran (THF), dimethyl sulfoxide (DMSO), acetonitrile, and also water. On the contrary, the membranes prepared without any other solvent, but simply by dissolving the GO nanofiller in the alcoholic solution (mixture of 1-propanol and ethanol in water, in about 1:1 weight ratio) of the Nafion, are quite homogeneous with a uniform dispersion of the nanofiller in the membrane. Most likely this is due to the partially hydrophobic nature of the alcohols that finds greater chemical affinity with the carbon layers of GO, while the water solvates the hydrophilic groups on the surface. Organo-modified GOs showed the same difficulties, like pristine GO, in being dissolved in these solvents; therefore, all the nanocomposite membranes in this work were prepared by using the method of nanofiller dispersion directly in the alcoholic solution of Nafion. The morphology of all the nanocomposite membranes was studied by SEM. Figure 3c shows SEM images of three nanocomposite membranes, Nafion/GO, Nafion/GO-SULF, and Nafion/GO-VAL, prepared with 3 wt% filler-to-polymer loading. What is immediately evident in all the samples is a structure that is particularly wrinkled and spongy, more accentuated in GO and GO-VAL composites, while it is smoother in the Nafion/GO-SULF. Therefore, the organo modification of the GO particles does not generate any important morphological change in the nanocomposite membranes. It is important to note that no big agglomerates are visible through the section or on the surface; this means that these particles can be dispersed homogeneously in the polymeric matrix, thereby maintaining submicrometric dimensions.

2.2.2. Structural Characterization

A powerful tool to evaluate the type of composites created after the incorporation of the hybrid layered nanofillers in the Nafion matrix is XRD. **Figure 4** shows the XRD patterns

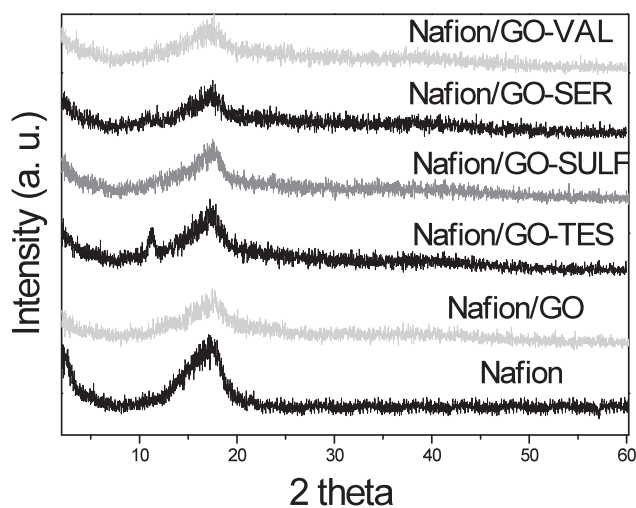


Figure 4. XRD patterns of filler-free Nafion and nanocomposite membranes with 3 wt% nanofillers.

of the filler-free Nafion and the nanocomposite membranes prepared with 3 wt% GO and organo-GO nanofillers. All the patterns show clearly a wide peak centered at 18° distinctive of the Nafion polymer arrangement (crystalline peak scattering from the polyfluorocarbon chains of Nafion).^[25] Except for the Nafion/GO-TES membrane, the absence of the 001 diffraction peak in the diffraction patterns of all the nanocomposites indicates the creation of fully exfoliated structures where all the individual graphene platelets lose their stacking after mixing with the polymeric mass (fully exfoliated nanocomposites). Organo-modified GO nanoplatelets are incorporated in the Nafion matrix by physical forces, such as electrostatic or van der Waals interactions. In the case of Nafion/GO-TES, a low-intensity 001 reflection peak appeared at 11.2° ($d_{001} = 7.9 \text{ \AA}$) indicating that a small fraction of GO platelets retain their stacking while the majority exist in fine dispersion between the polymer chains (creation of partially exfoliated nanocomposites). Furthermore, compared to filler-free Nafion, in the XRD patterns of all the nanocomposite membranes the broad band around 17° loses its intensity. This indicates changes in morphological features of the Nafion due to differences in crystallinity of the perfluorocarbon backbone of Nafion from the presence of the 2D graphene-based nanofillers. This broad band can be fitted to the experimental data (see Supporting Information, Figure S2) using two distinct diffraction peaks: a large amorphous halo centered at approximately 16° , and a superimposed Bragg peak centered at 17.5° corresponding to the crystalline fraction of the perfluorocarbon backbone.^[17a,c] The crystallinity of all nanocomposite membranes is lower than that of pristine Nafion membrane, which indicates that the presence of GO nanosheets (organo-modified or not) leads to membranes with essentially more amorphous structure.

Figure 5 (left) shows the Raman spectra of the nanocomposite membranes and of the filler-free Nafion for comparison. The two characteristic peaks at 1350 and 1595 cm^{-1} corresponding to graphite D and G bands, respectively, reveal the presence of the graphene-based nanofillers in the final nanocomposite membranes. Moreover, thermal analysis was also used to reveal the homogeneous distribution of the organo-GO platelets in the Nafion matrix. **Figure 5** (right) shows the DTA/TGA curves under air of the nanocomposite Nafion/GO-SULF and the filler-free Nafion. From the weight loss in the TGA curve it is calculated that until 280°C the total mass loss of the nanocomposite corresponds to about 11 wt% while in case of filler-free Nafion it is calculated to be about 6 wt%. This difference can be attributed to combustion of the SULF molecules that are attached on the GO surfaces and the removal of oxygen-containing groups of GO. Furthermore, from the TGA curves above 300°C , it is clear that in the case of nanocomposite loaded with 3 wt% GO-SULF, the decomposition of the perfluorocarbon backbone of Nafion is shifted to higher temperatures. In addition, the DTA curve of the filler-free Nafion membrane shows the main exothermic peak at 385°C , while in case of nanocomposite this exothermic peak is shifted at higher temperatures (395°C). The higher thermal resistance of the nanocomposite than that of the pure Nafion membrane is due to the strong interaction of polymer main chains with modified GO layers,

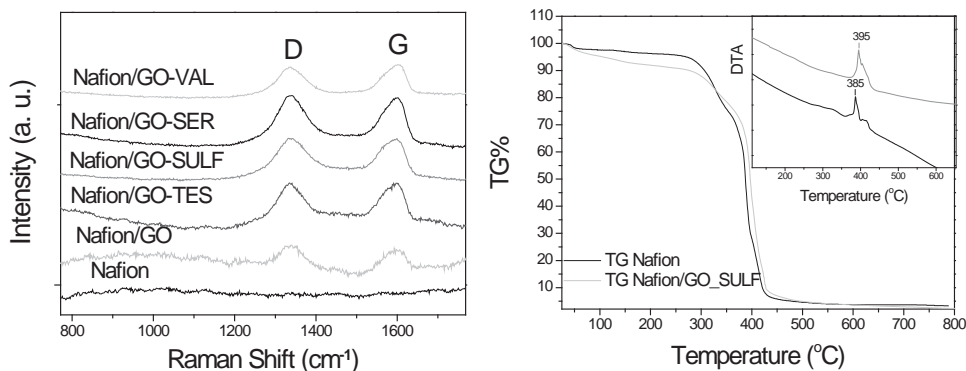


Figure 5. Left: Raman spectra of filler-free Nafion and nanocomposite membranes with 3 wt% nanofillers. Right: TGA/DTA curves of filler-free Nafion and Nafion/GO-SULF.

which provides evidence for the homogeneous dispersion of the graphene-based platelets in the polymeric matrix. Similar thermal improvement has been observed with other layered nanoadditives such as aluminosilicate clays.^[17c,25b,26] Analogous results were observed for all the series of nanocomposites (not shown here), thus indicating that all graphene nanofillers (apart from GO-TES) distributed homogeneously on the polymer matrix.

2.2.3. NMR (Diffusion, T_1 , and Spectral) Investigation

The strong relationship between water uptake of the electrolyte and the self-diffusion coefficients is well known.^[14,15] In general, electrolyte membranes that absorb more water exhibit higher diffusivity at room temperature, while an increased amount of adsorbed water is not necessary for good proton conductivity at high temperatures (above 80 °C). **Table 1** illustrates the maximum water uptake reached for filler-free Nafion and nanocomposite membranes. A small increase in the water uptake is observed for GO-SER (29 wt%), GO-TES (29 wt%), and GO-VAL (31 wt%) nanocomposites, as well as for the GO nanocomposite (27 wt%) compared to neat Nafion membrane, which absorbs about 24 wt% of water. The improvement in the water absorption is considerably higher in the case of Nafion/GO-SULF nanocomposite, which reaches the value of 50 wt% (the reason for this behavior is explained below).

Figure 6a shows the water self-diffusion coefficients of all nanocomposites measured by the pulsed field gradient

(PFG) NMR technique on completely swelled membranes, in the temperature range 20–140 °C. In particular, this graph displays the water mobility in Nafion nanocomposite membranes loaded with 3 wt% GO or organo-modified GO nanofillers in comparison with the filler-free Nafion. As expected,

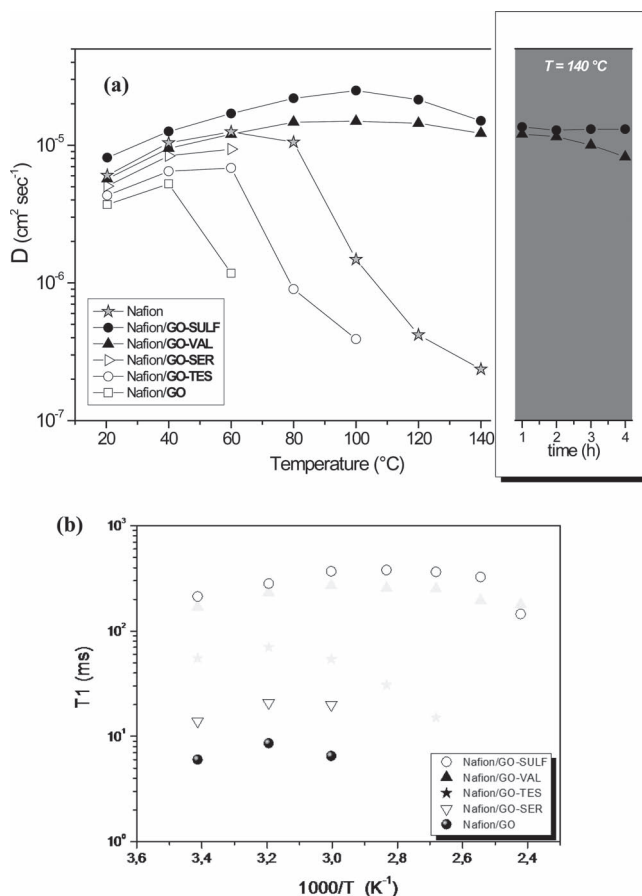


Figure 6. Self-diffusion coefficients D (a) and longitudinal relaxation times T_1 (b) as a function of the temperature (from 20 to 140 °C) of the water confined in completely swelled membranes of filler-free Nafion and nanocomposite membranes with 3 wt% loading of nanofillers (GO, GO-SULF, GO-VAL, GO-SER, and GO-TES). Inset in (a): graph of the data collected at 140 °C after several hours.

Table 1. Maximum water uptake of the filler-free Nafion and nanocomposite membranes with 3 wt% filler - to - polymer loading.

Membranes	Water uptake [wt%]
Nafion	24
Nafion/GO	27
Nafion/GO-TES	29
Nafion/GO-SER	29
Nafion/GO-VAL	31
Nafion/GO-SULF	50

at temperatures over 60–80 °C, the water diffusion in the filler-free Nafion decreases rapidly due to water evaporation from the membrane. The presence of unmodified GO platelets as filler in the polymer does not improve the performance of the membrane. On the contrary, at 60 °C almost all the water is lost from the composite and, practically, over this temperature no NMR signal is possible to measure its diffusion coefficient. Similar behavior has been observed by Giannelis et al.^[11a] who showed that Nafion reinforced with 5 wt% unmodified GO does not improve the conductivity of the membrane. On the other hand, the benefits from the surface modification of GO sheets with an organic molecule such as aminopropanesulfonic acid (SULF) are evident. Nafion/GO-SULF nanocomposite shows water diffusion coefficient values that are very high in all temperature ranges investigated. The diffusion increases linearly up to 100 °C and soon after, due to the evaporation of a certain amount of water from the membrane, it decreases slightly but remains constant, especially after several hours at 140 °C.

To clarify the water diffusive behavior in all the studied systems, we need to provide some information concerning the diffusion coefficients measured: 1) the water confined in the hydrophilic pores of the membranes shows a Gaussian self-diffusion behavior for all the investigated temperatures (the decay lines of the experimental data, $\ln A(g)$ vs. g^2 , are straight); as a consequence 2) we measure only one diffusion value, which is a weighted average between bound water and bulk-like water at a fast rate of proton exchange during the diffusion time. On the basis of these considerations, the reduction of the diffusion at temperatures above 100 °C can be explained by taking into account the fact that the water evaporation reasonably affects the bulk water because it is more “free” from electrostatic interactions; therefore, its contribution to the diffusion coefficient decreases, while the contribution of the bound water prevails.

It is important to underline that these measurements, as described in the Experimental Section, are conducted without providing additional humidification to the sample during heating. Therefore, this performance at high temperatures is truly remarkable and implies that a small amount of water (bound water) remains in the membrane, which ensures proton mobility and thus conductivity. This result can be ascribed to two effects: 1) the increment of the number of acid sites in the electrolyte is reflected in its ability to absorb and hold more water at high temperatures; and 2) the presence of organic molecules with sulfonic end groups makes the filler more compatible with the polymer and allows better dispersion, especially within the hydrophilic channels of Nafion. Moreover, increasing the loading of GO-SULF from 3 to 6 wt% (see Supporting Information, Figures S3 and S4) has a negative impact both in terms of water uptake (which falls to about 20 wt%) and proton diffusion at medium temperatures. This outcome can be directly related to the molecular confinement in the vicinity of the organic/inorganic interface, which drastically hinders the mobility of the polymer chains,^[11a] and to an obstruction effect that limits the mobility of the water in the ionic domains.

The Nafion/GO-VAL nanocomposite shows a performance analogous to that of Nafion/GO-SULF: the coefficients

are slightly lower^[14a,24] even if the sample absorbs much less water (the water uptake is about 30 wt% versus 50 wt% for the GO-SULF). By increasing the amount of GO-VAL nanofiller to 6 wt% (see Supporting Information, Figure S4), the diffusion at 25 °C is lower than that for the nanocomposite loaded with 3 wt% due to the consistently lower water uptake (about 20 wt%), and after 50–60 °C this membrane loses almost all the absorbed water. Therefore, once again, the increase in the filler loading does not give any improvement; on the contrary, for the reasons given before, it completely destroys the performance of the resulting composite. Finally, GO-SER and GO-TES nanocomposites show disappointing results: for example, Nafion/GO-SER shows an initial performance very similar to that of GO-VAL, but at 80 °C most of the water evaporates from the membrane and the proton NMR signal is not sufficient for determining the D coefficient. Instead, Nafion/GO-TES nanocomposite maintains a certain amount of water up to 100 °C but after this temperature the signal is lost. These data are indicative of systems not able to absorb/retain water, although both these fillers contain characteristic hydrophilic groups. This behavior is probably due to differences in the size and the stereochemical configuration of the four amine molecules. The TES and SER molecules occupy more volume, and thus surface, which inhibits the accessibility of water molecules in the remaining hydrophilic acid sites of the GO layers and thus reduces the insertion of more water molecules in the interlayer space of GO. On the other hand, in the case of primary amines SULF and VAL, which are linear molecules, the hydrophilic sites of the GO are more easily accessible by water molecules, which, in combination with the additional acidic functional groups of the organic molecules that have been added to the system, greatly enhances the total amount of absorbed water.

Figure 6b shows the temperature dependence of the NMR longitudinal (or spin–lattice) relaxation times (T_1) of water in the saturated nanocomposite membranes. Compared to diffusion, T_1 reflects more localized motions including both translation and rotation on a timescale comparable to the reciprocal of the NMR angular frequency (≈ 1 ns); therefore, higher T_1 values suggest more facile molecular rotational and translational motion. Nafion/GO-SULF and Nafion/GO-VAL nanocomposites with 3 wt% nanofiller show higher relaxation times, which indicates that the functionalization of GO surfaces with such molecules produces fillers able to increase the water absorption/retention properties and to facilitate molecular movements. On the contrary, GO-SER and GO-TES nanofillers as well as pristine GO show T_1 values lower by almost one order of magnitude, that is, a considerable reduction of the local water mobility that, as seen before, is reflected in the diffusion coefficients. At high temperatures the problem of water evaporation remains; these nanocomposites cannot retain water, and thus both diffusion and relaxation times fall down. Once again, these data demonstrate that the beneficial effects of some organo-modified GO particles (SULF and VAL) with respect to others (TES and SER) are attributable to structural modifications of the polymeric matrix, which facilitate more water motions with improved water-retention ability, and it is not merely a consequence of the fact that these particles are hygroscopic.

The proton NMR spectra collected on the various membranes can be useful to understand what happens when the temperature increases. **Figure 7** displays the temperature evolution of the ^1H NMR spectra of the GO-SULF, GO-VAL, and GO-TES nanocomposites at 3 wt% filler loading. These spectra were referenced against pure water set at 0 kHz, and were acquired with the same number of scans. For all the nanocomposites, one large, asymmetric peak was observed, the shape of which changes from one membrane to another. Due to the fluorinated character of the Nafion, the ^1H NMR signal arises essentially from the water absorbed by the membrane since the contribution of the hydrogen atoms of the sulfonic acid group and those of the organo fillers is practically negligible.

The asymmetric shape of the signal (non-Lorentzian curve) implies that different “types of water” coexist. It is well known that in a hydrated Nafion membrane, where the hydrophobic/hydrophilic duality for the matrix materializes in a nanoscale phase separation in hydrophobic and hydrophilic domains,^[27] water is shared between the solvation of the SO_3^- hydrophilic groups (as well as the hydrophilic groups of the organo-modified nanofillers in the case of nanocomposites) and bulk-like water.^[28] As we explained before, the distinction between the different states of water within the hydrophilic pores can be difficult to discern so what we see is only one peak, the shape of which is explicative of the complexity of the system and of the different structural modifications that each filler produces on the polymeric matrix. The intensity of this peak decreases upon heating due to the water evaporation from the membrane even though, at 140 °C in the GO-SULF and GO-VAL nanocomposites, there is still a discrete signal that remains unchanged for several hours and which is responsible for the proton diffusion revealed. However, what is interesting to note is the trend of the chemical shift of the peak versus temperature (insets in **Figure 7**) and how it is closely related to both the amount of water present in the membrane and the self-diffusion coefficients. The temperature contributes to the proton resonance variation because it affects the lifetime of the hydrogen bond. The heating causes a downfield shift of the resonance, and as a result a decrease of the chemical shift is observed. This reduction is more accentuated in the GO-SULF nanocomposite since is the membrane with higher water uptake (50 wt%), which corresponds to the higher chemical shift at room temperature (about 1.5 ppm); GO-VAL and GO-TES nanocomposites follow with 31 and 29 wt% water uptake, and 0.7 and 0.3 ppm chemical shift, respectively. The changing of the slope of that trend takes place at 120 °C for GO-SULF, 80 °C for GO-VAL, and 60 °C for GO-TES nanocomposites, which corresponds to a significant loss of water and therefore to an analogous reduction of the diffusion (see Figure 6a).

From these observations and from the comparative analysis of the diffusion data we can assert that before the minimum, the contribution to the chemical shift is mostly that of the bulk-like water, and the temperature effect is in fact practically that obtained for pure water. The increasing of the chemical shift soon after is explainable by considering that the residual water remaining in the membranes is the water bound to the hydrophilic groups; consequently,

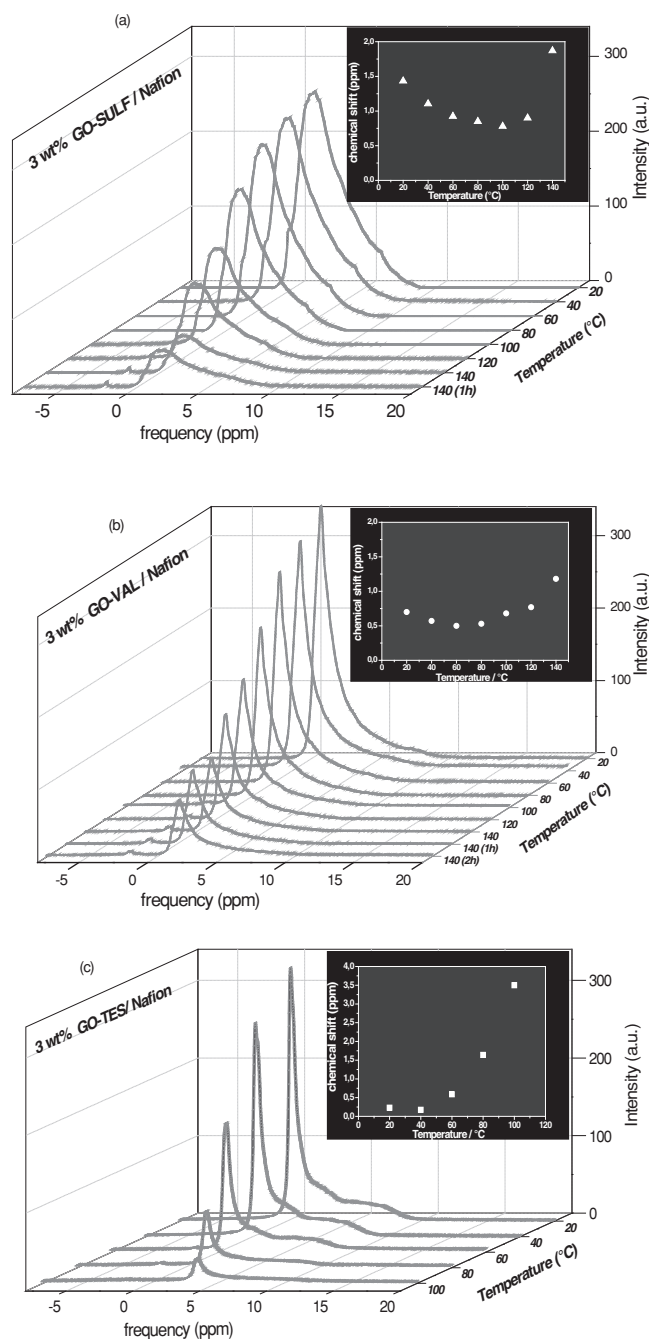


Figure 7. ^1H NMR spectral temperature evolution of the a) GO-SULF, b) GO-VAL, and c) GO-TES nanocomposites and chemical shift versus temperature.

the concentration of H^+ ions (the acidity of the water is a well-known property of water in Nafion) and the effect of induced fields by the polar groups (sulfonic, hydroxy, etc.) prevail on the temperature and bring an upfield shift of the resonance. In a nutshell, the variation of the chemical shift of the water resonance line with temperature dependence of the liquid water as well as on the “states” of the water confined in such membranes. In addition, this NMR analysis points to a strong correlation between the temperature behavior of the

D coefficients and the chemical shift: an increase of the diffusion corresponds to a decrease of the chemical shift (and vice versa) with an unexpected symmetry.

2.2.4. Dynamic Mechanical Analysis Investigation

The effect of GO and GO organo-modified nanofillers on the mechanical properties of the Nafion membrane was investigated by temperature ramp tests. **Figure 8** reports the temperature evolution of the storage modulus and $\tan \delta$ of the filler-free Nafion and some representative nanocomposites (Nafion/GO, Nafion/GO-VAL, and Nafion/GO-SULF). Pristine Nafion membrane shows a decline of storage modulus during heating and a relaxation event at about 125 °C, which can be attributed to the α -relaxation characteristic of the polar group clusters (the low-temperature β relaxation is outside the temperature range used in our measurements).^[29] This relaxation temperature remains almost unaltered in both the Nafion/GO-VAL and Nafion/GO-SULF nanocomposites (127 and 121 °C, respectively), while it clearly shifts at higher temperature, around 137 °C, for the Nafion/GO membrane. This implies that it is thermomechanically more stable than unmodified Nafion membrane.

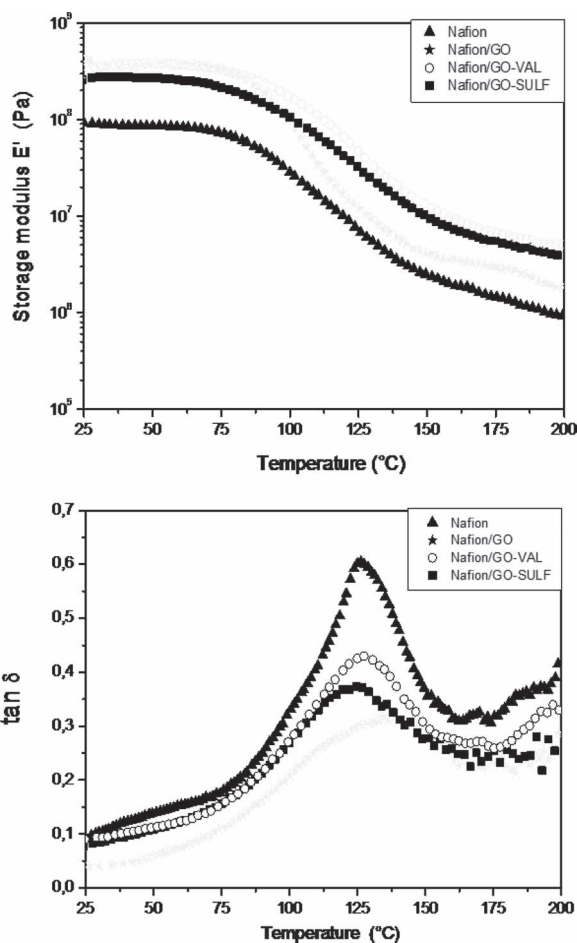


Figure 8. Storage modulus E' (top) and $\tan \delta$ versus temperature (bottom) of filler-free Nafion and nanocomposite membranes loaded with 3 wt% GO, GO-SULF, and GO-VAL.

From the literature, it is known that above 115 °C the network of hydrophilic clusters becomes extremely mobile, and the clustered structure finally collapses due to loss of water under dry and hot conditions.^[30] This high mobility of the backbone and cluster network is shown by a high value of the loss tangent for unmodified Nafion membrane, which reaches values of 0.62, as shown in Figure 8 (bottom). Instead, all the nanocomposites exhibit a strong decrease of the $\tan \delta$ value, down to 0.43 for Nafion/GO-VAL, 0.37 for Nafion/GO-SULF, and 0.30 for Nafion/GO. Such a result could be related to the presence of the nanofillers within the pores of the Nafion membrane and to their interactions with the polymeric chains, thus creating a membrane with lower flexibility; consequently, it becomes more stiff and can withstand higher temperatures.

By observing the E' modulus trend with the temperature, both Nafion/GO-VAL and GO-SULF show a slight decline above 100 °C with respect to the Nafion/GO composite; therefore, the organo modification of the GO produces membranes with higher solidity and without changing the α -relaxation temperature of the polymer, in agreement with the literature.^[29] In fuel cell applications, a nanocomposite membrane with high modulus might permit the employment of a thinner membrane, thus avoiding problems connected to the electrolyte resistance.^[17b] Finally, increasing of the filler loading from 3 to 6 wt% does not change the mechanical behavior of the Nafion/GO-VAL sample, while it even has a negative effect in the case of the GO-SULF nanocomposite (see Supporting Information, Figure S5).

3. Conclusion

Novel Nafion hybrid membranes based on organo-functionalized GO were synthesized by solution intercalation and characterized by different techniques. Functionalization of GO with amino derivatives having different terminal groups (5-aminovaleric acid, 3-amino-1-propanesulfonic acid, *N*-[tris(hydroxymethyl)methyl]-2-aminoethanesulfonic acid, and serine) was performed to increase not only the number of acid sites and consequently the water retention of the produced nanocomposite membranes, but also to improve the compatibility with the polymeric membrane. XRD results show that fully exfoliated nanocomposites were created while the crystallinity of all nanocomposite membranes was lower than that of pristine Nafion membrane, thus indicating that the presence of GO nanosheets (organo-modified or not) leads to membranes with essentially more amorphous structure. Vibrational spectroscopies (Raman and FTIR) reveal the presence of the 2D nanofillers in the final composite membranes. Thermal analysis indicates that graphene-based nanocomposite membranes show higher thermal resistance than that of pure Nafion membrane due to the strong interaction of polymer main chains with modified GO layers, which provides evidence for the homogeneous dispersion of the organographene platelets in the polymeric matrix. Nanocomposite membranes show a wrinkled and spongy structure as evidenced by SEM images.

The positive effect of the synthesized organo-modified GO nanofillers on Nafion properties was demonstrated by

NMR diffusion measurements. In particular, functionalization of GO with the SULF and VAL molecules resulted in composite membranes with high water diffusion coefficients over a wide range of temperatures (25–140 °C) and also promoted a higher hydration level with respect to filler-free Nafion, as revealed by water uptake measurements. However, the crucial outcome of this study is the behavior of these nanocomposites under very high temperature conditions. Nanocomposite membranes are able to retain a certain amount of water for several hours at temperatures as high as 140 °C without any further humidification. Diffusion and spectral analysis (line shape and chemical shift) have pointed out that the remaining water strongly interacts electrostatically with the hydrophilic groups present in the composite systems (“acid water”) but, at such high temperatures, the thermal molecular energy ensures a diffusion high enough to guarantee good proton conductivity. This result is very attractive in view of the potential application in fuel cells for transportation, where the cell stack must be able to perform without external humidification, which is a source of additional cost and complexity to the system. On the contrary, the other two nanocomposites prepared with the GO-TES and GO-SER fillers, even if they contain the same hydrophilic groups as SULF and VAL, did not show the same behavior probably due to differences in their size and stereochemical configuration.

Finally, the mechanical investigation of the nanocomposites indicated that the organo modification of the GO produces membranes more structured and with higher stiffness than the filler-free Nafion, which is a highly desirable characteristic for use in fuel cell applications.

4. Experimental Section

Materials: Nafion as a 20 wt% dispersion in water and lower aliphatic alcohols was supplied by Aldrich. The organic compounds used for the synthesis of the organo-GO were: 3-amino-1-propanesulfonic acid (denoted SULF), 2-amino-3-hydroxypropanoic acid or serine (SER), 2-[[2-hydroxy-1,1-bis(hydroxymethyl)ethyl]amino]ethanesulfonic acid (TES), and 5-aminovaleic acid (VAL), all of them purchased from Aldrich.

Preparation of GO: Aqueous dispersions of GO were produced using a modified Staudenmaier’s method^[31] from graphite powder. In a typical synthesis, powdered graphite (10 g, purum, powder ≤ 0.2 mm; Fluka) was added to a mixture of concentrated sulfuric acid (400 mL, 95–97 wt%) and nitric acid (200 mL, 65 wt%) while cooling in an ice-water bath. Potassium chlorate powder (200 g, purum, >98.0%; Fluka) was added to the mixture in small portions while stirring and cooling. The reaction was quenched after 18 h by pouring the mixture into distilled water, and the oxidation product was washed until the pH reached 6.0 and finally dried at room temperature. According to elementary analysis data, the C/O atomic ratio of the resulting product was 2.6.^[32]

Synthesis of Organo-Modified Graphene Oxides: For the preparation of organo-GO nanofillers, GO (100 mg) was dispersed in water (100 mL), followed by the addition of aliquots of 300 mg of the above amine derivatives in 40 mL of water (samples denoted as GO-SULF, GO-TES, GO-VAL, and GO-SER). After stirring for 24 h,

the organo-modified GOs were washed with water, separated by centrifugation, and air-dried by spreading on glass plates.

Preparation of Composite Membranes: Nafion hybrid nanocomposites were prepared by the solvent casting method. Two procedures were followed to obtain a homogeneous colloidal suspension of GO powder (and organo-modified GO) in the Nafion: 1) dispersion of the nanofillers and the polymer in an organic solvent (such as DMF, DMA, THF, DMSO, acetonitrile, etc.); 2) use of the same solution in which Nafion polymer was dispersed, that is, a mixture of water and propanol as purchased, to disperse directly the various filler powders. In the first procedure, an appropriate amount of Nafion solution was dried at about 60 °C and then redissolved in the organic solvent (DMF, DMA, etc.) until a clear solution was obtained. The filler was dispersed in the same solvent under stirring and ultrasonication and then added slowly to the polymer solution. The final solution was sonicated for 1 h and then stirred at 60 °C for several hours to ensure complete mixing. Finally, the suspension was cast on a petri dish at 80 °C overnight. In the second procedure, the filler was directly added to the Nafion solution (as purchased), ultrasonicated for 1 day, and stirred for another day at room temperature until a clear solution was obtained. After that, the dispersion was cast on a petri disk at 80 °C overnight to remove the solvents. The hybrid membranes were removed from the petri disk by immersing the glass plate in deionized water for several minutes.

To reinforce the membrane, it was sandwiched and pressed between two Teflon plates and placed in an oven at 150 °C for about 15 min. All composite membranes produced by casting were subsequently treated by rinsing in: 1) boiling HNO₃ solution (1 M) for 1 h to oxidize the organic impurities, 2) boiling H₂O₂ (3 vol%) for 1 h to remove all the organic impurities, 3) boiling deionized H₂O for 40 min three times, 4) boiling H₂SO₄ (0.5 M) for 1 h to remove any metallic impurities, and again 5) boiling deionized H₂O for 40 min twice to remove excess acid. According to MacMillan et al.^[33] an additional purification procedure was performed to ensure the removal of paramagnetic contaminants, which are particularly damaging to NMR experiments, such as the presence of copper that we found by electron paramagnetic resonance analysis. By this procedure membranes were soaked in ethylenediaminetetraacetic acid (EDTA) solution (0.001 M) for 1 day followed by a thorough rinse. Then they were soaked in HCl (2 M) at 80 °C for 2 h followed by boiling in freshly distilled–deionized water to remove any residual acids, and the treatment with EDTA was repeated. Finally, rinsing in boiled deionized water was carried out three times to remove residual EDTA and the membranes were stored at room temperature in the fully hydrated state.

Characterization Techniques: X-ray powder diffraction data were collected on a D8 Advance Bruker diffractometer by using Cu K α (40 kV, 40 mA) radiation and a secondary-beam graphite monochromator. The patterns were recorded in a 2θ range from 2 to 60°, in steps of 0.02° and counting time 2 s per step. Infrared spectra were measured in the region of 400–4000 cm⁻¹ with a FTIR 8400 spectrometer equipped with a deuterated triglycine sulfate (DTGS) detector. Raman spectra were recorded with a micro-Raman system RM 1000 Renishaw using a laser excitation line at 532 nm (Nd-YAG) in the range of 1000–2400 cm⁻¹. A power of 1 mW was used with 1 μ m focus spot to avoid photodecomposition of the samples. TGA and DTA were performed using a Perkin–Elmer Pyris Diamond TG/DTA system. Samples of approximately 5 mg were heated under air

from 25 to 850 °C, at a rate of 10 °C min⁻¹. Morphological studies were performed by using a QUANTA FEG 400 F7 FEI microscope operating in the e-SEM mode. The SEM images were acquired by collecting the backscattered electrons induced by using a 10 keV electron beam and 0.4 mbar of water humidity.

¹H NMR measurements were performed on a Bruker NMR spectrometer AVANCE 300 Wide Bore working at 300 MHz. Self-diffusion coefficients of water were obtained by using the pulsed field gradient spin-echo (PFGSE) method^[34] with a gradient pulse length δ ranging from 0.8 to 1.2 ms, a delay time for diffusion Δ of 10–12 ms, and varying the gradient amplitude from 10 to 700 G cm⁻¹. Under these conditions the uncertainty in the self-diffusion measurements was \approx 3%.

Longitudinal relaxation times (T_1) of water were measured by the inversion–recovery sequence (π – τ – $\pi/2$). Both self-diffusion and T_1 measurements were conducted by increasing the temperature step by step from 20 to 140 °C, with steps of 20 °C, and leaving the sample to equilibrate for about 15 min. Prior to the NMR measurements, membranes were dried in an oven, weighed, and then immersed in distilled water at room temperature. Upon removal from the water they were quickly blotted dry with a paper tissue (to eliminate most of the free surface liquid). The water content was determined by using a microbalance and recorded as: uptake% = $[(m_{\text{wet}} - m_{\text{dry}}) / m_{\text{dry}}] \times 100$. At this point the membranes were loaded into a 5 mm NMR Pyrex tube and hermetically sealed.

Dynamic mechanical analysis was carried out using a TTDMA instrument (Triton Technology, UK) equipped with a film/fiber tension clamp. The response, as a function of temperature, was measured by subjecting a rectangular film to a temperature ramp test from 25 to 200 °C at a rate of 5 °C min⁻¹. A periodic sinusoidal displacement was applied to the sample and the resultant force was measured. This measurement included the amplitude of the signals and also the phase difference between them.^[35] The damping factor, $\tan\delta$, is defined as the ratio of loss (E'') to storage (E') modulus. The study was performed by applying 1 Hz frequency and a small sinusoidal mechanical elongation. The α -relaxation temperature (T_g) of a material can be taken as either the peak of the loss modulus versus temperature curve or the peak of the $\tan\delta$ versus temperature curve. In the present work, T_g was obtained from the peak of $\tan\delta$ versus temperature data.

Supporting Information

Supporting Information is available from the Wiley Online Library or from the author.

Acknowledgements

The authors acknowledge co-funding of this research by the European Union–European Regional Development Fund and the Greek Ministry of Education/EYDE-ETAK through program ESPA 2007-2013/EPAN II/Action “SYNERGASIA” (project 09SYN-42-831). A.E. gratefully acknowledges the Academy of Athens for a Ph.D. fellowship. We also acknowledge use of the XRD unit of the Network of Laboratory Units and Centers of the University of Ioannina.

- [1] a) Y. Yurum, A. Taralp, T. N. Veziroglu, *Int. J. Hydrogen Energy* **2009**, *34*, 3784–3798; b) C. Moreno-Castilla, F. J. Maldonado-Hódar, *Carbon* **2005**, *43*, 455–465.
- [2] D. R. Paul, L. M. Robeson, *Polymer* **2008**, *49*, 3187–3204.
- [3] S. Sinha Ray, M. Okamoto, *Prog. Polym. Sci.* **2003**, *28*, 1539–1641.
- [4] F. R. Costa, M. Saphiannikova, U. Wagenknecht, G. Heinrich, *Adv. Polym. Sci.* **2008**, *210*, 101–168.
- [5] M. Moniruzzaman, K. I. Winey, *Macromolecules* **2006**, *39*, 5194–5205.
- [6] K. Litina, A. Miriouni, D. Gournis, M. A. Karakassides, N. Georgiou, E. Klontzas, E. Ntoukas, A. Avgeropoulos, *Eur. Polym. J.* **2006**, *42*, 2098–2107.
- [7] T. Kuilla, S. Bhadra, D. Yao, N. H. Kim, S. Bose, J. H. Lee, *Prog. Polym. Sci.* **2010**, *35*, 1350–1375.
- [8] J. R. Potts, D. R. Dreyer, C. W. Bielawski, R. S. Ruoff, *Polymer* **2011**, *52*, 5–25.
- [9] Y. Geng, S. J. Wang, J. K. Kim, *J. Colloid Interface Sci.* **2009**, *336*, 592–598.
- [10] A. B. Bourlinos, D. Gournis, D. Petridis, T. Szabo, A. Szeri, I. Dekany, *Langmuir* **2003**, *19*, 6050–6055.
- [11] a) S. Ansari, A. Kellarakis, L. Estevez, E. P. Giannelis, *Small* **2010**, *6*, 205–209; b) J. Li, S. Guo, Y. Zhai, E. Wang, *Electrochem. Commun.* **2009**, *11*, 1085–1088; c) J. Li, S. Guo, Y. Zhai, E. Wang, *Anal. Chim. Acta* **2009**, *649*, 196–201.
- [12] A. Kaniyoor, S. Ramaprabhu, *Carbon* **2011**, *49*, 227–236.
- [13] B. Seger, P. V. Kamat, *J. Phys. Chem. C* **2009**, *113*, 7990–7995.
- [14] a) I. Nicotera, A. Khalfan, G. Goenaga, T. Zhang, A. Bocarsly, S. Greenbaum, *Ionics* **2008**, *14*, 243–253; b) I. Nicotera, T. Zhang, A. Bocarsly, S. Greenbaum, *J. Electrochem. Soc.* **2007**, *154*, B466–B473.
- [15] I. Nicotera, L. Coppola, C. O. Rossi, M. Yousry, G. A. Ranieri, *J. Phys. Chem. B* **2009**, *113*, 13935–13941.
- [16] A. S. Arico, V. Baglio, V. Antonucci, I. Nicotera, C. Oliviero, L. Coppola, P. L. Antonucci, *J. Membr. Sci.* **2006**, *270*, 221–227.
- [17] a) R. H. Alonso, L. Estevez, H. Q. Lian, A. Kellarakis, E. P. Giannelis, *Polymer* **2009**, *50*, 2402–2410; b) E. Burgaz, H. Lian, R. H. Alonso, L. Estevez, A. Kellarakis, E. P. Giannelis, *Polymer* **2009**, *50*, 2384–2392; c) I. Nicotera, A. Enotiadis, K. Angjeli, L. Coppola, G. A. Ranieri, D. Gournis, *J. Phys. Chem. B* **2011**, *115*, 9087–9097; d) I. Nicotera, A. Enotiadis, K. Angjeli, L. Coppola, D. Gournis, *Int. J. Hydrogen Energy* **2012**, *37*, 6236–6245.
- [18] V. Tricoli, F. Nannetti, *Electrochim. Acta* **2003**, *48*, 2625–2633.
- [19] J.-M. Thomassin, J. Kollar, G. Caldarella, A. Germain, R. Jérôme, C. Detrembleur, *J. Membr. Sci.* **2007**, *303*, 252–257.
- [20] B. Choi, J. Hong, Y. C. Park, D. H. Jung, W. H. Hong, P. T. Hammond, H. Park, *ACS Nano* **2011**, *5*, 5167–5174.
- [21] a) R. Y. N. Gengler, A. Veligura, A. Enotiadis, E. K. Diamanti, D. Gournis, C. Jozsa, B. J. van Wees, P. Rudolf, *Small* **2010**, *6*, 35–39; b) H. F. Yang, C. S. Shan, F. H. Li, D. X. Han, Q. X. Zhang, L. Niu, *Chem. Commun.* **2009**, 3880–3882; c) I. Dékány, R. Krüger-Grasser, A. Weiss, *Colloid Polym. Sci.* **1998**, *276*, 570–576; d) S. Stankovich, D. A. Dikin, R. D. Piner, K. A. Kohlhaas, A. Kleinhammes, Y. Jia, Y. Wu, S. T. Nguyen, R. S. Ruoff, *Carbon* **2007**, *45*, 1558–1565.
- [22] W. W. Simons, *The Sadtler Handbook of Infrared Spectra*, Sadtler Research Laboratories, Philadelphia **1978**.
- [23] a) S. Stankovich, D. A. Dikin, R. D. Piner, K. A. Kohlhaas, A. Kleinhammes, Y. Jia, Y. Wu, S. T. Nguyen, R. S. Ruoff, *Carbon* **2007**, *45*, 1558–1565; b) S. P. Economopoulos, G. Rotas, Y. Miyata, H. Shinohara, N. Tagmatarchis, *ACS Nano* **2010**, *4*, 7499–7507.
- [24] I. Nicotera, T. Zhang, A. Bocarsly, S. Greenbaum, *J. Electrochem. Soc.* **2007**, *154*, B466–B473.
- [25] a) K. A. Mauritz, R. B. Moore, *Chem. Rev.* **2004**, *104*, 4535–4585; b) D. H. Jung, S. Y. Cho, D. H. Peck, D. R. Shin, J. S. Kim, *J. Power Sources* **2003**, *118*, 205–211.
- [26] R. Gosawit, S. Chirachanchai, S. Shishatskiy, S. P. Nunes, *Solid State Ionics* **2007**, *178*, 1627–1635.

- [27] K. A. Mauritz, R. B. Moore, *Chem. Rev.* **2004**, *104*, 4535–4585.
- [28] a) T. D. Gierke, G. E. Munn, F. C. Wilson, *J. Polym. Sci. Polym. Phys. Ed.* **1981**, *19*, 1687–1704; b) W. Y. Hsu, T. D. Gierke, *J. Membr. Sci.* **1983**, *13*, 307–326; c) G. Gebel, P. Atkins, *Polymer* **2000**, *41*, 5829–5838; d) S. J. Paddison, R. Paul, *Phys. Chem. Chem. Phys.* **2002**, *4*, 1158–1163.
- [29] a) V. Di Noto, R. Gliubizzi, E. Negro, G. Pace, *J. Phys. Chem. B* **2006**, *110*, 24972–24986; b) R. Herrera Alonso, L. Estevez, H. Lian, A. Kelarakis, E. P. Giannelis, *Polymer* **2009**, *50*, 2402–2410.
- [30] G. Alberti, M. Casciola, L. Massinelli, B. Bauer, *J. Membr. Sci.* **2001**, *185*, 73–81.
- [31] L. Staudenmaier, *Ber. Dtsch. Chem. Ges.* **1899**, *31*, 1481.
- [32] D. V. Stergiou, E. K. Diamanti, D. Gournis, M. I. Prodromidis, *Electrochem. Commun.* **2010**, *12*, 1307–1309.
- [33] B. MacMillan, A. R. Sharp, R. L. Armstrong, *Polymer* **1999**, *40*, 2471–2480.
- [34] E. O. Stejskal, J. E. Tanner, *J. Chem. Phys.* **1965**, *42*, 288–292.
- [35] P. Gabbott, *Principles and Applications of Thermal Analysis*, Blackwell, Oxford **2008**.

Received: March 21, 2012
Revised: April 26, 2012
Published online: July 25, 2012

NANO MICRO
small

Supporting Information

for *Small*, DOI: 10.1002/smll.201200609

**Graphene-Based Nafion Nanocomposite Membranes:
Enhanced Proton Transport and Water Retention by Novel
Organo-functionalized Graphene Oxide Nanosheets**

*Apostolos Enotiadis, Kristina Angjeli, Noemi Baldino, Isabella
Nicotera, * and Dimitrios Gournis**

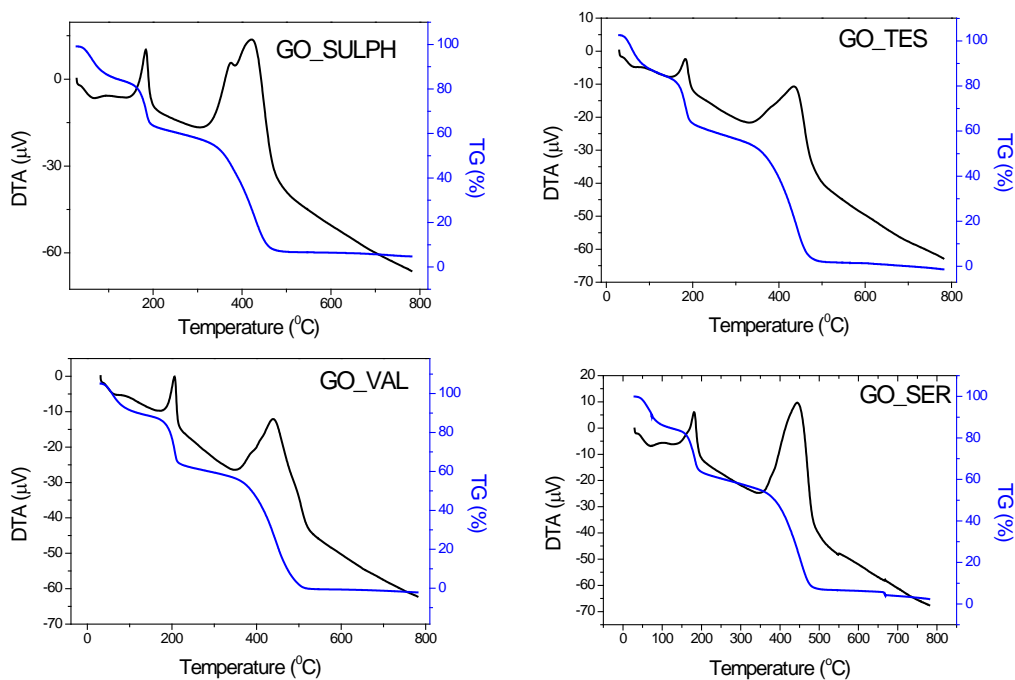
Supporting Information

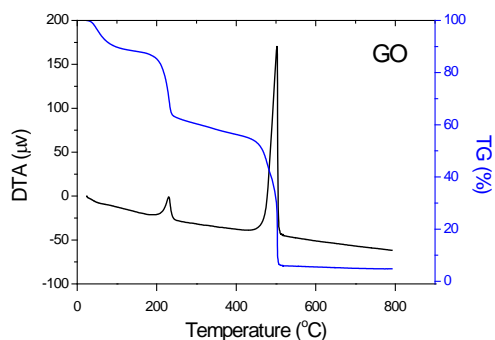
Graphene-based Nafion nanocomposite membranes: Enhanced proton transport and water retention by novel organo-functionalized graphene oxide nanosheets

Apostolos Enotiadis, Kristina Angjeli, Noemi Baldino, Isabella Nicotera and Dimitrios Gournis**

S1. DTA/TGA curves of organo-modified GOs.

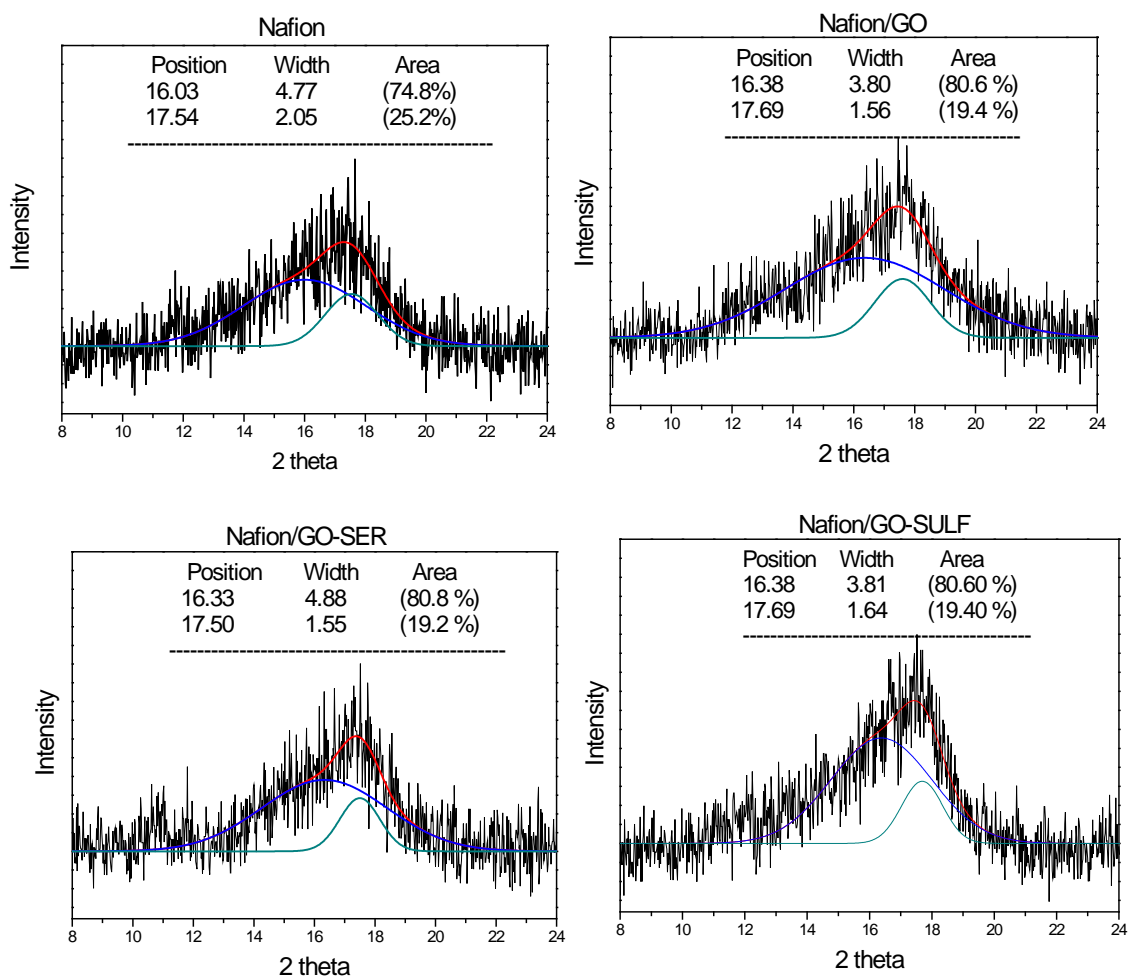
Figure S1 shows the DTA/TGA of a GO-SULF, GO-TES, GO-VAL and GO-SER as well as the pristine GO. DTA curve of pristine graphene oxide exhibits two exothermic peaks at 250 °C and 500 °C, attributed to the removal of oxygen containing groups (first peak) and to carbon combustion (second peak). The exothermic peak due to decomposition of graphene layers is very sharp with high intensity while in the case of the organo-GOs the peaks are broader and are shifted at lower temperatures due to the decomposition of the organic molecules. The TGA curves of the functionalized graphene materials show a considerable weight loss in the temperature range 280-400 °C due to the decomposition of the covalently grafted organic molecules. Finally, organo-GO fillers adsorb more water than the pristine GO as derived from the weight loss up to 120 °C.

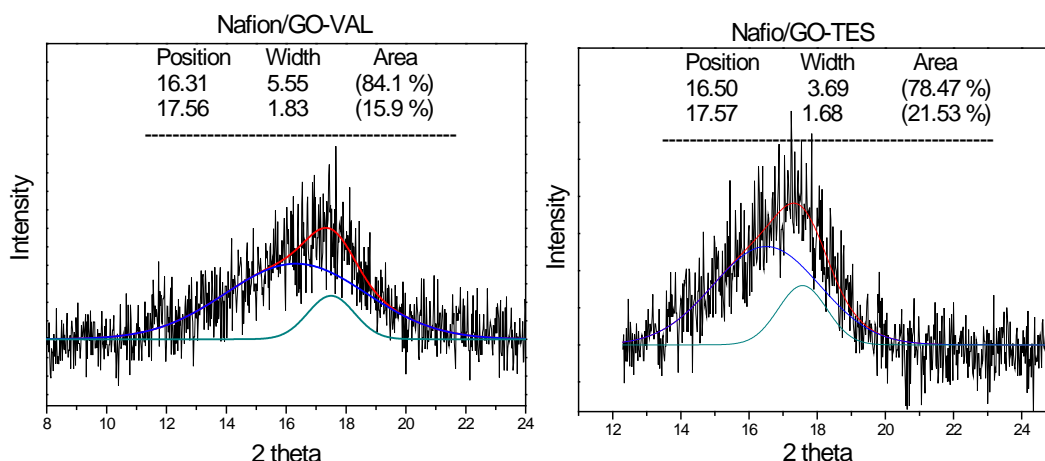




S2. Deconvolution of XRD patterns.

Figure S2 shows the deconvolution of the XRD diffractograms at $2\theta = 10\text{--}24^\circ$ of Nafion membranes. Fit curves of experimental data are deconvoluted into an amorphous ($\sim 16^\circ$) and crystalline (17.5°) scattering peaks.

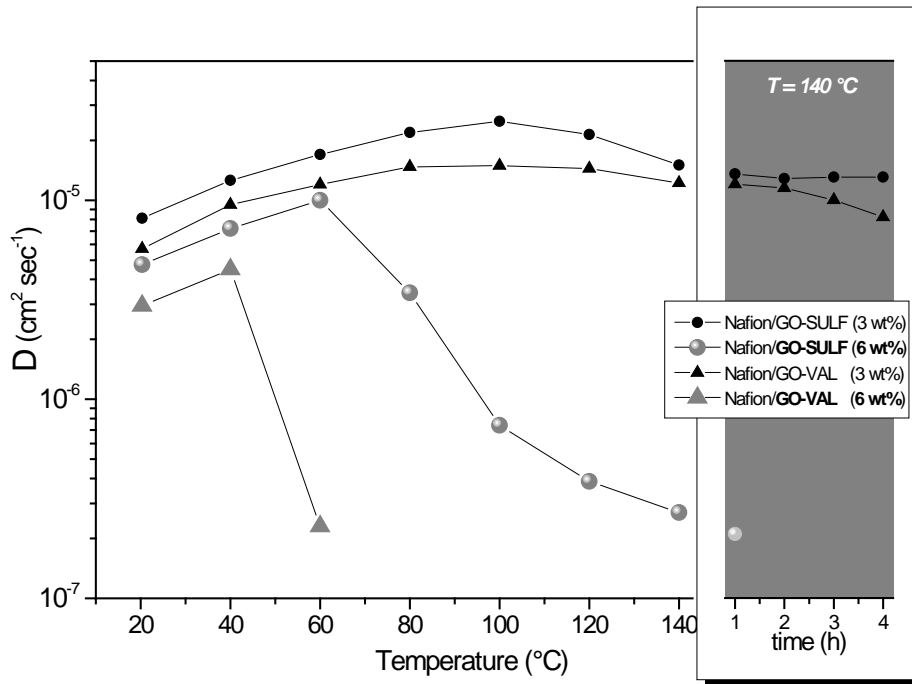




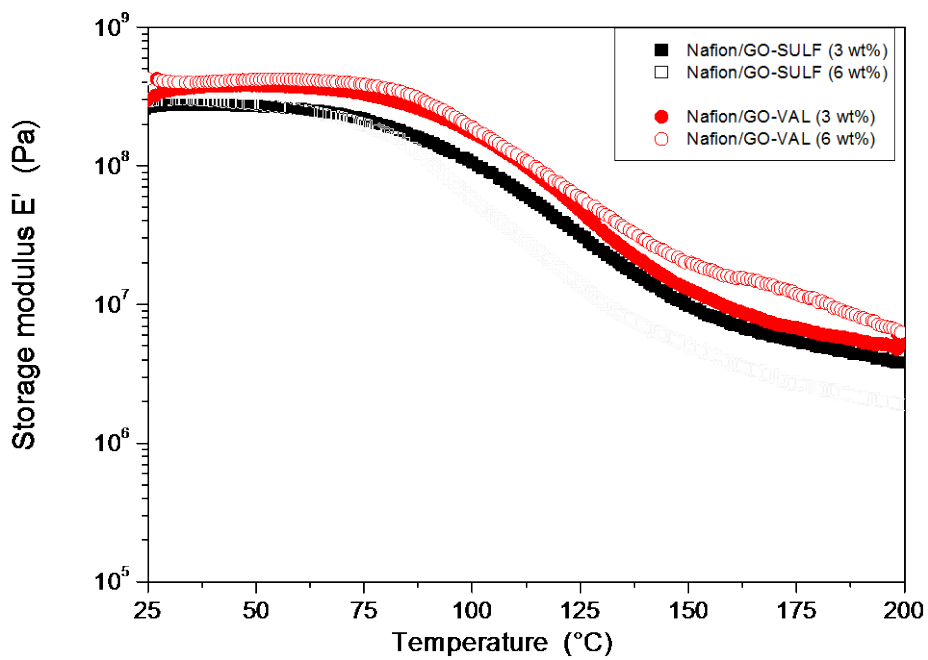
S3. Maximum water uptake of Nafion/GO-SULF and Nafion/GO-VAL nanocomposite membranes with 6 wt% filler to polymer loading.

<i>Membranes</i>	<i>Water uptakes (wt%)</i>	
	<i>6 wt%</i>	<i>3 wt%</i>
Nafion/GO-VAL	20	31
Nafion/GO-SULF	20	50

S4. Self-diffusion coefficients as function of the temperature (from 20 °C up to 140 °C) of the water confined in Nafion nanocomposite membranes loaded with 6 wt% GO-SULF and GO-VAL. For comparison, in the graph are also plotted the data of the composites with 3 wt% of loading.



S5. Storage modulus, E' , vs. temperature of Nafion/GO-SULF and Nafion/GO-VAL nanocomposites at 6 wt% filler loading in comparison with the 3 wt% loading.





Investigation of layered double hydroxide (LDH) Nafion-based composite membranes for high temperature PEFCs

Kristina Angjeli¹, Isabella Nicotera¹, Maria Baikousi², Apostolos Enotiadis², Dimitrios Gournis², A. Saccà³, E. Passalacqua³, Alessandra Carbone^{3*}

¹Department of Chemistry, University of Calabria, 87036 Rende (CS), Italy

²Department of Material Science and Engineering, University of Ioannina, GR-45110 Ioannina, Greece

³CNR-ITAE “Nicola Giordano”, Via S. Lucia sopra Contesse, 5 - 98126 Messina, Italy

Abstract

Polymer Electrolyte Fuel Cells (PEFCs) fed with H₂/air represent a highly efficient energy source at low environmental impact and it is suggested their use at temperatures above 80°C, due to an enhancement of electrochemical kinetics rates, waste heat recovery and catalyst tolerance for reformed hydrogen. For this aim, several Nafion membranes containing different fillers have been investigated. In this work, a new class of layered double hydroxide (LDH) nanoparticles as inorganic fillers was studied to be introduced in a Nafion matrix. LDHs with Mg²⁺/Al³⁺ metal cations (with metal ratio 2:1) and different countervailing anions (CO₃²⁻, ClO₄⁻, NO₃⁻) in the interlayer space were synthesised and composite membranes were prepared by a standardised casting method. Such membranes were characterised in terms of chemical-physical and electrochemical properties. In addition, a deep investigation on the water transport properties within the polymeric membranes was performed by a NMR technique. Interlayer anions affect the lambda value (mol H₂O/mol SO₃H) resulting in higher values compared to the recast Nafion, meaning a better hydration. Fuel cell tests performed in drastic conditions (1.5 abs. bar and 50%RH) at 100°C highlighted the influence of the different interlayer anions in composite membranes and a good performance was obtained for membrane containing LDH-ClO₄ with a power density of 300mW/cm² at 0.6V at 100°C.

Keywords: LDH, Nafion membranes, NMR, Proton conductivity, PEMFCs.

1. Introduction

Polymer electrolyte membrane fuel cells (PEMFCs) are promising environmentally friendly and efficient power sources for a wide range of different applications [1]. Proton conducting PEMs attract considerable attention because they are key-components in polymer electrolyte membrane fuel cells. The most widely employed proton-conducting polymer today is Nafion (a registered trademark of E. I. du Pont de Nemours and Co.). However the proton conductivity of Nafion membrane above 80 °C decreases drastically, proton conduction in turn, is dependent on hydration level of the membrane, technical need for maintaining the humidification of the membrane is established, since fuel cell operation at higher temperature (typically 130°C) and under low relative humidity is desirable. The preparation of hybrid inorganic-organic materials where a suitable filler is dispersed in a perfluorinated ionomer is one of the most promising methods to deal the drawbacks of the state-of-the-art proton-conducting membranes. Over the last years, several approaches have been attempted to improve the performance of Nafion at temperatures near and above the normal boiling point of water. Generally, Nafion conductivity is assigned to hydrated protons around the anionic sulphonic acid groups when these are fully hydrated, but the conductivity decreases when more drastic conditions than conventional ones are used, such as an increase of the temperature above 100°C produces a dehydration of membrane or a weakening of the polymeric matrix. The need In this context, great efforts have been made to develop composite films containing hygroscopic parts and/or proton conductors (hydrophilic fillers) that increase water retention and conductivity above the critical temperature. They include incorporation of a various of fillers such as hygroscopic inorganic oxide (SiO₂, TiO₂, ZrO₂), zeolite, heteropoly acids, zirconium hydrogen phosphate, layered additives such as Montmorillonite (MMT) and other clays (organomodified or not) to enhance the water retention property.[2-17]

Layered double hydroxides (LDHs) belong to a class of nano-sized materials, of anionic clay family, with a unique combination of physicochemical properties that make them valuable nanostructures in diverse fields. [18-21] A typical chemical

structure of anionic (or hydrotalcite-type) clay can be represented as $[M_{1-x}^{(II)} M_x^{(III)} (OH)_2]^{x+} [A^{m-}_{x/m}] \cdot nH_2O$, where $M^{(II)}$ is a divalent metal cation (Mg, Mn, Fe, Co, Ni, Cu, Zn, Ga) and $M^{(III)}$ is a trivalent metal cation (Al, Cr, Mn, Fe, Co, Ni, and La). A^{m-} represents an interlayer anion, such CO_3^{2-} , OH^- , NO_3^- , SO_4^{2-} or ClO_4^- . [22-24] The anionic clays structure is similar to brucite $Mg(OH)_2$ structure, and crystallize in a layer-type lattice. Such LDHs have an anion exchange capacity, which depends on the isomorphic substitution of Mg^{2+} ions by higher valence cations. As a consequence, the layers have a fixed positive charge and neutrality is obtained, for example, by hydrated anions present in the galleries. [25] The positive charge of the layers affects many fundamental properties of the LDHs, including anion exchange capacity, anion fixation, swelling ability, water holding, and high specific surface areas. These materials have the natural ability to absorb organic or inorganic guest anionic species (and even neutral polar molecules) from solutions, and it is this anion “storage” that gives unique properties to LDHs, which can be used in a wide range of applications, such as in the field of catalysis photochemistry, electrochemistry, polymerization, magnetization, biomedical science, and environmental applications. [22-23, 26-28] Moreover another important feature of LDH is their ionic/protonic conductivity, which makes them potentially useful for sensors, adsorbents, polymer stabilizers, as well as solid electrolyte materials for intermediate temperature fuel cell and other device applications. [29-30] Moreover, these synthetic layered nanostructures have been used by the scientific community as nanofillers in order to prepare polymer nanocomposite materials, enhancing mainly the thermal and mechanical properties of initial polymeric materials (such as polypropylene, polyethylene, poly(methyl methacrylate)).[31] Recently, polyelectrolyte nanocomposites with LDH have been extensively studied in order to improve the proton and methanol transport of pristine polymers. Wang et al prepared Mg-Al LDH intercalated with vinyl benzene sulfonate (VBS) anions and incorporated into polymer electrolyte based on acrylonitrile-sodium styrene sulfonic copolymer to decrease the methanol crossover, and enhance the electrical performance.[32] On the other hand, the group of Tsotsis [33] studied the addition of hydrotalcites nanoparticles in the polymer matrix of sulfonated – Polyetherethercetone (SPEEK), preparing membranes with low cost, increasing the proton conductivity and decreasing significantly the methanol permeability to 4.4×10^{-7} - 6.24×10^{-7} cm^2/s , a value one order of magnitude lower than this of the pure polymer ($\sim 2.4 \times 10^{-6}$ cm^2/s).

Lee and Nam introduced LDHs nanoparticles into a Nafion membrane in order to improve the direct methanol fuel cell (DMFC) performance at high feed concentrations of methanol. [34-35]

In this work, high proton conducting Nafion nanocomposite membranes were developed using Mg^{2+}/Al^{3+} layered double hydroxides as nanofillers. LDHs with a 2:1 Mg^{2+}/Al^{3+} metal ratios and various interlayer anions (CO_3^{2-} , ClO_4^- , NO_3^-) were prepared and incorporated in Nafion matrix, in order to evaluate the effect of nanofiller's chemical composition in the performance of the final nanocomposite membranes. Composite membranes were synthesized by solution intercalation with 3 wt% LDH loading (with respect to the polymer). The pristine LDHs and the nanocomposite membranes were investigated by a combination of powder X-ray diffraction, FTIR spectroscopy and thermal analysis (DTA/TGA). The characteristics of the membranes were studied mainly, in terms of transport properties by NMR spectroscopy, in order to study the water dynamics inside the electrolyte membranes, which is one of the key aspects in the evaluation of these materials.[36-40] Moreover, physico-chemical characterizations were carried out to investigate the effect of the filler-polymer interaction at higher temperature than conventional ($80^\circ C$), in particular the water retention and distribution in such operative conditions. Membrane electrode assembly (MEA) testing is the principal means of characterization pertaining to its electrochemical performance and proton conductivity.

2. Experimental

2.1 Synthesis of inorganic fillers

LDH nanofillers have been synthesized by co-precipitation of Mg^{2+} and Al^{3+} salts, in the presence of the appropriate anion, using an aqueous solution of sodium hydroxide. The $Mg^{2+}:Al^{3+}$ metal ratio was adjusted to 2:1, in particular, in 100ml of aqueous solution containing $Mg(NO_3)_2 \cdot 6H_2O$ (0.05 mol), $Al(NO_3)_3 \cdot 9H_2O$ (0.025 mol) and sodium salt of carbonate or nitrate anions (Na_2CO_3 or $NaNO_3$: 0.045mol) was added drop wise an aqueous solution of NaOH (2.5M) until pH value reached to 10. For the synthesis of LDH with perchlorate as interlayer anions, an aqueous solution (100 ml)

containing $\text{Mg}(\text{ClO}_4)_2$ (0.05 mol) and $\text{Al}(\text{ClO}_4)_3 \cdot 9\text{H}_2\text{O}$ (0.025 mol) was used, followed by the addition of aqueous 2.5 M NaOH solution (pH=10). The resulting precipitated LDH materials were stirred at 60 °C for 24 h and subsequently separated by centrifugation, washed several times with water and finally were dried in air at 80°C for 24 h. In the case of nitrate and perchlorate anions, the synthetic procedure was done under nitrogen gas flow and using decarbonated-deionized water.

2.2 Membranes Preparation

For membrane manufacture, a 5wt% Nafion[®] solution (Ion Power LQ1105) was used. The original solvents were completely eliminated by a rotary evaporator, in order to obtain a dry residue. Successively, it was diluted in dimethylformamide (DMF) as a solvent with a final concentration of 10 wt%. For composite membranes preparation a nominal amount of 3 wt% of filler was added to the polymeric solution before the reconcentration step. The filler was previously dispersed in the same solvent of the polymer under magnetic stirring, for about 18 h at room temperature. The solutions were then slow reconcentrated until a suitable viscosity was reached to be stratified with a doctor-blade. The obtained film was dried at 80°C for 3h to eliminate the solvent.

All the prepared membranes underwent a thermal treatment up to 155°C to increase the crystallinity of the polymer and consequently the mechanical properties.

All composite membranes produced by casting were subsequently treated by rinsing in: (i) HNO_3 solution (1:1 vol) at 80°C for 30 min. to oxidize the organic impurities, (ii) boiling in deionized H_2O for 15 min., (iii) H_2SO_4 (1 M) at 80°C for 30 min to remove any metallic impurities, (iv) boiling in deionized H_2O for 15 min three times to remove excess acid. According to McMillat et.al[41] an ulterior purification procedure was performed in order to ensure the removal of paramagnetic contaminants which are particularly damaging to an NMR experiment, such as the presence of copper that we found by Electron Paramagnetic Resonance analysis. By this procedure membranes were soaked in EDTA solution (0.001M) for 1 day after followed by a thorough rinse. Then soaked in 2 M HCl at a temperature of 80°C for 2 h followed by boiling in fresh distilled–deionized water to remove any residual acids and again repeated the treatment with EDTA. Finally, rinsing in boiled deionized water three times to remove residual EDTA and stored at room temperature at fully hydrated state.

In Table 1 the prepared membranes are reported.

Table 1. Developed membrane characteristics

Membrane	Filler	Thickness, μm
Nrecast	-	55
NLDH-NO3	Mg/Al-LDH-NO ₃ ²⁻	71
NLDH-CO3	Mg/Al-LDH-CO ₃ ²⁻	64
NLDH-CIO4	Mg/Al-LDH-CIO ₄ ⁻	47

2.4 Electrodes and MEAs Preparation

The electrodes were produced by spraying [42] the catalytic ink onto a commercial Gas Diffusion Layer (SGL Sigracet-24BC). A 50% Pt/C (Alfa Aesar) was utilised as an electrocatalyst. The same Platinum (Pt) loading of 0.5 mg cm⁻² for anodes and cathodes was used. Membrane-Electrode assemblies (MEAs) were manufactured by hot-pressing the electrodes onto the membrane at 125°C and 20kg/cm².

2.5 Characterization of nanofillers

The X-ray powder diffraction data were collected on a D8 Advanced Bruker diffractometer by using CuK_a (40 kV, 40 mA) radiation and a secondary beam graphite monochromator. The patterns were recorded in a 2-theta range from 2° to 60°, in steps of 0.02° and counting time 2sec per step. Infrared spectra were measured with a FT-IR 8400 spectrometer, in the region of 400-4000 cm⁻¹, equipped with a DTGS detector. Thermogravimetric (TGA) and differential thermal (DTA) analysis were performed using a Perkin Elmer Pyris Diamond TG/DTA. Samples of approximately 5 mg were heated under air from 25 to 850 °C, at a rate of 10 °C/min.

2.6 Membranes Characterization

2.6.1. Self-diffusion coefficient measurements

NMR measurements were performed on a Bruker NMR spectrometer AVANCE 300 Wide Bore working at 300 MHz on ¹H. The employed probe was a Diff30 Z-diffusion 30 G/cm/A multinuclear with substitutable RF inserts. The spectra were obtained by a single $\pi/2$ pulse sequence. The NMR pulsed field gradient spin-echo (PFG-SE) method [43] was used to measure self-diffusion coefficients. This technique consists of two rf

pulses, Hahn-echo sequence ($\pi/2-\tau-\pi$), with two identical pulsed-field gradients, the first applied between the 90° and 180° rf pulse (during the dephasing) and the second after the 180° rf pulse (during the rephasing) but before the echo. Following the usual notation, the pulsed-field gradients have magnitude g , duration δ , and time delay Δ (different from the degree of ionic association). The attenuation of the echo amplitude is represented by the Stejskal-Tanner equation:

$$A(g) = A(0) \exp[-\gamma^2 g^2 D \delta^2 (\Delta - (\delta/3))]$$

where D is the self-diffusion coefficient and γ is the nuclear gyromagnetic ratio and $A(0)$ is the amplitude of the echo at $g = 0$. Note that the exponent in the equation is proportional to the mean-squared displacement of the molecules over an effective time scale ($\Delta - (\delta/3)$). For the investigated samples, the experimental parameters, Δ and δ , are 10 and 1 ms, respectively. The gradient amplitude, g , varied from 10 to 600 G cm⁻¹. In this condition the uncertainty in the self-diffusion measurements is $\sim 3\%$.

Longitudinal relaxation times (T_1) of water were measured by the inversion-recovery sequence ($\pi-\tau-\pi/2$). Both self-diffusion and T_1 measurements were conducted by increasing temperature step by step from 20 to 130 °C, with steps of 20 °C, and leaving the sample to equilibrate for about 15 min. Prior to the NMR measurements, membranes were dried in oven, weighed and then immersed in distilled water at room temperature. Upon being removed from the water they were quickly blotted dry with a paper tissue (to eliminate most of the free surface liquid). The water content value was determined using a microbalance and recorded as described in the following formula:

$$Wup, \% = [(m_{wet} - m_{dry}) / m_{dry}] \cdot 100$$

At this point the membranes were loaded into a 5 mm NMR Pyrex tube and hermetically sealed.

2.6.2. Membranes Ion Exchange Capacity (IEC)

The acid-base titration was performed to determine the membrane Ion Exchange Capacity (IEC, meqSO₃H/g dry polymer) and was based on the neutralization of H⁺ ions becoming from the acid SO₃H groups. The experimental procedure is described elsewhere[44]. The IEC was calculated using the following formula:

$$IEC = (V_{tit} \cdot [M]) / m_{dry}$$

where: IEC = Ion Exchange Capacity (meq $-\text{SO}_3\text{H}/\text{m}(\text{g})$); V_{tit} = titrant volume (ml); $[M]$ = titrant concentration (M); m_{dry} = dry mass of the sample (g);

2.6.3. Membranes Water Uptake, λ and dimensional variations

The membrane water retention (Wup,%) was calculated as reported above, at three different temperatures (30°C, 80°C and 95°C). The dry mass (m_{dry}), was measured by drying the sample in a vacuum oven at 80°C for 2 h. The wet mass (m_{wet}) was determined after immersion of the dried sample in distilled water at 30°C for 24 hours, while at 80°C and 95°C for 2 h.

The λ value, expressed as the number of H₂O moles per SO₃H moles, was calculated by the ratio between water uptake and IEC.

The dimensional variations were calculated at the same conditions of water uptake, by measuring the thickness, the width and the length variation between the dried and wet samples.

2.7. Electrochemical methods

2.7.1. Proton Conductivity

The proton conductivity was measured in the temperature range 80-120°C at reduced humidification (50% RH) using a commercial cell (Bekktech)[44]. The measurements were carried out in the longitudinal direction of the sample with a four-probes technique and calculated using the formula:

$$\sigma = L/(R \cdot W \cdot T)$$

where: L = 0.425 cm, fixed distance between the two Pt electrodes; R = resistance in Ω ; W = sample width in cm; T = sample thickness in cm.

2.7.2. Fuel cell tests

The prepared MEAs were tested in a 25 cm² commercial single cell in a range of temperature 80°C-100°C with humidified H₂/air gases at 1.5 abs. bar and 50%RH. The polarisation curves were performed in a galvanodynamic mode with a constant stoichiometry. The gas fluxes were fixed at 1.5 times and 2 times the stoichiometric value for the fuel and the oxidant, respectively. The cell resistance was measured at the

open circuit voltage (OCV) with an Agilent milliohmmeter (mod. 4338B) at a frequency of 1 KHz.

Electrochemical impedance spectroscopy (EIS) was performed by using a potentiostat/galvanostat (AUTOLAB PGSTAT30) equipped with a frequencies response analyzer (FRA module) and a 20A BOOSTER. All impedance measurements were performed in the potentiostatic mode of fuel cell operation at a constant potential of 650mV. The impedance spectra were obtained varying the frequency of the voltage perturbation signal from 0.1 Hz to 100 kHz, by using amplitude of 10mV for the perturbing signal.

3. Results and Discussion

3.1. Structural characterization of the fillers

The structure of layered double hydroxides was characterized using powder X-ray diffraction and FT-IR spectroscopy. Figure 1a shows the XRD patterns of Mg/Al-LDH with Mg²⁺/Al³⁺ ratio 2:1 and CO₃²⁻, NO₃⁻ or ClO₄⁻ as interlayers anions. The diffraction patterns exhibit the characteristic (00l) reflections of LDHs layers such as (003) and (006) which are related to the interlayer space of LDH. The distance between two consecutive layers is defined by the size of ions presented in the interlayer space, and calculated from the basal spacing d₀₀₃ by subtracting the thickness of a single layer (0.48 nm)[23], from the XRD patterns of Mg/Al-LDH with CO₃²⁻, NO₃⁻ and ClO₄⁻ interlayer anions, where the basal spacing d₀₀₃ is 0.75, 0.88 and 0.92 nm, respectively. The corresponding interlayer space is equal to 0.27, 0.40 and 0.44 nm, in that order, confirming the presence of the different anions into the LDH interlayers.

Figure 1b displays the FT-IR spectra of Mg/Al-LDH with Mg²⁺:Al³⁺ ratio 2:1 and different interlayer anions. All spectra show two broad absorption bands: one at the frequency region of 3000-3700 cm⁻¹ due to stretching vibration modes of hydroxyl groups of LDH's layers and a second at the frequency region of 1635cm⁻¹ due to bending vibration modes of interlayer water molecules.[23, 45-46] In the spectrum of LDH with CO₂³⁻ as interlayer anions, there is also a shoulder at 3050 cm⁻¹ due to the stretching vibration modes of hydroxyl groups of the interlayer water molecules which

interact with the carbonate ions.[45, 47] This shoulder does not exist in the spectra of LDH with nitrates and perchlorates anions, which are not only larger in size than the carbonates, but they have a lower valence [48] resulting in weaker interactions with the interlayer water molecules. Moreover, in the low frequency region, at 500-1000 cm^{-1} , in all spectra appear absorption bands due to the vibration modes of hydroxyl groups that are mainly influenced by the divalent and trivalent metal in the LDH's layer structure (see Table 2). [45] Finally, the presence of the different interlayer anions into the LDH structure can be revealed by the presence of the characteristic bands of the corresponding interlayer anions in the spectra of LDHs (CO_3^{2-} : 1367, 871, 663, ClO_4^- : 1145, 1112, 1090, NO_3^- : 830, 1384 cm^{-1})[47]. The correlative attribution of vibrational peaks detected for all LDH is summarized in Table 2. In conclusion, the combination of XRD and infrared results confirms the successful synthesis of LDH nanofillers having various compensating interlayer anions.

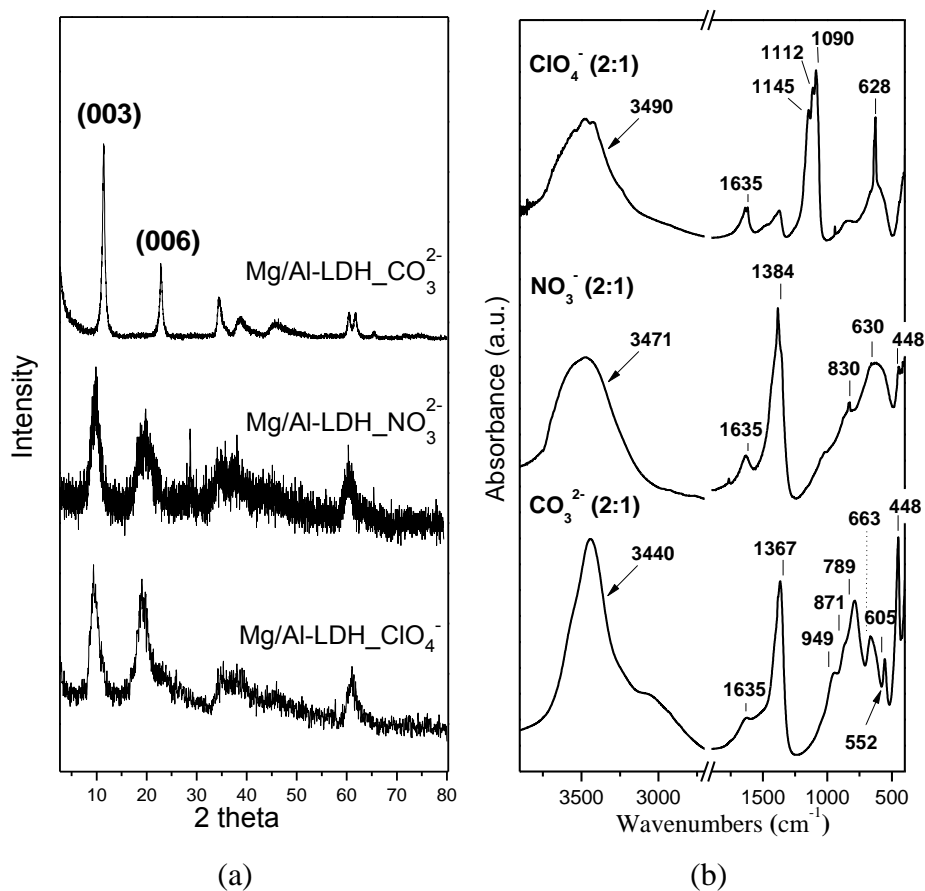


Figure 1: (a) XRD patterns of Mg / Al-LDH with Mg^{2+}/Al^{3+} ratios 2:1 and different interlayer anions (CO_3^{2-} , NO_3^- and ClO_4^-). (b) IR spectra of 2:1 Mg/Al-LDH with different interlayer anions.

Table 2: FTIR assignments of Mg/Al-LDHs with the different interlayer anions.

	Mg/Al-LDH-CO_3^{2-}	Mg/Al-LDH-ClO_4^-	Mg/Al-LDH-NO_3^-
Mg-OH	605	628	630
Al-OH	949,789,552,448	946	448
Anions	CO_3^{2-} : 1367, 871, 663	ClO_4^- : 1145, 1112, 1090	NO_3^- : 830, 1384

In order to verify the presence of the interlayer anions of Mg/Al-LDH in the composite membranes, after their treatment with the strong acids during the preparation procedure of the membranes, in Figure 2 are shown the FT-IR spectra of filler-free Nafion and N-LDH membranes, with NO_3^- ions, after the treatment of the nanocomposite membrane with acids (HNO_3 and H_2SO_4). The presence of the characteristic bands of NO_3^- (830, 1384 cm^{-1}) indicates that these anions did not exchange and remained into the interlayer space of Mg/Al-LDH.

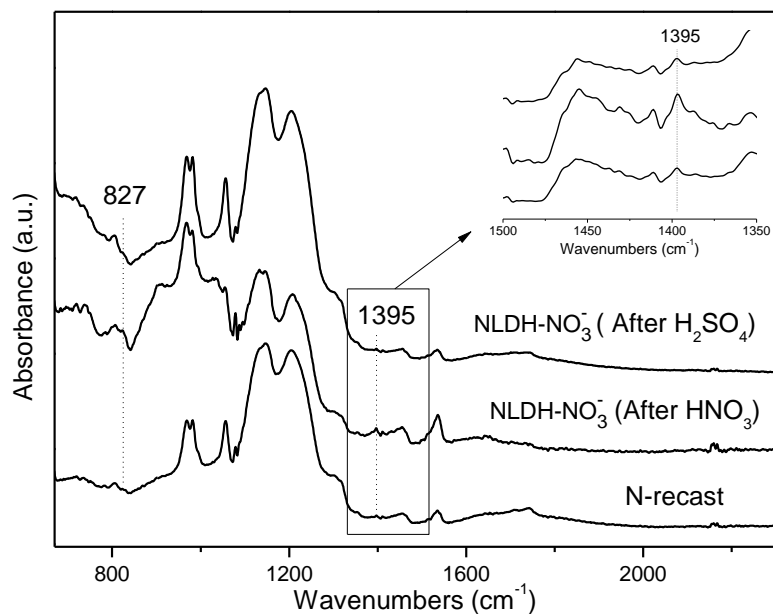


Figure 2: FTIR spectra of Nafion filler free membrane,, Nafion-Mg/Al-LDH membrane with metal ratio 2:1 and the NO_3^- ions after the treatment with strong acids, HNO_3 and H_2SO_4

3.2. Analysis of the nanocomposite membranes

Optimization of the water uptake and polymer swelling is essential for successful operation in a fuel cell at high temperatures. LDH-composite membranes showed a slightly higher water uptake than the recast Nafion, which can be attributed to the hydrophilicity of LDHs due to the hydroxyl groups present in the layered structure. Thermogravimetric curves were used to determine the amount of adsorbed water and in addition to reveal the homogenous distribution of the Mg/Al-LDH platelets in the Nafion matrix. TGA results (Figure 3), show a higher water loss (17 wt%) of the N-LDH(NO_3^-) from 20 to 120 °C, compared to the recast membrane (10 wt.%), indicating the higher ability of the nanocomposite to retain water. Furthermore, nanocomposite displays a higher thermal resistance than the recast Nafion since the polymer decomposition is shifted to higher temperatures. This is due to the strong interactions between the polymer chains and the nanoparticles which in fact provides evidence for

the homogeneous dispersion of the Mg/Al-LDH platelets in the polymeric matrix.[49-50] Similar results were obtained also for the other two composites.

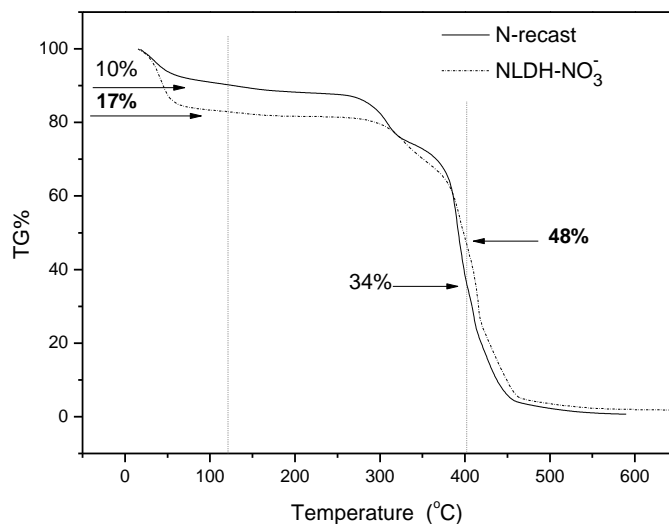


Figure 3: TGA curves of pure Nafion membrane and Nafion-Mg/Al-LDH nanocomposite membrane with 2:1 metal ratio and NO_3^- ions, in hydrated state.

Further information about the water distribution inside the membranes could be provided by λ data, which express the water molecules coordinated per sulphonic groups.

In Table 3 the IEC values for the composite membranes compared to the Nafion recast are reported. The insertion of filler produces a reduction of IEC values because no additive exchangeable protons are introduced. Moreover, the λ values of N-LDH membranes are more sensitive to the temperature increase than N-recast, depending on the LDH anions. In particular, at 95°C the λ values increase as follows: $\text{NO}_3^- < \text{ClO}_4^- < \text{CO}_3^{2-}$. This behavior could be correlated to the different capability of the interlayer anions to coordinate water molecules. These data are quite in accordance with NMR data as it is shown below, taking into account the different technique of measurements, e.g. λ measurements are performed in liquid water.

Table 3: Ionic exchange capacity and λ variations at different temperatures for composite and pure recast Nafion membranes

Membrane	IEC	λ 30°C	λ 80°C	λ 95°C
----------	-----	----------------	----------------	----------------

	meq/g	mol H ₂ O/SO ₃ H	mol H ₂ O/SO ₃ H	mol H ₂ O/SO ₃ H
N-recast	1.28	9	18	19
NLDH-NO₃	1.27	9	19	22
NLDH-CO₃	1.16	12	24	35
NLDH-CIO₄	1.19	13	27	32

The introduction of the filler also affects the water uptake and dimensional variations, in particular at high temperature, as shown in Figure 4. Obviously, the water uptake values are in accordance with the λ data. A different trend is visible for the volume percentage variation, in fact the values increase in the following order: NLDH-CO₃<NLDH-NO₃<N-recast<NLDH-CIO₄. This means that the anions of the filler entrap the water molecules in a different way, in accordance to the NMR data, that are discussed below. In fact, the membrane with the highest D (NLDH-CO₃) retains more water but the lowest volume percentage is measured, meaning that the water is predominantly bounded to the filler. On the contrary, in the membrane NLDH-CIO₄, with the lowest D but similar water uptake of NLDH-CO₃, the filler weakly coordinates the water molecules. This behavior indicates that the water molecules not bounded to the filler are mainly located in the polymer matrix, causing an increase of the volume % at the critical temperature of 95°C.

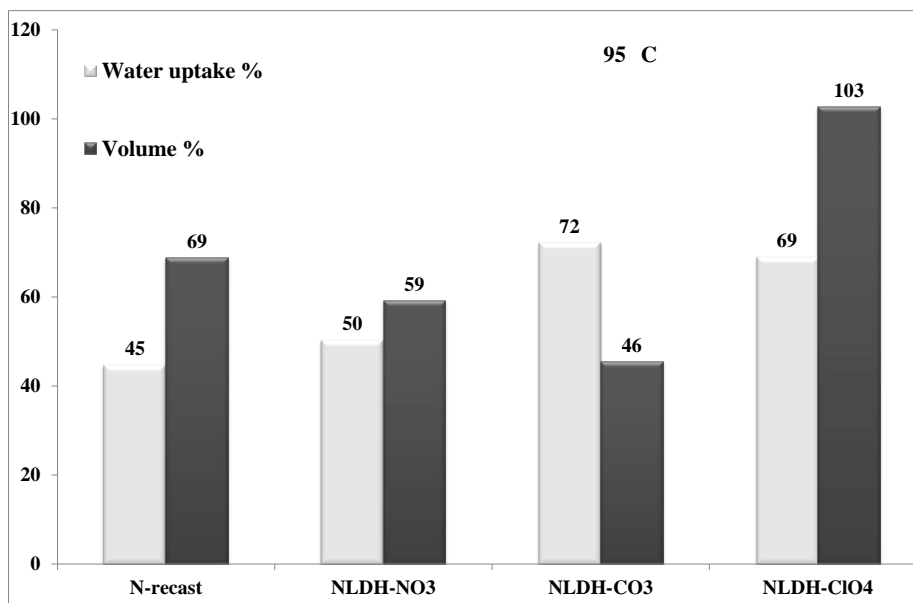


Figure 4: Chemical-physical variation at 95°C for composite membranes compared to filler free one.

PFG-NMR technique was used in this study to investigate the transport properties of the water absorbed in the nanocomposite electrolyte membranes in order to consider the effect of the LDH materials as hygroscopic nanofillers inside the Nafion polymer.

Figure 5 displays the plot of the water self-diffusion coefficients measured on completely swollen membranes (at the maximum water uptake, reported in the legend, achievable from each one at room temperature) in the temperature range 20-130 °C. The graph compares the diffusivity of water measured in the filler-free Nafion and in the composites obtained by dispersing 3 wt% of Mg/Al-LDH with the three different intercalated anions, CO₃²⁻, NO₃⁻, ClO₄⁻.

The effect of the intercalated anion seems to be a key factor not only, as previously seen, for the water uptake of the membranes, but mainly for the ability of the composite to keep in a hydrated state in the region of high temperature.

For example, the composite NLDH-CIO₄ has shown the highest degree of water absorption (27 wt% compared to 21 wt% of the recast Nafion), but this does not correspond to an equally high diffusion; in particular, at a temperature above 80 °C the diffusion coefficient collapses to a greater extent than in the recast Nafion, and at 130 °C there is no longer a sufficient NMR signal to be able to perform a measurement.

Different behavior was instead obtained for the other two composites: the NLDH-CO₃ has the highest diffusion throughout the temperature range 20-100 °C, while NLDH-NO₃ is much like the recast Nafion. At 130 °C the diffusion coefficients of water are almost identical, however, leaving the membranes for 1 hour at this temperature (obviously without any source of humidification, if not that of vapor present in the NMR tube), on the filler-free Nafion we cannot see any proton signal while the two composites have a weak signal but sufficient for the measurement; even NLDH-NO₃ after 2 hours there is still mobile water in the membrane with a coefficient D unaltered. Clearly, the water present at 130 °C is not bulk water but strongly bounded water to the hydrophilic groups of the system, sulphonic groups of the polymer and especially the hydroxyl groups contained in the interlayer space of LDH. Nitrate and carbonate anions show to have a superior ability to retain water than perchlorate anion, probably due to its greater charge delocalization that, as a consequence, affects the microstructure of the complex system “filler-polymer”.

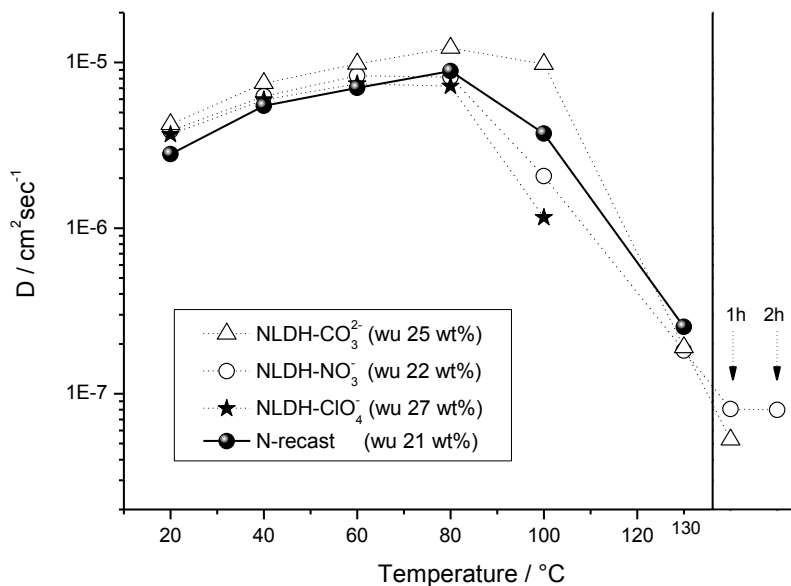


Figure 5: Self-diffusion coefficients of water confined in the LDH-composite membranes with different interlayer anions, NO₃⁻, CO₃²⁻, ClO₄⁻, from 20 °C up to 130 °C. Filler-free Nafion is also reported for comparison.

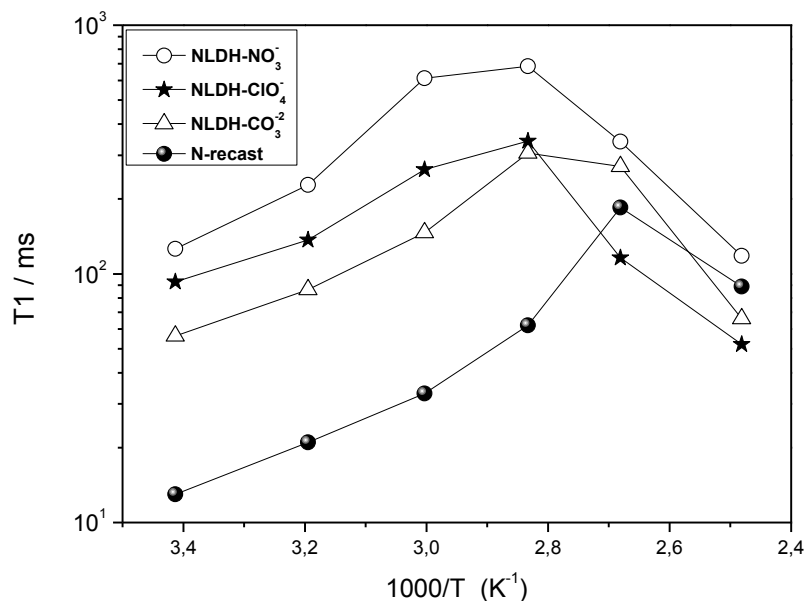


Figure 6: Arrhenius plot of water longitudinal relaxation times (T_1) measured in the temperature range from 20 °C up to 130 °C for recast Nafion and Mg/Al-LDH composite membranes at the maximum water uptake

Longitudinal (or spin-lattice) relaxation time (T_1) is affected by the strength of the spin interactions and the correlation time of the molecular tumbling (rotational diffusion). The stronger the interaction, the shorter the T_1 . In liquid samples with low viscosity, the shorter the tumbling correlation time, the longer relaxation T_1 . Because the molecular correlation time τ_c depends on temperature, when doing variable temperature measurements, one often observes a minimum in T_1 when $\omega\tau_c \sim 1$, where ω is the NMR frequency.[51] However, in the extreme narrowing limit (very fast motion and very short correlation time), i.e. when $\omega\tau_c \ll 1$, well above the T_1 minimum, higher T_1 values reflect more facile molecular rotational and translational motion on a time scale comparable to the reciprocal of ω (~1 ns).

Figure 6 reports the Arrhenius plot of the longitudinal relaxation times (T_1) of water collected on the nanocomposite membranes and recast Nafion in the same diffusion temperature range, 20-130 °C. The relaxation times of water in the composites are longer compared to the polymer recast and this is related to the greater hydration due to the presence of a larger number of hydrophilic sites. The T_1 gives a good discrimination

on the intercalated anion: the nitrate followed by perchlorate, and finally the carbonate. The nitrates and perchlorates ions are not only larger in size than the carbonates, but they have a lower valence [52] resulting in weaker interactions with the interlayer water molecules, additionally, the divalent anions are more strongly held in the interlayer than the monolayer anions [53]. This entails higher roto-translational degrees of freedom of the molecules of water in composites nitrates and perchlorates, while the double negative charge of the carbonate stiffens the molecular conformations and makes movements slower lowering the T_1 .

It is worth making a further observation at high temperatures, above 100 °C, where the T_1 decreases as a result of the evaporation of a certain amount of water, thus the measured times are related to the molecules more "linked" to the acid sites of the system. The composite with the perchlorate shows a more drastic reduction of the T_1 associated with a significant loss of hydration water, as is also apparent from the diffusion and spectral signal intensity, and the remaining water molecules are strongly interacting with the anions of the filler and consequently very little mobile.

For all membranes, the proton conductivity increases up to 100°C and then a different behavior is recorded (Figure 7). In fact, composite membranes decrease the conductivity by increasing the temperature, while a further increase is revealed only for the N-recast. This behavior could be associated to the different water distribution inside the membranes, as above discussed for water uptake and volume % variations.

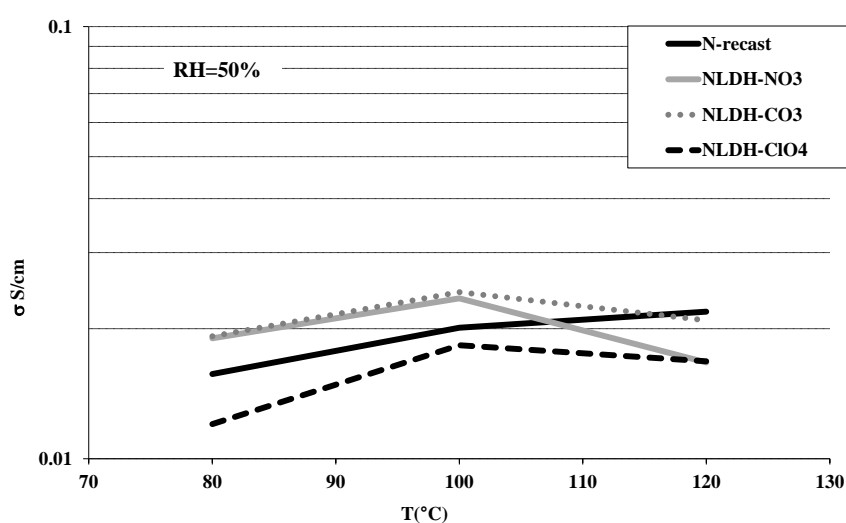


Figure 7: Proton conductivities comparison at low humidity level as a function of temperature

The polarisation curves at 80°C and 100%RH are reported in Fig.8 a. It is highlighted that the performance is quite similar for all the samples. In fact, in these optimal operative conditions for this kind of polymer, the inorganic introduction effect is negligible respect to the polymeric matrix.

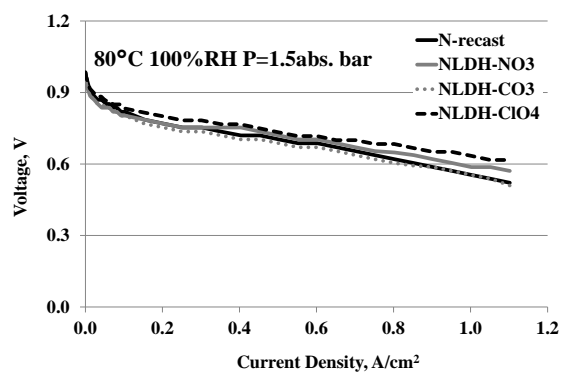


Figure 8a

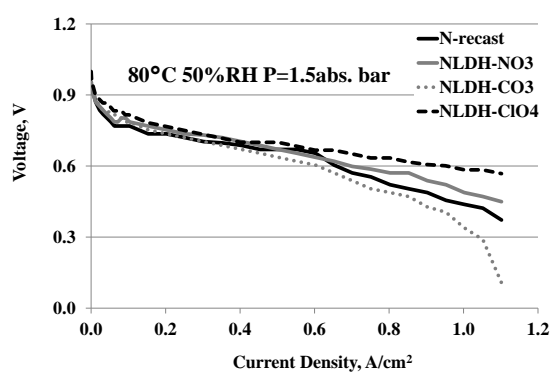


Figure 8b

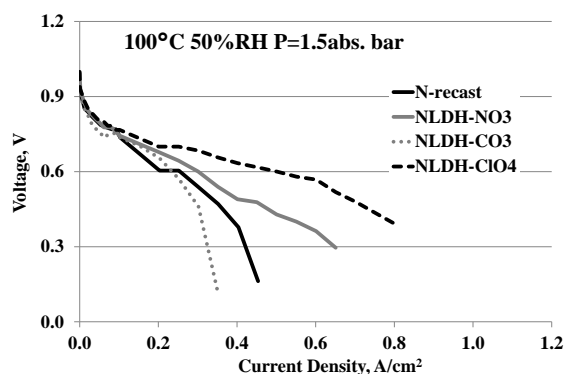


Figure 8c

Figure 8 a-c: Polarisation curves at fixed stoichiometry in the temperature range 80°C-100°C with low pressure and humidification

When the humidification is reduced until to 50%RH the effect of the filler presence becomes more evident (Figure 8-b). The NLDH-CIO4 presents a similar performance than the previous operative conditions, while the other samples reduce their performance, in particular the NLDH-CO3.

A further increase of temperature (Figure 8c) enhances this behaviour, in fact all the performance are reduced, in particular a drop of the performance for NLDH-CO3 is

recorded, with a limiting current of 350 mA/cm². The other two composite membranes show better performance than N-recast, meaning that the filler introduction has a beneficial effect in these drastic conditions. This trend is in accordance with the cell resistance (R) and open circuit voltage (OCV), as reported in tab.4

Table 4: Electrochemical parameters for prepared membranes obtained in fuel cell operative conditions

Membrane	80°C 100%RH		80°C 50%RH		100°C 50%RH	
	R _{cell} (Ω cm ²)	OCV (V)	R _{cell} (Ω cm ²)	OCV (V)	R _{cell} (Ω cm ²)	OCV (V)
N-recast	0.115	0.985	0.475	1	0.825	0.968
NLDH-NO3	0.099	0.985	0.533	0.952	0.43	0.976
NLDH-CO3	0.18	0.985	1.05	0.985	0.602	0.935
NLDH-CIO4	0.134	0.982	0.205	0.999	0.410	0.982

In any case the NLDH-CIO4 shows the best performance at each temperature, with a power density of 300mW/cm² at 0.6V at 100°C. As expected from the ex-situ membranes characterisations, the NLDH-CO3 would have to be the most promising membrane, but the fuel cell electrochemical tests contradict this expectation. This evidence could be due to instability of the filler containing CO₃²⁻ as anions in this electrochemical environment. As a consequence, the stability of the membrane could be affected, justifying a progressive reduction of single cell performance.

In tab.5 the comparison between the ex-situ (Bekktech cell) and in-situ (EIS in single cell) proton conductivity in different operative conditions is reported.

It is evident that the proton conductivity at 80°C and full humidification corresponds to the ex-situ measurement at the same temperature and 50%RH, for all membranes except for NLDH-CIO4 that is lower. Comparing the in-situ and ex-situ results at the same operative conditions a discrepancy in the data is more evident. In fact, the in-situ conductivity is always lower than ex-situ, due to the different technique of measurements. Moreover, these results seem to indicate that a lower humidification

level reaches the membrane during fuel cell operation. This effect could be caused by a not optimised electrodic structure for working at low humidification level[54]. Moreover, it is worthy to be noticed that, as reported in literature [55] all the ex-situ measurements do not always predict the fuel cell performance. In fact, despite ex-situ measurements (water uptake, water diffusion coefficients, proton conductivity, etc.) supply important information on the basic membrane properties other parameters (current density, gas composition, cell design, etc.) affect the performance under fuel cell operation.

Table 5: In-situ and Ex-situ proton conductivity data for developed membranes at different temperatures and humidification.

Membrane	method	Proton conductivity (mS/cm)		
		80°C 100%RH	80°C 50%RH	100°C 50%RH
N-recast	In-situ	15.7	11.6	7.59
	Ex-situ	-	15.7	20.1
NLDH-NO3	In-situ	18.9	8.11	11.4
	Ex-situ	-	19.0	23.5
NLDH-CO3	In-situ	19.7	9.48	18.3
	Ex-situ	-	19.2	24.3
NLDH-CIO4	In-situ	23.5	20.9	8.95
	Ex-situ	-	12.0	18.3

4. Conclusions

Composite Nafion membranes containing layered double hydroxides (LDHs) with different compositions as inorganic fillers, have been prepared and investigated for PEM fuel cells applications. Structural characterization of nanofillers and hybrid membranes proves the successful synthesis of Nafion-LDH nanocomposites. The chemical-physical characteristics of the used filler define the properties of the

corresponding composite membranes; in fact, the λ values at 95°C are higher than N-recast membrane, indicating an improved capability to coordinate water molecules for composite membranes. In particular, the different fillers possess a diverse capability to coordinate water molecules in relation to the interlayer anion: the carbonate ion has a higher valence resulting in stronger interactions with the interlayer water molecules. The water uptake values are in accordance with the λ data, while the volume variation data have a different trend and are in accordance to the NMR data. The discussed trend indicates that the water molecules not bounded to the filler are mainly located in the polymer matrix, causing an increase of the volume percentage at the critical temperature of 95°C and strongly influencing the proton conductivity. Furthermore the study of the water transport mechanism showed that some nanocomposite membranes possess a noteworthy behavior at 130 ° C retaining a small amount of "still mobile" water for a couple of hours without any further humidification.

Fuel cell tests in conventional operative conditions are less affected by the filler introduction, which, instead, strongly affects the performance in drastic conditions and in relation to the used interlayer anion. On the basis of the above discussed results, the most promising membrane seems to be the NLDH-ClO₄ that supplies a power density of 300mW/cm² at 0.6V and 100°C.

References

- [1] P. Jannasch, *Current Opinion in Colloid and Interface Science* 8 (2003) 96-102.
- [2] I. Nicotera, A. Enotiadis, K. Angjeli, L. Coppola and D. Gournis, *International Journal of Hydrogen Energy* 37 (2012) 6236-6245.
- [3] I. Nicotera, A. Enotiadis, K. Angjeli, L. Coppola, G. A. Ranieri and D. Gournis, *J Phys Chem B* 115 (2011) 9087-9097.
- [4] A. Enotiadis, K. Angjeli, N. Baldino, I. Nicotera and D. Gournis, *Small* 8 (2012) 3338-3349.
- [5] I. Nicotera, T. Zhang, A. Bocarsly and S. Greenbaum, *Journal of Electrochemical Society* 154 (2007) B466-B473.
- [6] I. Nicotera, A. Khalfan, G. Goenaga, T. Zhang, A. Bocarsly and S. Greenbaum, *Ionics* 14 (2008) 243-253.
- [7] K. T. Adjemian, S. J. Lee, S. Srinivasan, J. Benziger and A. B. Bocarsly, *J Electrochem Soc* 149 (2002) A256-A261.
- [8] K. T. Adjemian, S. Srinivasan, J. Benziger and A. B. Bocarsly, *Journal of Power Sources* 109 (2002) 356-364.
- [9] V. Baglio, A. S. Aricò, V. Antonucci, I. Nicotera, C. Oliviero, L. Coppola and P. L. Antonucci, *Journal of Power Sources* 163 (2006) 52-55.
- [10] G. Alberti, M. Casciola, L. Massinelli and B. Bauer, *Membr Sci* 185(1) (2001) 73-81.
- [11] A. Saccà, A. Carbone, E. Passalacqua, A. D'Epifanio, S. Licocchia, E. Traversa, E. Sala, F. Traini and R. Ornelas, *Power Sources* 152 (2005) 16-21.

- [12] A. Saccà, A. Carbone, R. Pedicini, M. Marrony, R. Barrera, M. Elomaa and E. Passalacqua, *Fuel Cells* 8 (2008) 225-235.
- [13] A. Saccà, R. Pedicini, A. Carbone, I. Gatto and E. Passalacqua, *ECS transaction* 11 (2007) 1553-1557.
- [14] A. Saccà, I. Gatto, A. Carbone, R. Pedicini and E. Passalacqua, *Journal of Power sources* 163 (2006) 47-51.
- [15] A. S. Arico, V. Baglio, V. Antonucci, I. Nicotera, C. Oliviero, L. Coppola and P. L. Antonucci, *Journal of Membrane Science* 270 (2006) 221-227.
- [16] M. A. Navarra, C. Abbati and B. Scrosati, *Journal of Power Sources* 183 (2008) 109-113.
- [17] Kongkachuichay P. and Pimprom S., *Chemical Engineering Research and Design* 88 (2010) 496-500.
- [18] H. F. W. Taylor, *Mineral. Mag.* 39 (1973) 377-389.
- [19] B. M. Choudary, M. Lakshmi Kantam, C. R. Venkat Reddy, K. Koteswara Rao and F. Figueras, *Journal of Molecular Catalysis A: Chemical* 146 (1999) 279-284.
- [20] M. J. Climent, A. Corma, S. Iborra and J. Primo, *Journal of Catalysis* 151 (1995) 60-66.
- [21] F. Li and X. Duan, edited by X. Duan and D. Evans (Springer Berlin / Heidelberg, 2006), Vol. 119, pp. 193-223.
- [22] F. Cavani, F. Trifiro and A. Vaccari, *Catalysis Today* 11 (1991) 173-301.
- [23] V. Rives, Nova Science Publishers, New York (2001).
- [24] S. Miyata, in *Clays and Clay Minerals* (1983), Vol. 31, pp. 305-311.
- [25] N. Kim, Y. Kim, T. T. Tsotsis and M. Sahimi, *The Journal of Chemical Physics* 122 (2005) 214713-214712.
- [26] S. P. Newman and W. Jones, *New Journal of Chemistry* 22 (1998) 105-115.
- [27] J. Guo, H. Lou, H. Zhao, D. Chai and X. Zheng, *Applied Catalysis A: General* 273 (2004) 75-82.
- [28] F. Li and X. Duan, *Structure and Bonding* 119 (2006) 193-223.
- [29] S. K. Yun and T. J. Pinnavaia, *Chemistry of Materials* 7 (1995) 348-354.
- [30] H.-S. Kim, Y. Yamazaki, J.-D. Kim, T. Kudo and I. Honma, *Solid State Ionics* 181 (2010) 883-888.
- [31] C. Manzi-Nshuti, P. Songtipya, E. Manias, M. M. Jimenez-Gasco, J. M. Hossenlopp and C. A. Wilkie, *Polymer* 50 (2009) 3564-3574.
- [32] A. Wang, Y. Bao, Z. Weng and Z. Huang, *Chinese Journal of Chemical Engineering* 16 (2008) 938-943.
- [33] T. W. Kim, M. Sahimi and T. T. Tsotsis, *Industrial & Engineering Chemistry Research* 48 (2009) 9504-9513.
- [34] K. Lee, J. H. Nam, J. H. Lee, Y. Lee, S. M. Cho, C. H. Jung, H. G. Choi, Y. Y. Chang, Y. U. Kwon and J. D. Nam, *Electrochemistry Communications* 7 (2005) 113-118.
- [35] K. Lee and J. D. Nam, *Journal of Power Sources* 157 (2006) 201-206.
- [36] J. R. P. Jayakody, P. E. Stallworth, E. S. Mananga, J. Farrington-Zapata and S. G. Greenbaum, *The Journal of Physical Chemistry B* 108 (2004) 4260-4262.
- [37] J. J. Fontanella, M. G. McLin, M. C. Wintersgill, J. P. Calame and S. G. Greenbaum, *Solid State Ionics* 66 (1993) 1-4.
- [38] T. A. Zawodzinski, M. Neeman, L. O. Sillerud and S. Gottesfeld, *The Journal of Physical Chemistry* 95 (1991) 6040-6044.
- [39] I. Nicotera, G. D. McLachlan, G. D. Bennett, I. Plitz, F. Badway, G. G. Amatucci and S. G. Greenbaum, *Electrochemical and Solid-State Letters* 10 (2007) A5-A8.
- [40] I. Nicotera, L. Coppola, C. O. Rossi, M. Youssry and G. A. Ranieri, *The Journal of Physical Chemistry B* 113 (2009) 13935-13941.
- [41] B. MacMillan, A. R. Sharp and R. L. Armstrong, *Polymer* 40 (1999) 2471-2480.
- [42] I. Gatto, A. Saccà, A. Carbone, R. Pedicini, F. Urbani and E. Passalacqua, *Journal of Power Sources* 171 (2007) 540-545.
- [43] E. O. Stejskal and J. E. Tanner, *The Journal of Chemical Physics* 42 (1965) 288-292.
- [44] A. A. Saccà, A. Carbone, R. Pedicini, G. Portale, L. D'Ilario, A. Longo, M. A. and E. Passalacqua, *Journal of Membrane Science* 278 (2006) 105-113.
- [45] J. T. Klopogge and R. L. Frost, *Journal of Solid State Chemistry* 146 (1999) 506-515.

- [46] W. Kagunya, R. Baddour-Hadjean, F. Kooli and W. Jones, *Chemical Physics* 236 (1998) 225-234.
- [47] J. T. Kloprogge, D. Wharton, L. Hickey and R. L. Frost, *American Mineralogist* 87 (2002) 623-629.
- [48] J. T. Kloprogge, D. Wharton, L. Hickey and R. L. Frost, in *American Mineralogist* (2002), Vol. 87, pp. 623-629.
- [49] R. Gosalawit, S. Chirachanchai, S. Shishatskiy and S. P. Nunes, *Solid State Ionics* 178 (2007) 1627-1635.
- [50] D. H. Jung, S. Y. Cho, D. H. Peck, D. R. Shin and J. S. Kim, *Journal of Power Sources* 118 (2003) 205-211.
- [51] C. P. Slichter, *Principles of Magnetic Resonance, 3rd ed.*, Springer ed. (Springer Series in Solid State Science, New York, 1990).
- [52] J. T. Kloprogge, D. Wharton, L. Hickey and R. L. Frost, *American Mineralogist* 87 (2002).
- [53] S. Miyata, *Clays and Clay Minerals*. (1983).
- [54] H. Xu, H. R. Kunz and J. M. Fenton, *Electrochimica Acta* 52 (2007) 3525-3533.
- [55] F. N. Büchi and G. G. Scherer, *Journal of Electroanalytical Chemistry* 404 (1996) 37-43.